

**Interaction between $\text{CO}_2/\text{HCO}_3^-$ and the
iron homeostasis in
*Corynebacterium glutamicum***

DISSERTATION

Von der Fakultät Energie-, Verfahrens- und Biotechnik der Universität
Stuttgart zur Erlangung der Würde eines Doktors der Naturwissenschaften

(Doctor rerum naturalium, Dr. rer. nat.)

genehmigte Abhandlung

vorgelegt von

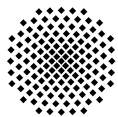
Felix Müller

aus Düsseldorf

Hauptberichter: Prof. Dr.-Ing. Ralf Takors

Mitberichter: Prof. Dr. Bernhard Eikmanns

Tag der mündlichen Prüfung: 05. Oktober 2020



University of Stuttgart
Germany

Institut für Bioverfahrenstechnik

2020

Deutscher Titel:

**Interaktion zwischen $\text{CO}_2/\text{HCO}_3^-$ und der
Eisenhomöostase in
*Corynebacterium glutamicum***

Meiner Familie.

Acknowledgements

More than three years of work are finally channeled into this manuscript. Many people have been involved, contributed to the work and supported myself during this time.

I want to express my deep appreciation.

First of all, I would like to thank Prof. Dr.-Ing. Ralf Takors, head of the Institute of Biochemical Engineering, my doctoral advisor. The professional setting, technical equipment and the scientific discussion have always supported my work in the most beneficial way. I am grateful, that the Prof. Dr. Bernhard Eikmanns agreed to the co-examination of this dissertation and that Prof. Dr. Georg Sprenger acceded to the examination chair.

I want to express my particular appreciation to Prof. Dr. Bastian Blombach for his scientific guidance. He performed the initial work in the predecessor project, accompanied my daily work and made me participate in the scientific network at international conferences.

I had to leave the microbiologist's comfort zone during the course of this project as I looked for the answers in chemical processes. Thanks to Dr. Stephan Hammer, Dr. Bettina Nestl and Dr. Bernd Nebel (Department of Technical Biochemistry, University of Stuttgart) as well as Prof. Dr. Herbert Riepel (Organic-Analytical Chemistry, Weihenstephan-Triesdorf University of Applied Sciences, Technical University of Munich, Campus Straubing) for their time during constructive discussions of chemical aspects. Thanks to Prof. Dr. Michael Bott for kindly providing the deletion plasmid *pK19mobsacB- Δ pup*.

I appreciate the excellent analytical expertise of André Feith, who performed the LC-MS-QTOF analysis of my samples. Thanks to Adrian Eilingsfeld, who introduced me

to the bioreactor setup. Thanks to Eugenia Münch, the technical assistant in our group, who supported my work inherently. I am very glad about the contributions of Johanna Rapp and Anna-Lena Hacker that helped me advancing the project.

At the IBVT, I was lucky enough to share my lab and office with some outstanding people. I want to single out Michaela Graf, Julian Lange and Andreas Schwentner, with whom I spent hours discussing scientific, annoying and private topics. Many thanks to our entire group of *Molecular Biotechnology* and all dear colleagues at the IBVT. I dedicate my special thanks to Silke Reu, who silently organises the professional non-scientific setting of the institute.

During my entire time in Stuttgart my parents, my girlfriend Rebecca and all my friends backed me up. I want to express my deepest thanks and appreciation for your permanent support.

This work was funded by the Deutsche Forschungsgemeinschaft (grant TA241/5-2).

Thank you all.

State of Affirmation

I declare herewith, that this thesis was prepared exclusively on my own without any help of a third party and that no other resources or means (including online sources and electronic media) were utilised than explicitly referred to. My work was assisted by my master student Johanna Rapp and my bachelor student Anna-Lena Hacker.

Parts of this work have been published in peer-reviewed journals and at international conferences as poster or oral presentations. This document has not been submitted identically or alike ever before. All analogously or literally employed statements are indicated precisely as such.

Peer-reviewed scientific articles:

Müller, F., Rapp, J., Hacker, A.-L., Feith, A., Takors, R., Blombach, B. (2020) CO₂/HCO₃⁻ accelerates iron reduction through phenolic compounds. *mBio* [accepted] <https://doi.org/10.1128/mBio.00085-20>.

Contributions at international conferences:

- poster
- oral

- **Müller, F.**, Rapp, J., Takors, R., Blombach, B. (2018) Reporter constructs in *Corynebacterium glutamicum* for the analysis of CO₂/HCO₃⁻ induced regulatory response. *VAAM annual conference*, 15 - 18 April 2018, Wolfsburg, Germany

- **Müller, F.**, Rapp, J., Takors, R., Blombach, B. (2018) Synthetic reporter constructs in *Corynebacterium glutamicum* for the analysis of CO₂/HCO₃⁻ imposed heterogeneities. *DECHEMA Himmelfahrtstagung*, 7 - 9 May 2018, Magdeburg, Germany

- **Müller, F.**, Rapp, J., Hacker, A.-L., Feith, A., Takors, R., Blombach, B. (2019) CO₂/HCO₃⁻ and PCA induced effects in the iron homeostasis of *Corynebacterium glutamicum*. *VAAM annual conference*, 17 - 19 March 2019, Mainz, Germany

- **Müller, F.**, Rapp, J., Hacker, A.-L., Feith, A., Takors, R., Blombach, B. (2019) Interaction between CO₂/HCO₃⁻ and the iron homeostasis in *Corynebacterium glutamicum*. *2nd annual meeting of the German Community of Corynebacterium glutamicum*, 1 - 2 August 2019, Jülich, Germany

Straubing, 25 October 2020

Felix Müller

Contents

Acknowledgements	I
State of Affirmation	III
List of Figures	XI
List of Tables	XIII
Nomenclature	XV
Abstract	1
Zusammenfassung	3
1 Introduction	5
1.1 Carbon dioxide	5
1.1.1 Physical properties	5
1.1.2 CO ₂ /HCO ₃ ⁻ in cell metabolism	7
1.1.3 CO ₂ /HCO ₃ ⁻ induced regulatory response and phenotypes	10
1.2 <i>Corynebacterium glutamicum</i>	14
1.2.1 Metabolism	15
1.3 Iron homeostasis	19
1.3.1 Iron transport	20
1.3.2 Iron storage	22
1.3.3 Iron mobilisation and reduction	23
1.3.4 Regulation of iron homeostasis	26

1.3.5	Iron homeostasis in <i>C. glutamicum</i>	28
1.3.5.1	Transport systems	28
1.3.5.2	Iron chelates	31
1.3.5.3	Iron storage and mobilisation	33
1.3.5.4	Regulation of iron homeostasis	33
1.3.5.5	The diphtheria toxin regulator (DtxR) protein	34
1.3.5.6	Transcriptional response of the DtxR regulon	37
1.4	Interference of iron homeostasis and CO ₂ /HCO ₃ ⁻	39
1.4.1	Chemical aspects	39
1.4.2	Biological interference	40
1.4.2.1	In plants	40
1.4.2.2	In other organisms	41
2	Objectives of this study	43
3	Material & Methods	45
3.1	Chemicals	45
3.2	Cultivation media	45
3.2.1	2x YT complex medium	45
3.2.2	BHI(S) complex medium	46
3.2.3	Agar plates	46
3.2.4	CgXII minimal medium	46
3.2.5	Antibiotics	47
3.3	Bacterial strains & plasmids	47
3.4	DNA manipulation & strain engineering	52
3.4.1	Quantification of the DNA concentration	52
3.4.2	DNA separation by agarose gel electrophoresis	52
3.4.3	PCR amplification	53
3.4.4	Colony PCR	55

3.4.5	DNA purification	56
3.4.5.1	Isolation of chromosomal DNA	56
3.4.5.2	Purification from PCR mix & restriction digest	56
3.4.5.3	Plasmid isolation	56
3.4.6	Plasmid linearisation	56
3.4.7	DNA ligation	57
3.4.8	Gibson assembly	57
3.4.9	Competent cells	58
3.4.9.1	<i>Escherichia coli</i>	58
3.4.9.2	<i>Corynebacterium glutamicum</i>	59
3.4.10	Transformation	59
3.4.10.1	<i>Escherichia coli</i>	59
3.4.10.2	<i>Corynebacterium glutamicum</i>	60
3.4.11	Sequencing & analysis	60
3.4.12	Chromosomal integration & deletion in <i>C. glutamicum</i>	60
3.5	Cultivation experiments	62
3.5.1	Cryogenic cultures	62
3.5.2	Generic seed train	62
3.5.3	Shaking flask experiments	62
3.5.3.1	Cultivation conditions	62
3.5.3.2	Fluorescence experiments	63
3.5.4	Bioreactor cultivation	64
3.5.5	BioLector cultivation	65
3.5.6	Biological replicates	65
3.6	Protein biochemistry	65
3.6.1	DtxR (over-)production	65
3.6.2	Protein purification	66
3.6.2.1	Cell disintegration	66
3.6.2.2	Ni-NTA affinity chromatography	66

3.6.2.3	Strep-Tactin affinity chromatography	67
3.6.3	Protein analysis	67
3.6.3.1	Quantification of the protein concentration	67
3.6.3.2	SDS-PAGE	67
3.6.3.3	native PAGE	69
3.6.3.4	Differential scanning fluorimetry	69
3.7	Pull-down experiments	70
3.7.1	Cultivation	71
3.7.2	Formaldehyde cross-linking	71
3.7.3	Sample preparation	71
3.7.4	Peptide analysis (commercial)	72
3.7.5	Manual re-processing & discrimination of data	72
3.8	Analytics	72
3.8.1	Quantification of the cell density	72
3.8.2	Fluorescence detection	73
3.8.3	Intracellular iron quantification	73
3.8.3.1	Cultivation & harvest	73
3.8.3.2	Cell disruption	73
3.8.3.3	Ferrozin based iron quantification	74
3.8.4	Iron reduction assay	74
3.8.5	Detection of Fe ³⁺ -PCA complexes	75
3.8.6	LC-MS-QTOF analysis of aromatic compounds	75
4	Results	77
4.1	<i>In vitro</i> characterisation of DtxR	77
4.1.1	Purification and PAGE	77
4.1.2	Differential scanning fluorimetry	79
4.2	Pull-down experiments	82
4.2.1	Cultivation & purification	82

4.2.2	Peptide identification & re-processing of the data	82
4.2.3	Hypothetical protein Cg2444	85
4.2.4	<i>Corynebacterium glutamicum</i> $\Delta cg2444$	86
4.3	Analysis of secreted compounds	88
4.4	Reporter strains	91
4.4.1	Design and construction	91
4.4.2	Validation	93
4.4.2.1	Responsiveness to iron	93
4.4.2.2	Responsiveness to the CO ₂ content	94
4.5	Shaking flask experiments	97
4.5.1	Scale-down	97
4.5.2	Acetate supplementation	99
4.5.3	Iron depleted growth	102
4.6	Intracellular iron quantification	104
4.7	Deletion mutant screening	107
4.8	Iron reduction assays	110
4.8.1	HCO ₃ ⁻ accelerates the iron reduction through PCA	110
4.8.2	Iron reduction by phenolic compounds	115
4.8.3	HCO ₃ ⁻ accelerates the formation of Fe ³⁺ -PCA complexes	116
5	Discussion	119
5.1	<i>C. glutamicum</i> growth performance responds to the iron availability	119
5.2	Iron is reduced by phenolic compounds	122
5.3	HCO ₃ ⁻ accelerates iron chelation and reduction	125
5.4	Secretion of reductants by <i>C. glutamicum</i>	126
5.5	Physiological relevance of <i>in vitro</i> iron reduction	127
5.6	HCO ₃ ⁻ is not the co-effector of DtxR	129
5.7	Cg2444 – an interaction partner of DtxR?	130
5.8	Iron transport and mobilisation in <i>C. glutamicum</i>	131

6 Conclusion	135
7 References	137
Appendix	161
Overview of aromatic compounds	161
Bioelector cultivation	162
Deletion mutants	163
<i>Corynebacterium glutamicum</i> $\Delta cg2444$ & Δftn	163
<i>Corynebacterium glutamicum</i> $\Delta cg0041-cg0042$	164
Chemicals	164
Enzymes	168
Kits	169
Laboratory equipment	169
Apparatus	170
Primer	171
GeneRuler TM 1 kb Plus DNA Ladder	176
Protein ladders PageRuler TM and nativeMark TM	177
Accepted manuscript at the proof-reading stage	178
Clarification on the work contributions	191

List of Figures

1	Major carboxylation and decarboxylation reactions in the central metabolism of <i>C. glutamicum</i>	8
2	Iron homeostasis in <i>C. glutamicum</i>	30
3	Protein structure of the DtxR protein from <i>C. glutamicum</i>	35
4	Standard seed train for <i>C. glutamicum</i> cultivation	63
5	Seed train for <i>C. glutamicum</i> cultivation under iron starvation and excess	64
6	Detection principle of iron reduction assays	75
7	SDS PAGE of purified DtxR-His and DtxR-Strep in the absence and presence of DTT	78
8	Native PAGE of purified DtxR-His with increasing DTT concentrations .	78
9	SDS PAGE of purified wt-DtxR and DtxR(C102D)	79
10	Thermal shift assay of purified DtxR with increasing concentrations of Ni ²⁺ and Mn ²⁺	81
11	SDS PAGE of DtxR in pull-down experiments	83
12	Genomic organisation of <i>cg2444</i>	85
13	SmartBLAST results of the Cg2444 carboxy-terminal protein sequence . .	87
14	Mechanism of activation in reporter strain <i>C. glutamicum</i> FEM1	91
15	Mechanism of activation in reporter strain <i>C. glutamicum</i> FEM3	92
16	Growth and fluorescence of <i>C. glutamicum</i> WT, FEM1 and FEM3 in iron starvation and excess	95
17	Growth and fluorescence of <i>C. glutamicum</i> FEM3 in bioreactor cultivations	96
18	Growth of <i>C. glutamicum</i> WT in shaking flask cultivations	98
19	Fluorescence of <i>C. glutamicum</i> FEM3 in shaking flask cultivations	100

List of Figures

20	Growth of <i>C. glutamicum</i> WT in iron-depleted shaking flask cultivations .	101
21	Calibration curve of the ferrozine based iron quantification assay	104
22	Intracellular iron quantification of <i>C. glutamicum</i> WT shaking flask cultivations	105
23	Growth of <i>C. glutamicum</i> WT and Δpup in shaking flask cultivations . .	108
24	Fluorescence of <i>C. glutamicum</i> FEM3 and FEM3 Δpup in shaking flasks cultivations	109
25	Iron reduction assays with PCA and HCO_3^-	112
26	Iron reduction assays with and without gas exchange	113
27	LC-MS-QTOF analysis of PCA degradation	114
28	Iron reduction assay with aromatic compounds	115
29	Fe^{3+} -PCA complex formation kinetics	117
30	pH and HCO_3^- dependence of Fe^{3+} -PCA absorbance maximum	118
S1	Classification of phenol, chetechol and benzoic acid derivatives	161
S2	Growth and fluorescence of <i>C. glutamicum</i> FEM3 in BioLector cultivations with and without BPS	162
S3	Growth of <i>C. glutamicum</i> WT, $\Delta cg2444$ and Δftn in shaking flask cultivations	163
S4	Growth of <i>C. glutamicum</i> WT and $\Delta cg0041-cg0042$ in BioLector cultivations	164
S5	GeneRuler™ 1 kb Plus DNA Ladder	176
S6	PageRuler™ and nativeMark™ Protein Ladder	177

List of Tables

1	Composition of the 2x YT complex medium	45
2	Composition of the BHI(S) complex medium	46
3	Composition of CgXII minimal medium	47
4	List of bacterial strains	49
5	List of plasmids	50
6	PCR reaction mixture for amplification using <i>Phusion</i> polymerase	53
7	PCR reaction mixture for amplification using <i>Q5</i> polymerase	53
8	PCR program for DNA amplification using the <i>Phusion</i> polymerase	54
9	PCR program for DNA amplification using the <i>Q5</i> polymerase	54
10	Reaction mixture for a colony PCR using <i>taq</i> polymerase	55
11	Program for a colony PCR using the <i>taq</i> polymerase	55
12	Composition of <i>Gibson ISO enzyme reagent mixture</i>	58
13	Composition of <i>Gibson 5x ISO reaction mixture</i>	58
14	Composition of 10 % SDS separating gels	68
15	Composition of 6 % SDS stacking gels	69
16	DtxR co-purified peptides	84
17	Benzoic acid derivatives	89
18	<i>C. glutamicum</i> growth rates in iron starvation and excess	94
S1	List of chemicals	164
S2	List of enzymes	168
S3	List of kits	169
S4	List of laboratory equipment	169
S5	List of apparatus	170

List of Tables

S6 List of primers 171

Nomenclature

<i>acn</i>	gene encoding aconitase
AraC	regulator of the arabinose metabolism
Arg	arginine residue
Asn	asparagine residue
Asp	aspartic acid residue
ATCC	American Type Culture Collection
ATP	adenosine triphosphate
aq	in aqueous solution
<i>B. anthracis</i>	<i>Bacillus anthracis</i>
<i>B. cereus</i>	<i>Bacillus cereus</i>
Bfd	bacterioferritin associated ferredoxin
BLAST	basic local alignment search tool
bp	base pairs (nucleotides)
<i>B. subtilis</i>	<i>Bacillus subtilis</i>
C	carbon
°C	degree Celsius
<i>C. glutamicum</i>	<i>Corynebacterium glutamicum</i>
<i>C. diphtheriae</i>	<i>Corynebacterium diphtheriae</i>
CDW	cell dry weight (g)
<i>C. rodentium</i>	<i>Citrobacter rodentium</i>
CoA	coenzyme A

<i>C. neoformans</i>	<i>Cryptococcus neoformans</i>
Cys	cysteine residue
DECHEMA	Deutsche Gesellschaft für chemisches Apparatewesen, Chemische Technik und Biotechnologie e.V.
kDa	kilodalton
DNA	deoxyribonucleic acid
dNTP	deoxynucleoside triphosphate
<i>dps</i>	gene encoding DNA protection during starvation protein
<i>dtxR</i>	gene encoding diphtheria toxin regulator (DtxR)
<i>E. coli</i>	<i>Escherichia coli</i>
EMSA	electrophoretic mobility shift assay
e.g.	<i>exempli gratia</i> , “for example”
et al.	<i>et alii</i> , “and other”
<i>fecABCDE</i>	operon encoding ferric citrate transport complex
<i>fecI</i>	gene encoding iron starvation sigma
<i>fecR</i>	gene encoding ferric citrate transport regulator
FeoAB	ferrous iron transporter
FhuF	ferrichrome reductase
fig.	figure
<i>ftn</i>	gene encoding ferritin (Ftn)
<i>fur</i>	gene encoding ferric uptake regulator (Fur)
g	gram
Gln	glutamine residue
Glu	glutamic acid residue
Gly	glycin residue
GRAS	generally recognized as safe
GTP	guanosine triphosphate
h	hour

H_i	Henry coefficient of substance i
His	histidine residue
HPLC	high performance liquid chromatography
IdeR	iron dependent regulator
i.e.	<i>id est</i> , “that is to say”
IRP	iron regulatory protein
IRE	iron regulatory element
K_i	equilibrium constant
K_D	dissociation constant
L	liter
<i>lacZ</i>	gene encoding β -galactosidase
LC-MS-QTOF	liquid chromatography coupled to hybrid quadrupole time of flight mass spectrometry
λ_{em}	emission wavelength
λ_{ex}	excitation wavelength
λ_{max}	wavelength of maximum absorbance
m	meter or milli (10^{-3} in combination with SI unit)
m/z	mass-to-charge ratio
μ	exponential growth rate or micro (10^{-6} in combination with SI unit)
M	molarity
Met	methionine residue
min	minute
<i>mtsABC</i>	operon encoding manganese and iron transport system
<i>M. tuberculosis</i>	<i>Mycobacterium tuberculosis</i>
n	nano (10^{-9} in combination with SI unit)
NAD ⁺	nicotinamide adenine dinucleotide (oxidised)
NADH	nicotinamide adenine dinucleotide (reduced)

Nomenclature

NADP ⁺	nicotinamide adenine dinucleotide phosphate (oxidised)
NADPH	nicotinamide adenine dinucleotide phosphate (reduced)
OD ₆₀₀	optical density at 600 nm
O/N	over night
oxPP	oxidative pentose phosphate pathway
p _i	(partial) pressure (of compound i)
PAGE	polyacrylamide gel electrophoresis
PCR	polymerase chain reaction
PEP	phosphoenolpyruvate
pH	negative decadic logarithm of the proton concentration
pI	isoelectric point
Phe	phenylalanine residue
P _{ripA}	promoter of <i>ripA</i>
Pro	proline residue
P _{tac}	hybrid <i>tac</i> promoter from <i>trp</i> and <i>lacUV5</i>
<i>pup</i>	gene encoding prokaryotic ubiquitin-like protein
RBS	ribosome binding site
<i>regA</i>	gene encoding exotoxin A regulatory protein (RegA)
RFU	relative fluorescence unit
<i>rhyB</i>	gene encoding iron responsive small RNA
<i>ripA</i>	gene encoding regulator of iron proteins A (RipA)
RNA	ribonucleic acid
ROS	reactive oxygen species
RT	room temperature or retention time
s	second
<i>sacB</i>	gene encoding levansucrase
<i>S. cerevisiae</i>	<i>Saccharomyces cerevisiae</i>

SH3	Src homology 3
<i>sitABCD</i>	gene encoding alkaline Mn ²⁺ transporter
<i>S. pyogenes</i>	<i>Streptococcus pyogenes</i>
<i>suf</i>	gene(s)/operon encoding iron sulfur cluster assembly machinery
t	time
tab.	table
TCA	tricarboxylic acid cycle
T _m	melting temperature
<i>toxA</i>	gene encoding exotoxin A
<i>toxT</i>	gene encoding toxin regulator (ToxT)
TSS	transcriptional start site
TPP	thiamine pyrophosphate
VAAM	Vereinigung für Allgemeine und Angewandte Mikrobiologie
<i>V. cholerae</i>	<i>Vibrio cholerae</i>
% (v/v)	volume per volume proportion
vvm	volume per volume per minute
vs.	<i>versus</i> “against”
% (w/v)	weight per volume proportion
WT	wildtype strain
XylS	transcriptional regulator XylS

Chemicals

2x YT (or 2x TY)	double concentrated yeast-tryptone
2,3-DHB	2,3-dihydroxybenzoic acid
3,4-DHB (=PCA)	3,4-dihydroxybenzoic acid (= protocatechuic acid)
3-HAA	3-hydroxyanthranilic acid (= 2-amino-3-hydroxybenzoic acid)
Amp	ampicillin
BHI(S)	brain heart infusion (with 91 g sorbitol L ⁻¹)
BPS	bathophenanthroline disulfonic acid
CaCl ₂	calcium chloride
Co ²⁺	divalent cobalt ion
CO ₂	carbon dioxide
CO ₃ ²⁻	carbonate
CuSO ₄	copper sulfate
DMSO	dimethyl sulfoxide
DTT	dithiothreitol
EDTA	ethylenediaminetetraacetic acid
Fe ²⁺	ferrous iron (reduced state)
Fe ³⁺	ferric iron (oxidised state)
FeCl ₃	ferric chloride
FeCO ₃	siderit
Fe(HCO ₃) ₂	ferrous bicarbonate
FeHCO ₃ ⁺	ferrous bicarbonate cation
H ⁺	hydrogen ion
H ₂ O ₂	hydrogen peroxide
HCl	hydrochloric acid
HCO ₃ ⁻	bicarbonate (hydrogen carbonate)
Kan	kanamycin

KHCO_3	potassium bicarbonate
K_2HPO_4	di-potassium phosphate
KH_2PO_4	potassium di-hydrogen phosphate
KOH	potassium hydroxide
Me^{2+}	divalent metal ion
MgSO_4	magnesium sulfate
Mn^{2+}	divalent manganese ion
MOPS	3-(<i>N</i> -morpholino)propanesulfonic acid
N_2	nitrogen
NaCl	sodium chloride
NaHCO_3	sodium bicarbonate
Ni^{2+}	divalent nickel ion
NiCl_2	nickel chloride
$(\text{NH}_4)_2\text{SO}_4$	Ammonium sulfate
O_2	oxygen
PCA (= 3,4-DHB)	protocatechuic acid (= 3,4-dihydroxybenzoic acid)
SDS	sodium dodecyl sulfate
Suc	sucrose
TAE buffer	tris-acetate with EDTA
VE- H_2O	demineralised water (“vollentsalzt”)
ZnSO_4	zink sulfate

Abstract

By addressing the physiological response to varying CO₂ contents in the inlet air of a bioreactor cultivation Blombach et al. (2013) disclosed recently a link between CO₂/HCO₃⁻ and the iron homeostasis of *Corynebacterium glutamicum*. Elevated CO₂ levels induced the transcriptional regulation of almost the entire DtxR regulon, which is known as the master regulator of iron homeostasis in *C. glutamicum*. Iron is one of the most abundant elements in the Earth's crust and possesses an essential role in central metabolism in almost all kind of life. Its accessibility is often limited by the poor solubility of ferric iron (Fe³⁺), which is the predominant oxidation state of iron in an oxygenic environment. Hence, the reduction of Fe³⁺ is of crucial importance to meet the cellular demand of Fe²⁺, but might become detrimental to the cell as excessive amounts of free Fe²⁺ are prone to the cytotoxic Fenton reaction in the presence of hydrogen peroxide. As a consequence, cells possess a tightly regulated network to balance the amount of free intracellular Fe²⁺. Homologues of the dual transcriptional regulator DtxR in *C. glutamicum* exist likewise in many bacterial pathogens, where they control the expression of virulence genes in response to the iron availability. Hence, understanding of the interaction level of CO₂/HCO₃⁻ and DtxR activation in *C. glutamicum* might be of interest with regard to human pathogens.

By means of a reporter strain *C. glutamicum* growth performance in CO₂/HCO₃⁻ and PCA supplemented cultures was found to respond to the DtxR activation state. This was apparently not attributed to any biological function, but the intracellular Fe²⁺ availability was increased by the iron reduction capacity of the cultivation medium. Under physiological conditions Fe³⁺ was chemically reduced at the expense of protocatechuic acid (PCA) and other phenolic compounds, resulting in seven-fold higher Fe²⁺ concen-

trations in an *in vitro* reduction assay compared to a reference lacking the reductant. The redox reaction was increased in the presence of HCO_3^- , which did not reduce iron itself. LC-MS-QTOF analytics revealed, that PCA was in fact degraded faster in the presence of HCO_3^- without affecting the oxidation products of PCA. Not only the iron reduction, but also the complex formation between Fe^{3+} and PCA was enhanced by 46 % in the presence of HCO_3^- and the wavelength of maximum absorbance of the complex was shifted to a shorter wavelength.

This work demonstrates, that the chemical iron reduction through phenolic compounds is accelerated in the presence of HCO_3^- . By that, the intracellular Fe^{2+} concentration was increased and growth was stimulated in *C. glutamicum*. Phenolic compounds, which were tested as the reductant in this study, are wide spread in nature and the same habitats can be characterised by high $\text{CO}_2/\text{HCO}_3^-$ contents. Hence, it can be concluded that the abiotic effect described here impacts other biological as well as geochemical systems. This finding might be of particular interest in the prediction of iron/bicarbonate controlled pathogenicity.

Zusammenfassung

In einer kürzlich veröffentlichten Studie untersuchten Blombach et al. (2013) die physiologische Antwort des industriellen Produktionsorganismus *C. glutamicum* auf unterschiedliche CO₂-Konzentrationen in der Zuluft einer Bioreaktor-Kultivierung. *C. glutamicum* induzierte die transkriptionelle Antwort beinahe des kompletten DtxR-Regulons in Antwort auf die CO₂-angereicherte Zuluft. Da DtxR in *C. glutamicum* als Eisen-Regulator bekannt ist, deuten die Ergebnisse auf eine Verbindung zwischen CO₂/HCO₃⁻ und der Eisenhomöostase hin. Eisen ist eines der am stärksten vertretenen Elemente in der Erdkruste und nimmt eine zentrale Rolle im Stoffwechsel fast aller Lebewesen ein. Die geringe Löslichkeit von oxidiertem Eisen (Fe³⁺), welches in einer sauerstoffreichen Umwelt überwiegt, begrenzt allerdings die Eisenverfügbarkeit und macht die Reduktion von Fe³⁺ unerlässlich, um den zellulären Bedarf an reduziertem Eisen (Fe²⁺) zu befriedigen. Eine große Menge an Fe²⁺ kann andererseits zu Problemen führen, da sie durch die Fenton-Reaktion in Gegenwart von Wasserstoffperoxid die Bildung zytotoxischer Sauerstoffradikale fördert. Folglich unterliegen die intrazelluläre Menge an freiem Eisen und das Gleichgewicht zwischen beiden Spezies einer strengen hierarchischen Kontrolle auf transkriptioneller Ebene. Homologe des dualen Transkriptionsfaktors DtxR in *C. glutamicum* existieren ebenso in vielen bakteriellen Pathogenen, in denen sie abhängig von der Eisenverfügbarkeit die Expression von Virulenzgenen kontrollieren. Daher ist ein tieferes Verständnis der Interaktion zwischen CO₂/HCO₃⁻ und DtxR-Aktivierung, welches im Fokus dieser Arbeit steht, auch im Hinblick auf Humanpathogene von Interesse.

Im Rahmen der vorliegenden Arbeit wurde zunächst ein Reporterstamm entwickelt, der den Aktivierungszustand von DtxR *in vivo* an die Produktion des fluoreszierenden Proteins eGFP koppelt. Mit Hilfe des Reporterstamm konnte gezeigt werden, dass unter-

schiedliche Wachstumsphänotypen von *C. glutamicum* in $\text{CO}_2/\text{HCO}_3^-$ oder Protocatechusäure (PCA) supplementierten Kultivierungen jeweils mit dem Aktivierungszustand von DtxR korrelieren. Die primäre Aktivierung von DtxR erfolgt durch Fe^{2+} und es konnten keine Hinweise darauf gefunden werden, dass HCO_3^- als Co-Stimulus fungiert. Die phänotypische Charakterisierung von Deletionsmutanten zeigte, dass HCO_3^- weder mit der intrazellulären Eisenspeicherung, noch mit der (enzymatischen) Eisenmobilisierung oder Reduktion interagiert. Stattdessen folgte die intrazelluläre Fe^{2+} -Verfügbarkeit offensichtlich der chemischen Eisenreduktionskapazität im Medium. *In vitro*-Reduktionsexperimente unter physiologischen Bedingungen zeigten, dass Fe^{3+} chemisch durch phenolische Substanzen reduziert wird, was zu einer siebenfachen Erhöhung der Fe^{2+} -Konzentration gegenüber einer Kontrolle ohne Reduktionsmittel führte. HCO_3^- beschleunigte die Redox-Reaktion ohne Eisen selbst zu reduzieren. In einem LC-MS-QTOF-Ansatz konnte nachgewiesen werden, dass die Degradation von PCA in Gegenwart von HCO_3^- tatsächlich schneller ablief, ohne dass sich die chemische Natur der nachgewiesenen Oxidationsprodukte von PCA veränderte. Die Gegenwart von HCO_3^- beschleunigte allerdings nicht allein die Eisenreduktion an sich, sondern auch die Fe^{3+} -PCA Komplexbildung lief etwa 46 % schneller ab und die maximale Absorption der Komplexe war in einen kurzwelligeren Bereich verschoben.

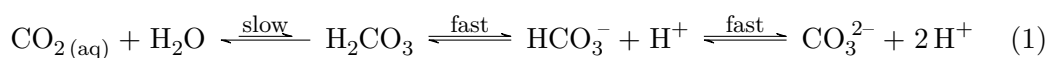
In dieser Arbeit konnte gezeigt werden, dass die chemische Eisenreduktion durch phenolische Substanzen in Gegenwart von HCO_3^- beschleunigt wird. Das resultierte in einer erhöhten intrazellulären Fe^{2+} -Verfügbarkeit und stimulierte das Wachstum von *C. glutamicum*. Phenole, die in dieser Studie als Eisenreduktionsmittel genutzt wurden, sind in der Natur weit verbreitet und in den selben Habitaten können ebenso hohe Konzentrationen an $\text{CO}_2/\text{HCO}_3^-$ vorkommen. Es kann daher geschlossen werden, dass der hier beschriebene abiotische Effekt auch Einfluss auf andere biologische sowie geochemische Systeme hat. Besonders im Hinblick auf Pathogene und die oft Eisen/Bicarbonat kontrollierte Infektiosität können diese Erkenntnisse von Bedeutung sein.

1.1 Carbon dioxide

Contributing to the atmospheric air with currently about 0.04 % (v/v), carbon dioxide is regarded as a trace gas. Nonetheless, it occupies a key position in the carbon cycle as the inorganic molecule is fixed in organic matter e.g. by the action of photosynthesis and released back into the atmosphere as the result of biotic and abiotic combustion processes.

1.1.1 Physical properties

In its gaseous form (at temperatures above the melting point $-56.6\text{ }^{\circ}\text{C}$) carbon dioxide is colorless, odorless and non-inflammable. The solubility of CO_2 in water is high, as reflected e.g. in a high Henry coefficient ($H_{\text{CO}_2} = 34.5\text{ mmol bar}^{-1}\text{ L}^{-1}$) compared to that of oxygen ($H_{\text{O}_2} = 1.3\text{ mmol bar}^{-1}\text{ L}^{-1}$) at $25\text{ }^{\circ}\text{C}$ (Blombach and Takors, 2015). Dissolved carbon dioxide ($\text{CO}_2_{(\text{aq})}$) can be hydrated to carbonic acid (H_2CO_3), which is then quickly deprotonated yielding bicarbonate (hydrogen carbonate, HCO_3^-) and carbonate (CO_3^{2-}) as in (1).



These species form a pH dependent dissociation equilibrium with the equilibrium constants for the first ($K_1 = 10^{-6.3}\text{ M}$) and second ($K_2 = 10^{-10.25}\text{ M}$) deprotonation, reflecting the respective equilibrium pH. These values highlight the predominance of bicarbonate species at physiological pH values. For the hydration of CO_2 to H_2CO_3 a reaction rate of 0.03 s^{-1} was determined, which is at least 6-times lower than for the reverse direction

(Bailey and Ollis, 1986; Blombach and Takors, 2015). Since deprotonation reactions proceed essentially faster than the hydration step, the occurrence of H_2CO_3 is typically ignored when balancing dissolved CO_2 species. At physiological pH conditions, the major part of dissolved inorganic carbon species is allocated in HCO_3^- . The distribution at pH 7 was calculated to 17 % CO_2 , 83 % HCO_3^- (Blombach and Takors, 2015). At the cultivation pH of 7.4 used in this study the distribution was even more drastically shifted towards bicarbonate (8 % CO_2 , 92 % HCO_3^-). The contribution of CO_3^{2-} to the overall inorganic carbon is negligible at these pH values. Difficulties, that arise when determining CO_2 transfer rates between gas and liquid phase, are also discussed in a review by Blombach and Takors (2015). In fact, CO_2 transfer might be slowed down as the hydration reaction represents the rate limiting step. Since CO_2 is highly soluble in water and permanently released by aerobically growing microbial cells, CO_2 availabilities might vary widely. Assuming a typical bioprocess is aerated with ambient air, dissolved concentrations will be around $0.5 \text{ mg CO}_2 \text{ L}^{-1}$ at the beginning of the fermentation and by a conservative estimation might rise to $650 \text{ mg CO}_2 \text{ L}^{-1}$ when 20 % CO_2 is released in the exhaust air. The variation factor of at least 1,000 might be further increased by the real process conditions. Dissolved CO_2 concentrations in over-pressurised bioreactors can be calculated by Henry's law, whilst medium components sometimes double the solubility (Blombach and Takors, 2015). In contrast to the well characterised transfer of oxygen from gas to liquid phase, the transfer of CO_2 proceeds most of the time in the opposite direction from liquid to gas phase. This will cause highest CO_2 concentrations in the liquid in close proximity to the cell (Blombach and Takors, 2015; Cummins et al., 2014).

CO_2 handling becomes cumbersome as bespoke deprotonation reactions shift the pH towards more acidic conditions when net CO_2 is released into the medium. As a consequence, cultivation media require sufficient buffer capacity or in the case of pH control titration of large amounts of a base, thus, increasing the osmolarity of the medium. On the other hand, when working with bicarbonate as supplement, concentrations decrease by gasing out of CO_2 , which in turn causes an increase of the pH.

1.1.2 CO₂/HCO₃⁻ in cell metabolism

In a heterotrophic lifestyle, carbon dioxide is mainly released in the TCA cycle, the preceding step providing acetyl-CoA for the TCA cycle and in the oxidative pentose phosphate pathway. The respective enzymes, isocitrate dehydrogenase, α -ketoglutarate dehydrogenase complex, pyruvate dehydrogenase complex and 6-phosphogluconate dehydrogenase, all belong to the class of oxidoreductases and, thus, yield one reduction equivalent during the oxidative decarboxylation of their respective substrate. In addition to this, CO₂ can be released in a number of reactions of anabolic as well as catabolic pathways, often catalysed by enzymes that are classified as transferases or lyases. During the non-oxidative decarboxylation of their substrate they do not generate reduction equivalents in turn (fig. 1).

CO₂/HCO₃⁻ represent the key intermediate at the transition between inorganic and organic carbon as it is the substrate of at least six independent pathways responsible for the energy demanding fixation of inorganic carbon in organic material, hence, forming the base of autotrophic life (Fuchs, 2010). But CO₂/HCO₃⁻ is likewise an essential substrate in heterotrophic bacteria during aerobic growth. Per round of the TCA cycle, one acetyl group is transferred onto one molecule of oxaloacetate. Following two decarboxylation steps, reduction equivalents for the respiratory chain are provided by the TCA cycle and one molecule of oxaloacetate is regenerated for a subsequent condensation reaction with acetyl-CoA. Since biosynthetic pathways of a number of different amino acids branch off, particularly at the level α -ketoglutarate and oxaloacetate, TCA intermediates need to be constantly refilled to prevent a draining of the TCA cycle in cells growing on glycolytic substrates (e.g. glucose, fructose). When using gluconeogenic substrates (e.g. acetate, ethanol) as the sole carbon and energy source decarboxylation of the C₄-molecules oxaloacetate and malate is vital to provide carbohydrates and flux into the oxidative pentose phosphate pathway via gluconeogenesis. An excellent review covering all reactions comprising the PEP-pyruvate-oxaloacetate node in different bacteria was given by Sauer and Eikmanns (2005). The organism-specific equipment involves up to two en-

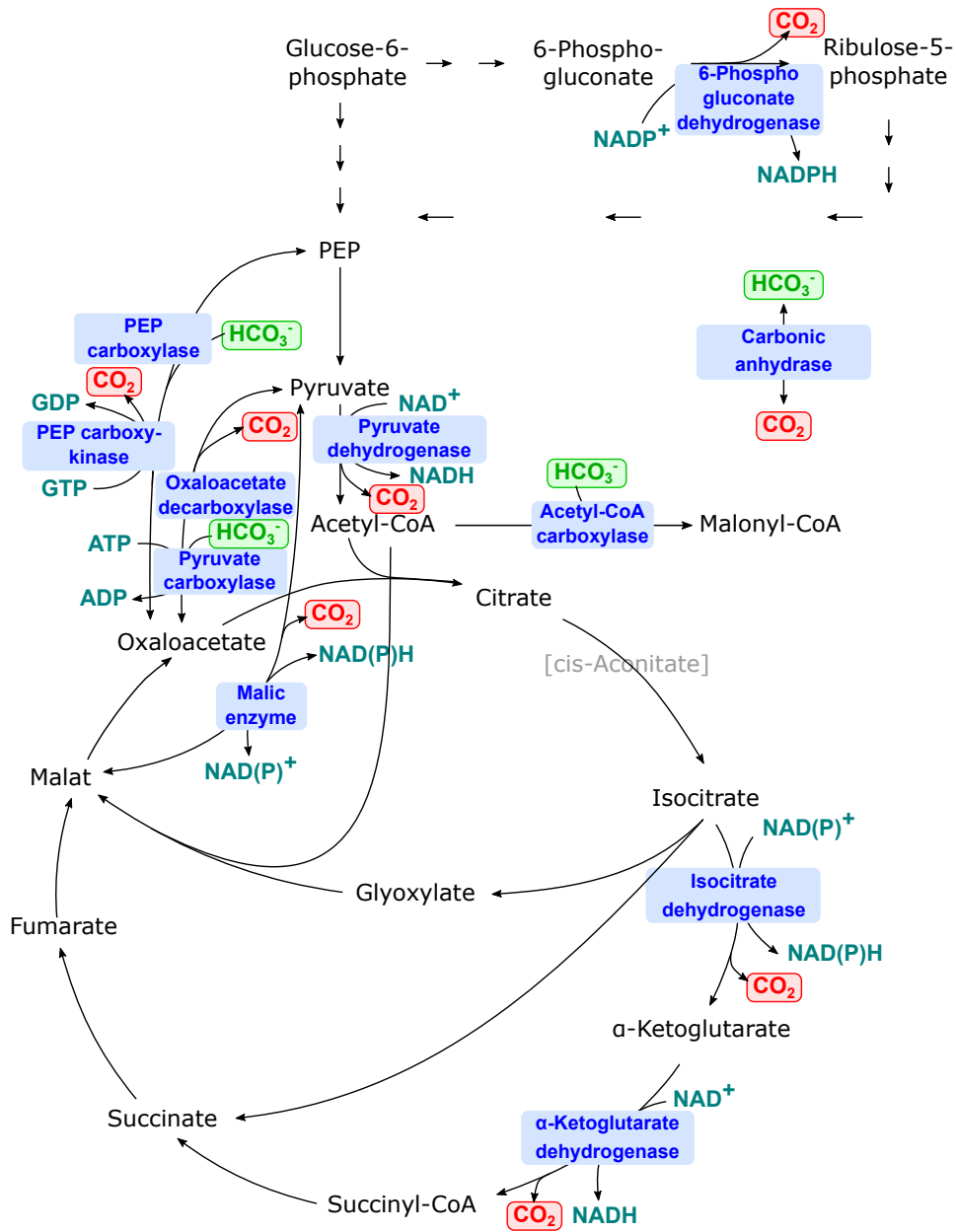


Figure 1: Schematic overview of the major carboxylation and decarboxylation reactions in the central carbon metabolism of *C. glutamicum* during aerobic growth. Only enzymes catalysing the relevant (de-)carboxylation reactions are annotated (in blue). The participation of reduction equivalents is indicated in cyan, CO_2 release in red and HCO_3^- fixation in green.

zymes catalysing the irreversible carboxylation of C₃-intermediates yielding oxaloacetate and up to three enzymes that catalyse primarily the reverse reaction yielding PEP or pyruvate through the decarboxylation of the C₄-intermediates oxaloacetate and malate. In contrast to large parts of central carbon metabolism that seem to be evolutionary conserved, a high degree of flexibility is found at the PEP-pyruvate-oxaloacetate node of different bacteria, that feature various combinations of enzymes (Sauer and Eikmanns, 2005). *C. glutamicum* is outstanding in this regard, as it possesses all five enzymes. Two enzymes catalyse the irreversible HCO₃⁻ fixation onto PEP or pyruvate. Both reactions yield oxaloacetate, but differ significantly with respect to the thermodynamics. Whereas the former reaction catalysed by the PEP carboxylase is thermodynamically favorable yielding one ATP/GTP per reaction, the latter is not. Pyruvate carboxylation is catalysed by the pyruvate carboxylase and must be energetically driven by the hydrolysis of ATP. In the reverse reaction oxaloacetate is decarboxylated to PEP (reversible, catalysed by PEP carboxykinase) or pyruvate (irreversible, catalysed by oxaloacetate decarboxylase). The physiological role of PEP carboxykinase has been found to differ with the organism and cultivation condition. Although it might be generally rather associated with the decarboxylation reaction, in rumen bacteria like *Mannheimia succiniproducens* that are exposed to CO₂ excess in their environment, PEP carboxykinase provides the primary anaplerotic enzyme (Lee et al., 2006). The malic enzyme constitutes the last piece of the PEP-pyruvate-oxaloacetate node that catalyses the reversible decarboxylation of malate yielding NAD(P)H. With respect to the NAD- or NADP-dependence of the enzyme in different organism its physiological role might be assigned either to the gluconeogenic flux or NADPH generation for biosynthetic pathways (Sauer and Eikmanns, 2005).

In contrast to the uncharged CO₂ molecule, which is typically released during decarboxylation and can easily pass the cell membrane by diffusion, the major substrate of carboxylation reactions, HCO₃⁻, cannot. Consequently, a fundamental function is attributed to the carbonic anhydrase. The enzyme catalyses the reversible hydration of CO₂ and, thus, eventually helps to establish the CO₂ – HCO₃⁻ equilibrium faster.

This conversion is crucial to provide sufficient HCO_3^- for carboxylation, e.g. for the anaplerotic reactions (Smith and Ferry, 2000).

The native regulation of the PEP-pyruvate-oxaloacetate node involves catabolite repression. However, it was suggested that a more sophisticated regulatory network might be required to ensure the efficient use of resources and avoid futile cycles (Sauer and Eikmanns, 2005).

1.1.3 $\text{CO}_2/\text{HCO}_3^-$ induced regulatory response and phenotypes

It appears plausible to hypothesise, that players of the PEP-pyruvate-oxaloacetate node are regulated in response to the $\text{CO}_2/\text{HCO}_3^-$ availability in addition to the regulation by the carbon source for growth. However, little is known about the $\text{CO}_2/\text{HCO}_3^-$ induced regulatory response in microorganisms and discrimination of the entangled effects, that are caused by $\text{CO}_2/\text{HCO}_3^-$, pH and osmolarity is particularly intricate (Cummins et al., 2014). Studies reporting on regulatory responses and phenotypes, that were provoked by the variation of $\text{CO}_2/\text{HCO}_3^-$ levels were reviewed by Lopes et al. (2014), Blombach and Takors (2015), Cummins et al. (2014), and Yu and Chen (2019) with the focus on biotechnological hosts, human pathogens or environmental microbes.

High CO_2 contents are often associated with growth inhibition in literature. However, a uniform picture of the CO_2 impact on microbial growth performance cannot be provided as even for the same organism publications might be inconsistent (Isenschmid et al., 1995). The effect of different CO_2 levels depends on the substrate and its metabolism (Bäumchen et al., 2007), as also reflected in the carbon flux at the PEP-pyruvate-oxaloacetate node, that is controlled differently with regard to the substrate (Sauer and Eikmanns, 2005). Variation of the total pressure but also differences of the experimental set-up might sometimes have an unexpectedly high impact on the experimental outcome. Undoubtedly, a high partial pressure of CO_2 ($p\text{CO}_2$) exerts antimicrobial activity and is therefore an established sterilisation technique e.g. during the preparation of food and pharmaceutical products. When stationary phase yeast cells of *Kluyveromyces fragilis*,

Saccharomyces cerevisiae and *Candida utilis* were subjected up to 100 bar pCO₂, the cell viability was reduced and described a sigmoidal curve shape with increasing pCO₂. However, up to pCO₂ = 20 bar, cell viability was hardly affected (< 10 % loss) regardless of the strain (Isenschmid et al., 1995). The reason for the antimicrobial effect of elevated pCO₂ is presumably the “anaesthesia effect”, which describes the disruption of the cell membrane integrity as a consequence of CO₂ penetrating the membrane, increasing its fluidity and permeability. Alternative explanations of the antimicrobial effect exist and emphasise (i) the pH gradient and (ii) enzymatic activities. (i) High CO₂ concentrations diffuse into the cell cytoplasm, acidify this as a consequence of dissociation equilibria, by that causing the collapse of pH gradient and proton motif force. (ii) Catabolic pathway activity could be abolished at high CO₂ content as the result of product inhibition of decarboxylating enzymes (Jones and Greenfield, 1982).

The effect of increasing pCO₂ on *E. coli* strains was investigated in a more moderate range (up to 300 mbar) in two independent studies (Castan et al., 2002; Baez et al., 2009). Whereas growth rates were found to decrease with increasing pCO₂ in 1 - 15 L bioreactor cultivations operating at ambient total pressure, the biomass per substrate yield $Y_{X/S}$ was enhanced. The improved $Y_{X/S}$ was attributed to the increased CO₂ fixation via the anaplerotic pathways. In another study, cultivations of the industrially applied bacterial systems *E. coli*, *C. glutamicum*, *S. cerevisiae* and *Arxula adenivorans*, were carried out in pressurised bioreactors that were operated in fed-batch mode and established growth rates below μ_{\max} (Knoll et al., 2007). In contrast to the previous two studies, neither growth rate nor $Y_{X/S}$ was affected by a high pCO₂ in comparison to the cultivation under non-pressurised conditions. Particularly on the basis of identical $Y_{X/S}$ (0.5 and 0.42 g cell dry weight per g glucose for *E. coli* and *C. glutamicum*, respectively) the authors argue, that in the given set-up, high pCO₂ did not cause energy demanding compensation of a negative effect. Further studies on the performance of *C. glutamicum* were performed by Bäumchen et al. (2007) and Blombach et al. (2013) and are outlined in more detail later (1.2.1). For comparison with the previous study, it should be anticipated here, that consistently, the growth rate was not affected by pCO₂ up to

300 mbar. However, Blombach et al. (2013) reported, that the $Y_{X/S}$ was increased by 63 % during the initial growth phase at elevated $p\text{CO}_2$ (this parameter was not reported by Bäumchen et al. (2007)).

Among different organisms, the group of capnophilic bacteria is particularly interesting as they do not grow at all unless surrounding CO_2 concentrations are sufficiently high. It was hypothesised, that the carbonic anhydrase function might be critical for these strains and decisive, whether they can grow or not at ambient $p\text{CO}_2$, because the $\text{CO}_2 - \text{HCO}_3^-$ interconversion is the critical step providing substrate for the PEP carboxylase (Ueda et al., 2008). In the well studied pathogenic capnophiles *Neisseria spp.* carbonic anhydrase as well as PEP carboxylase are responsible for CO_2 assimilation, whereas they lack other carboxylating enzymes (pyruvate carboxylase, PEP carboxykinase and PEP carboxytransphosphorylase). Since the HCO_3^- affinity of the PEP carboxylase is particularly low, this enzyme is probably not the reason for the high CO_2 demand of the organism (Hughes et al., 1995).

A concerted transcriptional response of *C. glutamicum* to elevated $p\text{CO}_2$ (1.2.1) was recently reported to involve the DtxR regulon (Blombach et al., 2013). The dual transcriptional regulator is the master regulator of iron homeostasis in *C. glutamicum*, but was named after its role in controlling toxin gene expression its pathogenic relative *Corynebacterium diphtheriae* (Wennerhold and Bott, 2006). In other pathogenic bacteria like *Bacillus anthracis*, *Vibrio cholerae*, *Pseudomonas aeruginosa* or *Citrobacter rodentium* the expression of toxin genes is increased at elevated concentrations of bicarbonate (Mekalanos, 1992; Cummins et al., 2014; Yang et al., 2008). $\text{CO}_2/\text{HCO}_3^-$ concentrations are about 100 times higher inside their respective hosts than outside – reaching typical bicarbonate concentrations of up to 140 mM in certain tissues (Blombach and Takors, 2015). In this regard $\text{CO}_2/\text{HCO}_3^-$ appears to be a suitable signal for the pathogen that must recognise its host environment and regulate toxins, colonisation and adherence factors accordingly (Cummins et al., 2014). RegA was identified as a key component in the mouse enteric pathogen *C. rodentium* modulating gene expression in

response to elevated CO₂ availability and a model of HCO₃⁻ binding to the N-terminal arm of RegA was proposed. The response of selected genes under control of RegA was analysed *in vivo* using fusion products with β -galactosidase and suggested a function as an anti-repressor and a release of self-repression in the presence of HCO₃⁻ (Yang et al., 2009). DNA binding of RegA was enhanced in the presence of 40 mM NaHCO₃ in 10 mM Tris-HCl buffered EMSA experiments during a preceding study (Yang et al., 2008). The authors state, that most AraC/XylS type virulence activators, to which RegA belongs, are stimulated by pH, osmolarity and temperature, but chemical effectors are not known. Nonetheless, a potential shift of pH in their experiments was unfortunately not discussed (Yang et al., 2008). However, such a shift of the pH must be expected as the addition of 36 mM NaHCO₃ to 10 mM Tris acetate buffer increased the pH from 7.4 to 8.6 in a different study (Thomson and Withey, 2014). The latter authors observed a doubling of the DNA affinity of the virulence regulator ToxT from *V. cholerae* in the presence of bicarbonate when EMSA experiments were run in parallel, although overall dissociation constants of identical experiments vary by almost a magnitude. Hence, despite various reports on the CO₂/HCO₃⁻ induced virulence of pathogenic bacteria, a conclusive mechanism for the activation cannot be provided.

1.2 *Corynebacterium glutamicum*

Corynebacterium glutamicum is a Gram-positive actinobacterium, that was originally isolated from soil samples and named *Micrococcus glutamicus* after its capacity to secrete large amounts of glutamic acid under biotin-limited growth conditions (Kinoshita et al., 1957; Eggeling and Bott, 2005). Cells typically display a rod-shaped morphology (sometimes described as “coryneform” from the Greek) and become visible in pairs under the microscope, that stick together in a “V”-formation after cell division (Liebl, 2005). *C. glutamicum* strains exhibit a moderately high GC-content (53.8 - 54.1 %) as summarised by Tauch (2008) and the entire genomic sequence of the wildtype (WT) strain ATCC 13032 used in this study as well as an other commonly employed strain (e.g. *C. glutamicum* R) was determined. More than 80 % of the 3,058¹ genes of strain ATCC 13032 putatively encoding proteins were annotated by homology (Kalinowski et al., 2003; Ikeda and Nakagawa, 2003). Information about the genomic organisation paired with a set of molecular biological tools makes this microorganism easily accessible for targeted genetic manipulation (reviewed e.g. in Kirchner and Tauch (2003)). *C. glutamicum* is generally regarded as safe (GRAS certified) and, thus, qualifies for the production of food and feed applications, particularly of amino acids. In this context, L-lysine and L-glutamate are produced at industrial scale, reaching a market volume of 2.6 and 3.2 million annual tons, respectively (Wendisch, 2019). Besides classical strain development approaches by continuous mutation and selection, *C. glutamicum* has been tailored for the biosynthesis of a wide range of natural and non-natural products comprising D- and L-amino acids, alcohols and organic acids, but also diamines or carotenoids (reviewed e.g. by Becker and Wittmann (2012), Heider and Wendisch (2015), and Wendisch (2019)).

¹https://coryneregnet.compbio.sdu.dk/v6e/CoryneRegNet/queryElement.php?organismID=NC_006958, accessed: 17/02/2019

1.2.1 Metabolism

C. glutamicum grows aerobically on a number of industrially relevant carbohydrates, organic acids and alcohols and co-metabolises several combinations without exhibiting diauxic growth. Examples and exceptions of the parallel consumption are nicely reviewed by Arndt and Eikmanns (2008). *C. glutamicum* possesses a facultatively anaerobic lifestyle. In the absence of oxygen it can use nitrate as alternative terminal electron acceptor for the oxidation of reduction equivalents catalysed by the NarKGHJI complex (Nishimura et al., 2007). However, biomass generation during nitrate respiration is limited, due to the accumulation of the toxic product nitrite in a closed system. Vassilev et al. (2018) demonstrated, that oxygen and nitrate were not the only electron acceptors, that could be utilised by *C. glutamicum*, since biomass generation was also observed in an anodic electro-fermentation approach operated under anaerobic conditions. In this experimental set-up, the lysine producer strain *C. glutamicum lysC* transferred electrons onto a ferricyanide mediator, that was constantly reoxidised by the anodic current.

Reduction equivalents cannot be reoxidised in the absence of a terminal electron acceptor, which causes an intracellular ATP limitation. It was shown recently, that this can be compensated by the addition of complex compounds like tryptone. When substantial amounts of tryptone or amino acids, that would otherwise require ATP-intensive biosynthesis, were provided alongside with the sugars glucose, fructose, sucrose or ribose as the major C-source, biomass was generated under oxygen deprivation conditions (and in the absence of nitrate) (Michel et al., 2015).

If terminal or intermediate electron acceptors or complex compounds are not provided, *C. glutamicum* converts glucose mainly to succinate, lactate and acetate via mixed acid fermentation without exhibiting substantial growth (Dominguez et al., 1993; Inui et al., 2004). This feature was exploited with engineered strains for several products of high reductive degree, i.e. succinate, isobutanol and L-valine, which benefit from both, improved supply of reducing equivalents and high conversion yields that can be obtained due to the lack of biomass formation (Okino et al., 2008; Blombach et al., 2011; Hasegawa

et al., 2013).

As outlined before (1.1.2), *C. glutamicum* metabolism is outstanding with regard to its enzymatic equipment at the PEP-pyruvate-oxaloacetate node. Unlike many other bacteria, *C. glutamicum* possesses both carboxylating enzymes, the PEP carboxylase and pyruvate carboxylase, and all three (mainly) decarboxylating enzymes, the PEP carboxykinase, oxaloacetate decarboxylase and malic enzyme (Eikmanns, 2005). It is interesting to note, that in *C. glutamicum* lacking a transhydrogenase, the role of an energy-demanding transhydrogenase might be functionally reconstituted by the action of pyruvate carboxylase, malate dehydrogenase and malic enzyme. Whilst pyruvate and HCO_3^- is recycled in this system (thus acting as a catalyst) one molecule of NADH is oxidised and yields one molecule of reduced NADPH (Blombach et al., 2011). The capacity to refuel oxaloacetate of the TCA cycle might be one inherent characteristic of *C. glutamicum* that contributes to the great production of pyruvate and TCA cycle derived amino acids. In contrast to *C. glutamicum*, *E. coli* features only the PEP carboxylase to replenish oxaloacetate (Sauer and Eikmanns, 2005). A comparison of the bicarbonate affinities is inconclusive as values differ e.g. between 0.63 and 2.8 mM for *C. glutamicum* PEP carboxylase or between 0.1 and 1.75 mM for the *E. coli* homologue and results might be heavily influenced by the assay conditions (Mori and Shiio, 1985; Chen et al., 2013; Smith, 1968; Yano et al., 1995; Kai et al., 1999). Particularly, the *pyc* gene encoding the pyruvate carboxylase was proven as an important target for strain engineering aiming at increased glutamate and lysine production (Peters-Wendisch et al., 2001).

Besides strain engineering approaches, the anaplerotic reactions can be enhanced by increasing the substrate availability of HCO_3^- and several studies addressed the impact of elevated pCO_2 during anaerobic production and aerobic growth of *C. glutamicum*. It was reported, that the initial bicarbonate concentration was critical during the production of succinate in order to fuel the reductive arm of the TCA cycle via anaplerotic reactions (Inui et al., 2004; Okino et al., 2008). In fact, the final succinate titer could be increased by the factor of three, when an oxygen deprived *C. glutamicum* cultivation using glucose as substrate was aerated with 100 % CO_2 (Radoš et al., 2014). Metabolic

flux analysis using ^{13}C -labelled CO_2 revealed, that in this case 97 % of succinate was produced via the reductive arm of the TCA cycle (fixing HCO_3^-), whereas only 3 % was produced following the oxidative arm. Michel et al. (2015) reported, that the growth rate and final biomass concentration of *C. glutamicum* was enhanced by increasing the CO_2 availability in an anaerobic bioreactor cultivation on glucose and tryptone. The authors argue, that this was not due to the increased carbon flux via the anaplerotic reactions, but that acetyl-CoA carboxylation and, thus, the biosynthesis of fatty and mycolic acids was enhanced. A positive impact of elevated CO_2 levels on the growth rate of *C. glutamicum* under aerobic conditions has not been postulated to date. Studies by Knoll et al. (2007), Bäumchen et al. (2007), and Blombach et al. (2013) investigated the impact of varying CO_2 levels on aerobic growth of *C. glutamicum* systematically and were briefly introduced above (1.1.3). In bioreactor cultivations in fed-batch mode *C. glutamicum* DSM 1730 growth on glucose was not affected by the pCO_2 up to 600 mbar with regard to the growth rate and biomass yield per substrate ($\mu = 0.16 \text{ h}^{-1}$, $Y_{\text{X/S}} = 0.42 \text{ gCDW gGlc}^{-1}$). The authors conclude, that there was no energy-demanding stress response induced by the exposure to high pCO_2 in their study (Knoll et al., 2007). The growth rate of *C. glutamicum* ATCC 13032 was essentially higher during the bioreactor cultivation in a different study ($\mu = 0.58 \text{ h}^{-1}$) and hardly affected at pCO_2 up to 260 mbar (Bäumchen et al., 2007). When the pCO_2 was further increased to 790 mbar, the growth rate declined to 0.37 h^{-1} . Finally, Blombach et al. (2013) analysed the phenotypic and transcriptional response of *C. glutamicum* ATCC 13032 to high as well as low CO_2 availability during bioreactor cultivations. In contrast to the standard conditions (aeration with pressurised air at 0.5 vvm), high pCO_2 was achieved by the aeration with 20 % CO_2 enriched air. The low pCO_2 was established by increasing the inlet air flow to 3 vvm, by this stripping excessive amounts of dissolved CO_2 . The exponential growth rate of $0.40 - 0.41 \text{ h}^{-1}$ was in accordance with the maximum growth rate of *C. glutamicum* ATCC 13032 for the given conditions (Grünberger et al., 2013) and not affected by the increased pCO_2 . Although the biomass-specific substrate uptake rate q_s remained unaltered, $Y_{\text{X/S}}$ was increased by 63 % during the initial phase at high pCO_2

(Blombach et al., 2013). The reason for this was presumably the increased flux in carboxylation reactions, particularly of the anaplerotic reactions. A growth defect became apparent at low pCO₂ and resulted in triphasic growth with a reduced rate of 0.19 h⁻¹ and concomitantly lower Y_{X/S} between 5 and 10 h of the cultivation. Interesting insights in the CO₂ induced regulatory response were moreover provided by the transcriptional analysis. At low pCO₂, *C. glutamicum* WT induced the expression of almost all genes contributing to the biosynthesis of thiamin pyrophosphate (TPP). The authors speculate, that by the biosynthesis of TPP, which is frequently found as enzyme cofactor of decarboxylation reactions, the lack of CO₂ in the environment might be compensated. Although there was no difference of the growth rate induced by the high pCO₂, the transcriptional response comprised the activation of the entire DtxR controlled regulon, indicating an involvement of the iron homeostasis (as described in 1.3.5.5). With regard to the PEP-pyruvate-oxaloacetate node, the transcription of *cg3335* encoding the malic enzyme in *C. glutamicum* (Klaffl and Eikmanns, 2010) was 3.32-fold upregulated at high pCO₂ and the transcription of *cg3169* encoding the PEP carboxykinase was 2.31-fold upregulated under low pCO₂. However, a joint regulatory circuit orchestrating the PEP-pyruvate-oxaloacetate node in response to the CO₂ availability could not be identified. One particular objective of this follow-up study was, therefore, to highlight the regulatory link between CO₂ availability and iron homeostasis.

It might be worth noting furthermore, that beyond biotechnological interest, *C. glutamicum* might serve as model organism for its pathogenic relatives *C. diphtheriae* and *Mycobacterium tuberculosis* (Burkovski, 2003).

1.3 Iron homeostasis

Iron is the fourth most abundant element in the earth's crust and of utmost importance for almost all kind of life. In fact, only a few bacterial examples exist, that grow entirely independent of iron. As such, a few members of the genus *Lactobacillus* were initially shown to be independent of iron and heme compounds as cofactors of key metabolic enzymes. These were apparently replaced by cobalt based vitamin B12, for instance, as reviewed by Neilands (1981).

Since the transition metal iron serves a wide range of redox potential from -500 to 300 mV (Proulx-Curry and Chasteen, 1995) as it switches from the ferrous iron (Fe^{2+}) to the ferric iron form (Fe^{3+}), it represents a well suited prosthetic group implemented in a number of inevitable redox reactions enabling heterotrophic (e.g. respiration, TCA cycle) as well as autotrophic life (e.g. photosynthesis). Several enzymes rely on iron as cofactor that participate in detoxification systems (catalase, peroxidase), N_2 assimilation or energy conservation processes (H_2 production/consumption)(Andrews et al., 2003). Iron is incorporated in these enzymes mainly as heme or iron sulfur cluster carrying a central ferrous iron atom (Fe^{2+}), which is the biologically accessible form of iron.

However, the availability of soluble Fe^{2+} (solubility = 0.1 M at pH 7.0) is limited in an oxidative environment under physiological conditions. As a consequence of corrosive reactions – especially the reaction of Fe^{2+} with oxygen – poorly soluble Fe^{3+} represents the predominant form (solubility = 10^{-18} M at pH 7.0), that exists in precipitates of various complexes formed with hydroxides, oxides but also phosphates or sulfates (Andrews et al., 2003; Schröder et al., 2003). The iron precipitates are *per se* inaccessible for bacterial life. Therefore, numerous strategies evolved in nature to counteract an iron limitation by increasing the iron solubility, e.g. through iron chelation and chemical reduction of ferric iron (Andrews et al., 2003).

In order to be equipped for times of extracellular iron shortage, cells can take up great quantities of iron, when excessive amounts are found in the environment. It is important at the same time to minimise the intracellular amount of free Fe^{2+} , as it does not only

represent the biologically active form of iron, but undergoes the Fenton reaction in the presence of oxidative stress molecules, i.e. hydrogen peroxide. The reaction products of the Fenton reaction (reactive oxygen species) exhibit a toxic effect on the cell as they damage DNA and proteins. A temporal surplus of iron is therefore stored in specialised iron storage proteins in the biologically inert Fe^{3+} form (Proulx-Curry and Chasteen, 1995). The players of iron homeostasis are generally not limited to prokaryotic life. However, due to the scope of this work, the aspects of iron homeostasis described here focus mainly on bacterial cells.

1.3.1 Iron transport

To cope with an iron restriction, a number of high-affinity iron uptake systems evolved that are specific for the transport of either ferrous iron or chelates of ferric iron. Selected transport systems and key characteristics are briefly introduced in the following. However, besides high-affinity iron transport systems the presence of low-affinity iron uptake must be considered. Evidence for the existence of the latter arises from the fact that iron concentrations above $10 \mu\text{M}$ sufficed for growth of several bacterial systems without high-affinity iron transport – although this not at maximum rates (Neilands, 1981; Andrews et al., 2003). The transport mechanism is poorly studied and, thus, it is not clear, whether this might be energy independent or even abiotic or proceed via promiscuity of other metal transport proteins.

High-affinity ferrous iron (Fe^{2+}) specific transport systems (Feo) are present in many bacteria. First discovered and, thus, eponymous for others was FeoAB in *E. coli*. It consists of a membrane bound protein (FeoB) that appears essential for iron uptake and a small 75 amino acid protein (FeoA) of unclear function, that is not present in all homologous Feo systems. Some debate persists about the energy-dependence of iron transport, since early studies reported on an ATPase function of the FeoB protein, that was later identified as GTPase function (Andrews et al., 2003; Lau et al., 2015) and rather involved in G-protein coupled intracellular signal transduction than energising

the iron transport itself.

By evidence, iron transport via the Feo system is essential in an anaerobic environment, in which Fe^{2+} represents the predominant iron species (Andrews et al., 2003; Lau et al., 2015). Since in an aerobic environment, Fe^{2+} tends to be oxidised to the poorly soluble Fe^{3+} at physiological pH, cells face the challenge of solubilising the iron to make it accessible for uptake. One global strategy to achieve the solubilisation of iron that is employed by many different types of organisms including bacteria, fungi and even plants, is the production of low molecular weight iron chelators. This heterogeneous group of molecules is termed siderophores (from greek for “iron carrier”) due to their extremely high binding affinity for Fe^{3+} with dissociation constants K_D up to 10^{-49} M (for enterobactin produced e.g. by *E. coli*; $K_D=10^{-35}$ M at physiological pH) (Lin et al., 2005; Harris et al., 1979). Siderophores are typically classified in accordance with their iron coordination moieties as (i) catecholate-, (ii) hydroxamate- or (iii) carboxylate-type (i.e. α -hydroxy-carboxylate). The term siderophore typically refers to molecules that combine several (usually three) identical or different (mixed-type) moieties in the same molecule, thus, providing a hexadentate ligand for octahedral coordination of the central Fe^{3+} . The octahedral coordination can also be achieved by smaller molecules providing a bidentate ligand each (e.g. catechol), and coordinate with a central Fe^{3+} atom at pH dependent stoichiometries. However, the latter display much lower K_D values and are typically considered as ferric iron chelates rather than ferri-siderophores.

The secretion of phenolic substances – and particularly catecholate compounds – in iron restricted growth media had been reported for a number of organisms. The precursor of catecholate siderophores, 2,3-dihydroxybenzoic acid (2,3-DHB), and derivatives of it had been identified in supernatants of *Bacillus subtilis* and *Paracoccus* (by then *Micrococcus*) *denitrificans* (Peters and Warren, 1968a; Tait, 1975) as reviewed by Neilands (1981). 2,3-DHB and derivatives are apparently involved in iron uptake, since mutants that do not produce these compounds were found to transport less iron and iron uptake could be enhanced by supplementation (Peters and Warren, 1968b). Protocatechuic acid (PCA, 3,4-dihydroxybenzoic acid) is structurally closely related with 2,3-DHB, but

less frequently used as the precursor of siderophores than the latter. Nonetheless, PCA represents the basic compound of the rare siderophore petrobactin (anthrachelin), that is produced by *Bacillus anthracis* and *Bacillus cereus* and might also be secreted itself in great amounts by both strains in response to iron limited cultivation conditions (Barbeau et al., 2001; Garner et al., 2004). The reason for enhanced iron uptake is generally assumed to be associated with the iron chelating function of catecholate compounds (Ratledge and Chaudhry, 1971). However, evidence has not been provided, that the ferric chelates are indeed taken up as a complex (Garner et al., 2004).

Interestingly, catecholate compounds bear the potential to reduce Fe^{3+} chemically (Peron and Brumaghim, 2009). Although this process is considered to be inhibited at physiological pH values, several links to the physiological relevance exist. The general reaction principle and constraints will be introduced later (1.3.3 Iron mobilisation and reduction).

In turn, the translocation of ferri-siderophores is well described and excellently reviewed by Andrews et al. (2003). In Gram-negative bacteria, iron-siderophore complexes bind to the outer membrane receptor and are translocated into the periplasm in a process that is energised by the ExbB-ExbD-TonB complex. A specialised periplasmic binding protein then guides the iron complex to the respective ABC permease for energy demanding transport across the cytoplasmic membrane. Since Gram-positive bacteria lack the outer membrane, iron-siderophore complexes are captured by membrane anchored binding proteins, that direct them to the dedicated ABC permease for uptake. It is believed that the iron-siderophore complex dissociates in the cytoplasm as a consequence of iron reduction. Potential mechanisms for the reduction are introduced below (1.3.3).

1.3.2 Iron storage

Once inside the cell, iron can be deposited in specialised storage proteins, if it is not incorporated in enzymes straight away. The three types of bacterial iron storage proteins,

namely ferritin, bacterioferritin and Dps - although only distantly related - share common features. A large spherical protein (500 kDa in case of (bacterio-)ferritin, 250 kDa in case of Dps) is formed by the assembly of 24 or, respectively, 12 identical subunits. The central cavity of the protein complex buries up to 4500 iron atoms within (bacterio-)ferritin and up to 500 iron atoms in the smaller Dps protein. Fe^{2+} enters the core through the ferroxidase centre, that forms part of each subunit. There it is oxidised at the expense of molecular oxygen (bacterioferritin and ferritin) or hydrogen peroxide (Dps) yielding poorly soluble Fe^{3+} , that is deposited as ferrihydrite or amorphous iron phosphate inside the protein. In fact, the oxidant of the ferroxidase reaction might give an insight into the functional diversity of the iron storage proteins. It was concluded, that the primary function of the Dps protein is related to the oxidative stress response rather than iron storage, as it favours H_2O_2 over O_2 as the electron acceptor. Thus, the protein was named “DNA protection during starvation protein” (Dps). The expression of respective genes encoding iron storage proteins are induced during stationary phase highlighting their importance of depositing iron during non-exponential growth (Andrews et al., 2003; Proulx-Curry and Chasteen, 1995).

1.3.3 Iron mobilisation and reduction

Iron, that was deposited in storage proteins during iron excess conditions, can be remobilised in times of external iron shortage and must be reduced to Fe^{2+} . However, in contrast to iron storage, much less is known about this process mechanistically. Four potential mechanisms for the release of ferritin iron were reviewed by Carmona et al. (2013) and classified as (i) driven by the chemical equilibrium, (ii) ferritin capsid degradation, (iii) Fe^{3+} release through chelating agents and (iv) Fe^{3+} reduction mediated by small biomolecules and subsequent chelation. Experimental evidence supported the fourth strategy, as ferritin iron was prone to reductive mobilisation in the presence of electron donors such as dithionite, dihydroriboflavin 5'-phosphate or thioglycolic acid in different studies (Sirivech et al., 1974; Funk et al., 1985).

An analogous role in the reductive iron mobilisation was also attributed to catecholate

(or diphenol) compounds including PCA (Boyer et al., 1988). These compounds had been introduced before (1.3.1) when focusing on the capability to chelate iron to make it better accessible. In accordance with this mechanistic understanding Crichton et al. (1980) reported, that ferritin iron was released by 2,3-DHB due to high affinity iron chelation. However, as anticipated above, diphenols and catecholate compounds have a second role as they can be oxidised in the presence of Fe^{3+} . By this, one electron is transferred to the iron atom, yielding reduced Fe^{2+} in turn. The reaction mechanism has been proposed for a number of structurally related substances including PCA (Avdeef et al., 1978; Kennedy and Powell, 1985) and was reviewed e.g. by Perron and Brumaghim (2009). A systematic overview of the aromatic compound nomenclature is provided in the appendix fig. S1 on page 161 including most substances used in this study.

Redox reactions within the iron-catecholate complex are restricted to acidic pH values, that favor an 1:1 stoichiometry between iron and catecholate. The reaction is inhibited, when at least the biscatecholate complex forms (Perron and Brumaghim, 2009; Avdeef et al., 1978). At pH values up to 4.5, PCA chelates iron predominantly in an 1:1 fashion (Kennedy and Powell, 1985), whereas a mix of 3:1 and 2:1 stoichiometric complexes (catecholate:iron) inhibits the iron reduction at physiological pH values (Perron and Brumaghim, 2009).

During the reduction of Fe^{3+} , two adjacent hydroxyl groups of the redox partner (diphenol or catecholate) are oxidised sequentially to the respective semiquinone and quinone form, respectively. The reaction yields two Fe^{2+} atoms by the full oxidation of one catechol molecule to the quinone (Perron and Brumaghim, 2009).

The reaction mechanism is not limited to ferritin iron, but free Fe^{3+} is reduced. However, due to pH range that is required for the reduction of iron, this reaction must be considered as physiologically irrelevant.

In the context of iron mobilisation from storage proteins, but also beyond this, the role of specialised ferric reductases is frequently discussed, considering the predominance of Fe^{3+} in the presence of oxygen. Its reduction seems to be a key element for all aer-

obic life in order to obtain biologically active Fe^{2+} . A lot of work has been spent to understand ferric reduction and was nicely reviewed by Schröder et al. (2003). Interestingly, most designated ferric reductases turned out to be flavin reductases in fact. The reduced flavins then acted as electron donor for Fe^{3+} in a subsequent non-enzymatic reaction. It was demonstrated recently in *Listeria monocytogenes*, that flavins can even be responsible for the reduction outside the cell. Protein-bound flavin was regenerated by extracellular electron transport machinery and acted as an extracellular electron mediator (Light et al., 2018).

Ferritin iron mobilisation following enzymatic iron reduction was solely described for bacterioferritin: The Bfr associated ferredoxin (Bfd) shares structural similarity with the ferrichrome reductase (FhuF) and appears to mediate the iron release from bacterioferritin under iron restricted conditions (Andrews et al., 2003). FhuF in turn catalyses the intracellular reduction of ferrichrome. It could be presumed, that iron mobilisation from bacterial ferritins and Dps proteins proceeds in a similar fashion. However, no studies have been published on that until recently. It could be demonstrated, that in *C. glutamicum* iron release from ferritin and Dps proteins was independent of ferric iron reduction. Instead, release of Fe^{3+} from ferritin and Dps was the result of pupylation mediated unfolding of the storage proteins (Küberl et al., 2016). Future studies are necessary to find out whether this mechanism is of wider importance for other organism and how ferric iron is reduced in *C. glutamicum*.

Studying the reduction of ferritin iron turns out to be particularly cumbersome and is therefore poorly understood. Considering the importance of iron reduction to enable growth, it is somewhat surprising that the reduction of free iron has not been determined to much greater extend. It cannot be stated with certainty, how nor where iron reduction typically takes place and there seem to be great variation between different organisms. The reduction step can be prior to iron transport, occur in a transport coupled fashion or happen intracellularly (Andrews et al., 2003; Schröder et al., 2003).

The reduction of Fe^{3+} from iron siderophores seems to exhibit mechanistic differences

that depend on the functional groups of the siderophore. I.e. reduction of ferric enterobactin is accompanied by an esterase catalysed cleavage of the siderophore, whereas hydroxamate based siderophores are thought to be recycled (Emery, 1971; O'Brien et al., 1971; Cooper et al., 1978).

The encapsulated yeast *Cryptococcus neoformans* reduces ferric iron prior uptake. Whilst the reduction by ferric reductases was dominant during exponential growth, iron reduction was mediated by secreted reductants during stationary phase. 3-Hydroxyanthranillic acid was identified as the major component responsible for the reducing capacity of the culture supernatants. However, the authors presume that there might be a contribution of additional unknown reductants (Nyhus et al., 1997). Further publications on the existence of extracellular ferric reductases have also been reviewed by (Andrews et al., 2003). The requirements for such a mode of extracellular iron reduction leave some space for discussion, considering the efficient export of reduction equivalents (NADH and NADPH), transport to the enzyme and reimport into the cell.

In contrast to most other players of the iron homeostasis, the expression of genes encoding ferric reductases (or better: flavin reductase expression) seems to be constitutive (Schröder et al., 2003), which might – again – support a rather secondary role of the reductases in iron metabolism. An exception from this is bespoke Bfd protein, that was found to be induced during iron starvation.

1.3.4 Regulation of iron homeostasis

The many players of iron homeostasis involved in transport, storage, reduction and utilisation require a regulatory circuit that orchestrates the different functions accordingly. The most prominent example of a transcriptional regulator of iron homeostasis is the ferric uptake regulator (Fur) protein present in *E. coli* and many other bacteria. The apo-protein is activated by Fe^{2+} inducing homodimerisation and thus DNA binding of the active repressor to a designated Fur box, that is located between -35 and -10 element of the respective promoter. The Fur controlled regulon is particularly large, i.e. it contains more than 90 genes in *E. coli*. In *Pseudomonas aeruginosa* 205 genes appear

to be regulated in response to iron – many of them are likely to be Fur dependent. At high Fe^{2+} availability Fur mediates the repression of genes encoding iron uptake systems and siderophore biosynthesis. On the other hand, the expression of genes encoding iron requiring enzymes and iron storage proteins were found to be upregulated under the same conditions (e.g. *acn*, *ftn* etc.). Lacking a Fur box upstream of these genes it was suggested, that they were only indirectly regulated by Fur.

The activation of these genes is mediated by the small non-coding RNA termed RhyB, which represses their expression under iron starvation. At iron excess, expression of the corresponding *rhyB* gene itself was repressed by active Fur protein and RhyB controlled genes are, thus, upregulated. Consequently, Fur induced genes were not upregulated upon *rhyB* inactivation (Andrews et al., 2003; Massé and Gottesman, 2002). Fur in conjunction with RhyB are the two major players in regulating the iron homeostasis in *E. coli* and many other bacteria.

A mutation of the *fur* gene in *E. coli* resulted in reduced iron contents by about 70 % (Andrews et al., 2003). This observation might be surprising at the first glance, considering that such mutants lack the ability to repress the expression of genes encoding iron transport systems. It highlights the presence of additional regulatory circuits that minimise the iron uptake when Fur is absent. The protein complex consisting of FecA, FecI and FecR sense the presence of ferric citrate (FecA) to induce the expression of the *fecABCDE* operon encoding a ferric citrate transport complex unless Fur represses its expression (at high Fe^{2+} availability). FecI belonging to the family of “iron starvation sigmas” provides an additional level of iron regulation besides the master regulator Fur. In mammals, the iron regulatory proteins (IRP1 and 2) possess a dual role. At iron sufficiency, IRP1 exhibits cytosolic aconitase function. The aconitase loses its iron-sulfur cluster under iron-starvation conditions and thereby its aconitase function. In this state it recognises mRNA instead and binds to the “iron regulatory element” (IRE). Depending on the IRE position this can result either in a translation block or mRNA stabilisation. A similar regulatory function of bacterial aconitases appears likely (Andrews et al., 2003).

An exception from the many bacteria possessing a Fur protein as master regulator of iron homeostasis is provided by some Gram-positive bacteria with high GC content (belonging e.g. to the genera *Corynebacteria* or *Mycobacteria*). Iron homeostasis in these bacteria is ultimately controlled by the diphtheria toxin regulator (DtxR) or homologues thereof. Although DtxR is only distantly related with Fur and displays poor sequence similarity with it, the functionality is analogous. DtxR homodimerises upon activation by two Fe^{2+} ions per monomer (instead of only one in Fur) and binds its recognition site on the DNA in a similar fashion. The DtxR protein itself is introduced in more detail below (1.3.5.5).

Pappenheimer and Johnson (1936) had already noted the marked influence of (unintentional) variations of the medium iron content on the production of diphtheria toxin production, which was repressed in *C. diphtheriae* at excessive iron availability. In fact, many examples of bacterial pathogens exist, that sense their host environment through iron availability and regulate their toxin expression accordingly, as reviewed e.g. by Litwin and Calderwood (1993). Just to mention a couple, expression of the shiga toxin in *E. coli* such as the diphtheria toxin in *C. diphtheriae* was controlled by the master regulator of iron homeostasis – Fur and DtxR, respectively (Mekalanos, 1992). The expression of *toxA* encoding exotoxin A in *P. aeruginosa* is not controlled by a transcriptional regulator, that senses Fe^{2+} immediately. However, the presence of the iron controlled transcriptional regulator RegA is vital for full *toxA* expression, as reviewed by Litwin and Calderwood (1993). Hence, production of exotoxin A is iron dependent in *P. aeruginosa* – even if it involves another regulatory element. Special emphasis is put on this observation, since RegA had been introduced above as bicarbonate sensing virulence regulator.

1.3.5 Iron homeostasis in *C. glutamicum*

1.3.5.1 Transport systems Experimental data on the iron transport mechanism in *C. glutamicum* is extremely scarce. Information is primarily gathered from similarities of

the annotated genome sequence with biochemically characterised homologues of other organism (Kalinowski et al., 2003; Frunzke and Bott, 2008). Fig. (2) provides an overview of the current understanding of iron homeostasis in *C. glutamicum* focusing only on elements, that were regarded as important for this project.

In the genomic sequence of *C. glutamicum* strain ATCC 13032 no genes could be identified so far, that constitute the biosynthetic pathways of siderophores (Wennerhold and Bott, 2006). It might be a surprise at the first glance, that despite lacking the capability of producing siderophores ATCC 13032 is well equipped regarding transport systems for iron siderophores. A total of 25 different genes encoding components of transport systems was identified in the genome, including five ABC transporters, five cytoplasmatic siderophore interacting proteins and 9 secreted lipoproteins for extracellular binding of different iron siderophore compounds (Frunzke and Bott, 2008). This fact strongly suggests, that in its natural environment *C. glutamicum* exploits secreted siderophores of other organisms for iron uptake (known as siderophore piracy, Traxler et al. (2012)). However, a monoseptical culture in defined salt medium should be free of siderophores and iron must be taken up by a different route.

Siderophore independent transport complexes for ferric iron are not annotated in the genome of *C. glutamicum*. Sequence similarities to the SfuABC of *Serratia marcescens* are found for the gene products of *cg0506-cg0508* but lack experimental validation (Frunzke and Bott, 2008).

Ferrous iron transport is in many bacteria mediated by the high affinity FeoB protein, that is absent in *C. glutamicum* (Frunzke and Bott, 2008). Matches for FeoB homologues (from *E. coli*) in a protein BLAST search (9 May 2019) could be attributed to the GTP binding domain of the protein (roughly 20 % sequence coverage). The gene products of *cg0041*, *cg0042* and *cg0043* reveal sequence similarity to the *sitABCD* encoded divalent metal transport systems from *Enterobacteriaceae* (Frunzke and Bott, 2008). Further homologues of the secreted substrate binding lipoprotein (putatively encoded by *cg0041*) could be identified e.g. in the MtsA protein of *Streptococcus pyogenes* responsible for binding Fe^{2+} alongside with bicarbonate as the synergistic anion (Sun et al., 2008).

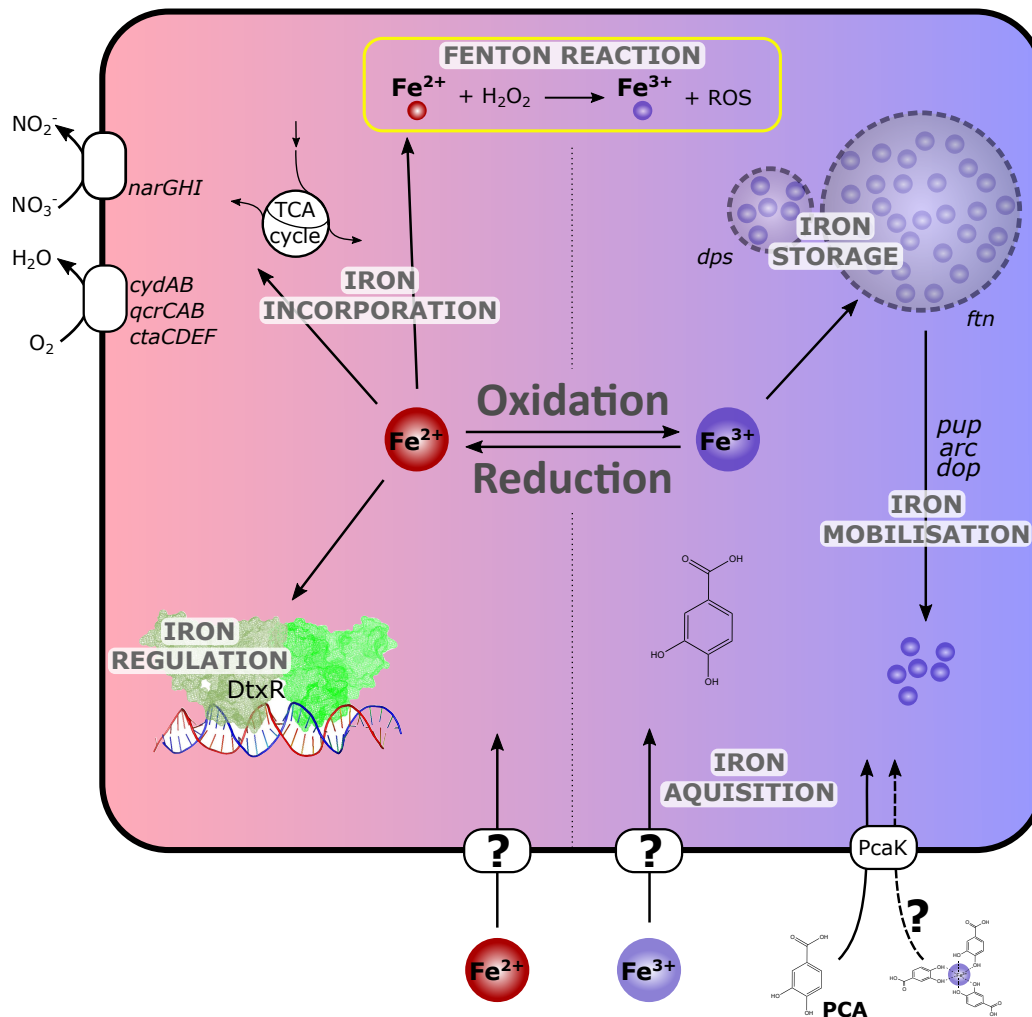


Figure 2: Schematic overview of the iron homeostasis in *C. glutamicum*. Several putative iron transport systems have been annotated in the genome of *C. glutamicum* due to sequence homologies, but were not experimentally validated (Kalinowski et al., 2003; Ikeda and Nakagawa, 2003). When PCA is utilised as carbon and energy source by *C. glutamicum*, the molecule is imported via the *PcaK* transporter (Shen and Liu, 2005). Whether Fe^{3+} -PCA complexes are transported following the same route requires experimental validation. Due to the detrimental effect of the Fenton reaction that Fe^{2+} undergoes in the presence of H_2O_2 , high concentrations are avoided by depositing Fe^{3+} in the storage proteins *Ftn* and *Dps*. The re-mobilisation of iron under starvation conditions is initiated by the pupylation of the storage proteins and subsequent unfolding (Küberl et al., 2016). Liberated Fe^{3+} must be reduced to Fe^{2+} to be incorporated in several enzymes. The master regulator of iron homeostasis *DtxR* senses only the concentration of biologically available Fe^{2+} . Because of simplicity reasons and relevance for this project, hemin uptake and mobilisation (Frunzke et al., 2011) is not included in the overview.

Cg0041 (ZnuA2) of *C. glutamicum* exhibits 28 % sequence identity with MtsA. Protein sequence alignment² against MtsA_{S.p.} confirmed, that the most critical two of the four amino acid residues involved in binding the Fe²⁺ ion (Sun et al., 2009) were conserved, whilst a third residue was mutated Asp281 → Glu (with respect to MtsA_{S.p.} sequence). The fourth and least important residue in iron binding was not conserved (Glu206 → His). The operon composed of *cg0041* and *cg0042* is under control of the zinc uptake regulator, Zur, in *C. glutamicum*. Wennerhold and Bott (2006) identified a DtxR binding site in the intergenic region of *cg0042* and *cg0043*, but DtxR controlled expression could not be manifested in DNA microarrays by the comparison of *C. glutamicum* WT and $\Delta dtxR$ under iron excess and limitation.

Despite the fact that *C. glutamicum* does not contain homologues of the transport systems for ferrichrome (FhuABCD) and ferric citrate (FecABCD), addition of these iron sources enabled growth (Nakayama et al., 1964a; von der Osten et al., 1989). In fact, in media containing 970 mg FeCl₃ · 6 H₂O L⁻¹ as the standard iron source, growth in the absence of casamino acids could be established by the addition of 5 mg ferrichrome L⁻¹, but also by great amounts of FeSO₄ · 7 H₂O (2.5 g L⁻¹) or L-ascorbic acid (1 g L⁻¹). The authors speculated, that it was not the excessive amount of iron salt itself, but rather some kind of chemical interaction with another constituent of the medium that enabled growth (Nakayama et al., 1964a). In a follow-up study, the same group identified chelating agents to be required for growth in defined medium, when glucose was sterilised separately. The authors argued that chelating agents might also be the product of autoclaving glucose together with all other medium ingredients (Nakayama et al., 1964b).

1.3.5.2 Iron chelates Besides undefined chelating agents, citrate supplementation enhanced growth of *C. glutamicum* in a synthetic minimal medium (von der Osten et al., 1989). Liebl et al. (1989) found that the addition of 10 μ M of the catechol or 3,4-dihydroxybenzoic acid (protocatechuic acid, PCA) sufficed to establish growth of

²<https://www.ebi.ac.uk/Tools/msa/clustalo/>; accessed: 05 July 2018

C. glutamicum in BMCG defined medium over a wide range of iron concentrations. Since similar iron chelating phenolic acids had already been identified in supernatants of actinomycetales under iron deprivation conditions, it is the general understanding that PCA enhances iron uptake (Liebl et al., 1989; Frunzke and Bott, 2008). Consequently, PCA became essential component of the CgXII minimal medium, that is utilised for cultivation of *C. glutamicum* in several labs (Keilhauer et al., 1993). It should be noted however, that other labs kept working with CgXII media lacking PCA without noticing growth deficiencies (Eikmanns et al., 1991). In accordance with this, Liebl et al. (1989) observed that cultures in BMCG minimal medium grew well when they were inoculated from a complex preculture, whereas an extended lag phase was observed when the cells were precultured in the same minimal medium or when the inoculum was washed excessively.

It might be undesirable, however, to use PCA in the standard broth, as it provides an additional carbon source that is co-consumed with glucose. PCA is taken up by *C. glutamicum* primarily via the hydroxybenzoate transporter PcaK and metabolised through the β -keto adipate pathway. The aromatic ring is cleaved open in a protocatechuate dioxygenase catalysed reaction (encoded by *pcaGH*) and broken down to one molecule succinyl-CoA and acetyl-CoA, each, that are further metabolised via the TCA cycle (Chaudhry et al., 2007; Merckens et al., 2005; Shen and Liu, 2005; Shen et al., 2012). The growth rate of *C. glutamicum* was essentially higher when protocatechuate was metabolised in parallel with glucose in microscale cultivations ($\mu = 0.61 \text{ h}^{-1}$) than on glucose alone ($\mu = 0.41 \text{ h}^{-1}$). Consequently, the authors suggested that metabolisation of PCA might give an alternative explanation of the growth promoting effect (Unthan et al., 2014).

Due to its inability to grow in the absence of strong chelating agents, it was concluded that *C. glutamicum* was siderophore auxotrophic and incapable of producing such components itself (Liebl et al., 1989). However, it was shown later, that *C. glutamicum* features the genetic basis to synthesise PCA by itself. (Teramoto et al., 2009). Expression of *qsuB* encoding a dihydroshikimate dehydratase, that catalyses the conversion

of 3-dehydroshikimate to protocatechuate, is controlled by the transcriptional activator QsuR in the presence of shikimate or quinate. Chorismate appeared to be an immediate effector molecule of QsuR suggesting that QsuR redirected carbon flux to the central metabolism when key intermediates of the shikimic acid pathway accumulated (Kubota et al., 2014). The native pathway could be exploited for PCA overproduction in a strain that was incapable of degrading it (Kallscheuer and Marienhagen, 2018). It is not clear whether PCA biosynthesis or degradation, respectively, might be regulated in response to the iron availability, but *qsuB* was not differentially transcribed in a $\Delta dtxR$ mutant (Brune et al., 2006; Wennerhold and Bott, 2006).

1.3.5.3 Iron storage and mobilisation Once inside the cell excessive amounts of iron are deposited in the two storage proteins encoded by *ftn* and *dps*, respectively. It was shown recently that iron release from both proteins is mediated by the pupylation machinery (Küberl et al., 2016). This mode of iron release was particularly essential under iron limitation, as a Δpup mutant revealed a stronger growth defect than the WT under this condition. Pupylated storage proteins are unfolded by the action of further constituents of the pupylation machinery and iron is subsequently released. Lacking the proteasome that is responsible for degradation of pupylated proteins in other *Actinobacteria*, Ftn and Dps proteins are apparently not degraded (not even by the action of other proteases). But they seem to be recycled afterwards. Two questions remain unanswered in this context: Given the fact, that the pupylation is vital under iron limitation, is there a regulation in response to the iron availability? So far, expression of *pup* and other components of this machinery was found dependent on the regulation by the oxidative stress regulator OxyR (Küberl et al., 2016; Milse et al., 2014). Interestingly, *ftn* and *dps* expression was also remarkably upregulated in a $\Delta oxyR$ mutant highlighting the protective function of iron storage proteins. Secondly, it remains unclear how Fe^{3+} liberated from ferritin is solubilised and reduced subsequently (Küberl et al., 2016).

1.3.5.4 Regulation of iron homeostasis The dual transcription factor DtxR is the master regulator of iron metabolism in *C. glutamicum* controlling the expression of

more than 60 genes, that are related to iron metabolism in an analogous fashion to the Fur regulator of e.g. *E. coli* (Frunzke and Bott, 2008).

Under conditions of iron excess the active DtxR homodimer represses the expression of genes encoding iron uptake systems and enhances the expression of genes, which encode iron storage proteins and the repair machinery of iron-sulfur clusters (i.e. the *suf* operon) (Brune et al., 2006; Wennerhold and Bott, 2006). In addition to this, DtxR regulates three genes, which code for transcriptional regulators themselves. One of them is the “repressor of iron proteins” (RipA), which represses the expression of several genes encoding enzymes that contain iron-sulfur clusters (many of them belonging to the TCA cycle), phosphoacetyltransferase and acetate kinase under standard conditions, but experiences itself a negative regulation by DtxR (Wennerhold et al., 2005). Hence, RipA functionality resembles RhyB of *E. coli*.

1.3.5.5 The diphtheria toxin regulator (DtxR) protein The DtxR protein (fig. 3) from *C. glutamicum* (DtxR_{C.g.}) forms a 228 amino acids³⁴ long polypeptide chain with a predicted size of 25.5 kDa and an isoelectric point of 4.65⁵. The crystal structure of this protein has not been resolved. However, homologues of the *C. glutamicum* DtxR, exist throughout a number of human pathogens, where they control e.g. the expression of the virulence genes (Boyd et al., 1990; Schmitt et al., 1995). Close relatives are DtxR of *C. diphtheriae* (DtxR_{C.d.}) and IdeR of *Mycobacterium tuberculosis*, whose iron-dependent activation is characterised and a vast amount of crystallographic structures (of the wildtype and mutants) is available. Sharing 72% amino acid sequence identity with DtxR_{C.d.}, it appears reasonable to assume an identical mechanism of activation (Wennerhold and Bott, 2006).

In *C. glutamicum* published work emphasised the transcriptional analysis of the DtxR

³<http://www.ncbi.nlm.nih.gov/protein/41326098?report=fasta>; accessed: March 2016

⁴<http://coryneregnet.netcompbio.sdu.dk/v6e/CoryneRegNet/queryElement.php?gene=cg2103>; accessed: March 2016

⁵http://web.expasy.org/compute_pi/; accessed: March 2016

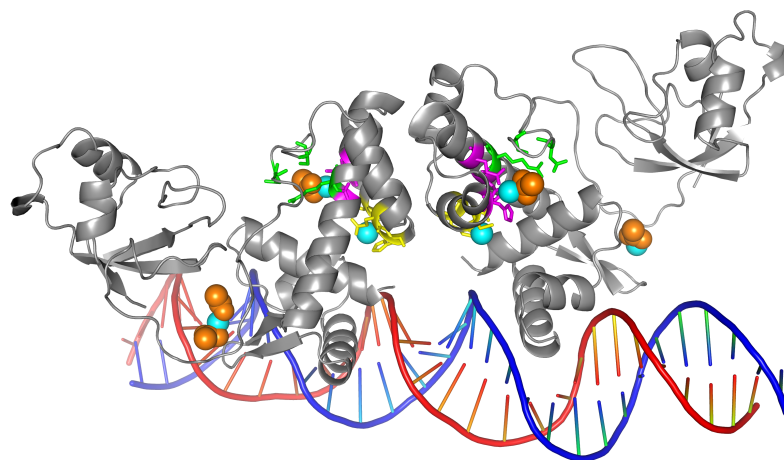


Figure 3: DNA binding of the DtxR_{C.g.} SWISS model on template 3GLX (D'Aquino et al., 2009); DNA (blue/red), Ni²⁺ ions (cyan) and acetate ions (orange) are imported from the crystal structure deposited as 2IT0; high affinity metal binding site 1 (ancillary) (magenta) and low affinity binding site 2 (primary) (yellow) are both occupied by a Ni²⁺ ion; the anion binding site (cation-anion binding site 1) (green) is occupied by an acetate ion

regulon (Brune et al., 2006; Wennerhold and Bott, 2006).

Each DtxR_{C.d.} monomer consists of three domains. In analogy to the Fur protein, the N-terminal domain (residues 1-73) contains a DNA-binding helix-turn-helix (HTH) motif, whilst two metal binding sites and the dimerisation interface are located in domain 2 (residues 77-144) (Qiu et al., 1995). The carboxy-terminal domain of DtxR is linked by a 23 amino acid long proline-rich tether and shows a higher degree of structural flexibility than the amino-terminal domain (Schiering et al., 1995). It reveals some similarity with a Src homology 3 motif, indicating a putative involvement in protein-protein interaction (Qiu et al., 1996).

Other DtxR-like metalloregulatory proteins such as TroR (*Treponema pallidum*) lack the C-terminal SH3-like domain but retain activity. This might suggest, that the C-terminal domain is not essential for iron recognition and DNA binding (Posey et al., 1999). Unlike its homologue in *T. pallidum*, TroR from *T. denticola* contains the carboxy-terminal

SH3-like domain. Brett et al. (2008) reported, that in *E. coli* TroR (from *T. denticola*) repressed *lacZ* expression, which was fused to a promoter-operator region (P/O_{tro}) from either *T. pallidum* or *T. denticola*, respectively, in an iron dependent manner. Truncation of the *T. denticola* TroR C-terminus resulted in a loss of repressor activity on the fusion construct including the *T. denticola* P/O_{tro} sequence. However, the same truncation remained without effect on the repression, when the P/O_{tro} from *T. pallidum* led the *lacZ* gene instead.

Another study with DtxR_{C.d.} found, that the SH3-like domain stabilised the apo-dimer under iron limiting conditions, and proposed a three-step model of DtxR activation (Love et al., 2004). Hence, the function of the carboxy-terminal domain of DtxR is not fully resolved. It might also be worth noting, that sequence similarity exists between the C-terminal domain of DtxR and FeoA (Andrews et al., 2003). The latter forms part of the Fe²⁺ transport system FeoA-FeoB of many bacteria. The function of FeoA in this context is not resolved either and FeoA is not an essential component throughout all bacteria containing FeoB (Lau et al., 2015).

Each DtxR_{C.d.} monomer possesses two distinct metal binding sites, which are sequentially occupied by Fe²⁺ ions, encouraging stable homodimerisation and DNA recognition at excessive iron concentrations (Tao et al., 1995).

The high affinity metal binding site 1 (ancillary) is formed by the three residues His79, Glu83 and His98 of domain 1 and might be complemented by the domain 3 residues Glu170 and Gln173, that are less conserved throughout different bacteria (Qiu et al., 1995; Love et al., 2003). Metal binding site 1 is first to be occupied by Fe²⁺, but not essential for DNA binding (D'Aquino et al., 2005). Binding of a second Fe²⁺ ion to the low affinity binding site 2 (primary), formed by Cys102, Glu105, His106 and Met20, induces structural changes in the N-terminal domain, which enable the interaction of DtxR with its recognition sequence (Qiu et al., 1995; Qiu et al., 1996; D'Aquino et al., 2005; Love et al., 2004; White et al., 1998). All amino acid residues involved in iron binding are conserved in *C. glutamicum*.

Alanine substitution of the metal-binding residues of site 1 and 2 as well as structural

analysis of the conformational changes induced by Fe^{2+} verified the predominant role of the low affinity binding site for nucleotide recognition (Goranson-Siekierke et al., 1999; D'Aquino et al., 2005). Furthermore, an anion binding site in close proximity to the metal binding site 1 (ancillary) is formed by the amino acid residues Arg80, Ser126 and Asn130 (Qiu et al., 1996) and appears to be of great importance for the functionality of DtxR. Single alanine substitutions of the anion binding residues were as detrimental as those of the primary metal binding site 2. In contrast, single alanine substitutions of the amino acids involved in the metal binding site 1 reduced DtxR activity on a *lacZ* reporter construct in *E. coli*, but did not entirely abolish it (Goranson-Siekierke et al., 1999). An important role for the structural stabilisation is inherent to the residue Glu20, which forms hydrogen bonds with Arg80 (Qiu et al., 1996).

Besides the physiological effector molecule of DtxR, Fe^{2+} , a number of additional divalent cations is capable of activating DtxR *in vitro* with the following order of affinity: $\text{Fe}^{2+} \approx \text{Ni}^{2+} > \text{Co}^{2+} \gg \text{Mn}^{2+}$ (Spiering et al., 2003). D'Aquino et al. (2005) determined binding affinities of both metal binding sites for Ni^{2+} by isothermal titration calorimetry (ITC) to $K_D = 2 \times 10^{-7}$ M for metal binding site 1 (ancillary) and $K_D = 6.3 \times 10^{-4}$ M for metal binding site 2 (primary).

Depending on the crystallisation conditions, the anion binding site of DtxR_{C,d.} was found to be occupied by different ions, such as SO_4^{2-} (Qiu et al., 1996), PO_4^{3-} (D'Aquino et al., 2009) or an acetate ion (in IdeR – Wisedchaisri et al., 2007). They participated always in the tetrahedral coordination of the Me^{2+} ion in the metal binding site 2 (ancillary) as a fourth ligand as proposed initially by Qiu et al. (1996). Although they proposed a mechanism involving a phosphate ion, the type of anion which binds under physiological conditions remains unclear.

1.3.5.6 Transcriptional response of the DtxR regulon The DtxR regulon of *C. glutamicum* was initially identified by Brune et al. (2006) and Wennerhold and Bott (2006), who analysed the transcriptomic response of a $\Delta dtxR$ mutant in comparison to the WT under iron excess and limitation conditions.

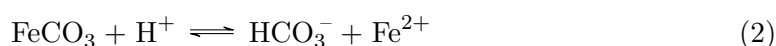
In subsequent studies, Küberl et al. (2016) noted a transcriptional response of the DtxR regulon that was in accordance with decreased Fe^{2+} availability in a Δpup mutant compared to the WT. Partial response of the same regulon was also observed in response to a variation of the medium pH. Decreasing the pH to 6.5 instead of 7.5 resulted in differential expression of some genes belonging to the DtxR regulon indicating a decrease of DtxR activation. Accordingly, when the pH was increased to 9, transcriptomic response resembled a higher activation state of DtxR, that would typically be caused by a larger Fe^{2+} pool (Follmann et al., 2009). Bioreactor fermentations of *C. glutamicum* under pH controlled conditions disclosed a very thorough activation of almost the entire DtxR operon as the result of elevated partial pressure of CO_2 (20 % in the inlet air) in comparison to a bioreactor that was aerated with ambient air (Blombach et al., 2013).

1.4 Interference of iron homeostasis and $\text{CO}_2/\text{HCO}_3^-$

The results of a study concerned about the $\text{CO}_2/\text{HCO}_3^-$ induced effects on *C. glutamicum* (Blombach et al., 2013) were outlined in more detail before (1.2.1). The transcriptional response disclosed an interference of high $\text{CO}_2/\text{HCO}_3^-$ levels with the iron homeostasis of *C. glutamicum*. However, the observation could not be explained mechanistically and was therefore the objective of this study. It might be interesting to highlight previous reports in this regard, that indicate an interference of CO_2 (and related species) and the iron homeostasis in *C. glutamicum*. Unthan et al. (2014) summarised carefully, that the need for the supplementation of chelating agents like PCA in CgXII medium coincided with the omission of CaCO_3 from *C. glutamicum* cultivation media (Liebl et al., 1989; von der Osten et al., 1989). Despite this strong indication of a direct relation between iron availability in *C. glutamicum* and the presence of $\text{CO}_2/\text{HCO}_3^-/\text{CO}_3^{2-}$, it has not been investigated further in the past.

1.4.1 Chemical aspects

Chemical aspects of iron interference with $\text{CO}_2/\text{HCO}_3^-/\text{CO}_3^{2-}$ have been investigated in a number of publications concerned about natural and ground water relations and soils. Dissolution and deposition of iron in ground water is governed by a number of principal equilibria. They include for instance (i) dissolution and precipitation of carbonates, (ii) redox reactions and (iii) formation of complex ions and chelation (Hem and Nolan, 1960). The occurrence of ferrous carbonate complexes has been observed particularly under reducing conditions and in the absence of oxygen, where they form insoluble complexes like siderit (FeCO_3). In accordance with the chemical equilibria given in (2), the presence of bicarbonate ions further restricts the solubility of Fe^{2+} from these complexes (Hem and Nolan, 1960). This fact is also supported by the observation, that the activity coefficient of iron in water is (at identical pH values) lower in the presence of bicarbonate, thus, lowering iron availability (Helgeson et al., 1969).



Under identical conditions (reducing, anoxic) soluble iron complexes include ferrous bicarbonate ($\text{Fe}(\text{HCO}_3)_2$) or soluble intermediates that might occur in supersaturated iron carbonate solutions (FeHCO_3^+). In the presence of dissolved CO_2 , iron can be solubilised as ($\text{Fe}(\text{HCO}_3)_2$) from insoluble siderite. Hence, high CO_2 concentrations represent one of the prerequisites for maintaining Fe^{2+} in solution (Hem and Nolan, 1960; Pohling, 2015).

The existence of such complexes might explain, why in natural and ground water studies iron is detected in solution often above solubility equilibria. Hem and Nolan (1960) noted during the experiments that iron had precipitated somewhere between sampling and lab. It appeared likely to them that the oxidation of ferrous carbonates was causative for the precipitates, since they are known to be poorly stable under oxidising conditions.

As the counterpart of cationic ferrous bicarbonate, the presence of a number of anionic ferric carbonates were isolated under certain conditions. The authors highlight, that soluble basic complex carbonates might exist in aqueous solutions and are entirely dependent on the HCO_3^- concentration (Sengupta and Nandi, 1974).

1.4.2 Biological interference

1.4.2.1 In plants The physiological response of plants to a variation of $\text{CO}_2/\text{HCO}_3^-$ availability has been addressed by many studies. There are several reports of the $\text{CO}_2/\text{HCO}_3^-$ interferences with iron nutrition across all types of plants. Iron chlorosis is defined as an insufficient iron nutritional status of the plant resulting in the lack of chlorophyll in the leaf. It can be provoked by the addition of different concentrations of bicarbonate to the (typically iron limited) growth medium (Lucena, 2000). Some inconsistency persists, whether this phenotype is caused by an inhibition of iron uptake or inefficient utilisation of iron due to interference with intracellular processes. In different studies, the inhibition of reducing capacity in the medium by bicarbonate (Alcántara et al., 2000), the buffering effect preventing the acidification (and thus lowering Fe^{3+} solubility) of the medium (Martínez-Cuenca et al., 2013) or reduced iron uptake by the roots (Alhendawi et al., 1997) were claimed to be responsible for the bicarbonate induced

iron chlorosis phenotype. In contrast to these studies, tomato plants (*Lycopersicon esculentum* “Zheza 809”) that were grown in iron restricted growth medium (providing Fe^{3+} oxide as iron source) exhibited a higher iron concentration in the shoot, when exposed to an elevated CO_2 concentration in the air. The authors suggest a multifaceted response of the plant that increased the capacity to solubilise iron from the poorly soluble source (Jin et al., 2009). It was mentioned by the authors, that the medium acidification due to elevated CO_2 might contribute to the solubilisation of Fe^{3+} . But unfortunately, control experiments to quantify this contribution had not been performed. In accordance with Jin et al. (2009), Sasaki et al. (1998) reported even earlier a several fold increase of ferric reductase activity and iron uptake capacity in the marine green algae *Chlorococcum littorale* in response to CO_2 enriched air (20 % CO_2 content), when it was cultivated in the absence of iron.

1.4.2.2 In other organisms Analogous information about the iron availability to microorganisms in response to the $\text{CO}_2/\text{HCO}_3^-$ content is scarce. It is worth noting, that bespoke ferrous iron transport complex SitABCD from *Salmonella enterica* or the homologous MtsABC from *Streptococcus pyogenes* might involve a HCO_3^- synergistic anion for Fe^{2+} binding (Sun et al., 2008). Likewise, iron binding to the transport protein transferrin in mammals is coordinated by a synergistic carbonate anion. The release of iron from transferrin is mediated by a drop of the endosomal pH that affects the protonation of CO_3^{2-} and conformational change of the protein itself (Steere et al., 2013).

Objectives of this study

This study was based on previous work disclosing a regulatory link between elevated levels of $\text{CO}_2/\text{HCO}_3^-$ and iron homeostasis in *C. glutamicum* (Blombach et al., 2013). First, low $\text{CO}_2/\text{HCO}_3^-$ levels provoked a growth defect of *C. glutamicum* in a bioreactor cultivation, that was not observed at standard (ambient CO_2 levels) and elevated concentrations (20 % CO_2 in the inlet air). Secondly, a remarkable transcriptional response was induced by elevated CO_2 contents, which comprised almost the entire regulon controlled by DtxR.

The dual transcriptional regulator DtxR is well characterised in literature, activated at a high concentration of Fe^{2+} and controls the expression of genes encoding enzymes involved in iron acquisition, utilisation and storage.

The objective of the follow-up project presented here was to identify the level of interaction between $\text{CO}_2/\text{HCO}_3^-$ and the DtxR regulated iron homeostasis in *C. glutamicum*. This included three working packages in particular, that were formulated at the beginning of the work: (i) Crystallographic structures of DtxR homologues from closely related pathogenic bacteria *Corynebacterium diphtheriae* and *Mycobacterium tuberculosis* revealed the presence of an anion binding site, that was essential for functionality of the transcriptional regulator. HCO_3^- represented an appropriate co-stimulus to recognise the host environment and regulate toxin expression accordingly. In fact, HCO_3^- sensors have been proposed in other bacteria but could not be identified in *C. glutamicum*. Thus, biochemical analysis of HCO_3^- binding by DtxR was intended for this project, to address the question, whether DtxR represents a $\text{CO}_2/\text{HCO}_3^-$ sensor as well. (ii) The DtxR protein holds an interesting structural feature in form of a C-terminal domain with similarity to SH3 like protein structures. Suggesting protein-protein inter-

action in this domain, potential interaction partners of DtxR should be identified with the focus on $\text{CO}_2/\text{HCO}_3^-$ sensors transmitting the signal to DtxR. (iii) Characterisation of deletion mutants of *C. glutamicum* regarding growth and intracellular Fe^{2+} levels are meant to provide insights in $\text{CO}_2/\text{HCO}_3^-$ interference with iron transport, storage and remobilisation. In the course of this project and caused by the gain of knowledge on iron homeostasis, the objective of this study was further broadened. As $\text{CO}_2/\text{HCO}_3^-$ seemed to interfere with the oxidation state of iron, it was decided to address this issue by chemical as well as biological characterisation of the phenomenon.

3.1 Chemicals

An overview of the most important chemicals is given in the appendix in tab. S1. All chemicals were of high purity ($\geq 97\%$). Enzymes, commercial kits and additional laboratory equipment are also outlined in the appendix (tab. S2, S3, S4).

3.2 Cultivation media

3.2.1 2x YT complex medium

The 2x yeast extract - tryptone complex medium (2x YT) was used for plasmid amplification, protein production (both in *E. coli*) and precultures of growth experiments with *C. glutamicum*. Media were prepared in accordance with Sambrook and Russell (2001) (tab. 1), sterilized (autoclaving, 20 min, 121 °C) and antibiotics were added aseptically where required immediately before inoculation.

Table 1: Composition of the 2x YT complex medium; Sambrook and Russell (2001)

Ingredient	Amount
Bacto Tryptone	16 g L ⁻¹
Yeast Extract	10 g L ⁻¹
NaCl	5 g L ⁻¹

3.2.2 BHI(S) complex medium

Brain heart infusion medium (BHI) and BHI medium containing sorbitol (BHIS) was used during the preparation of competent cells and selection of integrants in *C. glutamicum*. Components of the BHI(S) medium (tab. 2) were dissolved in VE-H₂O, autoclaved separately (20 min, 121 °C), and mixed aseptically, according to Liebl et al. (1989).

Table 2: Composition of the BHI(S) complex medium; Liebl et al. (1989)

Ingredient	Amount
BHI powder	37 g L ⁻¹
Sorbitol	91 g L ⁻¹

3.2.3 Agar plates

For the preparation of agar plates, 18 g agarose L⁻¹ was added to the complex medium (either 2x YT or BHIS) before sterilization. If required, antibiotics were added after sterilisation to the hand-warm medium immediately before pouring it into plastic petri dishes. Agar plates were stored up to four months at 4 °C.

3.2.4 CgXII minimal medium

Standard *C. glutamicum* growth experiments were performed in modified CgXII minimal medium (Eikmanns et al., 1991; Keilhauer et al., 1993). The precise composition was as described in tab. 3 for shaking flask experiments and BioLector cultivations or lacking urea and MOPS buffer when applied in bioreactor cultivations. Basic medium was prepared in VE-H₂O, the pH was adjusted to 7.4 with 5 M KOH, the appropriate volume was transferred to shaking flasks or bottles (bioreactor fermentations) and autoclaved (20 min, 121 °C). MgSO₄, CaCl₂, biotin and trace element solution were added aseptically from 1000x stock solutions. 20 g glucose L⁻¹ (40 g L⁻¹ in bioreactor cultivations) was added aseptically from the stock solution containing 500 g glucose L⁻¹. Other supplements (PCA, NaHCO₃) were likewise added aseptically to the medium after

autoclaving as indicated.

Table 3: Composition of CgXII minimal medium used for shaking flask experiments and bioreactor cultivations (lacking urea and MOPS buffer) modified after Eikmanns et al. (1991) and Keilhauer et al. (1993)

Ingredient	Amount
$(\text{NH}_4)_2\text{SO}_4$	5 g L ⁻¹
Urea	5 g L ⁻¹
MOPS	21 g L ⁻¹
K_2HPO_4	1 g L ⁻¹
KH_2PO_4	1 g L ⁻¹
<hr/>	
MgSO_4	0.25 g L ⁻¹
CaCl_2	0.01 g L ⁻¹
Biotin	0.2 mg L ⁻¹
Trace Element Solution (1000x stock)	1 mL L ⁻¹
<hr/>	
Trace Element Solution (1000x stock):	
$\text{FeSO}_4 \times 7 \text{ H}_2\text{O}$	16.4 g L ⁻¹
$\text{MnSO}_4 \times \text{H}_2\text{O}$	10 g L ⁻¹
CuSO_4	0.2 g L ⁻¹
$\text{ZnSO}_4 \times 7 \text{ H}_2\text{O}$	1 g L ⁻¹
$\text{NiCl}_2 \times 6 \text{ H}_2\text{O}$	0.02 g L ⁻¹

3.2.5 Antibiotics

Antibiotics were added aseptically to all media used during selection or for plasmid maintenance from 1000x stock solutions, as indicated. Working concentrations were 100 μg ampicillin mL⁻¹ or 50 μg kanamycin mL⁻¹.

3.3 Bacterial strains & plasmids

Bacterial strains and plasmids used in this work are listed in tab. 4 and 5, respectively. Chromosomal modifications in *C. glutamicum* were achieved with the integration/deletion plasmid pK19*mobsacB* (Schäfer et al., 1994). Deletion plasmids were always build in the same way. DNA sequences (500 bp) flanking the deletion target were

PCR-amplified from *C. glutamicum* ATCC 13032 chromosomal DNA with the appropriate primer pair as indicated in tab. S6. The two sequences were ligated adjacent to each other in BamHI and HindIII linearised pK19*mobsacB* by the isothermal assembling approach (3.4.8). For the construction of the reporter strains *C. glutamicum* FEM1 and FEM3 pK19*mobsacB* derived integration plasmids contained the P_{ripA}-*egfp*-T_{rrnB} or P_{ripA}-*lacI*-T_{rrnB} expression cassette, between the two 500 bp flanking regions, respectively. The promoter region of *ripA* and flanking sequences were amplified by PCR from *C. glutamicum* ATCC 13032 chromosomal DNA and the structural genes *egfp*, *lacI* and the strong terminator T_{rrnB} from plasmid pJOE7706.1 (Hoffmann and Altenbuchner, 2014) All fragments were ligated simultaneously into BamHI and NheI linearised pK19*mobsacB* as above. Reporter strain *C. glutamicum* FEM3 and all derivatives were completed with the replicative plasmid pJC4-P_{tac}-*egfp*. All fragments (P_{tac}, *egfp* and T_{rrnB}) were PCR-amplified from pJOE7706.1 (Hoffmann and Altenbuchner, 2014) with the appropriate primer pairs (tab. S6) and ligated simultaneously into XbaI and NotI linearised pJC4 (Cordes et al., 1992) by isothermal assembling (3.4.8).

DtxR protein was overproduced and purified in *E. coli* using the plasmids derived from pJOE6089.4 (carrying a C-terminal Strep-tag II, Hoffmann et al. (2012)) and pJOE6087.3 (carrying a C-terminal 6x His tag, Joe Altenbuchner, unpublished). The gene *dtxR* was amplified by PCR from the chromosomal DNA of *C. glutamicum* ATCC 13032 and ligated into NdeI and BamHI the linearised plasmids (3.4.7). The DtxR mutant C102D was generated in the same way. The *dtxR* gene was amplified in two pieces and the mutation was encoded in the primer overlap (see primer in tab. S6). Both fragments were assembled with the NdeI and BamHI linearised pJOE6089 simultaneously. The fragment *dtxR*-Strep-tag II was amplified from pJOE6089-*dtxR* and ligated into PstI and BamHI linearised pVWEx1 for IPTG inducible expression in *C. glutamicum* pull-down experiments.

Table 4: List of bacterial strains used in this study

Strain	Relevant characteristics	Reference
<i>E. coli</i> DH5 α	<i>supE44</i> Δ <i>lacU169</i> (<i>f80lacZ</i> Δ <i>M15</i>) <i>hsdR17</i> <i>recA1</i> <i>endA1</i> <i>gyrA96</i> <i>thi</i> <i>relA1</i>	Hanahan (1983)
<i>E. coli</i> JM109	<i>recA1</i> <i>endA1</i> <i>gyrA96</i> <i>thi</i> <i>hsdR17</i> <i>supE44</i> <i>relA1</i> λ^- Δ (<i>lac-proAB</i>)(<i>F'</i> <i>traD36</i> <i>proAB</i> ⁺ <i>lacI</i> ^q <i>lacZ</i> Δ <i>M15</i>)	Yanisch-Perron et al. (1985)
<i>C. glutamicum</i> ATCC 13032	wildtype strain (WT)	Abe et al. (1967), American Type Culture Collection
strains for <i>dtxR</i> overexpression		
<i>E. coli</i> DH5 α (pJOE6087- <i>dtxR</i>)	rhamnose inducible <i>dtxR</i> overexpression, C-terminal 6x His tag	this work
<i>E. coli</i> DH5 α (pJOE6089- <i>dtxR</i>)	rhamnose inducible <i>dtxR</i> overexpression, C-terminal Strep tag II	this work
<i>E. coli</i> DH5 α (pJOE6089- <i>dtxR</i> (C102D))	rhamnose inducible overexpression of <i>dtxR</i> mutant Cys102Asp, C-terminal Strep tag II	this work
strain for pull-down experiment		
<i>C. glutamicum</i> ATCC 13032 (pVWEx1- <i>dtxR</i>)	IPTG inducible overexpression of <i>dtxR</i> fused to a C-terminal Strep tag II	this work
reporter strains		
<i>C. glutamicum</i> FEM1	<i>C. glutamicum</i> ATCC 13032 (<i>cg3344-cg3345</i>)':P _{ripA} - <i>egfp</i>	this work
<i>C. glutamicum</i> FEM3	<i>C. glutamicum</i> ATCC 13032 (<i>cg3344-cg3345</i>)':P _{ripA} - <i>lacI</i> (pJC4-P _{tac} - <i>egfp</i>)	this work
deletion mutants		
WT background		
<i>C. glutamicum</i> ATCC 13032 Δ <i>dtxR</i>	deletion of the <i>dtxR</i> gene (<i>cg2103</i>) in <i>C. glutamicum</i> WT (<i>C. glutamicum</i> IB2103)	Brune et al. (2006)
<i>C. glutamicum</i> ATCC 13032 Δ <i>cg2444</i>	deletion of <i>cg2444</i> encoding a hypothetical protein in <i>C. glutamicum</i> WT	this work
<i>C. glutamicum</i> ATCC 13032 Δ <i>pup</i>	deletion of the <i>pup</i> gene (<i>cg1689</i>) in <i>C. glutamicum</i> WT using pK19 <i>mobsacB</i> - Δ <i>pup</i> (which was kindly provided by Michael Bott)	this work
<i>C. glutamicum</i> ATCC 13032 Δ <i>ftn</i>	deletion of the <i>ftn</i> gene (<i>cg2782</i>) in <i>C. glutamicum</i> WT	this work

Table 4: List of bacterial strains (continued)

Strain	Relevant characteristics	Reference
<i>C. glutamicum</i> ATCC 13032 Δdps	deletion of the <i>dps</i> gene (<i>cg3327</i>) in <i>C. glutamicum</i> WT	this work
<i>C. glutamicum</i> ATCC 13032 Δftn Δdps	double deletion of the <i>ftn</i> (<i>cg2782</i>) and <i>dps</i> (<i>cg3327</i>) genes in <i>C. glutamicum</i> WT	this work
<i>C. glutamicum</i> ATCC 13032 $\Delta cg1438-cg1441$	deletion of the operon <i>cg1438-cg1441</i> in <i>C. glutamicum</i> WT; annotated transport system	this work
<i>C. glutamicum</i> ATCC 13032 $\Delta cg0041-cg0042$	deletion of the operon <i>cg0041-cg0042</i> in <i>C. glutamicum</i> WT; annotated transport system	this work
reporter strain background		
<i>C. glutamicum</i> FEM3 $\Delta cg2444$	deletion of <i>cg2444</i> encoding a hypothetical protein in <i>C. glutamicum</i> FEM3	this work
<i>C. glutamicum</i> FEM3 Δpup	deletion of the <i>pup</i> gene (<i>cg1689</i>) in <i>C. glutamicum</i> FEM3 using pK19 <i>mobsacB</i> - Δpup (which was kindly provided by Michael Bott)	this work
<i>C. glutamicum</i> FEM3 Δftn	deletion of the <i>ftn</i> gene (<i>cg2782</i>) in <i>C. glutamicum</i> FEM3	this work
<i>C. glutamicum</i> FEM3 Δdps	deletion of the <i>dps</i> gene (<i>cg3327</i>) in <i>C. glutamicum</i> FEM3	this work
<i>C. glutamicum</i> FEM3 $\Delta ftn \Delta dps$	double deletion of the <i>ftn</i> (<i>cg2782</i>) and <i>dps</i> (<i>cg3327</i>) genes in <i>C. glutamicum</i> FEM3	this work
<i>C. glutamicum</i> FEM3 $\Delta cg1438-cg1441$	deletion of the operon <i>cg1438-cg1441</i> in <i>C. glutamicum</i> FEM3; annotated transport system	this work
<i>C. glutamicum</i> FEM3 $\Delta cg0041-cg0042$	deletion of the operon <i>cg0041-cg0042</i> in <i>C. glutamicum</i> FEM3; annotated transport system	this work

Table 5: List of plasmids utilized in this work

Plasmid	Relevant characteristics	Reference
pK19 <i>mobsacB</i>	shuttle vector for amplification in <i>E. coli</i> and integration/deletion in <i>C. glutamicum</i> ; pMB1 oriV _{E.coli} , oriT (RP4 <i>mob</i>), <i>lacZ</i> α , <i>sacB</i> _{B. subtilis} , Kan ^R	Schäfer et al. (1994)
pVWEx1	<i>E. coli</i> - <i>C. glutamicum</i> shuttle vector; oriV _{E. coli} , pCG1 oriV _{C. glutamicum} , P _{tac} , <i>lacI</i> ^Q , Kan ^R	Peters-Wendisch et al. (2001)

Table 5: List of plasmids (continued)

Plasmid	Relevant characteristics	Reference
pJC4	<i>E. coli</i> - <i>C. glutamicum</i> shuttle vector; oriV _{E. coli} , pCG1 oriV _{C. glutamicum} , Kan ^R	Cordes et al. (1992)
pJOE6089.4	rhamnose inducible overexpression plasmid in <i>E. coli</i> ; pBR322 oriV _{E. coli} , P _{rhaBAD} , <i>egfp</i> -Strep-tag II (C-terminal), T _{rrnB} , Amp ^R	Hoffmann et al. (2012)
pJOE6087.3	rhamnose inducible overexpression plasmid in <i>E. coli</i> ; pBR322 oriV _{E. coli} , P _{rhaBAD} , <i>egfp</i> -6x His tag (C-terminal), T _{rrnB} , Amp ^R	Joe Altenbuchner (unpublished)
pJOE7706.1	IPTG inducible overexpression shuttle plasmid for <i>E. coli</i> and <i>C. glutamicum</i> ; pBR322 oriV _{E. coli} , pCG1 oriV _{C. glutamicum} , <i>lacI</i> ^q , P _{tac} , <i>egfp</i> , T _{rrnB} , Kan ^R ,	Hoffmann and Altenbuchner (2014)
pJOE6089- <i>dtxR</i>	rhamnose inducible overexpression plasmid in <i>E. coli</i> ; pBR322 oriV _{E. coli} , P _{rhaBAD} , <i>dtxR</i> -Strep-tag II (C-terminal), T _{rrnB} , Amp ^R	this work
pJOE6089- <i>dtxR</i> (C102D)	codon exchange TGC → GAC introduced in pJOE6089- <i>dtxR</i> encoding the Cys102Asp substitution in DtxR; primer encoded codon exchange in <i>dtxR</i> re-inserted in NdeI and BamHI linearised vector	this work
pJOE6087- <i>dtxR</i>	rhamnose inducible overexpression plasmid in <i>E. coli</i> ; pBR322 oriV _{E. coli} , P _{rhaBAD} , <i>dtxR</i> -6x His tag (C-terminal), T _{rrnB} , Amp ^R	this work
pVWEx1- <i>dtxR</i>	<i>dtxR</i> with C-terminal Strep-tag II inserted in PstI and BamHI linearised pVWEx1 for IPTG inducible overexpression of <i>dtxR</i> in <i>C. glutamicum</i>	this work
pJC4-P _{tac} - <i>egfp</i>	P _{tac} - <i>egfp</i> -T _{rrnB} inserted in XbaI and NotI linearised pJC4 for controlled expression of <i>egfp</i> (in FEM3 and derivatives)	this work
integration plasmids		
pK19 <i>mobsacB</i> -flank1(3' <i>cg3344</i>)-P _{ripA} - <i>egfp</i> -T _{rrnB} -flank2(5' <i>cg3345</i>)	plasmid for the integration of <i>egfp</i> under control of the <i>ripA</i> promoter (P _{ripA}) in the intergenic region between <i>cg3344</i> and <i>cg3345</i> (defined as CgLP13 by Lange et al. (2017)) in the <i>C. glutamicum</i> genome; all fragments inserted simultaneously in BamHI and NheI linearised pK19 <i>mobsacB</i>	this work
pK19 <i>mobsacB</i> -flank1(3' <i>cg3344</i>)-P _{ripA} - <i>lacI</i> -T _{rrnB} -flank2(5' <i>cg3345</i>)	plasmid for the integration of <i>lacI</i> under control of the <i>ripA</i> promoter (P _{ripA}) in the intergenic region between <i>cg3344</i> and <i>cg3345</i> (defined as CgLP13 by Lange et al. (2017)) in the <i>C. glutamicum</i> genome; all fragments inserted simultaneously in BamHI and NheI linearised pK19 <i>mobsacB</i>	this work
deletion plasmids		
pK19 <i>mobsacB</i> - Δ <i>pup</i>	pK19 <i>mobsacB</i> derivative for markerless deletion of the <i>pup</i> gene (<i>cg1689</i>) in <i>C. glutamicum</i>	Küberl et al. (2014)

Table 5: List of plasmids (continued)

Plasmid	Relevant characteristics	Reference
pK19 <i>mobsacB</i> - Δ <i>cg2444</i>	pK19 <i>mobsacB</i> derivative for markerless deletion of <i>cg2444</i> in <i>C. glutamicum</i> ; homologous sequences* inserted in HindIII and BamHI linearised pK19 <i>mobsacB</i> plasmid backbone	this work
pK19 <i>mobsacB</i> - Δ <i>ftn</i>	pK19 <i>mobsacB</i> derivative for markerless deletion of the <i>ftn</i> gene (<i>cg2782</i>) in <i>C. glutamicum</i> ; homologous sequences* inserted in HindIII and BamHI linearised pK19 <i>mobsacB</i> plasmid backbone	this work
pK19 <i>mobsacB</i> - Δ <i>dps</i>	pK19 <i>mobsacB</i> derivative for markerless deletion of the <i>dps</i> gene (<i>cg3327</i>) in <i>C. glutamicum</i> ; homologous sequences* inserted in HindIII and BamHI linearised pK19 <i>mobsacB</i> plasmid backbone	this work
pK19 <i>mobsacB</i> - Δ <i>cg1438-cg1441</i>	pK19 <i>mobsacB</i> derivative for markerless deletion of the operon <i>cg1438-cg1441</i> in <i>C. glutamicum</i> ; homologous sequences* inserted in HindIII and BamHI linearised pK19 <i>mobsacB</i> plasmid backbone	this work
pK19 <i>mobsacB</i> - Δ <i>cg0041-cg0042</i>	pK19 <i>mobsacB</i> derivative for markerless deletion of the operon <i>cg0041-cg0042</i> in <i>C. glutamicum</i> ; homologous sequences* inserted in HindIII and BamHI linearised pK19 <i>mobsacB</i> plasmid backbone	this work

*) 500 bp sequences up- and downstream of the deletion target (*C. glutamicum* WT genomic sequence)

3.4 DNA manipulation & strain engineering

3.4.1 Quantification of the DNA concentration

The DNA concentration was determined by the absorbance at 260 nm using the Nano-drop spectrophotometer (ND-1000, Thermo Fisher Scientific Inc., Bremen, Germany) from 1 μ L solution.

3.4.2 DNA separation by agarose gel electrophoresis

DNA fragments were separated according to their size by agarose gel electrophoresis. 8 g agarose L⁻¹ was dissolved in 1x TAE buffer (4.84 g Tris L⁻¹, 0.4 % (v/v) acetic acid, 0.37 g EDTA L⁻¹) by heating it up in a microwave. For a small gel, 4 μ L GelRed™ (#41003, Biotrend, Cologne, Germany) was added to 50 mL agarose solution and the gel was allowed to polymerize at RT after casting it into a gel tray. The gel was submerged in 1x

TAE buffer in an electrophoresis chamber (Mini-Sub Cell System, Bio-Rad Laboratories, Inc., Hercules, CA, USA) and loaded with 6 μL of the DNA sample (diluted to an estimated 5 - 50 ng μL^{-1} in VE- H_2O) including 1 μL of DNA Gel Loading Dye (6x) (#R0611 Thermo Fisher Scientific Inc., Bremen, Germany). 5 μL GeneRuler™ 1 kb Plus DNA ladder (Thermo Fisher Scientific Inc., Bremen, Germany, fig. S5 in the appendix) was loaded at least in one of the lanes as the marker DNA of known size. DNA fragments were finally separated by size in a voltage field (80-100 V) for 45-60 min (provided by Biometra Power Pack P25, Analytik Jena, Jena, Germany).

3.4.3 PCR amplification

Genetic material was amplified for cloning purposes in a polymerase chain reaction (PCR) (Mullis and Faloona, 1987; Saiki et al., 1985; Saiki et al., 1988) using either *Phusion* or *Q5* polymerase. Reaction mixtures were prepared as outlined in tab. 6 and 7, respectively, and placed in a Thermocycler to control the PCR program given in tab. 8 and 9, respectively.

Table 6: PCR reaction mixture for amplification using *Phusion* polymerase

Compound	Volume
template DNA	(10-100 ng)
5x HF buffer (incl. MgCl_2)	10 μL
dNTPs (2 mM)	5 μL
forward primer (10 μM)	2 μL
reverse primer (10 μM)	2 μL
DMSO	2 μL
<i>Phusion</i> polymerase	1 μL
H_2O	ad 50 μL

Table 7: PCR reaction mixture for amplification using *Q5* polymerase

Compound	Volume
template DNA	(10-100 ng)
5x Q5 reaction buffer	10 μL

Table 7: PCR reaction mixture for amplification using *Q5* polymerase (continued)

Compound	Volume
dNTPs (2 mM)	5 μL
forward primer (10 μM)	2.5 μL
reverse primer (10 μM)	2.5 μL
5x <i>Q5</i> high GC enhancer	10 μL
<i>Q5</i> polymerase	0.5 μL
VE-H ₂ O	<i>ad</i> 50 μL

Table 8: PCR program for DNA amplification using the *Phusion* polymerase; *) Annealing temperature was either set to 55 °C or calculated using the NEB online tool (tmcalculator.neb.com)

	Step	Temperature	Time
	Initial Denaturation	98 °C	5 min
30 cycles	Denaturation	98 °C	30 s
	Annealing	55 °C	30 s
	Elongation	72 °C	15-30 s kb ⁻¹
	Final Extension	72 °C	8 min
	Hold	4 °C	∞

Table 9: PCR program for DNA amplification using the *Q5* polymerase

	Step	Temperature	Time
	Initial Denaturation	98 °C	30 s
30 cycles	Denaturation	98 °C	10 s
	Annealing	55 °C	30 s
	Elongation	72 °C	20-30 s kb ⁻¹
	Final Extension	72 °C	2 min
	Hold	4 °C	∞

3.4.4 Colony PCR

The purpose of colony PCR was to discriminate positive/negative transformants and confirm the integration/deletion success. Biological material was taken from agar plates, resuspended in 50 μL VE-H₂O and heated for 10 min at 95 °C. The suspension was centrifuged (Eppendorf Minispin, 1 min, 13,400 rpm) and 10 μL supernatant was used as DNA template in the reaction mixture. Composition of reaction mixture and PCR program for the colony PCR are given in tab. 10 and 11.

Table 10: Reaction mixture for a colony PCR using *taq* polymerase

Compound	Volume
template DNA (lysed cell supernatant)	10 μL
10x buffer S (incl. MgCl ₂)	2.5 μL
dNTPs (2 mM)	2.5 μL
forward primer (10 μM)	0.5 μL
reverse primer (10 μM)	0.5 μL
DMSO	1 μL
<i>taq</i> polymerase (Genaxxon)	0.1 μL
VE-H ₂ O	<i>ad</i> 25 μL

Table 11: Program for a colony PCR using the *taq* polymerase

Step	Temperature	Time	
Initial Denaturation	95 °C	5 min	
30 cycles	Denaturation	95 °C	
	Annealing	55 °C	
	Elongation	72 °C	1 min kb ⁻¹
	Final Extension	72 °C	8 min
Hold	4 °C	∞	

3.4.5 DNA purification

3.4.5.1 Isolation of chromosomal DNA Chromosomal DNA of *C. glutamicum* ATCC 13032 was extracted with the *DNeasy Blood & Tissue kit* (Qiagen, Hilden, Germany) according to the manufacturers instructions for Gram positive bacteria. DNA was finally eluted from the spin-columns with 50 μL 70 °C VE-H₂O.

3.4.5.2 Purification from PCR mix & restriction digest PCR products and linearised plasmid DNA were purified using the *NucleoSpin Gel and PCR Clean-up kit* (Macherey-Nagel, Düren, Germany). Instead of elution buffer, 70 °C VE-H₂O was used for elution and storage of the DNA. Linearised plasmid DNA was eluted in a smaller volume of about 10-15 μL to achieve higher DNA concentrations.

3.4.5.3 Plasmid isolation Vector plasmids were amplified in *E. coli* DH5 α cells and isolated with the *E.Z.N.A Plasmid Mini Kit I* (Omega Bio-Tek Inc., Norcross, Georgia, USA). Cells were grown in 5 mL 2x TY tubes O/N at 37 °C shaking (120 rpm). 3 mL culture was harvested by centrifugation (2x 1.5 mL, 1 min, 13,400 rpm in Eppendorf Minispin). Plasmid DNA was finally eluted with 50 μL 70 °C VE-H₂O.

3.4.6 Plasmid linearisation

Vector plasmids were linearised in a double digest using two compatible restriction enzymes (Thermo Fisher Scientific Inc., Bremen, Germany). Any digest was prepared in a total volume of 20 μL containing about 500 ng plasmid DNA, 2 μL of the recommended buffer the appropriate volume of both restriction enzymes according to the online DoubleDigest Finder⁶.

⁶ThermoFisher Scientific DoubleDigest Finder; <https://www.thermofisher.com/de/de/home/brands/thermo-scientific/molecular-biology/thermo-scientific-restriction-modifying-enzymes/restriction-enzymes-thermo-scientific/double-digest-calculator-thermo-scientific.html>

3.4.7 DNA ligation

Most plasmids were generated by ligating several fragments into one construct using homologous overlaps as outlined below (3.4.8). The two plasmids pJOE6087-*dtxR* and pJOE6089-*dtxR* for overexpression of *dtxR* and purification of the protein by affinity chromatography were built by conventional restriction and ligation. NdeI and BamHI linearised plasmid backbone and amplification product of *dtxR* (obtained by PCR from *C. glutamicum* ATCC 13032 chromosomal DNA with the appropriate primer pair as indicated in tab. S6) were ligated using the T4 DNA ligase (New England Biolabs, Frankfurt, Germany) according to the manufacturers instructions. Reaction mixtures were set up in 20 μL containing 2 μL of supplied ligation buffer and 500 - 1000 ng DNA that was provided in a molar 3:1 excess of insert:plasmid. After the addition of 1 μL T4 DNA ligase, the reaction was statically incubated for 20 - 30 min at RT.

3.4.8 Gibson assembly

Plasmids with two or more inserts were constructed in an isothermal assembling approach (Gibson assembly), that allows the simultaneous integration of multiple fragments (Gibson et al., 2009). Overlapping regions (20 bp length) were encoded at the 5' end of the PCR primers used for amplification of DNA fragments (according to tab. S6) and determine the correct orientation of all fragments. *Gibson ISO enzyme reaction mixture* (tab. 12) was prepared by adding the appropriate enzymes to the *Gibson 5x ISO reaction mixture* (tab. 13) in accordance with Gibson (2011) and 15 μL aliquots were stored frozen at -20 °C until use. DNA fragments and linearised plasmid were mixed in the recommended ratio (Gibson, 2011) and 5 μL was pipetted into the lid of a PCR tube containing 15 μL *Gibson ISO enzyme reaction mixture*. The tube was briefly centrifuged to bring both liquids together, placed in a pre-heated Thermocycler and incubated for 60 min at 50 °C. 5 μL of the reaction mixture was applied to the transformation of competent DH5 α cells (3.4.10.1).

Table 12: Composition of *Gibson ISO enzyme reagent mixture* prepared in accordance with Gibson (2011) and stored at -20°C.

Compound	Volume
5x ISO reaction mixture (tab. 13)	320 μ L
T5 exonuclease (10 U mL ⁻¹)	0.64 μ L
<i>Phusion</i> polymerase (2 U mL ⁻¹)	20 μ L
T4 DNA ligase (40 U mL ⁻¹)	160 μ L
VE-H ₂ O	<i>ad</i> 1.2 mL

Table 13: Composition of *Gibson 5x ISO reaction mixture* prepared in accordance with Gibson (2011)

Compound	Amount
PEG-8000	1.5 g
Tris-HCl (1 M) pH 7.5	3 mL
MgCl ₂ (2 M)	150 μ L
DTT (1 M)	300 μ L
dNTPs (100 mM)	60 μ L each
NAD (100 mM)	300 μ L

3.4.9 Competent cells

3.4.9.1 *Escherichia coli* Electro-competent cells of *E. coli* (Dower et al., 1988) were prepared as described by Lange et al. (2017). A 250 mL culture in 2x YT medium was inoculated with 0.5 mL of an overnight (O/N) culture in 5 mL 2x YT reaction tubes. The main culture was incubated at 37 °C (120 rpm on a rotary shaker) and the optical density at 600 nm (OD₆₀₀) of the culture was monitored. At an OD₆₀₀ between 0.3 and 0.5, the culture was harvested in 50 mL falcon tubes (Eppendorf Centrifuge 5804 R, 15 min, 5,000 rpm, 4 °C), washed twice in 20 mL ice-cold VE-H₂O and once with ice-cold 10 % (v/v) glycerol. The cells were eventually resuspended in 1 mL ice-cold 10 % (v/v) glycerol and 50 μ L aliquots in 1.5 mL Eppendorf cups were frozen in liquid nitrogen. The aliquots were stored frozen at -70 °C until further use.

3.4.9.2 *Corynebacterium glutamicum* Competent *C. glutamicum* cells for electroporation were prepared following a modified protocol by Kirchner and Tauch (2003). A reaction tube containing 5 mL BHI medium was inoculated with a single colony, incubated for 6 h at 30 °C shaking and used to inoculate 50 mL BHIS in a 500 mL baffled shaking flask, that was incubated O/N. The main culture (250 mL BHIS in a 1 L baffled shaking flask) was inoculated with 5 mL of the O/N culture, incubated as before and the optical density at 600 nm of the culture was monitored. At $OD_{600} = 1.75$, the culture was harvested in 50 mL falcon tubes (20 min, 5,000 rpm, 4 °C, Eppendorf Centrifuge 5804 R). The pellets were washed three times in 20 mL ice-cold 10 % (v/v) glycerol and centrifuged (15 min, 5,000 rpm, 4 °C) increasing the centrifugation time by 2 min each round. Cell suspension was pooled at the beginning of the washing to process only two falcon tubes at the same time. Each pellet was finally resuspended in 0.8 mL ice-cold 10 % (v/v) glycerol and 150 μ L aliquots were frozen in liquid nitrogen. The aliquots were stored frozen at -70 °C until used. Electro-competent cells for the transformation with replicative plasmids were prepared by a modified protocol from 5 mL BHI culture in reaction tubes. Fresh medium was inoculated with a single colony and incubated for 6 h at 30 °C shaking at 120 rpm. The culture was harvested in 15 mL falcon tubes (Eppendorf Centrifuge 5804 R, 10 min, 5,000 rpm, 4 °C) and the pellet was resuspended in 1 mL ice-cold 10 % (v/v) glycerol. The suspension was transferred to an 1.5 mL Eppendorf cup and centrifuged in a bench-top centrifuge (Eppendorf Minispin, 1 min, 13,400 rpm). The washing step was repeated twice, the cell pellet was resuspended in 80 μ L ice-cold 10 % (v/v) glycerol and stored as before.

3.4.10 Transformation

3.4.10.1 *Escherichia coli* Competent cells of *E. coli* were transformed with plasmid DNA by electroporation (Dower et al., 1988). Per aliquot of competent cells, 3-5 μ L of DNA was added (aiming at a total of about 500 ng DNA) and the suspension was transferred to the electroporation cuvette (Eppendorf, 1 mL, 2 mm gap width). A 2,500 V electroporation pulse was given (4-5 ms time constant), the suspension was

mixed with 1 mL 2x YT medium and transferred to another fresh 4 mL of the same medium in a reaction tube. After recovery (50 min, 37 °C shaking at 120 rpm) 100 μ L of the culture was spread on selective agar plates and incubated at 37 °C O/N.

3.4.10.2 *Corynebacterium glutamicum* Likewise, competent *C. glutamicum* cells were transformed by electroporation. Having added 3-5 μ L plasmid DNA (about 500 ng) to one aliquot of electro-competent cells, the suspension was transferred to a clean electroporation cuvette (Eppendorf, 1 mL, 2 mm gap width) and incubated for 5 min on ice. After electroporation (2,500 V pulse, 3.5-4.0 ms time constant), cells were resuspended in 1 mL of BHIS medium, transferred to another 4 mL remaining in the reaction tube and subjected to an additional heat shock (6 min in a 46 °C water bath) as described by van der Rest et al. (1999) before leaving them to recover (50 min, 30 °C, shaking at 120 rpm). The entire cell suspension was concentrated to a final volume of 100 μ L by centrifugation, spread on selective agar plates and incubated for 2 days at 30 °C.

3.4.11 Sequencing & analysis

Inserts in the final plasmid that resulted from PCR amplification were routinely checked by sequencing to be free of mutations. 400-500 ng plasmid DNA and 2.5 μ M of the appropriate sequencing primer were mixed in a total volume of 10 μ L and sent for sequencing by the *GATC LIGHTrun* tube service (GATC Biotech AG, Constance, Germany). At least duplicate coverage of the amplified insert sequence was assured by the selection of suitable number and binding location of the sequencing primer. Online sequencing results were processed and aligned against the reference structure using the *DNA Baser* software (HeracleBiosoft, Pitesti, Romania).

3.4.12 Chromosomal integration & deletion in *C. glutamicum*

Integrations and deletions in the *C. glutamicum* genome were performed with pK19*mob-sacB* derived plasmids (Schäfer et al., 1994). Two homologous regions of 500 bp length, each, were used to target the correct integration/ deletion site in the genome of *C. glu-*

tamicum. Recombinant genetic information was inserted between *cg3344* and *cg3345* (designated as CgLP13, Lange et al. (2017)). The desired integration sequence was flanked by 500 bp sequences homologous to the target site as described before. In the other case, entire genes or operons were deleted by cloning 500 bp homologous regions into pK19*mobsacB* adjacent to each other. The genomic cassette exchange is governed by the selection/ counter-selection principle provided by the vector backbone. After transformation of competent cells with plasmid DNA by electroporation according to the protocol (3.4.10.2), cells were selected on BHIS agar plates containing 50 μg kanamycin mL^{-1} (2 days at 30 °C). Since pK19*mobsacB* does not replicate in *C. glutamicum*, kanamycin resistance was only conferred by integration of the entire plasmid by homologous recombination inside one of the two homologous regions. Excision of the vector backbone was ensured by counter-selection on 2x YT agar plates containing 100 g sucrose L^{-1} . The production of levansucrase encoded by the *sacB* gene on pK19*mobsacB* is lethal for *C. glutamicum* in the presence of sucrose unless the functional expression of *sacB* is somehow prevented - either by a second homologous recombination or by a mutation of *sacB* itself or its promoter. Single kanamycin resistant (Kan^{R}) colonies were cultivated in reaction tubes containing 5 mL 2x YT liquid medium for 6 h at 30 °C (shaking at 120 rpm) and 100 μL 10^{-2} dilutions in VE- H_2O were spread on 2x YT agar plates containing 100 g sucrose L^{-1} (incubation for 2-3 days at 30 °C). Suc^{R} cells had to be checked for the correct genotype in the following: Undesired mutations inside *sacB* or its promoter were identified by patch-plating on sucrose containing vs. kanamycin containing 2x YT agar plates. Only kanamycin sensitive (Kan^{S}) cells had undergone a second homologous recombination. Discrimination between cells having excised the entire plasmid and those having excised only the vector backbone was finally performed by colony PCR on Kan^{S} Suc^{R} cells.

3.5 Cultivation experiments

3.5.1 Cryogenic cultures

All strains were maintained in cryogenic cultures (30 % (v/v) glycerol stocks) at -70 °C. Strains were cultivated starting from single colonies in 5 mL 2x YT complex medium to mid-exponential phase (6 h) at the appropriate growth conditions (*E. coli* at 37 °C, *C. glutamicum* at 30 °C; shaking at 120 rpm). 700 µL of the cell suspension was added to 300 µL glycerol in cryogenic tubes, that had been sterilized previously, and stored frozen at -70 °C.

3.5.2 Generic seed train

The standard seed train for all cultivation experiments is outlined graphically in fig. 4 on the next page. Each replicate of an experiment was started from cryogenic cultures that were streaked on (selective) 2x YT agar plates and incubated for 2-4 days at 30 °C. A reaction tube containing 5 mL 2x YT liquid culture was inoculated from a single colony and incubated O/N at 30 °C shaking (120 rpm). The entire culture was transferred to a fresh 50 mL 2x YT liquid culture (in a 500 mL baffled shaking flask) and incubated 6-8 h at identical conditions. An appropriate volume of the culture was harvested by centrifugation (Eppendorf Centrifuge 5804 R, 10 min, 5000 rpm, RT), resuspended in 2 mL sterile 0.9 % (w/v) NaCl and used to inoculate the last preculture (50 mL CgXII in a 500 mL baffled shaking flask) to a starting OD₆₀₀ of 1. The preculture was incubated O/N at 30 °C shaking at 120 rpm and again the appropriate volume of culture was harvested as before and resuspended in 2 mL sterile 0.9 % (w/v) NaCl. The main culture (50 mL CgXII medium in 500 mL baffled shaking flask) was inoculated to a starting OD₆₀₀ of 1 and incubated for 24-25 h at 30 °C shaking at 120 rpm.

3.5.3 Shaking flask experiments

3.5.3.1 Cultivation conditions When the strain performance in different growth conditions (media) was tested, the set of main cultures was inoculated from identical precul-

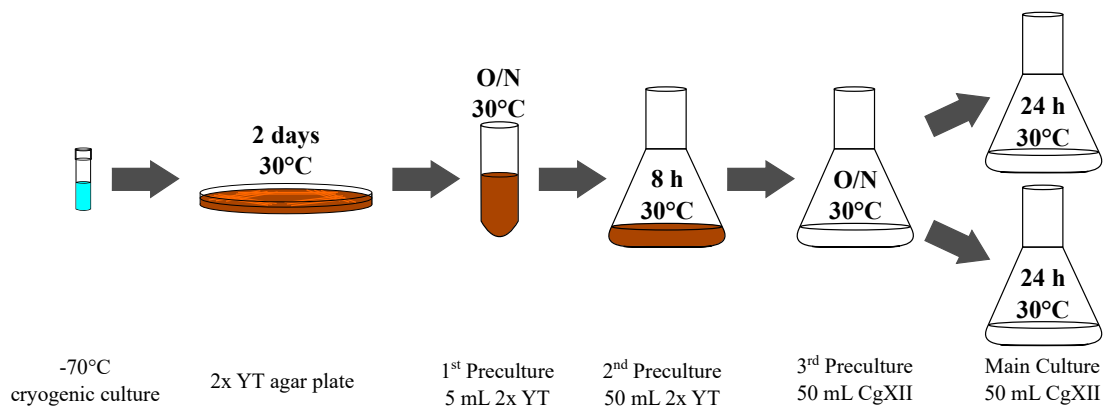


Figure 4: Schematic depiction of the generic seed train applied for growth experiments comparing different cultivation conditions. Main cultures differing e.g. in the supplementation (with/without PCA, NaHCO_3) were inoculated from an identical preculture in CgXII minimal medium (3.2.4).

ture conditions. The standard screening approach of each strain in CgXII minimal medium (3.2.4) consisted of (i) reference culture without supplements, (ii) medium supplemented with $195 \mu\text{M}$ protocatechuic acid (PCA) and (iii) medium supplemented with 30 mM NaHCO_3 . Iron starvation and excess conditions during the validation of reporter strains (1 and $100 \mu\text{M}$ FeSO_4 , respectively) were already established in the last CgXII preculture (fig. 5) as described by Wennerhold and Bott (2006). Iron depleted medium (trace element solution without FeSO_4) was established by the addition of $250 \mu\text{M}$ of the Fe^{2+} specific chelator 2,2-bipyridyl in the main culture (Frunzke et al., 2011). Iron depleted main cultures were inoculated from precultures in minimal medium containing $100 \mu\text{M}$ FeSO_4 (iron excess).

To monitor growth, the cell density of cultures was measured every hour for at least 11 hours by the optical density at 600 nm (OD_{600}).

3.5.3.2 Fluorescence experiments Two types of fluorescence experiments were carried out: When the bioreporter strains were validated in iron excess and starvation, fluorescence was detected in parallel with the cell density over the full range of sampling. When fluorescence should be analysed in the standard screening approach, the seed train was

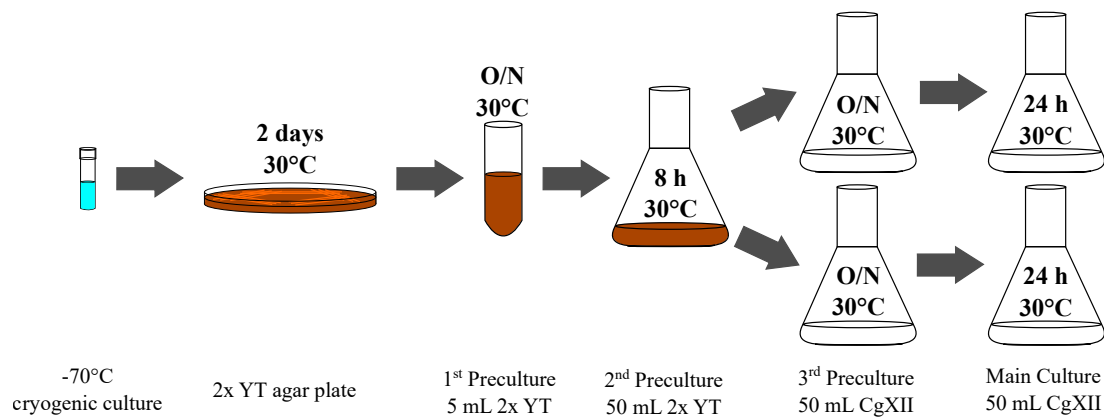


Figure 5: Schematic depiction of a seed train imposing differences in iron availability. Iron starvation ($1 \mu\text{M}$) and excess ($100 \mu\text{M}$) conditions were already established in the CgXII preculture (Wennerhold and Bott, 2006).

performed as described above (3.5.2) with strain FEM3 and derivatives thereof. The main culture was incubated for 24 h at 30°C shaking at 120 rpm and OD_{600} as well as fluorescence was detected at the end point.

3.5.4 Bioreactor cultivation

Controlled bioreactor cultivations were performed in batch mode in 1.5 L stainless steel bioreactors with a starting volume of 800 mL CgXII basic medium lacking urea and MOPS buffer. The identical bioreactor equipment was described before (Blombach et al., 2013). $40 \text{ g glucose L}^{-1}$ was provided as the sole carbon and energy source. The temperature was controlled at 30°C and the cultivation pH was maintained at 7.4 by the addition of 25 % ammonium hydroxide. Always, two parallel fermentations were inoculated from identical precultures to a starting $\text{OD}_{600} = 2$. Both reactors were operated at a total pressure of 1.5 bar and contained six-blade rushton-type impellers starting at 300 rpm that were individually upregulated to maintain the dissolved oxygen concentration above 35 %. Reactor 1 was aerated with 0.5 vvm pressurised air (ambient/standard pCO_2) and reactor 2 with synthetically mixed gas containing 20 % CO_2 , 21 % O_2 and 59 % N_2 (high pCO_2).

3.5.5 BioLector cultivation

Miniaturised cultivations were performed in the BioLector (m2p-labs Baesweiler, Germany). One cavity of the MTP-48-FlowerPlate was filled with 1 mL culture in CgXII standard medium (3.5.2) containing 20 g glucose L⁻¹ and incubated for > 24 h shaking at 30 °C at a constant 1000 rpm. Cell density (backscatter at a wavelength $\lambda = 620$ nm, gain 20) and fluorescence ($\lambda_{\text{ex}} = 488$ nm, $\lambda_{\text{em}} = 520$ nm, gain 75) were measured automatically at intervals < 20 min. Backscatter values of a blank control (medium without inoculum) of each condition was measured on the same plate and subtracted from samples as background. Biomass specific fluorescence was calculated by normalising fluorescence data to the backscatter value of the respective culture. Growth conditions were chosen as before and the addition of 1 mM of the Fe²⁺ specific chelator bathophenanthroline disulfonic acid (BPS) in the same cultures was tested.

3.5.6 Biological replicates

Cultivation experiments were performed at least in three independent biological replicates. By definition, this comprises cultivation on different days in individually prepared growth media that were inoculated from individual seed trains. Seed trains were started by streaking out cryogenic cultures on agar plates. If not explicitly stated otherwise, data represent mean values of the triplicates with error bars indicating the standard deviation. When appropriate, differences between strains and cultivation conditions were tested for statistical significance by a (Student's) two-sample t-test.

3.6 Protein biochemistry

3.6.1 DtxR (over-)production

Wildtype DtxR protein and derivatives were purified by a C-terminal purification tag for biochemical characterisation. Plasmid-encoded expression of *dtxR* was performed in *E. coli* DH5 α and specific differences of the expression hosts are listed in tab. 4. Protein production was always performed by using the standard protocol. Cryogenic cultures

(glycerol stocks) were streaked on 2x YT agar plates containing $100 \mu\text{g mL}^{-1}$ ampicillin (Amp¹⁰⁰) and incubated for 24 h at 37 °C. Cell material from these plates was used to inoculate 5 mL 2x YT Amp¹⁰⁰ liquid cultures (test tubes) and incubated O/N at 37 °C shaking at 120 rpm. 1.5 mL of the O/N culture was transferred to 150 mL 2x YT Amp¹⁰⁰ in 1 L baffled shaking flasks and incubated under identical conditions. At an OD₆₀₀ of 0.84 *dtxR* expression was induced by the addition of L-rhamnose to a final concentration of 0.2 % (w/v) (transferring 1.5 mL of a 20 % (w/v) stock solution to the main culture). The cultivation was continued for 6 h at 30 °C before harvesting 3 x 50 mL by centrifugation (50 mL falcon tubes in Eppendorf Centrifuge 5804 R, 10 min, 5,000 rpm, 4 °C). Cell pellets were stored frozen at -20 °C until further processing.

3.6.2 Protein purification

3.6.2.1 Cell disintegration Biomass was thawed on ice for about 15 min. Cell pellets were resuspended in 2 mL buffer NP (50 mM NaH₂PO₄, 300 mM NaCl, pH 8.0 adjusted with NaOH) containing 10 mM imidazole and 2 mg mL⁻¹ lysozyme (His tagged proteins) or buffer NP containing only 2 mg mL⁻¹ lysozyme (Strep tagged proteins). The suspension was transferred to 15 mL falcon tubes and cell disruption was performed by 5 cycles of sonication (Sonopuls HD2200, Bandelin, Berlin, Germany, tip type MS73, 30 s, power: 40 %). The cell suspension was maintained on ice during sonication and left 1 min on ice for cooling down between two cycles. Cellular debris was finally removed by centrifugation (30 min, 14,000 rpm, 4 °C in Eppendorf 5804 R centrifuge).

3.6.2.2 Ni-NTA affinity chromatography His tagged protein was purified with the *QIAexpress Ni-NTA fast start kit* (Qiagen, Hilden, Germany) as described in the *Protocol: purification of 6x His tagged proteins under native conditions* (QIAexpress Ni-NTA Fast Start Handbook 07/2011, page 17-18). Cell lysate was applied to a Fast Start Column containing nickel-nitriloacetic acid (Ni-NTA) resin. The column was washed twice with 4 mL native wash buffer and protein was recovered in two consecutive elution steps with 1 mL native elution buffer, each. The column was regenerated with two times 10 mL

0.5 M NaOH and finally stored in 30 % (v/v) ethanol at 4 °C.

3.6.2.3 Strep-Tactin affinity chromatography Proteins carrying a Strep tag II were purified according to the *Protocol: Batch Purification of Strep-tagged Proteins using Strep-Tactin Superflow Plus* (Strep-tagged Protein Purification Handbook 07/2011, Qiagen, Hilden, Germany). Cell lysate was mixed with 2 mL Strep-Tactin Superflow Plus resin suspension (Qiagen, Hilden, Germany) in a 15 mL falcon tube and incubated for 60 min at 4 °C shaking. The suspension was transferred to a column and washed twice with 4 mL buffer NP (3.6.2.1). Purified protein was eluted with six times 0.5 mL buffer NPD (buffer NP containing 2.5 mM desthiobiotin). Strep-Tactin Superflow Plus resin was regenerated by several wash steps with Strep-Tactin Regeneration buffer (5 x 6 mL; buffer NP containing 1 mM hydroxyphenylazobenzoic acid) and buffer NP (2 x 8 mL). The resin was eventually stored in buffer NP at 4 °C.

3.6.3 Protein analysis

3.6.3.1 Quantification of the protein concentration The protein concentration was determined using the Pierce™ BCA Protein Assay kit (#23227, Thermo Fisher Scientific Inc., Bremen, Germany) according to the manufacturers instructions for 96-well plate scale. The absorbance at 562 nm was eventually measured on a Synergy 2 (BioTek Instruments, Bad Friedrichshall, Germany) and the protein concentration was deduced from the comparison with a 9-point calibration utilising the BSA standard solution provided in the kit.

3.6.3.2 SDS-PAGE Protein analysis and evaluation of the purification success was routinely performed by sodium dodecyl sulfate-polyacrylamide gel electrophoresis (SDS-PAGE) following the protocol provided by Sambrook and Russell (2001). Denatured peptides covered with the negatively charged molecule SDS are separated in an electric field according to their molecular mass. If not stated otherwise, gels consisted of a 10 % separating gel and 6 % stacking gel, that were prepared as indicated in tab. 14 and

15, respectively. 4.5 mL of the 10 % separating gel was pipetted between two glass plates, layered with isopropanol to obtain a straight gel edge and left for 30-60 min until the polymerisation was finished. After removing the isopropanol, the remaining slice was filled with the 6 % stacking gel and a comb was inserted. The gel was left for another 30-60 min to solidify. The gel was placed in a vertical SDS-PAGE chamber (BioRad Laboratories Inc., Hercules, California, USA) filled with running buffer (25 mM Tris/HCl, 192 mM glycine, 0.1 % (w/v) SDS). Protein samples were mixed with an equal amount of 2x SDS sample buffer (10 mM Tris/HCl pH 6.8, 4 % (w/v) SDS, 0.02 % (w/v) bromophenol blue, 20 % (v/v) glycerol, 200 mM DTT) and heated for 5 min at 95 °C (heating block) to support unfolding. The gel pockets were loaded with either 5 μ L of the protein ladder PageRuler™ (art. no. #26616, Thermo Fisher Scientific Inc., Bremen, Germany, fig. S6a in the appendix) or 10 μ L of the protein samples. Proteins of different sizes were then separated for 50 min at 200 V (Biometra Power Pack P25, Analytik Jena, Jena, Germany). The glass plates were removed and the gel was washed once with VE-H₂O before staining it O/N in Coomassie Brilliant Blue stain solution (50 % (v/v) methanol, 10 % (v/v) acetic acid, 1 g Coomassie Brilliant Blue L⁻¹). The gel was finally destained 3-4 times (30-60 min) in fresh destaining solution (20 % ethanol, 10 % acetic acid) until the protein bands became nicely visible.

Table 14: Composition of 10 % separating gels; volumes were prepared to cast at least 4 gels at the same time; protocol adapted from Sambrook and Russell (2001)

Compound	Volume
40 % acrylamide	8 mL
VE-H ₂ O	15.3 mL
1.5 M Tris/HCl (pH 8.8)	8 mL
10 % (w/v) SDS	320 μ L
10 % (w/v) ammonium persulfate	320 μ L
TEMED	32 μ L
total volume	32 mL

Table 15: Composition of 6 % stacking gels; volumes were prepared to cast at least 4 gels at the same time; protocol adapted from Sambrook and Russell (2001)

Compound	Volume
40 % acrylamide	3 mL
VE-H ₂ O	14.1 mL
1 M Tris/HCl (pH 6.8)	2.5 mL
10 % (w/v) SDS	200 μ L
10 % (w/v) ammonium persulfate	200 μ L
TEMED	20 μ L
total volume	20 mL

3.6.3.3 native PAGE Protein dimerisation was analysed by native PAGE. Gels and buffer were prepared and conditions applied as described for SDS PAGE (3.6.3.2) leaving out denaturing agents such as SDS, DTT and omitting heating of the samples. During native PAGE, the migration of peptides in the electric field depends on its net charge. If the isoelectric point (pI) of the protein is lower than the buffer pH it presents a negative net charge and migrates towards the positively charged anode (as it was the case for DtxR at pH 8.8). 5 μ L nativeMark™ unstained protein standard (art. no. #LC0725, Thermo Fisher Scientific Inc., Bremen, Germany, fig. S6b in the appendix) was loaded at least to one lane of the gel in order to estimate the molecular weight of proteins of interest. In order to analyse DtxR dimerisation upon different concentrations of divalent metal ions and reductants, samples were mixed as indicated and incubated for 30 min at RT on top of the bench before loading it on the gel.

3.6.3.4 Differential scanning fluorimetry Protein stability is the product of a number of parameters such as pH and osmolarity of the buffer or the concentration of cofactors and interaction partners. Denaturation of proteins can be monitored in thermal shift assays by an increase of the fluorescence signal as the fluorophore binds to gradually exposed hydrophobic areas of the unfolding protein (Niesen et al., 2007). The melting temperature (T_m) of the protein at the given conditions is defined as the inflection

point of the melting curve (fluorescence over temperature). 50 μL sample consisted of 5 μL protein solution (approx. 0.5 mg mL⁻¹, precipitation removed by centrifugation) in 100 mM buffer (HEPES or KOH at pH 7.4), 600 mM NaCl and 5 mM DTT. 1 μL SYPRO™ Orange (Thermo Fisher Scientific Inc., Bremen, Germany) was added immediately before starting the assay. Divalent metal ions were provided as NiCl₂ (0.1 μM - 1 mM), MnCl₂, MgCl₂ and CaCl₂ (0.1 μM - 5 mM). When anions were supplied as potassium phosphate, ammonium sulfate (10 - 100 mM) or sodium bicarbonate (10 - 200 mM), the total osmolarity of the sample was compensated by reducing the NaCl concentration accordingly. The temperature gradient was controlled by the Mastercycler EP Realplex² (epgradient S) (Eppendorf, Hamburg, Germany); 20 °C for 15 s, 20 °C → 90 °C in 30 min, 90 °C for 15 s; lid heating off. Output data was further processed manually by plotting the absorbance at 550 nm over the temperature. T_m was determined in the inflection point of a 4th order polynomial fit through the data points in the relevant temperature range. For every single condition, mean T_m and standard deviations were calculated from at least four replicates. Dissociation constants (K_D) are indicative for the binding affinity of specific metal ions to the protein. K_D values were determined for Ni²⁺ and Mn²⁺ interacting with wt-DtxR and DtxR(C102D) in the absence and presence of NaHCO₃ by fitting the simple cooperative model (Vivoli et al., 2014) to our data.

3.7 Pull-down experiments

For the identification of potential DtxR interaction partners, Strep-tagged DtxR was overexpressed in *C. glutamicum* WT. In theory, following a cross-linking step with formaldehyde, that linked the interacting proteins covalently to DtxR, the standard purification procedure yielded “co-purified” proteins alongside with DtxR, which were sent for protein sequencing.

3.7.1 Cultivation

C. glutamicum WT (pVWEx1-*dtxR*) was cultivated in the parallel bioreactor fermentation set up as outlined above (3.5.4). Main cultures were inoculated to a starting OD₆₀₀ of 1 from a complex preculture in 2x YT to mimic the original seed train (Blombach et al., 2013). The CgXII cultivation medium contained an additional 0.5 mM IPTG for induction of *dtxR* expression. At an approximate OD₆₀₀ = 4, 4 h after inoculation 250 mL suspension was withdrawn from each bioreactor and filled into 50 mL falcon tubes.

3.7.2 Formaldehyde cross-linking

In accordance with the protocol established by Herzberg et al. (2007) 810 μ L 37 % formaldehyde was added to each tube containing 50 mL cell culture and incubated for 20 min at 30 °C in a water bath. By this cross-linking reaction covalent bonds are supposed to be formed between macromolecules located to each other at a distance of 2 Å or closer. Biomass was eventually harvested by centrifugation (Eppendorf Centrifuge 5804 R, 10 min, 5,000 rpm, 4 °C) and pellets were stored at -20 °C until further processing.

3.7.3 Sample preparation

Frozen cell pellets were thawed on ice, resuspended in 400 μ L buffer NP containing 10 % (v/v) glycerol and transferred to cryo tubes filled with 300 μ L glass beads (0.1 mm). Biomass was disintegrated with the Precellys 24 homogenizer (Peqlab, Erlangen, Germany) for 3x 20 s at 6,500 rpm, 5 min cooling on ice between each run. Glass beads and debris were removed by centrifugation (Eppendorf Centrifuge 5804 R, 10 min, 14,000 rpm, 4 °C). Supernatants were pooled and Strep-tagged DtxR protein with covalently bonded interaction partners was purified by affinity chromatography as described above (3.6.2.3). The protein concentration was enhanced by the SDS/ KCl precipitation protocol provided by Dennison (2013) and peptides were separated by SDS PAGE

(3.6.3.2). Distinct protein bands that were found exclusively at high CO₂ cultivations were cut out with a scalpel and sent for sequencing.

3.7.4 Peptide analysis (commercial)

For peptide analysis the commercial service offered by Proteome Factory AG (Berlin, Germany) was employed. After solubilising proteins from the gel slices and tryptic digest, resulting peptides were analysed by mass spectrometric means using a nanoLC-MS/MS device. Peptide sequences were mapped onto bacterial proteomes and protein hits were presorted according to the number of hits by different and identical peptides using bioinformatic tools.

3.7.5 Manual re-processing & discrimination of data

Raw data (= list of peptides) was re-processed in order to restrict hits to the *C. glutamicum* proteome (BLAST search⁷). Proteins with only a single hit were ignored due to the randomness of the result. Proteins that were present in the sample as suggested by multiple hits were sorted by the total number of hits from different peptides in the sample, identical peptides in the sample and total number of peptides from all samples taken together. The assessment of biologically plausible interaction partners was finally based on the knowledge of the intracellularly abundant proteome (Hansmeier et al., 2006; Schaffer et al., 2001; Schluesener et al., 2005; Schluesener et al., 2007).

3.8 Analytics

3.8.1 Quantification of the cell density

Growth of *C. glutamicum* cultures was monitored by the optical density of the suspension at 600 nm (OD₆₀₀). The biomass concentration as g cell dry weight (CDW) L⁻¹ was calculated from the OD₆₀₀ given the correlation factor $CDW = OD_{600} * 0.21$ determined

⁷blast.ncbi.nlm.nih.gov/Blast.cgi?PROGRAM=blastp&PAGE_TYPE=BlastSearch&LINK_LOC=blasthome; accessed: December 2016 - January 2019

previously (Schwentner et al., 2019) and is specific for this spectrophotometer (Ultrospec 10 Cell Density Meter, GE Healthcare, Little Chalfont, UK).

3.8.2 Fluorescence detection

The DtxR activation state was monitored in the bioreporter strains *in vivo* by fluorescence. 100 μL culture was transferred into one well of a 96-well microtiter plate and the fluorescence was detected using the Synergy 2 device (BioTek Instruments, Bad Friedrichshall, Germany) at 37 °C with the following settings: excitation wavelength = 485/20 nm, emission wavelength 528/20 nm (wavelength/bandwidth) as by Failmezger et al. (2016). When the cell density of the culture was higher than $\text{OD}_{600} = 11$, it was appropriately diluted with 0.9 % (w/v) NaCl. Nonspecific fluorescence of the culture background was subtracted from the biomass fluorescence after removing cells by centrifugation. To account for the different growth kinetics, fluorescence values were typically provided as biomass specific fluorescence (RFU CDW^{-1}).

3.8.3 Intracellular iron quantification

3.8.3.1 Cultivation & harvest For the quantification of the total intracellular amount of iron, 50 mL *C. glutamicum* WT main cultures in CgXII medium were set up as described before (3.5.3.1). Several identical cultures were set up and inoculated from the same preculture. After inoculation every 2 h OD_{600} of one of the identical 50 mL shaking flask cultures was determined and the entire culture was harvested in 50 mL falcon tubes by centrifugation (Eppendorf Centrifuge 5804 R, 20 min, 5000 rpm, 4 °C), washed in 20 mL 0.9 % NaCl and the cell pellet was stored frozen at -20 °C until further use.

3.8.3.2 Cell disruption Biomass was thawed on ice, resuspended in an appropriate volume of 50 mM NaOH to achieve an OD_{600} between 70-100. The precise OD_{600} was determined and about 850 μL of the suspension was transferred to a cryo tube containing 250 μL glass beads (0.1 mm). The entire biomass was disintegrated using a Precellys 24

homogenizer (Peqlab, Erlangen, Germany) for 4 x 180 s at 6,000 rpm. Disruption was carried out in technical duplicates.

3.8.3.3 Ferrozin based iron quantification The total iron content of the biomass was finally determined by a slightly modified method described by Riemer et al. (2004). 100 μL cell suspension was mixed with 100 μL 10 mM HCl and 100 μL iron release reagent (equal amounts of 4.5 % (w/v) KMnO_4 and 1.4 M HCl) and incubated for 2 h at 60 °C shaking at 1,100 rpm (Thermomix 5436, Eppendorf, Hamburg, Germany) in order to liberate the entire amount of incorporated and stored iron. Once cooled down to RT, 100 μL detection reagent (1 M ascorbic acid, 2.5 mM ammonium acetate, 6.5 mM ferrozin, 6.5 mM neocuproin) was added and incubated for another 30 min shaking at RT. Precipitations were removed by centrifugation (Eppendorf Minispin, 3 min, 13,400 rpm), 100 μL of each sample supernatant was transferred to the wells of a 96-well microtiter plate and the absorbance was detected at 550 nm using the Synergy 2 device (BioTek Instruments, Bad Friedrichshall, Germany). Iron was detected in complex with Fe^{2+} specific ferrozin following the reduction of ferric iron (Fe^{3+}) thorough ascorbic acid. Iron concentrations were calculated by a 17-point external calibration curve of FeCl_3 dissolved in 10 mM HCl at concentrations ranging from 0 to 300 μM .

3.8.4 Iron reduction assay

Iron reduction assays are based on the detection principle described above (3.8.3) and depicted schematically in fig. 6. Fe^{2+} is captured by Fe^{2+} specific iron chelators (ferrozin or BPS) leaving characteristic absorbance peaks that can be detected spectrophotometrically (Smith et al., 1952; Cowart et al., 1993; Riemer et al., 2004). The optimized reaction mixture comprised 0.5 mM FeCl_3 (from a 10x stock solution in 10 mM HCl) and 3.5 mM NaOH for neutralisation, 200 mM MOPS buffer to maintain the solution pH at 7.4 and 6.5 mM BPS. Where indicated, protocatechuic acid or other benzoic acid derivatives were added at a final concentration of 19.5 μM . NaHCO_3 or KHCO_3 were applied at a concentration of 50 mM. It is also indicated, when reaction mixtures were

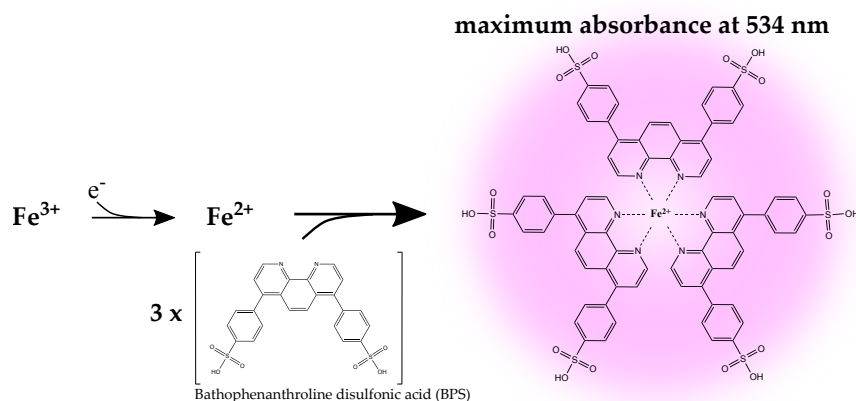


Figure 6: Iron reduction assay principle. Ferrous iron (Fe^{2+}) resulting from the chemical reduction of ferric iron (Fe^{3+}) forms complexes with bathophenanthroline disulfonic acid (BPS). The oxidation half of the redox reaction was in the focus of interest. BPS binds Fe^{2+} in a 3:1 stoichiometry with the absorbance peaking at 534 nm (Coward et al., 1993). The Fe^{2+} -BPS coordination was taken from Mudasir et al. (1998).

different from this optimised protocol, e.g. lacking buffer. If not stated otherwise, the reaction was started by the addition of the chelator BPS and 100 μL was transferred to one well of a 96-well microtiter plate for the detection of a reaction kinetic at 534 nm using the Synergy 2 device (BioTek Instruments, Bad Friedrichshall, Germany).

3.8.5 Detection of Fe^{3+} -PCA complexes

To monitor the formation of Fe^{3+} complexes with protocatechuic acid (PCA), reaction mixtures were set up as before (3.8.4) omitting BPS and increasing the PCA concentration to about 1.5 mM (to achieve a 3:1 stoichiometry for PCA:iron). The reaction kinetic was detected at 560 nm measuring every 5 min. Wavelength scans were performed at a step width of 1 nm between 400 and 700 nm.

3.8.6 LC-MS-QTOF analysis of aromatic compounds

The degradation of PCA during an extended reaction time was monitored by a decrease of the peak area measured by LC-MS-QTOF. Samples containing FeCl_3 , PCA, BPS

and NaHCO_3 or lacking NaHCO_3 (3.8.4) were prepared in a larger volume (1 mL) than before and incubated in 1.5 mL Eppendorf cups with closed lids. The reaction was started by the addition of BPS and after 0, 5 and 22 h 200 μL samples were transferred to a fresh 1.5 mL Eppendorf cup and stored frozen at $-20\text{ }^\circ\text{C}$ until further processing. Sample preparation and analysis was kindly performed by André Feith. Once thawed, samples (and commercial standards) were prepared for analysis in 60 % (v/v) acetonitrile, 0.75 mM EDTA and 10 mM ammonium acetate buffer (pH 9.2). An Agilent 1260 bio-inert HPLC system (Agilent Technologies, Waldbronn, Germany) coupled to an Agilent 6540 Accurate-Mass QTOF (Agilent Technologies, Santa Clara, CA, USA) was used for separation and detection, respectively. Alkaline HILIC LC and QTOF-MS parameters were chosen as described previously, and the analysis was carried out in the negative mode with a fragmentor voltage of 100 V in the MS mode (Teleki et al., 2015; Feith et al., 2019). The extraction of chromatograms and integration was carried out in MassHunter Qualitative Analysis software (Agilent Technologies, Waldbronn, Germany) using the *Find by Formula* algorithm. Potential oxidation products were identified via the molecular formula calculator feature based on the accurate mass, isotope abundances, and isotope spacing (B.07.00, Agilent Technologies, Santa Clara, CA, USA).

4.1 *In vitro* characterisation of DtxR

4.1.1 Purification and PAGE

In vitro characterisation of purified DtxR protein tried to address the question, whether CO₂ or its related species HCO₃⁻ could serve as a co-stimulus, thus, mediating the DtxR controlled regulatory response. In a first attempt, DtxR purification via (i) a C-terminal 6x His tag (DtxR-His) and (ii) a C-terminal Strep tag II (DtxR-Strep) was run in parallel. The protein concentration of DtxR-His elutions (1.22 mg mL⁻¹ and 0.68 mg mL⁻¹) was slightly higher than DtxR-Strep elutions 1 (0.51 mg mL⁻¹) and 2 (0.98 mg mL⁻¹). Qualitative differences between both affinity chromatographic purification approaches were not noted, as a single protein band of the expected molecular weight for DtxR (25.5 kDa⁸) became visible on a SDS PAGE gel (fig. 7), when the purified protein samples were denatured in the presence of DTT, following the standard protocol (3.6.3.2). However, when disulfide bond reducing DTT was omitted from the sample treatment, a second protein band appeared at around 60 kDa size, indicating the occurrence of DtxR dimers. The formation of covalently linked DtxR dimers was confirmed by native PAGE analysis (fig. 8) and could be abolished by increasing DTT concentrations in the sample treatment. A visible band indicating dimeric DtxR disappeared completely at 5mM and higher concentrations of DTT. In the following, 5 mM DTT was added during the purification procedure to prevent disulfide bond formation during purification and storage.

⁸http://web.expasy.org/compute_pi; accessed: 02/2016

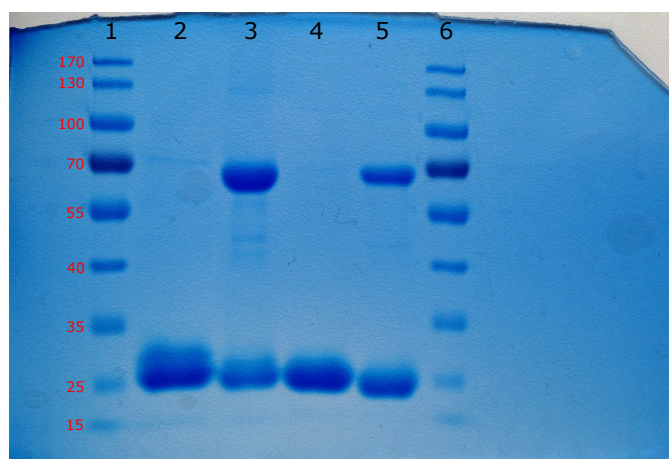


Figure 7: SDS PAGE of DtxR-His and DtxR-Strep in the absence and presence of disulfide bond reducing DTT; lane 1+6: ThermoScientific prestained PageRuler (the corresponding fragment sizes in kDa are indicated on the left), lane 2: DtxR-His + 0.1 M DTT, lane 3: DtxR-His without DTT, lane 4: DtxR-Strep + 0.1 M DTT, lane 5: DtxR-Strep without DTT

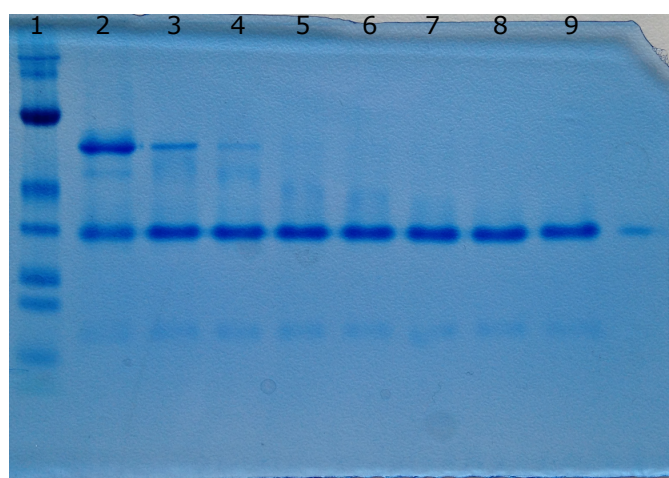


Figure 8: Native PAGE of DtxR-His incubated for 30 min at RT with increasing amounts of DTT; 12 % separating gel pH 8.8, 6 % stacking gel pH 6.8; gel run at 200 V for 60 min. lane 1: ThermoScientific prestained PageRuler, lane 2: 0 mM DTT, lane 3: 1 mM DTT, lane 4: 2 mM DTT, lane 5: 5 mM DTT, lane 6: 7.5 mM DTT, lane 7: 10 mM DTT, lane 8: 15 mM DTT, lane 9: 20 mM DTT; note that prestained PageRuler is not indicative for the size of native protein bands

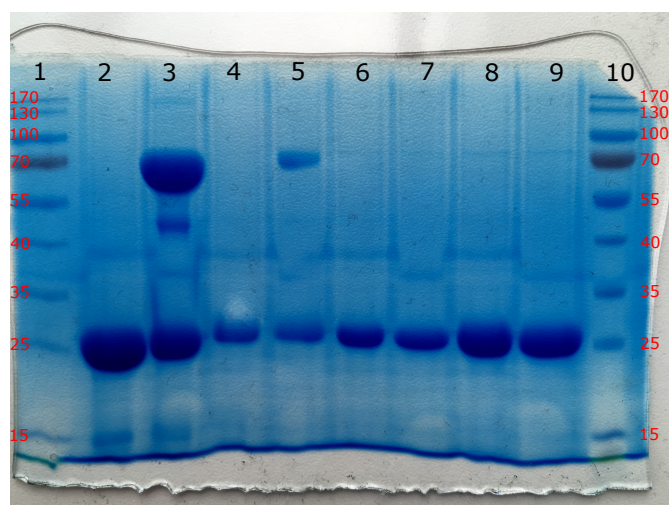


Figure 9: SDS PAGE comparing wt-DtxR (lane 2-5) and DtxR(C102D) (lane 6-9) spontaneous dimerisation; 12 % separating gel, 6 % stacking gel; lane 1: Thermo Scientific prestained PageRuler (corresponding fragment sizes in kDa are indicated on the left and right), lane 2: wt-DtxR (elution 2) + 0.1 M DTT, lane 3: wt-DtxR (elution 2) without DTT, lane 4: wt-DtxR (elution 3) + 0.1 M DTT, lane 5: wt-DtxR (elution 3) without DTT, lane 6: DtxR(C102D) (elution 1) + 0.1 M DTT, lane 7: DtxR(C102D) (elution 1) without DTT, lane 8: DtxR(C102D) (elution 2) + 0.1 M DTT, lane 9: DtxR(C102D) (elution 2) without DTT, lane 10: Thermo Scientific prestained PageRuler

In a second approach to counteract the irreversible denaturation of DtxR under oxidative conditions, the only thiol group within amino acid residue Cys102 of the DtxR protein was substituted with an Asp residue by a codon exchange (TGC → GAC) in the genetic sequence of *dtxR*. The mutated gene was overexpressed within pJOE6089 and purified by the Strep tag II as before. SDS PAGE analysis of the resulting protein DtxR(C102D) revealed no difference regarding the absence or presence of DTT during sample preparation (fig. 9). The protein band of 60 kDa size was completely vanished in all DtxR(C102D) samples, leaving only the monomeric protein band at 25 kDa.

4.1.2 Differential scanning fluorimetry

The melting temperature (T_m) of wt-DtxR in the absence of stabilising metal ions (46.3 ± 3.5 °C) was significantly increased in the presence of certain divalent metal ions. Addi-

tion of 1 mM Ni²⁺ increased the melting temperature by $\Delta T_m = 22.5 \pm 3.3$ °C (p-value of a t-test = 0.0006) and 5 mM Mn²⁺ by $\Delta T_m = 25.6 \pm 4.6$ °C (p-value < 0.0001). The stabilising effect of both metal ions was dose-dependent (fig. 10). Corresponding dissociation constants were calculated to $K_D(\text{Ni}^{2+}) = 5.3 \pm 1.1$ μM and $K_D(\text{Mn}^{2+}) = 21.8 \pm 3.6$ μM .

Unlike Ni²⁺ and Mn²⁺, DtxR could not be thermally stabilised in the presence of Mg²⁺ or Ca²⁺ (data not shown).

As outlined above, mutant DtxR(C102D) was constructed to prevent the irreversible denaturation of protein by the spontaneous formation of disulfide bonds between two DtxR monomers. T_m of DtxR(C102D) was reduced by approximately 4 °C under all tested conditions in comparison with wt-DtxR (fig. 10). However, the metal affinity of the protein remained unaffected by the amino acid substitution.

The dose dependent effect of anions, that are likely to interact with DtxR from literature (Qiu et al., 1996), on the DtxR thermal stability was analysed in the absence of metal ions and at 10 μM NiCl₂. The addition of 100 mM NaHCO₃ was tested over the full concentration range of NiCl₂ and MnCl₂. None of the tested anions (bicarbonate, sulfate or phosphate) could markedly increase the T_m of DtxR or DtxR(C102D) in any condition. It was concluded from these experiments, that bicarbonate does not provide a co-stimulus for the DtxR protein itself and, consequently, the focus of further experiments was shifted to investigate alternative activation mechanisms.

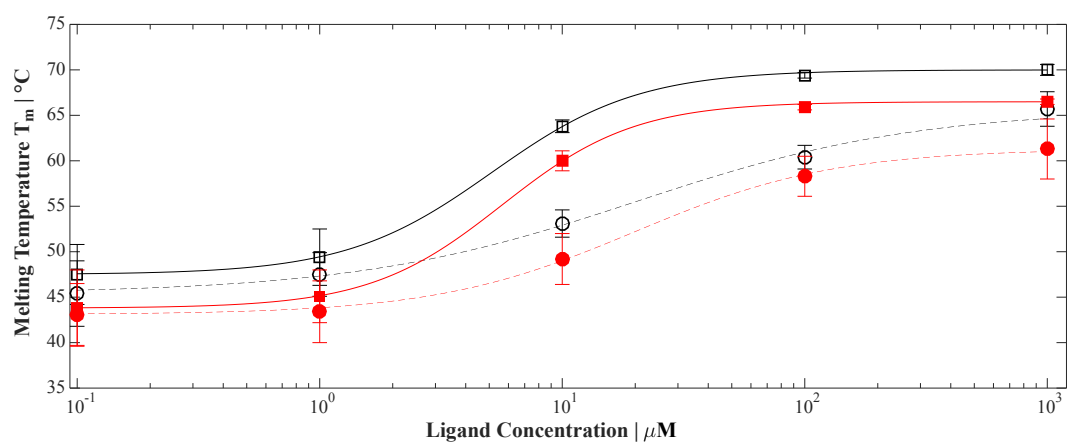


Figure 10: Thermal stabilisation of purified wt-DtxR (\square , \circ) and DtxR(C102D) (\blacksquare , \bullet) protein by different concentrations of the divalent metal ions Ni^{2+} (\square , \blacksquare) and Mn^{2+} (\circ , \bullet).

4.2 Pull-down experiments

Since differential scanning fluorimetry experiments indicated, that bicarbonate did not provide a direct stimulus for DtxR (4.1.2), the possibility was addressed next, that it could be an indirect DtxR stimulus. One could imagine that the CO₂ or HCO₃⁻ molecule binds to a CO₂/HCO₃⁻ sensing protein, which transmits the signal to DtxR via protein-protein interaction, in turn. Pull-down experiments were conducted with the aim to identify potential interaction partners of DtxR, that might represent such a modulator protein.

4.2.1 Cultivation & purification

The *dtxR* gene fused to a C-terminal Strep tag II for purification was overexpressed in the *C. glutamicum* WT background from the replicative plasmid pVWEx1 under control of the strong inducible P_{tac} promoter. *C. glutamicum* WT (pVWEx1-*dtxR*) grew comparably under both conditions revealing exponential growth rates of $\mu = 0.31 \text{ h}^{-1}$ (high pCO₂) and $\mu = 0.30 \text{ h}^{-1}$ (standard pCO₂). At the harvest point 4 h after inoculation both cultures had reached optical densities of OD₆₀₀ = 4.0 (equivalent to biomass concentrations of 0.84 g L⁻¹). After purification of Strep tagged DtxR and covalently bonded putative interaction partners, the protein solution was 10-fold concentrated in order to increase the visibility of faint protein bands on the gel. A set of protein bands was unique in the protein solution purified from the high pCO₂ cultivation (fig. 11). Five protein bands were selected from the high pCO₂ condition as indicated and sent for peptide sequencing at Proteome Factory AG.

4.2.2 Peptide identification & re-processing of the data

A tryptic digests of the bands containing DtxR and cross-linked proteins results in peptides of typically 10-20 amino acids length, which were analysed by a nanoLC-MS/MS approach at Proteome Factory AG (Berlin, Germany) and the peptide sequences were reported back to us. To figure out the origin of the individual peptides, a BLAST search

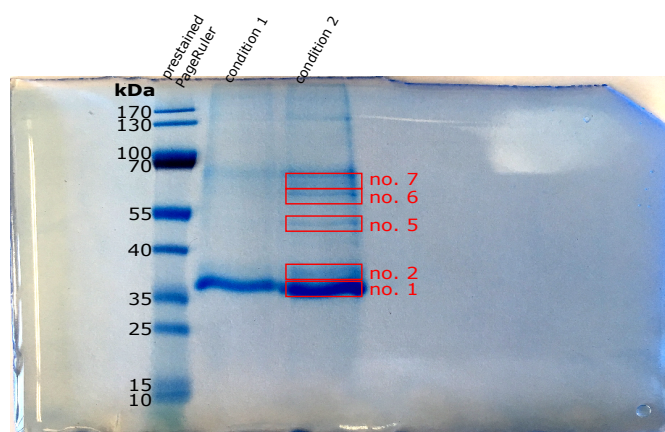


Figure 11: SDS PAGE of DtxR and potential interaction partners after formaldehyde cross-linking. lane 1: prestained protein ladder Page Ruler™ (Thermo Fisher Scientific), approx. molecular weight of the protein bands is indicated on the left. DtxR was purified from standard conditions aerated with ambient air (conditions 1 - lane 2) or high pCO₂ conditions aerated with 20 % CO₂ in the synthetically mixed inlet air (condition 2 - lane 3). Protein bands indicated as no. 1, 2, 5, 6 and 7 of lane 3 were cut out with a clean scalpel and sent to Proteome Factory AG for identification.

against the *C. glutamicum* ATCC 13032 (Bielefeld) proteome was performed⁹. In all five samples, most peptides belonged to the DtxR protein itself. Other proteins were ranked according to the total number of peptides which matched them (tab. 16). For each sample, the number of individual peptides mapping on the same protein were summed up as well as the total number including identical peptides that were identified multiple times. A final score was obtained from the addition of all the peptides in all samples that were attributed to the same protein. Proteins that were matched by a single peptide were ignored due to the randomness of the result.

Remarkably, the so far uncharacterised hypothetical protein encoded by *cg2444* was identified in every single sample and, thus, obtained the highest score. Most other proteins were considered to be highly abundant as they belonged to the central carbon metabolism (e.g. enolase or D-3-phosphoglycerate dehydrogenase) or protein biosynthesis (e.g. elongation factor Tu or charperone GroEL2) and therefore encountered in close

⁹blast.ncbi.nlm.nih.gov/Blast.cgi?PROGRAM=blastp&PAGE_TYPE=BlastSearch&LINK_LOC=blasthome; accessed: January - February 2017

Results

proximity to the DtxR protein which, in turn, increases the likelihood of being cross-linked to it.

Table 16: DtxR co-purified peptides. Pull-down experiments were performed *via* Strep tagged DtxR after formaldehyde crosslinking. Peptides resulting from a tryptic digest were analysed by nanoLC-MS/MS (Proteome Factory AG, Berlin, Germany) and mapped on the *C. glutamicum* ATCC 13032 (Bielefeld) proteome (BLAST). Proteins were ranked according to the number of peptides (identical and different) which could be attributed to it.

Gene	Annotated function	Number of different (all) peptides per sample mapped on the protein					Score
		1	2	5	6	7	
<i>cg2444</i>	Hypothetical Protein	1 (3)	2 (6)	3 (7)	3 (12)	2 (9)	37
<i>cg1111</i>	Eno - enolase (2-phosphoglycerate dehydratase)				4 (7)	8 (23)	30
<i>cg0587</i>	elongation factor Tu			8 (23)		1 (1)	24
<i>cg3011</i>	GroEL2 - molecular chaperone					8 (12)	12
<i>cg1451</i>	SerA - D-3-phosphoglycerate dehydrogenase				5 (9)		9
<i>cg1487</i>	LeuC - 3-isopropylmalate dehydratase large subunit				1 (1)	5 (8)	9
<i>cg2840</i>	ActA - acetyl-CoA hydrolase				6 (9)		9
<i>cg0802</i>	AccBC - biotin carboxylase and biotin carboxyl carrier protein			1 (1)	1 (1)	4 (6)	8
<i>cg1145</i>	FumC - fumarate hydratase				2 (3)	2 (4)	7
<i>cg0898</i>	PdxS - pyridoxal biosynthesis lyase		4 (6)				6
<i>cg0811</i>	methylmalonyl-CoA carboxyltransferase / acetyl-propionyl-CoA carboxylase / detergent sensitivity rescuer dtsR2					2 (4)	4
<i>cg1368</i>	AtpD - ATP synthase F0F1 subunit beta				3 (4)		4
<i>cg2291</i>	Pyk - pyruvate kinase					2 (4)	4
<i>cg2361</i>	cell division initiation protein					3 (4)	4
<i>cg0812</i>	methylmalonyl-CoA carboxyltransferase / acetyl-propionyl-CoA carboxylase / detergent sensitivity rescuer DtsR1					2 (3)	3
<i>cg1133</i>	GlyA - serine hydroxymethyltransferase			2 (3)			3
<i>cg3096</i>	Ald - aldehyde dehydrogenase				2 (3)		3
<i>cg0655</i>	RpoA - DNA-directed RNA polymerase subunit alpha			2 (2)			2
<i>cg0699</i>	GuaB2 - inosine 5'-monophosphate dehydrogenase					2 (2)	2
<i>cg2366</i>	FtsZ - cell division protein					2 (2)	2

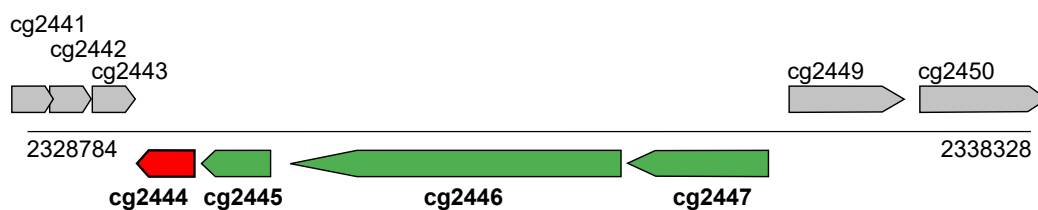


Figure 12: Genetic organisation around *cg2444* (in red) on the *C. glutamicum* ATCC 13032 genome displaying the putative operon structure (coloured, bold). Figure was generated in accordance with the genomic context displayed on the internet page coryneregnet.compbio.sdu.dk/v6e/CoryneRegNet/queryElement.php?gene=cg2446 (accessed: 29/03/2017).

4.2.3 Hypothetical protein Cg2444

The *cg2444* gene (NCgl2145 / Cgl2226) encodes an uncharacterised hypothetical protein¹⁰ consisting of 181 amino acids with a calculated molecular mass of 19.8 kDa and a pI of 4.3¹¹. Protein BLAST search did not reveal high similarity to known proteins and also secondary structure/ architecture prediction stayed without result. The gene might be expressed either in the predicted operon *cg2444* – *cg2445* – *cg2446* – *cg2447* with a transcriptional start site (TSS) upstream of *cg2447* (fig. 12) or as monocistronic transcript with individual TSS (Pfeifer-Sancar et al., 2013). Adjacent genes in the former operon encode proteins belonging to the iron uptake/utilisation group, i.e. *cg2445* encoding the heme oxygenase HmuO (Frunzke et al., 2011).

The amino acid sequence of Cg2444 exhibits a remarkably Gly-Pro rich C-terminus. Motifs consisting of the three amino acid Gly-Pro-Asp and Gly-Pro-Phe, respectively, appear in triplicates and are highlighted in bold:

```
>Cg2444
MVRSL GCKAH FGTRQ EVRNS TMAIK LSIDL SDATF AELSA VIGYA HQLGV
DADEK LTFEG TVLNI EFDGD LQFDD VFDAF DEAEI ELDNP REDGP IYADD
```

¹⁰as annotated in CoryneRegNet (coryneregnet.compbio.sdu.dk) and Uniprot (www.uniprot.org); query = *cg2444*; both accessed: 29/03/2017

¹¹web.expasy.org/compute_pi; accessed: 29/03/2017

LIDED EDYRA QTKSQ INDEV INEIR DGISS FVDGI VNGLG QGRRG GRYGD
FG **GPR GPR GPR** ND **GPF GPF GPF** GPG YRGPR F

A BLAST search of the C-terminal sequence, however, did not disclose similarities to proteins of other organisms. SmartBLAST detected > 50 % identity to the protein sequences of scavenger receptor class A member 5 and collectin-12, both from the zebra fish *Danio rerio* (fig. 13). The former protein forms part of the transferrin dependent iron delivery.

4.2.4 *Corynebacterium glutamicum* $\Delta cg2444$

A deletion mutant lacking the *cg2444* gene was constructed in the WT background. *Corynebacterium glutamicum* $\Delta cg2444$ behaved like the WT in shaking flask experiments (fig. S3a, CgXII medium with 20 g glucose L⁻¹ as carbon and energy source, with the standard supplements applied for screening as introduced in 4.5) and failed to produce unambiguous results when exposed in bioreactor cultivations to high and standard CO₂ content in the inlet air. A reporter strain of *Corynebacterium glutamicum* to monitor the DtxR activation state *in vivo* is introduced in 4.4 and experiments with the *cg2444* deletion in the reporter background of strain FEM3 are presented later (4.7). However, it should be anticipated here, that there were no indications of an altered DtxR activation/ functionality in response to the *cg2444* deletion. By this, Cg2444 could be neither confirmed nor denied as interaction partner of DtxR.

scavenger receptor class A member 5 [Danio rerio]
Sequence ID: [NP_001025361.1](#) Length: 499 Number of Matches: 1

Range 1: 306 to 334 [GenPept](#) ▼ Next Match ▲ Previous Match

Score	Expect	Method	Identities	Positives	Gaps	Frame
34.7 bits(78)	0.010()	Composition-based stats.	17/31(55%)	20/31(64%)	3/31(9%)	
Query 14	FGGPRGPRGPRNDGPFPGPFPG-PCYRGPR		43			
	F GP GP+G + D GP GP G PG+ GPR					
Sbjct 306	FQGPPGPKGZKGD--VGFLGPDGIPGWIGPR		334			

[GenPept](#)

PREDICTED: collectin-12 isoform X1 [Danio rerio]
Sequence ID: [XP_005163514.1](#) Length: 740 Number of Matches: 1

Range 1: 516 to 547 [GenPept](#) ▼ Next Match ▲ Previous Match

Score	Expect	Method	Identities	Positives	Gaps	Frame
32.7 bits(73)	0.046()	Composition-based stats.	17/32(53%)	18/32(56%)	1/32(3%)	
Query 12	GDFGGPRGPRGPRNDGPFPGPFPG-GRGPF		42			
	G+ G P P P DG GP GP GP G RGP					
Sbjct 516	GERGDFGIPGMPGRDQPGFTGPGQGPQLRGP		547			

Figure 13: SmartBLAST search of the carboxy-terminal protein sequence of Cg2444 (pos. 137-181: query sequence = GLGQRRRGGRYGDFFGGPRGPRG-PRNDGPFPGPFPGPFPGYRGPRF). Screenshot of the two hits for proteins of known function

4.3 Analysis of secreted compounds

So far, *in vitro* characterisation of DtxR and pull-down experiments were designed to investigate the potential activation of DtxR through CO₂/HCO₃⁻ directly as well as indirectly. However, the primary function of DtxR as master regulator is the control of iron homeostasis in response to the intracellular Fe²⁺ concentration. It might be assumed, that the latter is increased by elevated CO₂ levels and, thus, explain the transcriptional response of the DtxR regulon. In response to poor iron availability many microorganism secrete siderophores or small compounds, which chelate iron, increase the solubility of Fe³⁺ and facilitate the iron transport into the cell. Consequently, culture supernatants of bioreactor cultivations were kindly analysed by André Feith using an untargeted LC-MS-QTOF approach with the aim to identify differences in the occurrence and relative concentration of secreted compounds at high and standard CO₂ content in the inlet air. The focus was particularly on the appearance of protocatechuic acid or other known chelators in either of the two conditions, that would explain the greater iron availability at elevated CO₂ content.

Small PCA concentrations were detected in the samples, that varied neither with the CO₂ content nor with the cultivation time. In the negative detection mode, the peak area of the ion mass-to-charge ratio (*m/z*) 152.0365 increased remarkably during the cultivation, but exhibited no difference between high and low CO₂ contents. The molecular formula C₇H₇NO₃ could be proposed via accurate mass, natural isotope intensities and spacing. PubChem¹² suggestions for the molecular formula include a number of benzoic acid derivatives with structural similarities to PCA (tab. 17).

Consequently, a set of commercially available amino-hydroxy (bi-)functionalised benzoic acid derivatives was applied to the same analytical procedure for the identification of the unknown substance via the retention time (RT = 15.8 min). However, none of the tested substances coincided with the RT determined before and the set of candidate substances with the correct chemical formula and molecular weight (154 g mol⁻¹) is large,

¹²<https://www.ncbi.nlm.nih.gov/pccompound?term=c7h7no3>; accessed: February 2018

because positioning of the functional groups at the benzene ring allows a high degree of freedom. Since the purified substances are expensive – if commercially available at all – the screening was ceased at this point. A potentially iron chelating compound that was secreted by *C. glutamicum* but could not be identified successfully.

Table 17: Benzoic acid derivatives

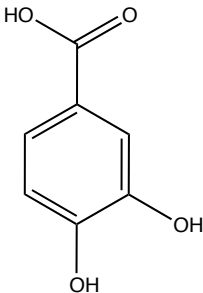
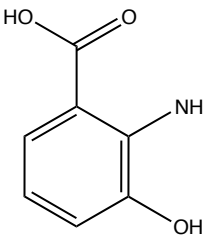
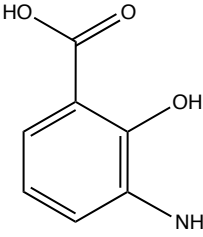
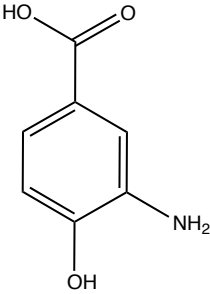
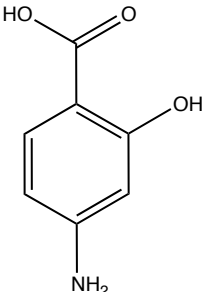
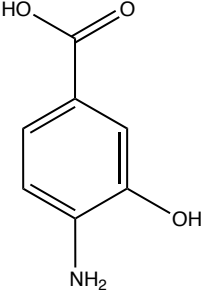
Abbreviation	Substance (trivial name)	Retention time	Structure
PCA	3,4-dihydroxybenzoic acid (protocatechuic acid)	17.8 min	
2A-3HBA	2-amino-3-hydroxybenzoic acid (3-hydroxyanthranilic acid)	14.4 min	
3A-2HBA	3-amino-2-hydroxybenzoic acid (3-aminosalicylic acid)	8.6 min	

Table 17: Benzoic acid derivatives (continued)

Abbreviation	Substance (trivial name)	Retention time	Structure
3A-4HBA	3-amino-4-hydroxybenzoic acid	17.2 min	
4A-2HBA	4-amino-2-hydroxybenzoic acid (<i>para</i> -aminosalicylic acid)	12.2 min	
4A-3HBA	4-amino-3-hydroxybenzoic acid	16.0 min	

4.4 Reporter strains

Previous experiments tried to address the activation of purified DtxR in *in vitro* or analysed the culture supernatants. Both approaches did not shed light on the $\text{CO}_2/\text{HCO}_3^-$ induced transcriptional response of the DtxR regulon. A couple of biosensors was designed with the objective, to report the DtxR activation state *in vivo*. The immediate output signal was expected to afford attribution of DtxR activation to a wider set of cultivation conditions.

4.4.1 Design and construction

In general, the activation state of DtxR was monitored by a reporter gene that was expressed under control of the promoter of *ripA* (P_{ripA}), which appeared as a suitable target, because in *C. glutamicum* WT *ripA* expression was supposed to be solely controlled by DtxR (Wennerhold et al., 2005). In a first attempt, an expression cassette consisting of the reporter gene *egfp* (encoding the enhanced green fluorescent protein) under control of P_{ripA} was integrated in the *C. glutamicum* WT genome (fig. 14). Greater activation of DtxR in the resulting strain *C. glutamicum* FEM1 should be reported by lower fluorescence, as *egfp* expression under P_{ripA} becomes repressed.

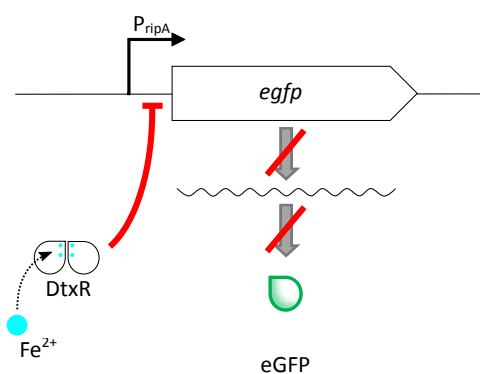


Figure 14: Schematic representation of the functionality of reporter strain *C. glutamicum* FEM1. Active DtxR (e.g. at high intracellular Fe^{2+} concentration) represses the expression of *egfp* under control of P_{ripA} . Negative correlation between DtxR activation and eGFP production.

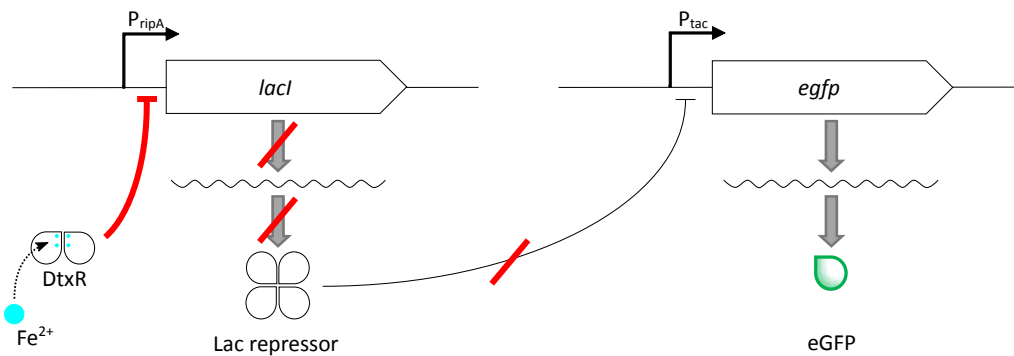


Figure 15: Schematic representation of the functionality of reporter strain *C. glutamicum* FEM3. Active DtxR (e.g. at high intracellular Fe^{2+} concentration) represses the expression of *lacI* under control of P_{ripA} , thus, rendering *egfp* expression under P_{tac} constitutive. Positive correlation between DtxR activation and eGFP production. Figure was published in the attached manuscript (Müller et al., 2020).

In order to keep the perturbation of the endogenous DtxR regulon at a minimum possible level, the synthetic cassette (P_{ripA} -*egfp*) was provided as a single copy, in contrast to typical approaches providing a higher copy number through replicative plasmids. To compensate potentially low expression under P_{ripA} a more elaborated biosensor was constructed in parallel (fig. 15). In this design, the expression of *egfp* was under the strong hybrid promoter P_{tac} , that can be repressed by the Lac repressor (LacI). Expression of *lacI* was under control of P_{ripA} , thus, rendering eGFP production responsive to the DtxR activation state. In comparison to the simpler design, P_{tac} regulation through LacI provided not only a signal enhancer but also a converter, since eGFP production should correlate positively with DtxR activation.

Strain *C. glutamicum* FEM2 carrying both elements (P_{ripA} -*lacI* and P_{tac} -*egfp*) as genomic integrations did not exhibit higher fluorescence than the autofluorescence of the WT (data not shown) and was therefore not further characterised in this work. Finally, *C. glutamicum* FEM3 carried the P_{ripA} -*lacI* genomic integration and P_{tac} -*egfp* on the replicative plasmid pJC4 in *C. glutamicum*.

4.4.2 Validation

Correct functionality of the reporter strains FEM1 and FEM3 needed to be validated. In a first step, responsiveness of the systems towards varying FeSO_4 concentrations in the medium was tested in accordance with Wennerhold and Bott (2006). The more sensitive reporter strain was then applied to the bioreactor cultivation established by Blombach et al. (2013) to confirm DtxR activation under the high pCO_2 test conditions.

Fluorescence detection was established in 100 μL sample volume in 96-well microplates and the linear range was determined between 50 and 80,000 arbitrary units (a.u.). RFU values below 50 in the culture samples were not further considered for evaluation. At cell densities $> \text{OD}_{600}=11$, a meniscus of the liquid level formed in the wells and disturbed the accurate detection. Cultures were diluted with 0.9 % (w/v) NaCl appropriately to ensure that such physical parameters caused by the cell density did not interfere with the measurements. Background fluorescence of the culture supernatants increased over the cultivation time and was therefore subtracted from each sample individually.

4.4.2.1 Responsiveness to iron No differences in the growth performance of *C. glutamicum* WT, FEM1 and FEM3 was detected between the strains when cultivated in iron starvation (1 μM FeSO_4) or excess (100 μM FeSO_4). The iron availability itself had a strong impact on the growth phenotype (fig. 16a). In iron excess all three strain grew exponentially at rates $\mu = 0.44$ or 0.45 h^{-1} between 1 and 8 h after inoculation. The exponential growth phase was reduced by two hours in iron starvation without affecting the growth rate markedly (tab. 18). Growth proceeded after the exponential phase at reduced rates to a final biomass concentration of $4.62 \pm 0.20 \text{ g L}^{-1}$ after 24 h (compared to $8.21 \pm 0.25 \text{ g L}^{-1}$ after 24 h in iron excess). A lag phase with very low biomass generation appeared in the first hour of cultivation under iron starvation conditions that was absent when iron was provided in excess.

Table 18: Exponential growth phases and rates of *C. glutamicum* WT, FEM1 and FEM3 cultivated under iron starvation (1 μM FeSO_4) or excess conditions (100 μM FeSO_4); WT duplicates were stated individually; mean values \pm standard deviations of FEM1 and FEM3 were calculated from four biological replicates

Condition	1 μM FeSO_4	100 μM FeSO_4
Exponential phase	1 - 6 h	1 - 8 h
Strain		
WT	$\mu_1=0.43 \text{ h}^{-1}; \mu_2=0.43 \text{ h}^{-1}$	$\mu_1=0.45 \text{ h}^{-1}; \mu_2=0.44 \text{ h}^{-1}$
FEM1	$\mu=0.45 \pm 0.02 \text{ h}^{-1}$	$\mu=0.45 \pm 0.00 \text{ h}^{-1}$
FEM3	$\mu=0.44 \pm 0.01 \text{ h}^{-1}$	$\mu=0.44 \pm 0.00 \text{ h}^{-1}$

Autofluorescence of *C. glutamicum* WT was below the detection limit during the first 4 h of cultivation. After that, biomass specific fluorescence (RFU CDW^{-1}) ranged between 10 and 40 a.u. $\cdot (\text{g L}^{-1})^{-1}$ until 10 h after inoculation (fig. 16b). Fluorescence of FEM1 and FEM3 was comparable to autofluorescence in the condition, that was supposed to suppress eGFP production (iron excess for FEM1 and starvation for FEM3). Biomass specific fluorescence of FEM1 was detectable after 4 h under iron starvation conditions and increased gradually in the following to $113 \pm 5 \text{ a.u.} \cdot (\text{g L}^{-1})^{-1}$ after 10 h (fig. 16c). FEM3 fluorescence was already detected after 1 h in iron excess and ranged between 91 and 153 a.u. $\cdot (\text{g L}^{-1})^{-1}$ throughout the cultivation (fig. 16d). Due to the higher sensitivity of FEM3 at the beginning of the cultivation, it was applied as the reporter strain and background for further strain manipulation in all following experiments.

4.4.2.2 Responsiveness to the CO_2 content Parallel cultivation of *C. glutamicum* FEM3 in bioreactors at high and standard pCO_2 revealed differences in the growth behavior (fig. 17a). At an elevated CO_2 content of 20 % (v/v) in the inlet air cultures grew exponentially at $\mu = 0.35 \pm 0.02 \text{ h}^{-1}$ between 1 and 10 h. When the same strain in the identical set-up was aerated with ambient air (approx. 0.04 % (v/v) CO_2) instead, it exhibited a reduced biomass generation for the first 7 h. After this, growth recovered to comparable rates as high pCO_2 ($\mu = 0.34 \pm 0.05 \text{ h}^{-1}$). It is inconclusive whether the first growth phase might be interpreted as a limitation or another exponential growth phase.

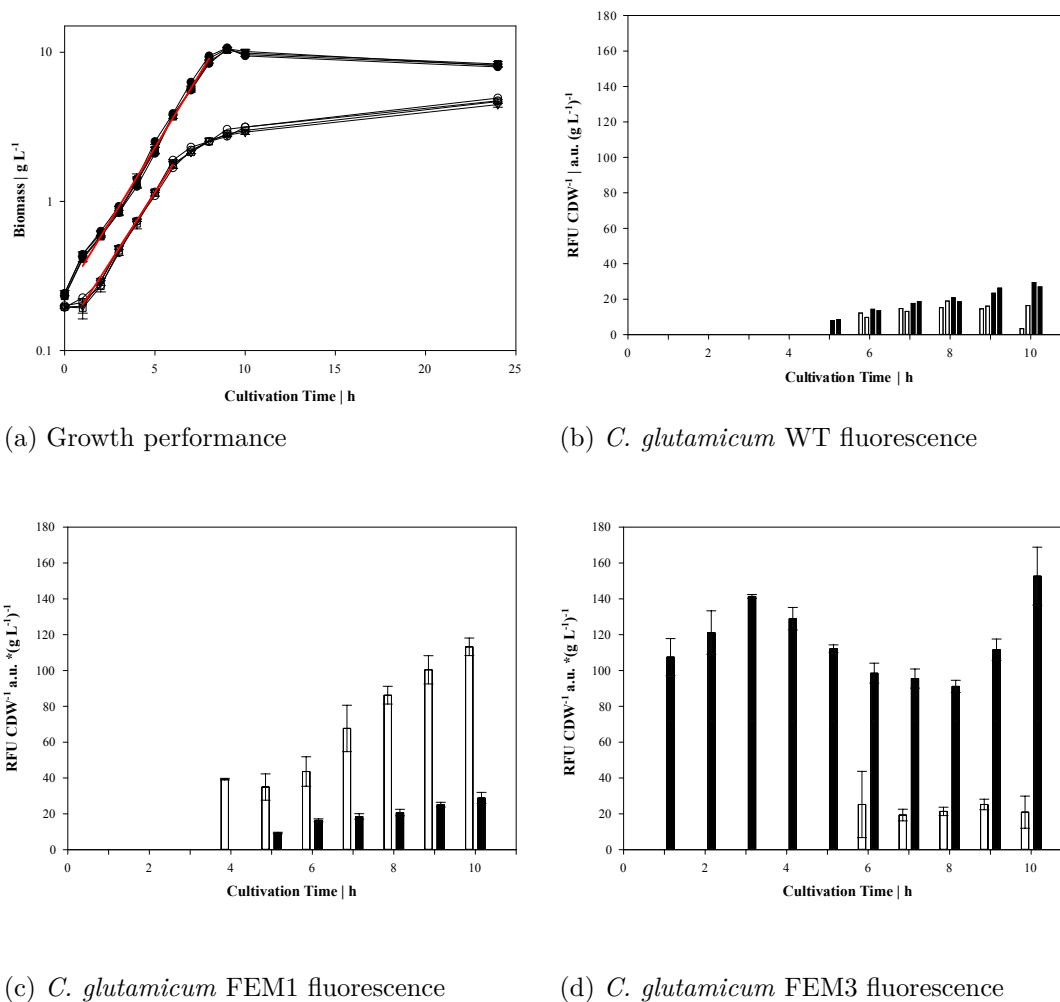
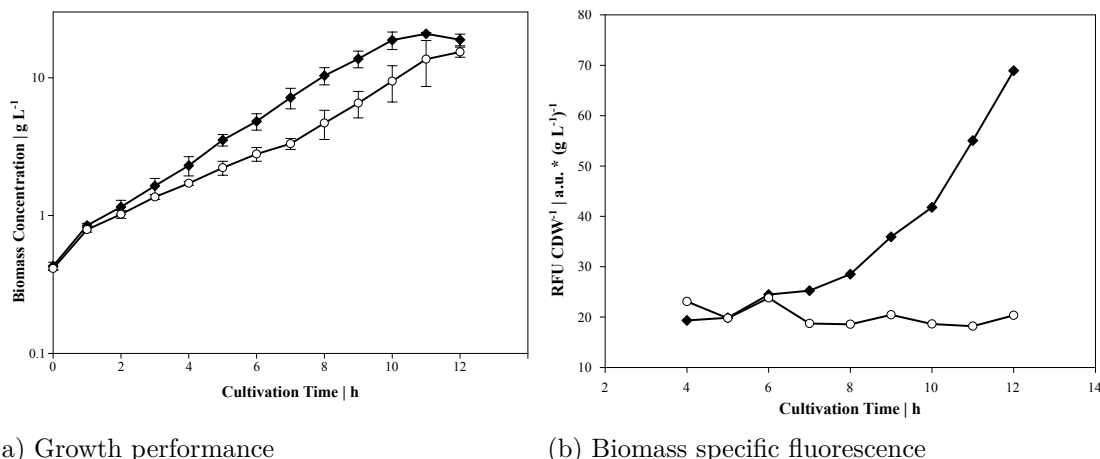


Figure 16: Growth and fluorescence of *C. glutamicum* strains under iron starvation and excess conditions. 16a) Biomass concentration over the cultivation time of WT (●), FEM1 (■) and FEM3 (▼) in iron excess (filled symbols) and starvation (open symbols). Red lines indicate the exponential growth phase. 16b-16d) Biomass specific fluorescence during the cultivation in iron excess (filled bars) and starvation (open bars). Biological duplicates of the WT strain are depicted as single points and bars in 16a and 16b, respectively, other data points represent mean values and error bars indicate the standard deviation of four biological replicates



(a) Growth performance

(b) Biomass specific fluorescence

Figure 17: Bioreactor cultivation of *C. glutamicum* FEM3 in a parallel set-up aerated either with ambient air (standard pCO₂, ○) or 20 % CO₂ in the inlet air (high pCO₂, ◆). 17a) Biomass concentration during 12 h of cultivation. Data points represent mean values and error bars indicate standard deviations of biological triplicates. 17b) Biomass specific fluorescence of a single parallel bioreactor cultivation - exemplarily shown for the triplicate. Parts of this figure were published in the attached manuscript (Müller et al., 2020).

Therefore, calculated $\mu = 0.25 \pm 0.03 \text{ h}^{-1}$ in this phase (1-6 h) should be considered with reservations.

Biomass specific fluorescence of FEM3 during the parallel cultivation was exemplarily shown for one of the triplicates in fig. 17b. Identical RFU CDW⁻¹ values were detected in both conditions until 6-7 h cultivation. RFU CDW⁻¹ diverged thereafter with high values at high pCO₂ and lower values at standard pCO₂. The fluorescence regime was qualitatively the same in all three experiments. However, the initial fluorescence levels – putatively resulting from the preculture conditions – failed to be standardised. Optimization of the inoculum size and harvest point of the preculture were overshadowed by batch-to-batch variation between the experiments. Reproducibility of RFU CDW⁻¹ was higher towards the end of the main cultivation, yielding e.g. after 12 h process time $77 \pm 9 \text{ a.u.} * (\text{g L}^{-1})^{-1}$ at high pCO₂ and $26 \pm 5 \text{ a.u.} * (\text{g L}^{-1})^{-1}$ at standard pCO₂.

4.5 Shaking flask experiments

Growth differences of *C. glutamicum* FEM3 between high and standard CO₂ contents in the inlet air of a bioreactor cultivation reminded of non-documented differences that were observed in the past (oral communication). Exponential growth was by then stabilised through the supplementation of PCA – in accordance with a publication on the requirement for chelating agents to ensure sufficient iron availability in *C. glutamicum* (Liebl et al., 1989). Consequently, PCA supplementation was included as variation parameter in the following shaking flask cultivations.

4.5.1 Scale-down

At the given operation parameters of the bioreactor cultivation (1.5 bar total pressure, 20 % (v/v) CO₂ in the inlet air, 30 °C, pH 7.4) the HCO₃⁻ concentration can be estimated to about 110 mM in aqueous solutions. This concentration exceeds the buffer capacity of CgXII minimal medium due to the mutual interaction of CO₂/HCO₃⁻ and pH (e.g. by gassing out). In a scale-down approach from the bioreactor to shaking flasks, the high CO₂ cultivation was represented by the addition of (only) 30 mM NaHCO₃, whilst non-supplemented cultures were intended to represent standard pCO₂ cultivations.

In fact, growth of *C. glutamicum* WT under non-supplemented (reference) conditions resembled growth at ambient CO₂ content exhibiting a growth deficit during the first 6-7 h and recovery to exponential growth thereafter (fig. 18). The transition from limitation to exponential growth was preponed by 2-3 h through the supplementation of 30 mM NaHCO₃ in the culture broth. However, a complete relief of the growth limitation was only obtained by the supplementation of 195 μM protocatechuic acid, resulting in exponential growth between 1 and 9 h of cultivation. During the exponential phase, all strains grew at comparable rates ($\mu = 0.40 \pm 0.01 \text{ h}^{-1}$ (PCA), $\mu = 0.40 \pm 0.03 \text{ h}^{-1}$ (NaHCO₃) and $\mu = 0.37 \pm 0.01 \text{ h}^{-1}$ (reference)). Identical results were obtained in cultivations of *C. glutamicum* FEM3 (data not shown).

The dynamic of time-resolved fluorescence (appendix fig. S2d on page 162) does not nec-

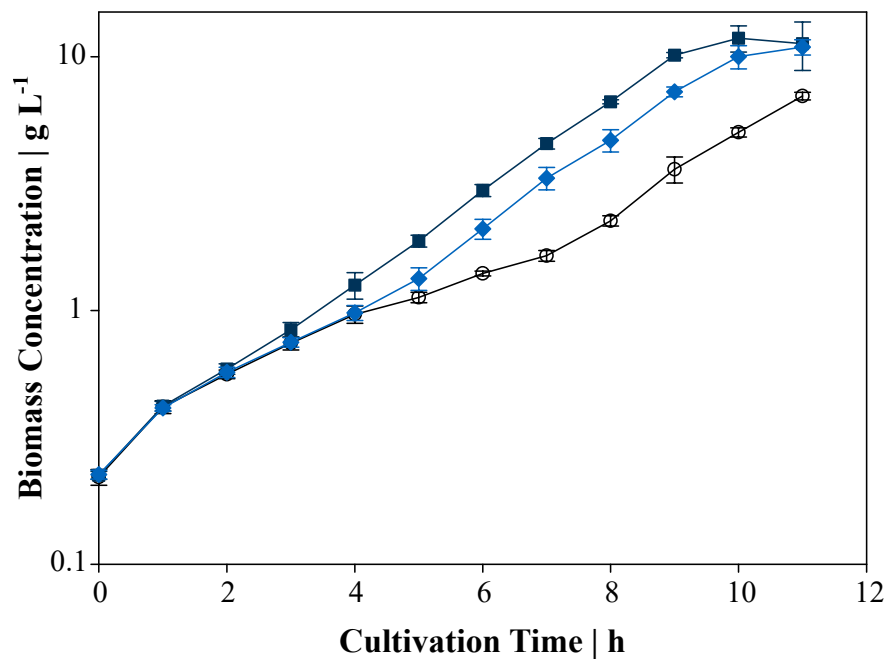


Figure 18: Biomass generation of *C. glutamicum* ATCC 13032 (WT) in shaking flask cultivations. \circ : standard conditions (no supplements), \blacksquare : 195 μM protocatechuic acid (PCA) supplemented, \blacklozenge : 30 mM NaHCO_3 supplemented. Data points represent mean values and error bars indicate standard deviations of three independent experiments. Parts of this figure were published in the attached manuscript (Müller et al., 2020).

essarily reflect the time-resolved DtxR activation. It might be hampered by maturation of eGFP as well as production/degradation kinetics. In order to compensate such potential fluctuations, fluorescence experiments were performed as end point reading after 25 h cultivation in the following experiments. Fluorescence results of the three screening conditions were in accordance with the growth experiments as highest RFU CDW⁻¹ was detected in PCA supplemented cultures, followed by the NaHCO₃ supplemented cultures. Reference cultures exhibited the lowest biomass specific fluorescence (fig. 19). Although differences between reference and NaHCO₃ supplemented cultures appeared to be small, they were highly reproducible and statistically significant.

Synergistic effects of PCA and NaHCO₃ were tested by a joint supplementation. Although growth was not enhanced over the solely PCA supplemented culture, RFU CDW⁻¹ values were by tendency higher when both supplements were provided. High variance of the results hampered the statistical analysis, such that no significant differences could be proven by a two-sample Student's t-test. However, considering the parallel cultivation in different conditions (on the same day), RFU CDW⁻¹ was always markedly higher when NaHCO₃ was additionally provided alongside PCA.

4.5.2 Acetate supplementation

Besides enhancing the iron transport in *C. glutamicum* (Liebl et al., 1989), PCA is metabolised in the β -ketoacid pathway and eventually fuels the TCA cycle (Shen et al., 2012). The PCA metabolisation resulted in higher growth rates at microscale cultivation level compared to growth on glucose (Unthan et al., 2014). To test, whether the growth promoting effect of PCA was due to an initially increased TCA cycle activity, experiments were performed with C-equimolar amounts of acetate, which is co-metabolised with glucose (Wendisch et al., 2000). However, supplementation of 600 μ M acetate did not enhance growth of *C. glutamicum* WT over a reference culture (data not shown).

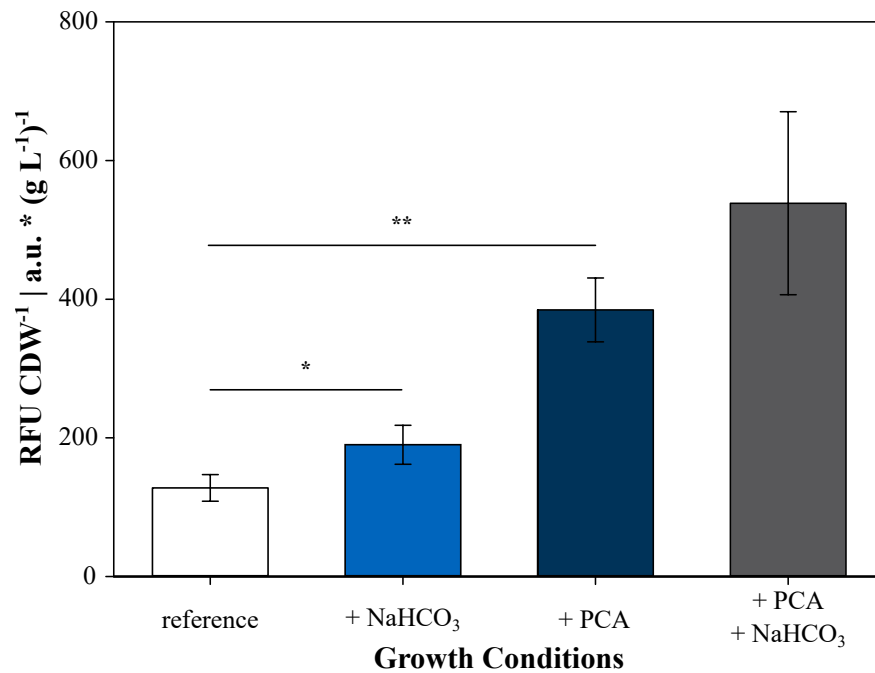


Figure 19: Biomass specific fluorescence of *C. glutamicum* FEM3 after 25 h cultivation in shaking flasks that were supplemented as indicated at the bottom. Bars represent mean values and error bars indicate standard deviations of three independent experiments. Asterisks indicate significance levels of a two-sample t-test by the following cut-off values: *) $p \leq 0.05$, **) $p < 0.01$. Figure was published in the attached manuscript (Müller et al., 2020).

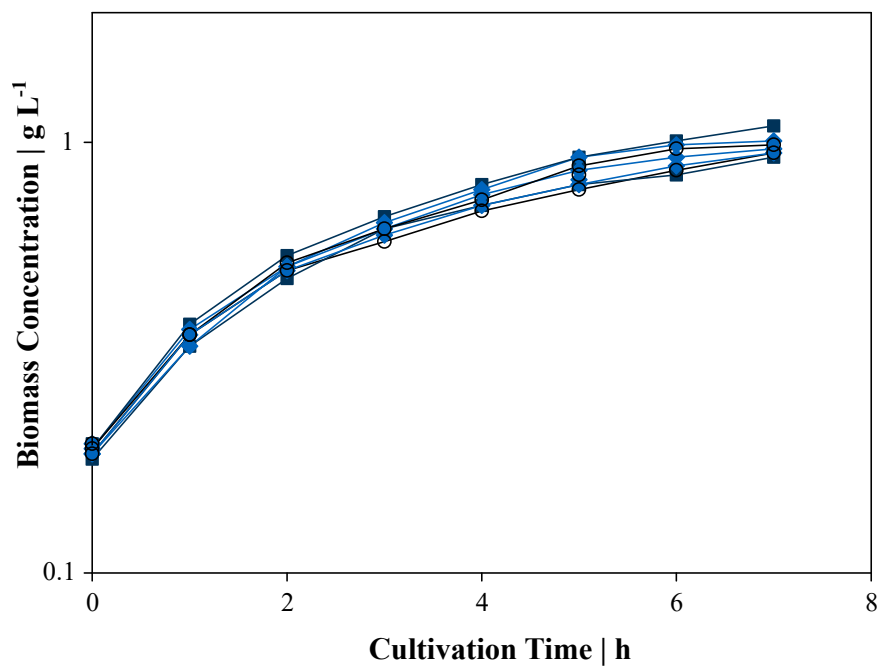


Figure 20: Biomass generation of *C. glutamicum* ATCC 13032 (WT) in iron-depleted shaking flask cultivations. ●: standard conditions (no supplements), ■: 195 μM protocatechuic acid (PCA) supplemented, ◆: 30 mM NaHCO_3 supplemented. Data of each experiment is plotted individually (duplicates, triplicates at $t = 0$ h and $t = 5$ h). Figure was published in the attached manuscript (Müller et al., 2020).

4.5.3 Iron depleted growth

To further address the role of PCA and NaHCO₃, growth effects provoked by the supplementation in iron depleted medium were tested. The seed train for this experiment was slightly adapted to ensure (i) iron replete conditions in the preculture and (ii) iron depleted main cultures. Therefore, (i) the last preculture was supplemented with 100 μM FeSO₄ and (ii) main cultures contained no iron, but 250 μM of the strong ferrous iron chelator 2,2-bipyridyl, in accordance with (Frunzke et al., 2011). Iron depleted medium provoked a strong growth defect in *C. glutamicum* WT, which could not be compensated by the supplementation of either PCA or NaHCO₃ (fig. 20). All cultures reached a final biomass concentration of about 1 g_{CDW} L⁻¹ after 7 h shaking flask cultivation, which did not further increase upon extended cultivation for several days (data not shown).

The question about the role of PCA and NaHCO₃ was addressed in a similar setting at a later point. Cultivations were performed in a medium-throughput BioLector system (appendix fig. S2a-S2d). Growth phenotypes of *C. glutamicum* FEM3 in the different conditions (PCA, NaHCO₃) were comparable to the shaking flask approach. However, the differences were less pronounced. The experiments were performed in the standard medium composition with or without the addition of 1 mM of the Fe²⁺-chelator BPS. It was visually assured, that Fe³⁺-PCA complexes had formed at the time of BPS addition to the vials. *C. glutamicum* FEM3 growth was largely impaired by the presence of 1 mM BPS and poorly reproducible. A growth stimulatory effect of PCA or NaHCO₃ supplementation could not be noted and all cultures reached reduced final backscatter values (by 20 % in average). The biomass specific fluorescence decreased during the cultivation in the presence of 1 mM BPS and reached a final value of < 0.1 regardless of the supplementation. By this, the biomass specific fluorescence represented only about 50 %, 30 % and 10 %, respectively, of reference, NaHCO₃ and PCA supplemented cultures lacking BPS.

Hence, these experiments confirm, that the growth promoting effect of PCA and NaHCO₃

is related to the iron availability because their supplementation remains without effect in iron-depleted conditions.

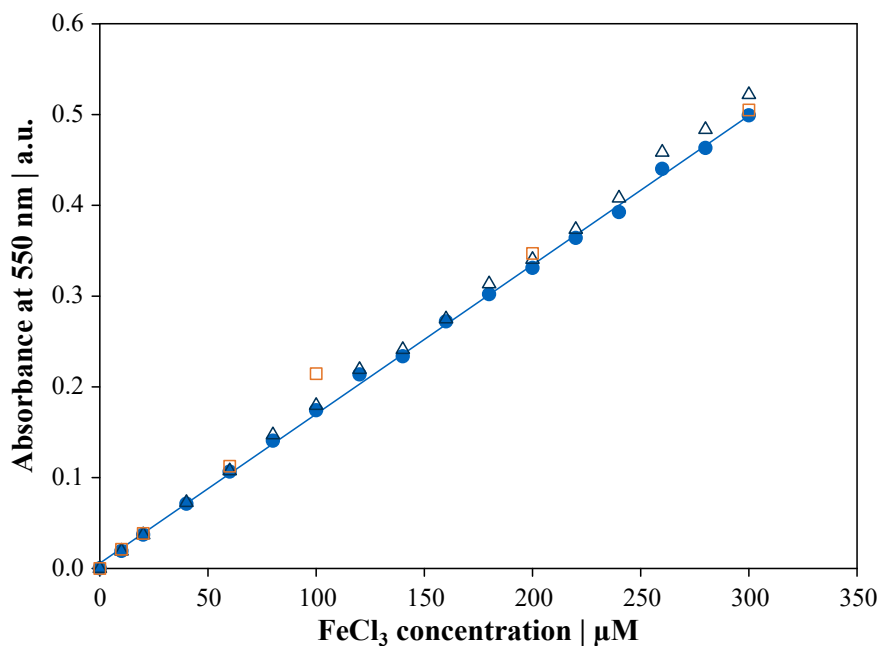


Figure 21: Calibration curve of the iron quantification assay using FeCl_3 . Linear regression ($f(x) = 0.0016x + 0.0057$) of the calibration (\bullet) delivered an $R^2 = 0.9992$. Robustness of the calibration was addressed upon extended incubation (\triangle) and day-to-day variation (\square).

4.6 Intracellular iron quantification

It is generally assumed, that the iron uptake of *C. glutamicum* can be enhanced by the supplementation of PCA (Liebl et al., 1989; Frunzke and Bott, 2008). A method for the intracellular iron quantification was established in the following with the objective to find out, whether the higher Fe^{2+} availability detected *in vivo* could be correlated with the increased iron transport. In analogy with PCA one might expect the greater intracellular Fe^{2+} concentration in the presence of NaHCO_3 to be due to its involvement in iron uptake.

While establishing the iron quantification assay, reproducibility could be increased by the addition of 100 μL detection reagent instead of 30 μL as originally (Riemer et al., 2004). A linear increase of Fe^{2+} -ferrozin complexes was monitored by the absorbance at 550 nm over the range of FeCl_3 concentrations (0 - 300 μM) and the linear regression fit-

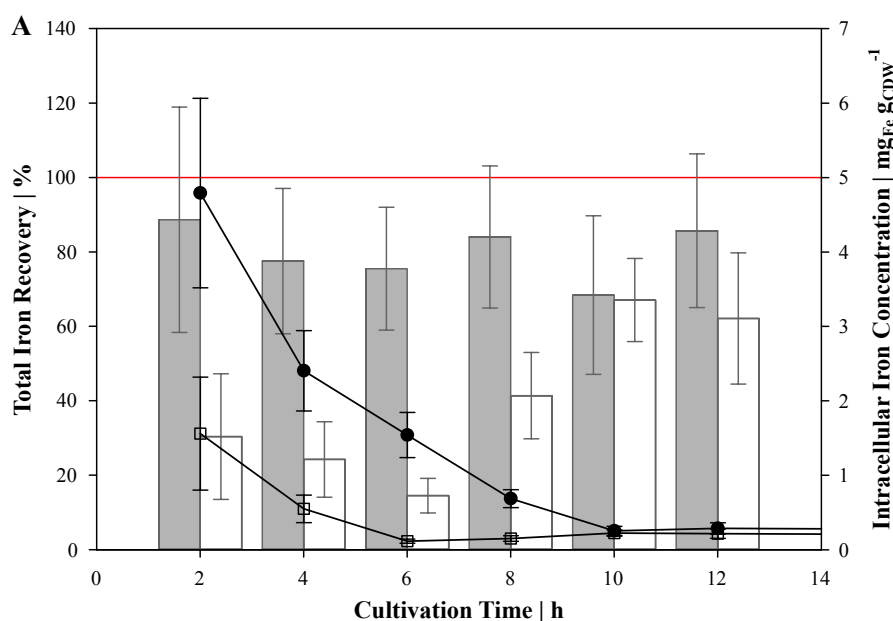


Figure 22: Iron uptake assay. Iron was quantified in cell pellets of reference and PCA supplemented *C. glutamicum* WT cultivations. The total amount of iron recovered (grey bars) and intracellular iron concentration (●) of the reference cultivations were not further considered due to solubility issues, that might hamper the assay performance in this case. Due to the iron chelations, intracellular iron concentration (□) as well as total iron recovery (open bars) of the PCA supplemented cultivations might be valid. Data points and bars represent mean values with error bars indicating the standard deviation of independent biological triplicates.

ted at high quality ($R^2 = 0.9992$). The calibration curve was robust towards an extended incubation (90 min) and identical absorbance values were obtained on a different day, when the assay was prepared freshly (fig. 21). The calibration curve was routinely integrated every time the assay was performed and did not differ markedly (data not shown).

In the next step, the iron concentration was determined in the washed cell pellets of reference and PCA supplemented *C. glutamicum* WT cultivations. Determining carefully the biomass concentration which was applied to the assay the total intracellular iron concentration was calculated and related to the iron source, thus, allowing an iron balance (% total iron recovery). As soon as 2 h after inoculation of a reference culture

90 % of the supplied iron was recovered in the biomass and consequently high intracellular iron concentrations were obtained (fig. 22). However, the discussion must already be anticipated here, in order to emphasize that these results should be taken with precaution. It was the intention of this work to remove the supernatant of *C. glutamicum* WT cultivations including the entire amount of iron, that had not been internalised before. To get rid of impurities, cell pellets were additionally washed with 20 mL 0.9 % (w/v) NaCl. As outlined in 5.2 cultivation conditions as well as the washing buffer, might support soluble ferrous iron (as it is provided – FeSO_4). However, Fe^{2+} will be quickly oxidised in the presence of O_2 yielding poorly soluble Fe^{3+} , which might have sedimented with the cell pellet and could not be removed from it during the washing step. As a consequence, intracellular iron concentrations and recovery of the reference cultivation were not considered in the following. The results obtained in a NaHCO_3 supplemented cultivation resembled the reference (data not shown).

In contrast to the NaHCO_3 supplemented and reference cultivation, results from the PCA supplemented culture might be valid. Providing PCA at $> 3:1$ stoichiometry with iron, the amount suffices to maintain the entire Fe^{3+} in solution. About 30 % of the entire iron was taken up in a PCA supplemented cultivation 2 h after inoculation, reaching the highest intracellular iron concentration throughout the cultivation ($1.56 \pm 0.76 \text{mg}_{\text{Fe}} \text{g}_{\text{CDW}}^{-1}$). No net increase of the recovered iron was noted until 6 h of cultivation and a sharp stepwise increase after 8 and 10 h cultivation to a maximum of about 60 % (fig. 22).

4.7 Deletion mutant screening

A set of deletion mutants was generated in *C. glutamicum* WT and FEM3 background, respectively, to analyse the impact of PCA and CO₂/HCO₃⁻ in accordance with the experiments outlined in 4.5.

Deletion targets were selected (i) based on the current knowledge about iron homeostasis in *C. glutamicum*, (ii) deduced from the pull down experiment (4.2) or (iii) as the annotated putative bicarbonate transport system. Deletion mutants from (i) addressed the master regulator encoded by *dtxR* (only in WT background), iron storage proteins encoded by *ftn* and *dps* (single and double deletion mutant) as well as the pupylation protein initialising iron mobilisation from storage proteins encoded by *pup*. Gene *cg2444* was the only deletion target derived from (ii), which was suspected to interact with DtxR in a modulating fashion. Searching for transport systems that might translocate iron alongside HCO₃⁻ as the counter-ion in *C. glutamicum* delivered the transport systems encoded by *cg1438-cg1441* and *cg0041-cg0042*.

Growth of the deletion mutants was monitored in the standard screening approach in parallel with the WT as outlined in 4.5 and the biomass specific fluorescence was determined after 25 h. Except for the Δpup mutant, none of the deletion mutants revealed a remarkable difference from the WT and FEM3 phenotype, respectively. Compared to the WT growth, *C. glutamicum* Δpup exhibited a severer growth retardation in reference conditions yielding only roughly half of the biomass concentration after 10 h cultivation. Supplementation of PCA and NaHCO₃ improved growth over the reference and resembled the growth phenotype of the WT in the respective condition (fig. 23). The biomass specific fluorescence reporting the intracellular Fe²⁺ concentration of strain FEM3 Δpup was not different from the FEM3 base strain under reference and NaHCO₃ supplemented conditions. In the presence of PCA, the biomass specific of FEM3 Δpup was in tendency reduced when it was compared with FEM3 (fig. 24). Shaking flask screenings of *C. glutamicum* $\Delta cg2444$ and *C. glutamicum* Δftn as well as the BioLector cultivation of *C. glutamicum* $\Delta cg0041-cg0042$ revealed no differences compared to the

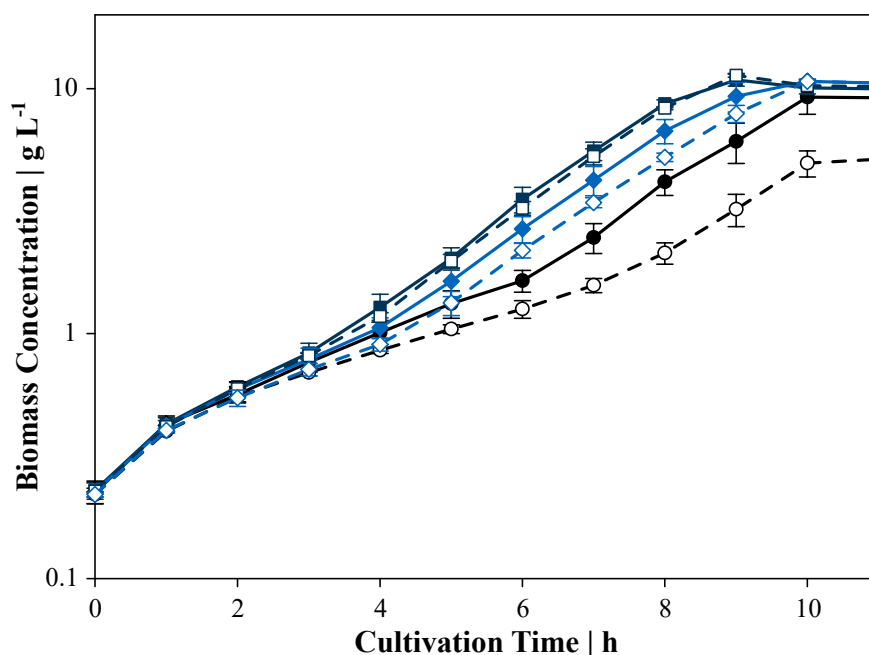


Figure 23: Biomass generation of *C. glutamicum* WT and *C. glutamicum* Δpup in shaking flask cultivations. ●: WT - standard conditions (no supplements), ■: WT - 195 μM protocatechuic acid (PCA) supplemented, ◆: WT - 30 mM NaHCO_3 supplemented ○: Δpup - standard conditions (no supplements), □: Δpup - 195 μM protocatechuic acid (PCA) supplemented, ◇: Δpup - 30 mM NaHCO_3 supplemented. Data points represent mean values and error bars indicate standard deviations of three independent experiments. Figure was published in the attached manuscript (Müller et al., 2020).

WT regarding growth and fluorescence (fig. S3a, b and S4a-d in the appendix).

In summary, there was no evidence provided by the deletion mutants tested here, that the elevated intracellular Fe^{2+} concentration was provoked by the interaction of PCA or NaHCO_3 with iron transport (via the two investigated transport systems) nor with the iron mobilisation from storage proteins. The lower biomass specific fluorescence of FEM3 Δpup , when it was cultivated in the presence of PCA, might suggest, that iron can be reduced intracellularly by PCA succeeding iron mobilisation by pupylation. However, storage proteins are not the only iron source for the interaction with PCA, because a Δftn mutant and the $\Delta ftn \Delta dps$ double deletion mutant lacking both storage proteins achieved WT-like intracellular Fe^{2+} concentrations as reported by fluorescence.

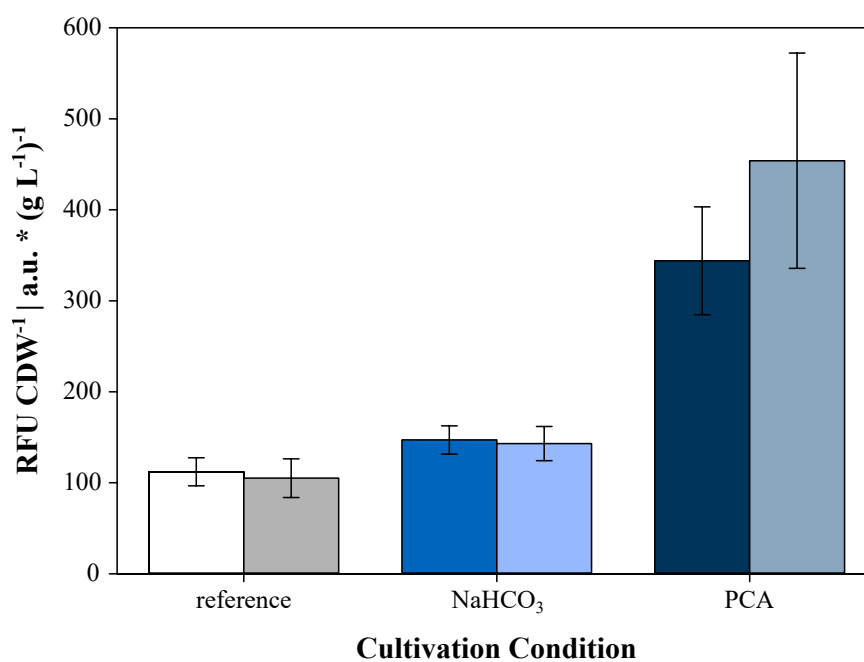


Figure 24: Biomass specific fluorescence of *C. glutamicum* FEM3 (right bar) and *C. glutamicum* FEM3 Δ pup (left bar) after 25 h cultivation in shaking flasks that were supplemented as indicated at the bottom. Bars represent mean values and error bars indicate standard deviations of three independent experiments.

4.8 Iron reduction assays

Intracellular concentrations of Fe^{2+} were found to be increased in *C. glutamicum* in the presence of PCA or NaHCO_3 but could be attributed neither to transport nor intracellular storage and subsequent mobilisation of iron. The last experimental part concentrates, therefore, on the abiotic interaction of iron, PCA and NaHCO_3 , considering that it might be uncoupled of biological mechanisms. An assay to address the chemical reduction of iron was inspired by the detection principle used for total iron quantification. Iron was initially provided as FeCl_3 (Fe^{3+}) in the reaction mixture. Only upon reduction Fe^{2+} ions could be detected by the formation of coloured complexes with Fe^{2+} specific chelators. First, the reduction assay was established with the chelator ferrozine, that was already used for total iron quantification (4.6), and the absorbance monitored at 550nm wavelength. Ferrozine was later replaced with BPS during the assay development, as the latter did not acidify the sample mixture and provided a broader pH range for operation (Blair and Diehl, 1961; Cowart et al., 1993). Fe^{2+} -BPS complexes exhibited a maximum absorbance at 534 nm wavelength. A sketch summarising the assay principle graphically has been provided in fig. 6.

The assay was initially conducted at a physiological pH of 7.4 – 7.5 by adjusting it with 50 mM NaOH. While working with bicarbonate solutions, continuous CO_2 degassing from (unsealed) samples during incubation shifted the pH towards alkaline conditions. Consequently, the assay was modified during the course of experiments and the sample pH was additionally buffered with 200 mM MOPS adjusted to pH 7.4 with 5 M KOH (reflecting conditions of the cultivation medium), if not stated otherwise.

4.8.1 HCO_3^- accelerates the iron reduction through PCA

Samples containing only FeCl_3 and BPS served as a negative control and exhibited a marginal increase of the absorbance during 300 min incubation (fig. 25). The addition of PCA itself up to a concentration of 19.5 μM made no contribution to the absorbance at 534 nm (A_{534}) in the absence of BPS. However, Fe^{2+} -BPS complex formation was speed

up in the presence of PCA and described a saturation curve. Iron reduction could be further enhanced by an additional 50 mM NaHCO₃ added alongside of PCA. Particularly the initial formation rate was increased and A₅₃₄ reached a plateau after 150 min at higher values (about 15 % after 300 min) than samples containing only PCA. During the initial phase up to 100 min incubation time, > 50 % more Fe²⁺-BPS complexes were detected in the presence of NaHCO₃. The promoting effect was attributed to the HCO₃⁻ anion itself as identical results were obtained when NaHCO₃ was replaced with KHCO₃ (fig. 25). On the contrary, addition 50 mM NaCl did not affect the complex formation (data not shown) and the addition of 50 mM NaHCO₃ to samples lacking PCA had a negligible effect on complex formation compared to the negative control.

Considering the extinction coefficient determined by Blair and Diehl (1961) and Cowart et al. (1993), $50.8 \pm 1.7 \mu\text{M}$ Fe²⁺-BPS had formed after 300 min in the presence of PCA, compared to $58.8 \pm 3.2 \mu\text{M}$ when PCA and NaHCO₃ were added. The reduction of iron in the presence of PCA was not limited to free iron. Iron reduction could also be observed, when iron loaded ferritin was provided as the iron source instead of FeCl₃ (data not shown).

To provide evidence, that PCA serves as the electron donor for iron reduction, but is not simply the catalyst, the fate of PCA was monitored by a LC-MS-QTOF approach. In contrast to previous experiments, that were incubated in unsealed 96-well plates, 1 mL unbuffered samples were prepared for the LC-MS analytic and incubated in 1.5 mL Eppendorf cups with closed lids. Surprisingly, samples that were taken after 5 and 22 h revealed remarkably less absorbance (at 534 nm) than typically measured before.

These results were also reproduced in a more systematic approach. Unbuffered reaction mixtures were prepared in a larger stock and 150 μL of it was aliquoted into 200 μL PCR tubes and incubated with closed lids as before. Every 30 min the absorbance of one of the aliquots was determined. For comparison, 100 μL of the same preparation was incubated on unsealed 96-well plates. Samples, that were incubated on 96-well plates, were qualitatively similar to the previous experiments, although PCA addition

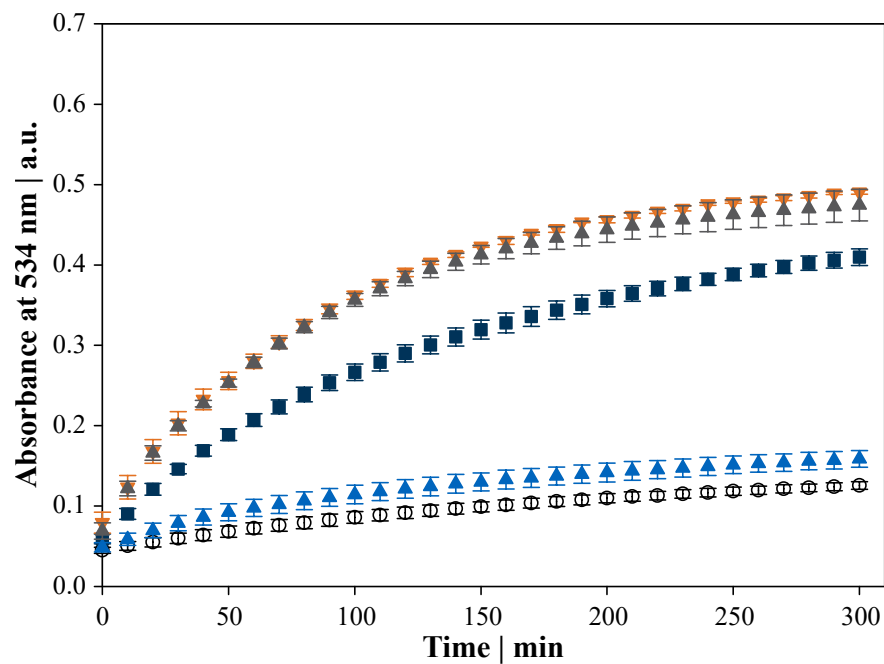


Figure 25: Iron reduction assay. Fe^{2+} -BPS complex formation was monitored by an increase of the absorbance at 534 nm in samples with no further additions (\circ), 19.5 μM PCA (\blacksquare), 50 mM NaHCO_3 (\blacktriangle), 19.5 μM PCA and 50 mM NaHCO_3 (\blacktriangle) or 19.5 μM PCA and 50 mM KHCO_3 (\blacktriangledown). Data points represent mean values with error bars indicating standard deviations of four to six independent replicates. Figure was published in the attached manuscript (Müller et al., 2020).

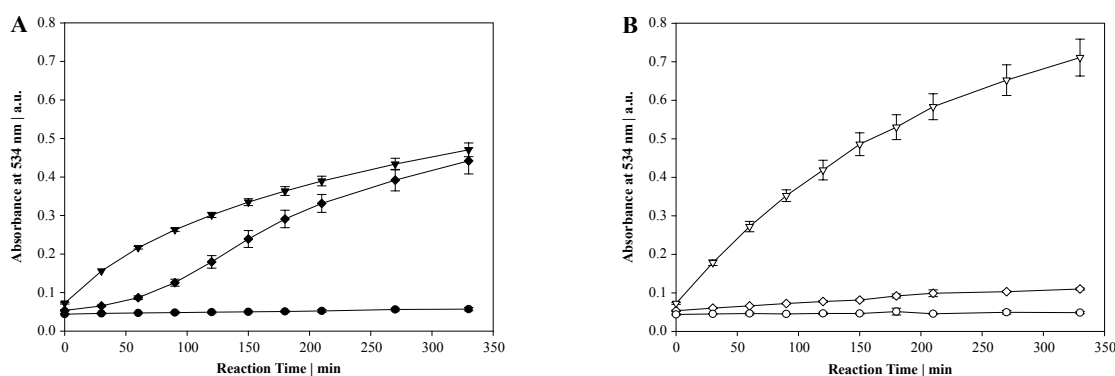


Figure 26: Iron reduction assays. Unbuffered reaction mixtures were prepared in one stock and (A) incubated on the plate permitting gas exchange or (B) incubated in 200 μL closed PCR tubes filled with 150 μL sample. Samples contained 19.5 μM PCA (\blacklozenge , \blacklozenge), 19.5 μM PCA and 50 mM NaHCO_3 (\blacktriangledown , \blacktriangledown) or no additives (\bullet , \circ) as a negative control. Data points represent mean values with error bars indicating the standard deviation of triplicates.

resulted in a rather sigmoidal curve (fig. 26). However, when the same reaction mixture containing 19.5 μM PCA was incubated in closed reaction cups, almost no increase in absorbance could be detected. The addition of 50 mM NaHCO_3 under these conditions resulted in higher final absorbance values than obtained during incubation on the plates (fig. 26), indicating that gas exchange was essential for the reaction unless sufficient NaHCO_3 was provided.

In accordance with this, LC-MS-QTOF analysis revealed differences of the PCA degradation in the absence and presence of NaHCO_3 . The peak area of PCA decreased by 65.3 ± 14.8 % within 5 h in the presence of 50 mM NaHCO_3 , compared to 23.7 ± 8.0 % in the absence of NaHCO_3 (fig. 27). After 22 h, the PCA peak area was reduced by 99.5 ± 17.3 % and 62.5 ± 21.0 % in the presence and absence of NaHCO_3 , respectively (fig. 27). Regarding the oxidation products of PCA, the corresponding semiquinone and quinone could not be detected. However, two degradation products might be described by the chemical formula $\text{C}_7\text{H}_6\text{O}_6$ and $\text{C}_7\text{H}_8\text{O}_6$ that were identified in the samples.

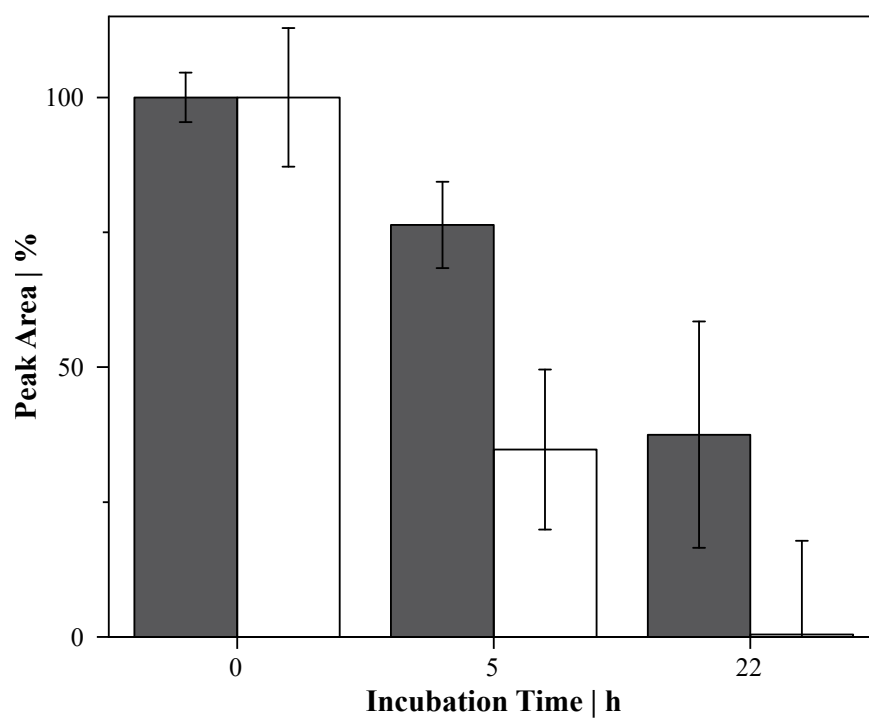


Figure 27: LC-MS-QTOF analysis of PCA degradation in the iron reduction assay. The degradation was monitored by a decrease of the peak area in the absence of NaHCO₃ (grey bars) or in the presence of 50 mM NaHCO₃ (open bars). The initial peak area at 0 h was set as 100 %. Peak areas at the later time points are calculated as the fraction of the initial area. Bars represent mean values of three individual experiments with error bars indicating the standard deviation. Figure was published in the attached manuscript (Müller et al., 2020).

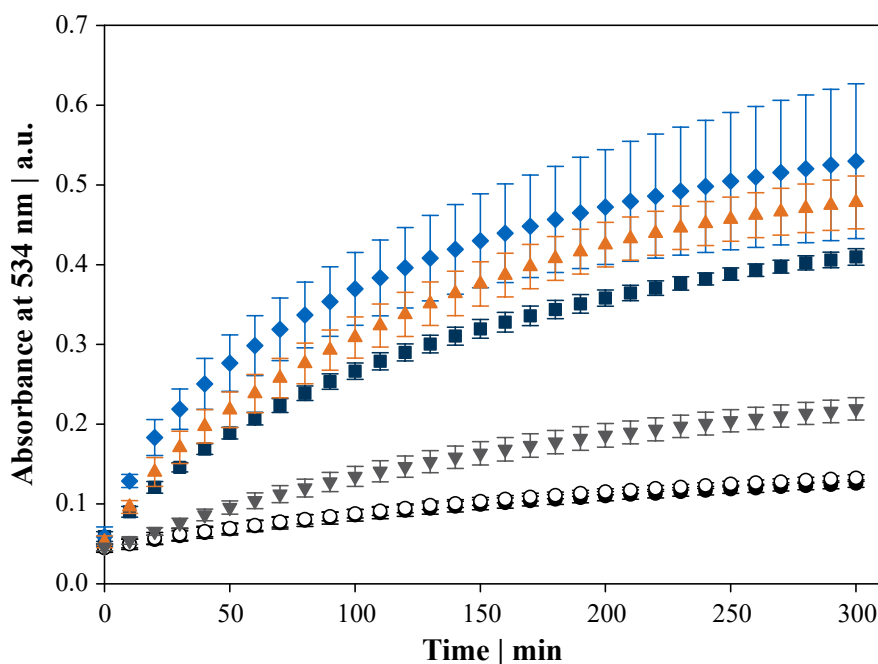


Figure 28: Iron reduction assay to investigate the reduction capacity of a number of aromatic compounds. Fe^{2+} -BPS complex formation was monitored by an increase of the absorbance at 534 nm in samples with no further additions (\bullet) or 19.5 μM PCA (\blacksquare), catechol (\blacklozenge), 3-HAA (\blacktriangle), 2-amino-4-hydroxybenzoic acid (\blacktriangledown) or benzoic acid (\circ). Data points represent mean values with error bars indicating standard deviations of four to six independent replicates. Figure was published in the attached manuscript (Müller et al., 2020).

4.8.2 Iron reduction by phenolic compounds

To deepen the understanding of iron reduction, a set of functionalised aromatics was assayed for their reduction capacity at PCA equivalent concentrations (fig. 28). Fe^{2+} -BPS complex formation in the presence of catechol and 2-amino-3-hydroxybenzoic acid (3-hydroxyanthranilic acid, 3-HAA) was comparable to PCA. Interestingly, benzoic acid did not promote this formation and addition of 4-amino-2-hydroxybenzoic acid (amino and hydroxy group are not adjacent to each other) exhibited only an intermediate effect on complex formation. The addition of 50 mM NaHCO_3 to either substance enhanced iron reduction in the same way that was observed with PCA (data not shown).

4.8.3 HCO_3^- accelerates the formation of Fe^{3+} -PCA complexes

While having seen that the redox reaction between Fe^{3+} and PCA was speed up by the presence of HCO_3^- , the mechanistic role remained unclear. Prior to the electron transfer, PCA complexes with the poorly accessible Fe^{3+} must have formed. Consequently, this last experiment was designed to answer the question, whether HCO_3^- could already enhance the formation of Fe^{3+} -PCA complexes. In order to monitor iron chelation in Fe^{3+} -PCA complexes, BPS was omitted from the reaction and the PCA concentration was increased to 1.5 mM providing a 3:1 stoichiometry between PCA and iron. The formation of coloured complexes was eventually detected at 560 nm.

Apparently, HCO_3^- accelerated the formation of Fe^{3+} -PCA complexes significantly (fig. 29, mean values \pm standard deviation of 5 replicates, p-value of a two-sided t-test = 0.0119). A linear increase of the absorbance during the first 35 min of the assay indicated a complex formation rate of $7.6 \pm 1.3 \Delta\text{mA}_{560} \text{ min}^{-1}$ in the presence of 50 mM NaHCO_3 , which was approximately 46 % higher than in the absence of NaHCO_3 ($5.2 \pm 1.0 \Delta\text{mA}_{560} \text{ min}^{-1}$). In addition to this, wavelength scans disclosed that the absorbance peak shifted from $561 \pm 9 \text{ nm}$ to $538 \pm 8 \text{ nm}$ upon addition of 50 mM NaHCO_3 without affecting the pH of the reaction mixture (fig. 30). The intentional pH perturbation in control experiments with equimolar amounts of HCl and KOH failed to reproduce a comparable wavelength shift of the complex maximum absorbance. Again, NaHCO_3 could be substituted with KHCO_3 , likewise, but not with NaCl.

These experiments provide an abiotic explanation for the greater intracellular Fe^{2+} availability in *C. glutamicum* when exposed to elevated $\text{CO}_2/\text{HCO}_3^-$ levels by demonstrating that the chemical reduction of Fe^{3+} is accelerated. The reason for this might already be the interference of HCO_3^- with Fe^{3+} solubility.

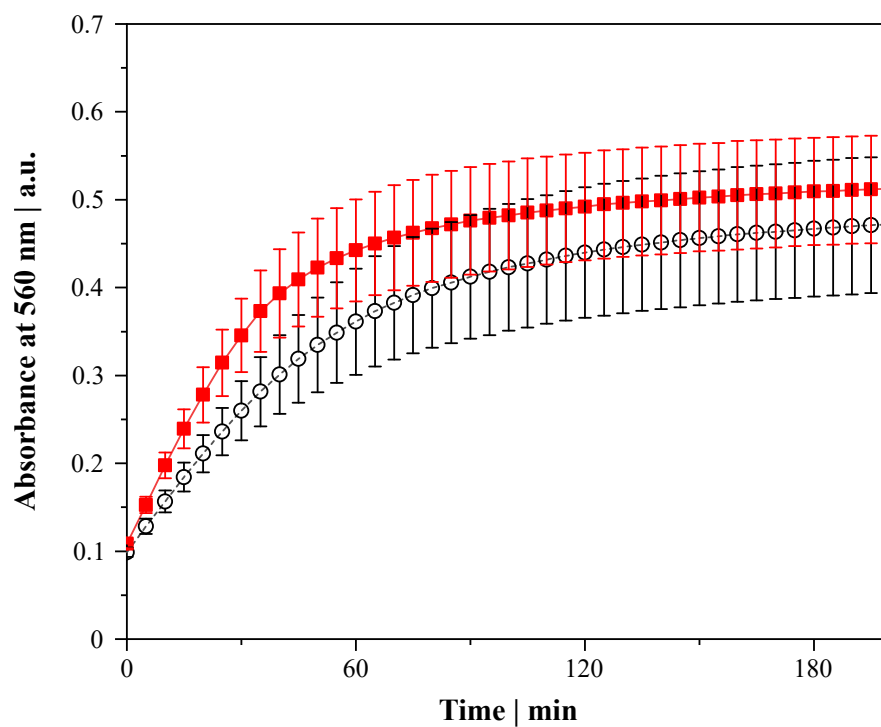


Figure 29: Complex formation kinetic between Fe³⁺ and PCA in the absence (○) and presence of 50 mM NaHCO₃ (■) monitored by an increase of the absorbance at 560 nm. Data points represent mean values with error bars indicating standard deviations of five replicates. Figure was published in the attached manuscript (Müller et al., 2020).

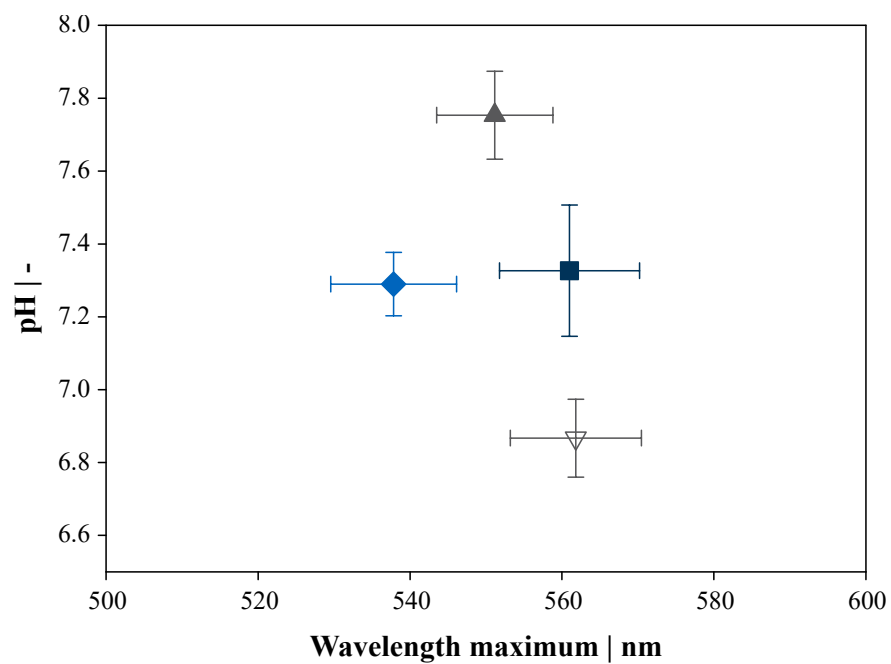


Figure 30: Wavelengths of maximum absorbance λ_{\max} and pH values of Fe^{3+} -PCA complexes in the absence (■) and presence of 50 mM NaHCO_3 (◆) or when the pH was intentionally perturbed by the addition of 50 mM KOH (▲) or 50 mM HCl (▽). Data points represent mean values with error bars indicating standard deviations of at least three independent replicates. Standard deviations of the x-axis (λ_{\max}) was calculated by error propagation. Figure was published in the attached manuscript (Müller et al., 2020).

It was demonstrated in this work that the chemical reduction of free Fe^{3+} through phenolic compounds is accelerated in the presence of $\text{CO}_2/\text{HCO}_3^-$. This abiotic mechanism was monitored at physiological pH and, thus, might be of broad significance in geochemical as well as living systems. *In vivo* effects were exemplarily described in *C. glutamicum*, where elevated $\text{CO}_2/\text{HCO}_3^-$ availability increased the intracellular Fe^{2+} pool and stimulated growth.

5.1 *C. glutamicum* growth performance responds to the iron availability

It was shown recently, that exposure of *C. glutamicum* to an elevated CO_2 content in the inlet air of a bioreactor cultivation caused the transcriptional activation of almost the entire DtxR regulon (Blombach et al., 2013). The key objective of this follow-up study was, therefore, the deeper analysis of $\text{CO}_2/\text{HCO}_3^-$ induced effects in the iron homeostasis of *C. glutamicum*. In this regard the present work demonstrates, that the DtxR activation is not caused by a regulatory interference involving $\text{CO}_2/\text{HCO}_3^-$ as (co-)stimulus, but is the immediate result of the increased intracellular Fe^{2+} concentration.

Reporter constructs were designed initially, in order to generate a straightforward read-out of the DtxR activation state by fluorescence. For this purpose, the expression of *egfp* was placed under control of the *ripA* promoter, which is itself repressed by DtxR (Wennerhold et al., 2005). Strong DtxR activation resulted in low fluorescence of the reporter construct designated FEM1, as it was expected. The coupling of DtxR activation and the fluorescence level was inverted in a second reporter construct designated

FEM3, which comprised a signal enhancer in form of the strong P_{tac} promoter and converter by its repression through LacI. Since biomass specific fluorescence of the reporter constructs was linked to low (FEM1) or high iron availability (FEM3), respectively, it was also concluded, that *egfp* expression did not simply follow growth performance. In the non-induced state of the biosensors, fluorescence of the two strains resembled autofluorescence of the WT, indicating generally a tight regulation. *C. glutamicum* FEM3 was selected for validation of the CO₂ induced DtxR response, because this strain exhibited overall a stronger signal and provided a logic connection of DtxR activation with the onset of eGFP production. The dynamic of eGFP production during a bioreactor cultivation as well as final biomass specific fluorescence of FEM3 after 24 h indicated higher DtxR activation at 20 % CO₂ in the inlet air, thus, supporting previous findings (Blombach et al., 2013). The low activation state of DtxR was coupled to a growth retardation at the ambient CO₂ content in the present study, which has not been noted by Blombach et al. (2013). It was concluded that the differences were induced by the seed train variation, as precultures had previously been carried out in 2x YT medium containing 10 g glucose L⁻¹ instead of minimal medium used in this study. Regarding growth, similar observations had been made by Liebl et al. (1989) who described an extended lag phase, when precultures were set up in minimal medium or when cell pellets were washed extensively before inoculation. Addition of the iron chelators citrate, PCA or catechol promoted growth (Liebl et al., 1989; von der Osten et al., 1989) and, consequently, PCA was in the following added to the CgXII medium variant used by several labs (Keilhauer et al., 1993). The growth stimulating effect of the PCA supplementation of shaking flask cultivations during this work was, thus, in accordance with the previous publications and provoked highest intracellular Fe²⁺ concentrations reported by FEM3. PCA can also be utilised as sole carbon and energy source by *C. glutamicum* (Shen et al., 2012) and it was reported that growth on PCA enabled extremely high growth rates in a microscale cultivation (Unthan et al., 2014). To test the effect of the additional carbon flux in the TCA cycle, equimolar amounts of carbon were supplemented as acetate. Acetate is co-metabolised with glucose (Wendisch et al., 2000) and fuels the the TCA

cycle. However, the supplementation in shaking flasks did not promote growth over the reference culture, indicating that PCA metabolisation was not the reason for the growth benefit.

It was noted with interest, that the requirement for iron chelating agents in *C. glutamicum* defined medium arose when CaCO_3 was omitted (Liebl et al., 1989; von der Osten et al., 1989; Unthan et al., 2014). Given the fact, that sufficient $\text{CO}_2/\text{HCO}_3^-$ levels dispensed the need for iron chelating compounds to support *C. glutamicum* growth, a direct interaction with the intracellular iron availability is suggested. However, the interaction level of dissolved CO_2 species (including HCO_3^- and CO_3^{2-}) with the iron availability had not been addressed in *C. glutamicum* before.

The growth stimulating effect of $\text{CO}_2/\text{HCO}_3^-$ was qualitatively robust and could be reproduced in three different settings (bioreactor, shaking flasks and BioLector). Although an enhanced growth phenotype seemed to follow higher intracellular Fe^{2+} availability, further increase of the intracellular Fe^{2+} concentration through the synergistic effect of PCA and HCO_3^- could not increase the growth rate itself over a PCA supplemented cultivation. By this, it is suggested, that iron availability is not the growth limiting factor in a PCA supplemented cultivation any longer.

Consistent with the Fe^{2+} limited growth under non-supplemented conditions, the Δpup mutant, exhibited an even stronger growth retardation than the WT under reference conditions. *C. glutamicum* Δpup growth performance had been studied on a number of different carbon sources and stress conditions. Only in a cultivation under iron starvation conditions, the growth phenotype differed remarkably from the WT, indicating that it sensed a stronger iron limitation (Küberl et al., 2016).

In summary, different growth phenotypes of *C. glutamicum* were redundantly correlated with the intracellular Fe^{2+} availability. A growth retardation under reference conditions was caused by the insufficient iron availability and both could be increased apparently at elevated $\text{CO}_2/\text{HCO}_3^-$ contents.

5.2 Iron is reduced by phenolic compounds

Iron in CgXII medium is provided as FeSO_4 , and thus, Fe^{2+} after dissolution. However, 99 % of the initial iron concentration will be oxidised to poorly soluble Fe^{3+} within 15 min of an aerobic cultivation (Davison and Seed, 1983). At atmospheric conditions typical dissolved oxygen concentrations ($7.5 - 8 \text{ mg L}^{-1}$) exceed the iron concentration at least by the factor of four (Blombach and Takors, 2015). Hence, it is plausible, that the iron source is completely oxidised even before starting the experiment, considering typical preparation times of the medium.

Since increased intracellular Fe^{2+} levels were reported by *C. glutamicum* FEM3, either the Fe^{2+} oxidation state was stabilised or iron reduction must have been enhanced under PCA and $\text{CO}_2/\text{HCO}_3^-$ supplemented conditions.

Intracellular (total) iron concentrations in *C. glutamicum* might range between 0.4 and 3 $\text{mmol}_{\text{Fe}} \text{ L}^{-1}$ depending on the growth media (Liebl, 2005) and assuming cell volumes of $1.7 \mu\text{L mg}_{\text{CDW}}^{-1}$ as determined by Bröer and Krämer (1990). In order to meet physiological conditions, *in vitro* assays were conducted at an FeCl_3 concentration of 0.5 mM and 19.5 μM of reductants (e.g. PCA), which represents 10 % of the PCA concentration in CgXII medium at the beginning of the cultivation. Iron reduction experiments in conjunction with LC-MS-QTOF analytics provided evidence, that PCA served indeed as the electron donor in the reduction of Fe^{3+} . The secretion of catecholate, phenolate and derivatives in iron deprived cultivations had been described in a number of organisms (Peters and Warren, 1968a; Tait, 1975; Neilands, 1981; Barbeau et al., 2001). Due to their iron chelating properties, they are generally associated with the enhanced iron transport (Peters and Warren, 1968b; Liebl et al., 1989; Frunzke and Bott, 2008; Rattledge and Chaudhry, 1971). By tracking the radioactively labeled iron (^{59}Fe) isotope it was shown, that 2,3-DHB supplementation enhanced the iron uptake rate in *B. subtilis* (Peters and Warren, 1968b). The authors speculate, that the entire 3:1 complex of 2,3-DHB (or derivatives) and iron was internalised. However, the mode of iron uptake was not studied experimentally.

In the present study, the increased intracellular Fe^{2+} concentration correlated with the reduction of iron through PCA *in vitro*. This observation was in accordance with literature focussing on the chemical reactions in iron-catechol and -catecholate complexes, that was reviewed e.g. by Perron and Brumaghim (2009). Redox reactions in iron-catechol/-catecholate complexes were observed at acidic pH values favoring 1:1 binding stoichiometries (Avdeef et al., 1978). The redox reaction was also demonstrated in iron-PCA complexes, in particular (Kennedy and Powell, 1985). Establishing a mix of 3:1 and 2:1 complexes, at physiological pH values iron reduction was not expected to occur (Perron and Brumaghim, 2009). Hence, the present data contribute to the general understanding of iron reduction by showing that the reaction is not restricted to acidic conditions, because all experiments were conducted at physiological pH (7.4). Findings, that ferritin iron was also extracted and reduced by PCA were in accordance with the literature (Boyer et al., 1988), where experiments were conducted, however, at rather unphysiological pH 5.5. Crichton et al. (1980) found that chelating agents including 2,3-DHB removed iron from ferritin at pH 7.4. But they did not observe the reduction of it, as experiments were not conducted with a Fe^{2+} specific iron chelator like ferrozine or BPS. It is discussed below, to what extent the outcome might vary with the experimental setup.

LC-MS-QTOF results supported the interpretation of iron reduction assay, that PCA served as the electron donor of the reaction, by showing that it was degraded over time. Interestingly, semiquinone and quinone form of the PCA molecule, that were expected as the primary oxidation products emerging during iron reduction (Perron and Brumaghim, 2009), could not be detected by the LC-MS approach. This might be due to the analytical setup or indicate the thorough degradation of PCA considering sampling point (after 5 h) and the lack of appropriate sample processing to stop the reaction. Thus, PCA oxidation might have continued, and the analytes resulting from it ($\text{C}_7\text{H}_6\text{O}_6$ and $\text{C}_7\text{H}_8\text{O}_6$) might represent the downstream oxidation products β -carboxy-*cis-cis*-muconic acid or β -carboxy- γ -carboxymethyl- $\Delta^{\alpha,\beta}$ -butenolide and butene-1,2,3-tricarboxy acid. These compounds had been identified before, when PCA was oxidised

under harsh reaction conditions with peroxyacetic acid (Morgan, 1962) and appear also during the enzymatic degradation of PCA in the β -ketoadipate pathway (Shen et al., 2012).

Structurally related with catecholate compounds is 3-hydroxyanthranilic acid (2-amino-3-hydroxybenzoic acid), in which one hydroxyl group of 2,3-DHB is substituted with a functional amino group. 3-HAA was secreted during stationary phase and mediated the reduction of iron, that is required for iron uptake by *C. neoformans*. This was concluded particularly from the fact, that the addition of BPS to the culture broth abolished growth of *C. neoformans*, indicating iron was reduced extracellularly and prior to uptake (Nyhus et al., 1997) because it resembled a previous study in *S. cerevisiae* perfectly (Lesuisse et al., 1987). However, the reaction mechanism was not further specified. Since *in vitro* iron reduction performance of 3-HAA was similar to catechol and PCA in this study, it might be assumed that the reaction mechanism is also analogous, thus, oxidising the amino group to the primary imine.

The presence of 1 mM BPS in *C. glutamicum* cultures (BioLector) caused a growth retardation, that could not be compensated with PCA nor NaHCO_3 supplementation, but did not completely abolish it as in *C. neoformans* (Nyhus et al., 1997). The intracellular Fe^{2+} availability was always low in BPS supplemented cultivations and could not be increased by either supplement. BPS was not utilised as C-source itself and apparently not internalised. The results suggest that iron is reduced prior to uptake in *C. glutamicum* and the mode of iron transport seemed to be independent of the cultivation condition. However, question marks remain, and might be addressed in future work. It is not clear whether iron was necessarily taken up to afford growth. In iron depleted medium two to three cell divisions could be observed in accordance with Frunzke et al. (2011) and are presumably enabled by the mobilisation of iron storages.

It was proposed, that during exponential growth of *C. neoformans* iron was reduced predominantly through the action of an extracellular ferric reductase (Nyhus et al., 1997). Oxidoreductase function depends on sufficient concentrations and the constant regeneration of cofactors like NAD(P)H, which need to be efficiently transported across the

membrane for the extracellular reductase activity. But such transport systems have not been described (Schröder et al., 2003).

Beyond the location of ferric reductases, many turned out to be designated flavin reductases in fact, which catalyse the regeneration of reduced flavin. Subsequently, Fe^{3+} is reduced in a chemical reaction yielding Fe^{2+} and (re-)oxidised flavin (Schröder et al., 2003). It was shown recently, that extracellular flavin is a mediator which shuttles electrons from the extracellular electron transport (EET) machinery of *Listeria monocytogenes* to an anode or Fe^{3+} , respectively (Light et al., 2018). Considering that the redox recycling of flavin relies on the interconversion of its quinole/quinone form, the mechanistic similarities with phenolic or catecholic compounds in iron reduction are striking and raise the question whether they can serve analogously as extracellular electron mediators. Put the case, that oxidised PCA can indeed be recycled in a similar fashion, e.g. by the interaction with the *C. glutamicum* EET, it might be an interesting mediator to improve *C. glutamicum* performance in a bioelectrochemical system, that is currently hampered by the efficiency of electron transport (Kracke et al., 2015; Vassilev et al., 2018).

5.3 HCO_3^- accelerates iron chelation and reduction

It is the major outcome of this work, that the reduction of iron was accelerated in the presence of bicarbonate. Regardless of the electron donor, which was established in the previous section, the presence of HCO_3^- enhanced the redox reaction *in vitro*. This included 4-amino-2-hydroxybenzoic acid, which exhibited lower iron reduction capacity than PCA. But HCO_3^- remained without effect, when a suitable electron donor was lacking in the assay.

The role of HCO_3^- might even be essential for the iron reduction through PCA. When the standard setup (incubation in 96-well microtiter plates) was changed and the assay was incubated in closed vials, iron reduction was almost completely abolished unless providing NaHCO_3 . Further experiments were conducted with PCA, exemplarily, in

order to investigate the mechanistic interaction between HCO_3^- , Fe^{3+} and PCA. A λ_{max} shift of the Fe^{3+} -PCA complex suggests an active participation of HCO_3^- in the complex itself. Analogously, shifts of the maximum absorbance were found to be caused by the presence of OH^- in mono- and biscatecholate complexes Fe^{3+} (Kennedy and Powell, 1985). Due to the mutual interaction between $\text{CO}_2/\text{HCO}_3^-$ and pH (Blombach and Takors, 2015), one might expect variations of the OH^- concentration as the explanation for the λ_{max} shift. In order to rule out this possibility, pH effects were addressed. By monitoring the pH value it was ensured that the buffer capacity of the assay sufficed to maintain the pH at 7.4. The intentional perturbation of the assay pH failed to reproduce the λ_{max} shift in the presence of HCO_3^- . In this view, it appears plausible that HCO_3^- substituted OH^- at one or more sites for the octahedral Fe^{3+} coordination. This might reduce the number of catecholate ligands (to a mono- or bis-coordinated complex) and, thus, facilitate the electron transfer as discussed above. However, an increase of the initial Fe^{3+} -PCA complex formation rate by 46 % might suggest that HCO_3^- increases the Fe^{3+} availability for PCA, e.g. by enhancing its solubility in ferric bicarbonate, $\text{Fe}(\text{HCO}_3)_3$ (Byrne and Kester, 1976). The precise nature of such complexes could be addressed e.g. by Mössbauer spectroscopy in the future.

5.4 Secretion of reductants by *C. glutamicum*

The *in vitro* iron reduction was only accelerated in the presence of HCO_3^- when phenolic compounds were provided alongside of it, whilst the effect of HCO_3^- alone was negligible. It might be concluded, that the growth stimulating effect *in vivo* with higher intracellular Fe^{2+} concentrations inherently relies on the natural secretion of reductants by *C. glutamicum*. It is a surprise in this regard, that *C. glutamicum* is genetically equipped for the biosynthesis of PCA, but does not regulate the respective gene expression in response to iron deprivation (Teramoto et al., 2009; Kubota et al., 2014). In contrast, *B. anthracis* secreted PCA in iron restricted cultivations, when PCA was not incorporated as the precursor in the siderophore anthrachelin (Garner et al., 2004). Small amounts of PCA could be detected in culture supernatants of a *C. glutamicum* FEM3 bioreactor

cultivation, but did not vary with the CO₂ content and were not quantified. Besides PCA secretion of a compound with the chemical formula C₇H₇NO₃ was qualified. The chemical formula coincides with 3-HAA, that mediates iron reduction in the siderophore deficient *C. neoformans* (Nyhus et al., 1997). However, neither 3-HAA nor the four regioisomers tested here, could be confirmed as the secreted amino-hydroxybenzoic acid via the retention time. Hence, it remains to be elucidated, what is the major reductant in *C. glutamicum*, if it is possible to single out one in particular.

5.5 Physiological relevance of *in vitro* iron reduction

There is a continuous debate about the physiological relevance of redox reactions in Fe³⁺ catecholate complexes. Contradictory observations were made in the past and the role of catecholates discussed ranges from antioxidant to pro-oxidant as reviewed e.g. by Perron and Brumaghim (2009) and Schweigert et al. (2001). Hence, it should be noted, that the experimental setup is always essentially decisive for its result.

This fact is particularly striking when considering two publications by Crichton et al. (1980) and Boyer et al. (1988), respectively, that investigated ferritin iron release through catecholates. Probably more important than buffer pH, was the use of the Fe²⁺ specific chelator ferrozine in the latter study. Consequently, emerging Fe²⁺ was detected and the reductive iron release through PCA was postulated. On the contrary, lacking this type of chelator Fe²⁺ resulting from the reduction was not detected to the same extend in the former study (Crichton et al., 1980).

Besides the detection principle, the presence of oxygen shifts the experimental outcome. Whereas Fe²⁺ is stabilised under anaerobic conditions, it will be rapidly (re-)oxidised in the presence of oxygen as outlined above (Davison and Seed, 1983). The use of BPS in this study to detect emerging Fe²⁺ was beneficial as (i) the complex protected Fe²⁺ from reoxidation. (ii) Capturing Fe²⁺ in the complex shifted the chemical equilibrium constantly, by that favoring the reduction reaction.

Thus, does the *in vitro* assay represent physiologically irrelevant conditions? To be incorporated as the enzyme cofactor, iron is usually assembled in iron sulfur clusters. The

first enzyme involved in this machinery, IscA in *E. coli*, exhibits a high Fe^{2+} affinity ($K_D = 3.3 - 5 * 10^{-20}$ M, Ding and Clark (2004) and Ding et al. (2005)), which is also in line with the iron affinity of human transferrin ($K_D = 2.1 * 10^{-21}$ M and $4.2 * 10^{-20}$ M, respectively, Aisen et al. (1978)). Hence, it can be concluded, that the use of high affinity iron chelators like BPS provides a suitable representation of the physiological situation. The chemical structure of iron reductants appeared to be a phenol moiety containing at least one additional (amino or hydroxy) group. However, a simple phenol was not tested. Suitable compounds are vastly abundant in nature as they form part of the central metabolism and comprise intermediates of the shikimic acid pathway in particular. High concentrations of phenolic and catecholic substances can be encountered in soils, where they are released during the degradation of biomass, e.g. lignin (Schweigert et al., 2001). Likewise, great titers accumulate in the human plasma short after ingestion of plant derived food products (Perron and Brumaghim, 2009). The functional groups discussed here are present in the classes of phenolate- and catecholate-type siderophores (Butler and Theisen, 2010; Wilson et al., 2016) and can also be found within a number of stress hormones and neurotransmitters including dopamine, adrenaline and norephedrine. In fact, the latter have been reported to liberate Fe^{3+} from host iron storages, lactoferrin and transferrin, reduce it to Fe^{2+} and promote bacterial growth (Coulanges et al., 1998; Freestone et al., 2000; Freestone et al., 2007; Sandrini et al., 2010). The same habitats might be characterised by the presence of great amounts of CO_3^{2-} or HCO_3^- considering calcareous soils or the human body. Constantly high concentrations of both (reductant and CO_2 species) might shift the general equilibrium of iron species, whereas variations of either availability (reductant and CO_2 species) might induce a sudden iron reduction and Fe^{2+} availability peak.

Amongst the inhabitants of the human body, pathogens possess an outstanding role. They encounter in a constant battle for iron, which might be reflected in the iron availability issue of *C. glutamicum* under reference conditions (Wilson et al., 2016). By reviewing the currently most threatening human pathogens, at least *Pseudomonas aeruginosa*, *Staphylococcus aureus*, *Klebsiella pneumoniae*, *M. tuberculosis* and pathogenic *E.*

coli strains as well as several other pathogens turned out to regulate the virulence expression in response to the Fe^{2+} availability (Litwin and Calderwood, 1993; Torres et al., 2010; Lin et al., 2011; Zondervan et al., 2018). Hence knowledge of the environmental impact on Fe^{2+} availability, might be particularly interesting in order to understand and predict pathogenicity and the course of disease and, consequently, chose the right therapy.

5.6 HCO_3^- is not the co-effector of DtxR

An anion binding site had been postulated in the DtxR protein, that is essential for the coordination of Fe^{2+} (and analogous divalent metal ions *in vitro*) at the high affinity metal binding site (Qiu et al., 1996). Having observed the $\text{CO}_2/\text{HCO}_3^-$ induced transcriptional response (Blombach et al., 2013), it appeared reasonable to wonder, whether HCO_3^- provides the co-stimulus for DtxR activation *in vivo*. Because the physiological stimulus of DtxR, Fe^{2+} , undergoes rapid oxidation, when anaerobic assay conditions are not established, the experiments were performed with divalent nickel (Ni^{2+}) and manganese (Mn^{2+}) ions in this work. The results obtained here were in good qualitative accordance with previous reports analysing the DtxR homologue from *C. diphtheriae* (Spiering et al., 2003). It was concluded that the high T_m shift by about 20 °C provoked through Ni^{2+} and Mn^{2+} binding represented the more drastic conformational change of DtxR upon occupation of the primary metal binding site (Goranson-Siekierke et al., 1999). If this holds true, the dissociation constant for Ni^{2+} obtained in the described setup ($K_D(\text{Ni}^{2+}) = 5.3 \pm 1.1 \mu\text{M}$) was about 100 times lower than reported for DtxR_{C.d.} (D'Aquino et al., 2005). Irreversible dimerisation and denaturation of the wt-DtxR protein hampered the initial experiments. Therefore, the DtxR mutant C102D was constructed in analogy to Tao and Murphy (1993). DtxR(C102D) exhibited a reduction of T_m by roughly 4 °C over the full range of test conditions and performed qualitatively like wt-DtxR. Experimental data from thermal stability assays with both, wt-DtxR and DtxR(C102D), did not support the hypothesis of HCO_3^- acting as the co-stimulus for DtxR activation. In fact, several anions had been found to occupy the binding site of

DtxR and homologues including acetate (which shares the highest structural similarity with HCO_3^-), but also sulfate and phosphate ions had been identified in crystallographic structures (Qiu et al., 1996; D'Aquino et al., 2009; Wisedchaisri et al., 2007). None of these anions could be proven beneficial for the thermal stability of DtxR. This might be a surprise at the first glance. However, the anion is involved in metal coordination at the high affinity binding site. This site is first occupied and binding does not induce comparable conformational changes, as this is the predominant role of the low affinity iron binding site (Goranson-Siekierke et al., 1999; D'Aquino et al., 2005). It cannot be excluded, that the anion binding site of DtxR is occupied by HCO_3^- under physiological conditions. But it appears unlikely to provide the co-stimulus for DtxR activation considering the binding order of the effector molecules.

5.7 Cg2444 – an interaction partner of DtxR?

The C-terminal domain of DtxR is particularly interesting, as it shares significant sequence identity with FeoA (Andrews et al., 2003). It was proposed, that the C-terminal domain is not essential for DtxR function, because not all DtxR homologues comprise this domain (Posey et al., 1999). Comparably, not all genetic loci encoding the transport protein FeoB contain the *feoA* gene (Andrews et al., 2003). The SH3-like structure of the C-terminal domain had been noted in the past and it was postulated, that amino acid residues of this domain contributed to iron binding by DtxR, thus revealing intra-protein-protein interaction (Qiu et al., 1996; Feese et al., 2001; Love et al., 2003). The functional role of FeoA in iron transport has not been disclosed to date. However, a potential (inter-protein-protein) interaction with FeoB has been reviewed e.g. by Lau et al. (2015). It was formulated at the beginning of this work, that the C-terminal domain of DtxR could also be the target region to integrate further stimuli by interaction with a putative modulator protein.

Trying to identify potential interaction partners, the abundance of Cg2444 protein fragments in DtxR pull-down experiments was remarkable. Literature research revealed,

that *cg2444* was not expressed in an operon with *cg2445*, as transcript levels of both genes were not found to be strictly coupled in a $\Delta dtxR$ strain (Brune et al., 2006; Wenerhold and Bott, 2006), although the operon structure could have been expected from the genomic sequence (Pfeifer-Sancar et al., 2013). Interestingly, *cg2445* is also involved in the iron homeostasis as it encoded the heme oxygenase HmuO (Frunzke et al., 2011). Since the $\Delta cg2444$ mutant did not reproducibly show a growth phenotype in response to different CO₂ levels (bioreactor) or in the shaking flask screening approach, this target was not further pursued as potentially CO₂/HCO₃⁻ induced regulator/modulator. However, because of the abundance of Cg2444 co-purified with DtxR and the genomic context of *cg2444* (Kalinowski et al., 2003; Frunzke et al., 2011), this target remains interesting for future analysis in the context of DtxR modulation.

5.8 Iron transport and mobilisation in *C. glutamicum*

Intracellular iron concentrations had been quantified in astrocyte cells (Riemer et al., 2004) and the same approach was successfully applied to *C. glutamicum* cells when they were cultivated with 1 μ M FeSO₄ in the presence of PCA (Küberl et al., 2016). Therefore, it was expected, that the assay could be readily adapted for the purpose of this study. However, providing PCA in about 200 times excess (over iron) in the latter study, the entire iron pool might be maintained in solution throughout the experiment. In contrast, in CgXII medium lacking PCA the entire iron pool might be rapidly oxidised in accordance with the kinetics proposed by Davison and Seed (1983), as discussed previously (5.2). This would result in the precipitation of a large proportion of Fe³⁺ soon after starting the cultivation. PCA and iron chelates were not externally supplemented in the present study unless explicitly indicated. As a consequence, iron precipitates might have formed in the reference cultivation and it cannot be assumed that these have been removed quantitatively during the washing step.

The assay results appeared to be very reliable in principle, as the iron balance was closed to 80 – 100 % throughout the reference cultivation. However, future work is required, to

remove potential iron precipitates from the cell pellet quantitatively, without extracting intracellular iron at the same time. The use of EDTA during iron detection with BPS is not recommended as it interferes with the colour development (Derman et al., 1989). Hence, the results obtained for iron uptake by *C. glutamicum* under reference conditions were not further considered. PCA supplemented medium, provided a > 3-fold excess with regard to the iron concentration enabling complexation of the entire amount of iron in 3:1 stoichiometry (Kennedy and Powell, 1985). Therefore, the iron uptake data obtained in the PCA supplemented cultivation seemed more reliable. The highest intracellular iron concentration of a PCA supplemented shaking flask cultivation ($1.6 \pm 0.8 \text{ mg}_{\text{Fe}} \text{ g}_{\text{CDW}}^{-1}$) was detected after 2 h and represents > 5-fold and about 40-fold the *C. glutamicum* iron concentration determined before in BMCG and CgIII medium, respectively (Liebl, 2005).

The intracellular Fe^{2+} concentration is not necessarily coupled to the concentration of total iron because lower intracellular Fe^{2+} levels had been found in a Δpup mutant revealing the identical total iron content of the WT (Küberl et al., 2016). Quantification of the intracellular iron content would improve the understanding of iron uptake in *C. glutamicum*, particularly to address the transport mode. Thus far, it is assumed from growth and fluorescence experiments in the presence and absence of iron and BPS, that Fe^{2+} is transported into the cell after the extracellular reduction by PCA. However, this study provides no evidence, that Fe^{3+} -PCA complexes cannot be internalised by *C. glutamicum*.

It was not the objective of this study to investigate iron transport systems in *C. glutamicum* in principle. Wondering how elevated $\text{CO}_2/\text{HCO}_3^-$ might affect iron uptake, the focus was set on potential symporters. Although the gene product of *cg0041-0042* appeared particularly interesting in this context, as Fe^{2+} - HCO_3^- symport was postulated in *S. pyogenes* containing a protein that shares 28 % sequence identity with Cg0041, the deletion strain generated in this study did not differ from the WT regarding growth performance and fluorescence. This might be either due to redundant transport systems or HCO_3^- independent iron uptake. Deletion mutants of the genes encoding storage

proteins in *C. glutamicum* (Δftn , Δdps or the double deletion mutant $\Delta ftn \Delta dps$) were generated in order to determine the iron source for reduction through PCA. It must be concluded from the present data (growth and phenotypes resembled WT), that storage proteins were not the primary iron source for reduction. On the contrary, PCA could be proven to reduce ferritin iron *in vitro* using purified ferritin, in accordance with the literature (Boyer et al., 1988). Lacking data on basal expression levels of *ftn* and *dps* or quantification on the proteome level, it remains unclear whether Ftn and Dps are present (and loaded with iron) under standard conditions. Both genes are co-regulated by OxyR, and thus, de-repressed in the presence of H₂O₂ (Milse et al., 2014). Brune et al. (2006) found *ftn* and *dps* to be differentially transcribed in the $\Delta dtxR$ mutant, whereas this was not observed in a similar setting by Wennerhold and Bott (2006). The CO₂ induced transcriptional response included almost the entire DtxR regulon. But alternated transcript levels of *ftn* and *dps* were not detected, either (Blombach et al., 2013). Hence, the physiological impact of PCA and CO₂/HCO₃⁻ on the intracellular iron reduction might be dependent on the growth condition and did not provoke a phenotypical response in our experiments.

Conclusion

This study was started with the intention to shed light on the interaction of $\text{CO}_2/\text{HCO}_3^-$ and the iron homeostasis causing DtxR activation in *C. glutamicum*. The mode of interference was eventually identified as purely chemical. HCO_3^- accelerated the complex formation of Fe^{3+} -PCA and the subsequent redox reaction yielding Fe^{2+} . Contrasting the common literature, phenolic compounds reduced iron *in vitro* at physiological conditions and provoked a greater intracellular Fe^{2+} availability in *C. glutamicum*. The positive interference of $\text{CO}_2/\text{HCO}_3^-$ with Fe^{2+} pools had not been addressed in the past. Since all required components are wide spread in nature, the abiotic effect described in this study might be of broad significance for other biological and geochemical systems, which experience the greater Fe^{2+} availability, as a consequence. Hence, this study contributes with its results to the general understanding of the global iron cycle.

Future research might show, whether Fe^{3+} is reduced only extracellularly or if the iron reduction mechanism is general and proceeds also inside the cell. In addition to this it will be interesting to specify the mechanistic role of $\text{CO}_2/\text{HCO}_3^-$ with regard to the redox reaction. Is the electron transfer restricted to Fe^{3+} ions, transition metals or has it the potential to increase transfer reactions in electrobiochemical approaches?

- (1) Abe, S., Takayama, K. I., and Kinoshita, S. (1967). Taxonomical studies on glutamic acid-producing bacteria. *The Journal of General and Applied Microbiology* 13, 279–301.
- (2) Aisen, P., Leibman, A., and Zweier, J. (1978). Stoichiometric Iron to Human and Site Characteristics Transferrin*. *Journal of Biological Chemistry* 253, 1930–1937.
- (3) Alcántara, E., Romera, F. J., Cañete, M., and De la Guardia, M. D. (2000). Effects of bicarbonate and iron supply on Fe(III) reducing capacity of roots and leaf chlorosis of the susceptible peach rootsrock "Nemaguard". *Journal of Plant Nutrition* 23, 1607–1617.
- (4) Alhendawi, R. A., Römheld, V., Kirkby, E. A., and Marschner, H. (1997). Influence of increasing bicarbonate concentrations on plant growth, organic acid accumulation in roots and iron uptake by barley, sorghum, and maize. *Journal of Plant Nutrition* 20, 1731–1753.
- (5) Andrews, S. C., Robinson, A. K., and Rodríguez-Quñones, F. (2003). Bacterial iron homeostasis. *FEMS Microbiology Reviews* 27, 215–237.
- (6) Arndt, A. and Eikmanns, B. J. In *Corynebacteria: Genomics and Molecular Biology*, Burkovski, A., Ed.; Caister Academic Press: Norfolk, UK, 2008; Chapter 7, pp 155–182.
- (7) Avdeef, A., Sofen, S. R., Bregante, T. L., and Raymond, K. N. (1978). Coordination Chemistry of Microbial Iron Transport Compounds. 9.1 Stability Constants

- for Catechol Models of Enterobactin. *Journal of the American Chemical Society* 100, 5362–5370.
- (8) Baez, A., Flores, N., Bolívar, F., and Ramírez, O. T. (2009). Metabolic and transcriptional response of recombinant *Escherichia coli* to elevated dissolved carbon dioxide concentrations. *Biotechnology and Bioengineering* 104, 102–110.
- (9) Bailey, J. and Ollis, D., *Biochemical Engineering Fundamentals*, 2nd; Bailey, J. and Ollis, D., Eds.; McGraw-Hill: New York, NY, 1986.
- (10) Barbeau, K, Rue, E. L., Bruland, K. W., and Butler, A (2001). Photochemical cycling of iron in the surface ocean mediated by microbial iron(III) - binding ligands. *Nature* 413, 409–413.
- (11) Bäumchen, C., Knoll, A., Husemann, B., Seletzky, J., Maier, B., Dietrich, C., Amoabediny, G., and Büchs, J. (2007). Effect of elevated dissolved carbon dioxide concentrations on growth of *Corynebacterium glutamicum* on D-glucose and L-lactate. *Journal of Biotechnology* 128, 868–874.
- (12) Becker, J. and Wittmann, C. (2012). Bio-based production of chemicals, materials and fuels - *Corynebacterium glutamicum* as versatile cell factory. *Current Opinion in Biotechnology* 23, 631–40.
- (13) Blair, D. and Diehl, H. (1961). Bathophenanthrolinedisulphonic acid and bathocuproinedisulphonic acid, water soluble reagents for iron and copper. *Talanta* 7, 163–174.
- (14) Blombach, B. and Takors, R. (2015). CO₂ - Intrinsic product, essential substrate, and regulatory trigger of microbial and mammalian production processes. *Frontiers in Bioengineering and Biotechnology* 3, 1–11.
- (15) Blombach, B., Riester, T., Wieschalka, S., Ziert, C., Youn, J.-W., Wendisch, V. F., and Eikmanns, B. J. (2011). *Corynebacterium glutamicum* tailored for efficient isobutanol production. *Applied and environmental microbiology* 77, 3300–10.

-
- (16) Blombach, B., Buchholz, J., Busche, T., Kalinowski, J., and Takors, R. (2013). Impact of different $\text{CO}_2/\text{HCO}_3^-$ levels on metabolism and regulation in *Corynebacterium glutamicum*. *Journal of Biotechnology* 168, 331–340.
- (17) Boyd, J., Oza, M. N., and Murphy, J. R. (1990). Molecular cloning and DNA sequence analysis of a diphtheria *tox* iron-dependent regulatory element (*dtxR*) from *Corynebacterium diphtheriae*. *Genetics* 87, 5968–5972.
- (18) Boyer, R. F., Clark, H. M., and LaRoche, A. P. (1988). Reduction and Release of Ferritin Iron By Plant Phenolics. *Journal of Inorganic Biochemistry* 32, 171–181.
- (19) Brett, P. J., Burtnick, M. N., Fenno, J. C., and Gherardini, F. C. (2008). *Treponema denticola* TroR is a manganese- and iron-dependent transcriptional repressor. *Molecular Microbiology* 70, 396–409.
- (20) Bröer, S. and Krämer, R. (1990). Lysine uptake and exchange in *Corynebacterium glutamicum*. *Journal of Bacteriology* 172, 7241–7248.
- (21) Brune, I., Werner, H., Hüser, A. T., Kalinowski, J., Pühler, A., and Tauch, A. (2006). The DtxR protein acting as dual transcriptional regulator directs a global regulatory network involved in iron metabolism of *Corynebacterium glutamicum*. *BMC genomics* 7, 21.
- (22) Burkovski, A. (2003). Ammonium assimilation and nitrogen control in *Corynebacterium glutamicum* and its relatives: An example for new regulatory mechanisms in actinomycetes. *FEMS Microbiology Reviews* 27, 617–628.
- (23) Butler, A. and Theisen, R. M. (2010). Iron(III)-siderophore coordination chemistry: Reactivity of marine siderophores. *Coordination Chemistry Reviews* 254, 288–296.
- (24) Byrne, R. H. and Kester, D. R. (1976). Solubility of hydrous ferric oxide and iron speciation in seawater. *Marine Chemistry* 4, 255–274.

- (25) Carmona, F., Palacios, Ò., Gálvez, N., Cuesta, R., Atrian, S., Capdevila, M., and Domínguez-Vera, J. M. (2013). Ferritin iron uptake and release in the presence of metals and metalloproteins: Chemical implications in the brain. *Coordination Chemistry Reviews* 257, 2752–2764.
- (26) Castan, A., Näsman, A., and Enfors, S. O. (2002). Oxygen enriched air supply in *Escherichia coli* processes: Production of biomass and recombinant human growth hormone. *Enzyme and Microbial Technology* 30, 847–854.
- (27) Chaudhry, M. T., Huang, Y., Shen, X. H., Poetsch, A., Jiang, C. Y., and Liu, S. J. (2007). Genome-wide investigation of aromatic acid transporters in *Corynebacterium glutamicum*. *Microbiology* 153, 857–865.
- (28) Chen, Z., Bommarreddy, R. R., Frank, D., Rappert, S., and Zeng, A.-P. (2013). Deregulation of Feedback Inhibition of Phosphoenolpyruvate Carboxylase for Improved Lysine Production in *Corynebacterium glutamicum*. *Applied and Environmental Microbiology* 80, 1388–1393.
- (29) Cooper, S. R., Mcardle, J. V., and Raymond, K. N. (1978). Siderophore electrochemistry: Relation to intracellular iron release mechanism. *Proceedings of the National Academy of Sciences* 75, 3551–3554.
- (30) Cordes, C., Möckel, B., Eggeling, L., and Sahm, H. (1992). Cloning, organization and functional analysis of *ilvA*, *ilvB* and *ilvC* genes from *Corynebacterium glutamicum*. *Gene* 112, 113–116.
- (31) Coulanges, V., Andre, P., and Vidon, D. J. (1998). Effect of siderophores, catecholamines, and catechol compounds on *Listeria spp.* growth in iron-complexed medium. *Biochemical and Biophysical Research Communications* 249, 526–530.
- (32) Cowart, R. E., Singleton, F. L., and Hind, J. S. (1993). A comparison of bathophenanthrolinedisulfonic acid and ferrozine as chelators of iron(II) in reduction reactions. *Analytical Biochemistry* 211, 151–155.
- (33) Crichton, R. R., Roman, F., and Roland, F. (1980). Iron mobilization from ferritin by chelating agents. *Journal of Inorganic Biochemistry* 13, 305–316.

-
- (34) Cummins, E. P., Selfridge, A. C., Sporn, P. H., Sznajder, J. I., and Taylor, C. T. (2014). Carbon dioxide-sensing in organisms and its implications for human disease. *Cellular and Molecular Life Sciences* 71, 831–845.
- (35) D’Aquino, J. A., Denninger, A. R., Moulin, A. G., D’Aquino, K. E., and Ringe, D. (2009). Decreased Sensitivity to Changes in the Concentration of Metal Ions as the Basis for the Hyperactivity of DtxR(E175K). *Journal of Molecular Biology* 390, 112–123.
- (36) D’Aquino, J. A., Tetenbaum-Novatt, J., White, A., Berkovitch, F., and Ringe, D. (2005). Mechanism of metal ion activation of the diphtheria toxin repressor DtxR. *Proceedings of the National Academy of Sciences of the United States of America* 851, 196–198.
- (37) Davison, W. and Seed, G. (1983). The kinetics of the oxidation of ferrous iron in synthetic and natural waters. *Geochimica et Cosmochimica Acta* 47, 67–79.
- (38) Dennison, C, *A Guide to Protein Isolation*, 2nd ed.; Springer Science & Business Media: 2013, pp 211–212.
- (39) Derman, D. P., Green, A., Bothwell, T. H., Graham, B., Mcnamara, L., MacPhail, A. P., and Baynes, R. D. (1989). A systematic evaluation of bathophenanthroline, ferrozine and ferene in an ICSH-based method for the measurement of serum iron. *Annals of Clinical Biochemistry* 26, 144–147.
- (40) Ding, H. and Clark, R. J. (2004). Characterization of iron binding in IscA, an ancient iron-sulphur cluster assembly protein. *Biochemical Journal* 379, 433–440.
- (41) Ding, H., Harrison, K., and Lu, J. (2005). Thioredoxin reductase system mediates iron binding in IscA and iron delivery for the iron-sulfur cluster assembly in IscU. *Journal of Biological Chemistry* 280, 30432–30437.
- (42) Dominguez, H, Nezondet, C, Lindley, N. D., Coccagn, M, National, I., and Ranguelil, C. S. D. (1993). Modified carbon flux during oxygen limited growth of *Corynebacterium glutamicum* and the consequences for amino acid overproduction. *Biotechnology Letters* 15, 449–454.

- (43) Dower, W. J., Miller, J. F., and Ragsdale, C. W. (1988). High efficiency transformation of *E. coli* by high voltage electroporation. *Nucleic acids research* *16*, 6127–45.
- (44) Eggeling, L. and Bott, M., *Handbook of Corynebacterium glutamicum*; Eggeling, L. and Bott, M., Eds.; CRC Press: 2005.
- (45) Eikmanns, B. J. In *Handbook of Corynebacterium glutamicum*, Eggeling, L. and Bott, M., Eds.; CRC Press: 2005; Chapter 11, pp 243–278.
- (46) Eikmanns, B. J., Metzger, M., Reinscheid, D., Kircher, M., and Sahm, H. (1991). Amplification of three threonine biosynthesis genes in *Corynebacterium glutamicum* and its influence on carbon flux in different strains. *Applied Microbiology and Biotechnology* *34*, 617–622.
- (47) Emery, T. (1971). Role of Ferrichrome as a Ferric Ionophore in *Ustilago sphaerogena*. *Biochemistry* *10*, 1483–1488.
- (48) Failmezger, J., Nitschel, R., Sánchez-Kopper, A., Kraml, M., and Siemann-Herzberg, M. (2016). Site-specific cleavage of ribosomal RNA in *Escherichia coli*-based cell-free protein synthesis systems. *PLoS ONE* *11*, 1–18.
- (49) Feese, M. D., Ingason, B. P., Goranson-Siekierke, J., Holmes, R. K., and Hol, W. G. J. (2001). Crystal Structure of the Iron-dependent Regulator from *Mycobacterium tuberculosis* at 2.0 Å Resolution Reveals the Src Homology Domain 3-like Fold and Metal Binding Function of the Third Domain. *Journal of Biological Chemistry* *276*, 5959–5966.
- (50) Feith, A., Teleki, A., Graf, M., Favilli, L., and Takors, R. (2019). HILIC-enabled ¹³C metabolomics strategies: Comparing quantitative precision and spectral accuracy of QTOF High- and QQQ low-resolution mass spectrometry. *Metabolites* *9*, 1–21.
- (51) Follmann, M., Ochrombel, I., Krämer, R., Trötschel, C., Poetsch, A., Rückert, C., Hüser, A., Persicke, M., Seiferling, D., Kalinowski, J., and Marin, K. (2009). Functional genomics of pH homeostasis in *Corynebacterium glutamicum* revealed

- novel links between pH response, oxidative stress, iron homeostasis and methionine synthesis. *BMC Genomics* 10, 621.
- (52) Freestone, P. P., Lyte, M., Neal, C. P., Maggs, A. F., Haigh, R. D., and Williams, P. H. (2000). The mammalian neuroendocrine hormone norepinephrine supplies iron for bacterial growth in the presence of transferrin or lactoferrin. *Journal of Bacteriology* 182, 6091–6098.
- (53) Freestone, P. P. E., Walton, N. J., Haigh, R. D., and Lyte, M. (2007). Influence of dietary catechols on the growth of enteropathogenic bacteria. *International Journal of Food Microbiology* 119, 159–169.
- (54) Frunzke, J. and Bott, M. In *Corynebacteria: Genomics and Molecular Biology*, Burkovski, A., Ed.; Horizon Scientific Press: Norwich, UK, 2008; Chapter 11, pp 241–266.
- (55) Frunzke, J., Gätgens, C., Brocker, M., and Bott, M. (2011). Control of heme homeostasis in *Corynebacterium glutamicum* by the two-component system HrrSA. *Journal of Bacteriology* 193, 1212–1221.
- (56) Fuchs, G., *Alternative Pathways of Carbon Dioxide Fixation: Insights into the Early Evolution of Life?*; 1, 2010; Vol. 65, pp 631–658.
- (57) Funk, F., Lender, J.-P., Crichton, R. R., and Schneider, W. (1985). Reductive mobilisation of ferritin iron. *European Journal of Biochemistry* 152, 167–172.
- (58) Garner, B. L., Arceneaux, J. E., and Byers, B. R. (2004). Temperature control of a 3,4-dihydroxybenzoate (protocatechuate)-based siderophore in *Bacillus anthracis*. *Current Microbiology* 49, 89–94.
- (59) Gibson, D. G. (2011). Enzymatic assembly of overlapping DNA fragments. *Methods in Enzymology* 498, 349–61.
- (60) Gibson, D. G., Young, L., Chuang, R.-Y., Venter, J. C., Hutchison, C. a., and Smith, H. O. (2009). Enzymatic assembly of DNA molecules up to several hundred kilobases. *Nature Methods* 6, 343–5.

- (61) Goranson-Siekierke, J., Pohl, E., Hol, W. G. J., and Holmes, R. K. (1999). Anion-coordinating residues at binding site 1 are essential for the biological activity of the diphtheria toxin repressor. *Infection and Immunity* 67, 1806–1811.
- (62) Grünberger, A., van Ooyen, J., Paczia, N., Rohe, P., Schiendzielorz, G., Eggeling, L., Wiechert, W., Kohlheyer, D., and Noack, S. (2013). Beyond growth rate 0.6: *Corynebacterium glutamicum* cultivated in highly diluted environments. *Biotechnology and Bioengineering* 110, 220–228.
- (63) Hanahan, D. (1983). Studies on Transformation of *Escherichia coli* with Plasmids. *Journal of Molecular Biology* 166, 557–580.
- (64) Hansmeier, N., Chao, T. C., Pühler, A., Tauch, A., and Kalinowski, J. (2006). The cytosolic, cell surface and extracellular proteomes of the biotechnologically important soil bacterium *Corynebacterium efficiens* YS-314 in comparison to those of *Corynebacterium glutamicum* ATCC 13032. *Proteomics* 6, 233–250.
- (65) Harris, W. R., Carrano, C. J., Cooper, S. R., Sofen, S. R., Avdeef, A. E., McArdle, J. V., and Raymond, K. N. (1979). Coordination Chemistry of Microbial Iron Transport Compounds. 19. Stability Constants and Electrochemical Behavior of Ferric Enterobactin and Model Complexes. *Journal of the American Chemical Society* 101, 6097–6104.
- (66) Hasegawa, S., Suda, M., Uematsu, K., Natsuma, Y., Hiraga, K., Jojima, T., Inui, M., and Yukawa, H. (2013). Engineering of *Corynebacterium glutamicum* for High-Yield L-Valine Production under Oxygen Deprivation Conditions. *Applied and Environmental Microbiology* 79, 1250–1257.
- (67) Heider, S. A. and Wendisch, V. F. (2015). Engineering microbial cell factories: Metabolic engineering of *Corynebacterium glutamicum* with a focus on non-natural products. *Biotechnology Journal* 10, 1170–1184.
- (68) Helgeson, H. C., Garrels, R. M., and MacKenzie, F. T. (1969). Evaluation of irreversible reactions in geochemical processes involving minerals and aqueous solutions - II. Applications. *Geochimica et Cosmochimica Acta* 33, 455–481.

-
- (69) Hem, J. D. and Nolan, T. B. (1960). Restraints on Dissolved Ferrous Iron Imposed by Bicarbonate Redox Potential, and pH chemistry of iron in natural water.
- (70) Herzberg, C., Weidinger, F. A. L., Dörrbecker, B., Hübner, S., Stülke, J., and Commichau, F. M. (2007). SPINE : A method for the rapid detection and analysis of protein – protein interactions in vivo. *Proteomics* 7, 4032–4035.
- (71) Hoffmann, J and Altenbuchner, J (2014). Hyaluronic acid production with *Corynebacterium glutamicum*: effect of media composition on yield and molecular weight. *Journal of Applied Microbiology* 117, 663–678.
- (72) Hoffmann, J., Bóna-Lovász, J., Beuttler, H., and Altenbuchner, J. (2012). *In vivo* and *in vitro* studies on the carotenoid cleavage oxygenases from *Sphingopyxis alaskensis* RB2256 and *Plesiocystis pacifica* SIR-1 revealed their substrate specificities and non-retinal-forming cleavage activities. *FEBS Journal* 279, 3911–3924.
- (73) Hughes, N. J., Chalk, P. A., Clayton, C. L., and Kelly, D. J. (1995). Identification of carboxylation enzymes and characterization of a novel four-subunit pyruvate:flavodoxin oxidoreductase from *Helicobacter pylori*. *Journal of Bacteriology* 177, 3953–3959.
- (74) Ikeda, M. and Nakagawa, S. (2003). The *Corynebacterium glutamicum* genome: Features and impacts on biotechnological processes. *Applied Microbiology and Biotechnology* 62, 99–109.
- (75) Inui, M., Murakami, S., Okino, S., Kawaguchi, H., Vertès, A. A., and Yukawa, H. (2004). Metabolic analysis of *Corynebacterium glutamicum* during lactate and succinate productions under oxygen deprivation conditions. *Journal of Molecular Microbiology and Biotechnology* 7, 182–196.
- (76) Isenschmid, A., Marison, I. W., and von Stockar, U. (1995). The influence of pressure and temperature of compressed CO₂ on the survival of yeast cells. *Journal of Biotechnology* 39, 229–237.

- (77) Jin, C. W., Du, S. T., Chen, W. W., Li, G. X., Zhang, Y. S., and Zheng, S. J. (2009). Elevated Carbon Dioxide Improves Plant Iron Nutrition through Enhancing the Iron-Deficiency-Induced Responses under Iron-Limited Conditions in Tomato. *Plant Physiology* 150, 272–280.
- (78) Jones, R. P. and Greenfield, P. F. (1982). Effect of carbon dioxide on yeast growth and fermentation. *Enzyme and Microbial Technology* 4, 210–223.
- (79) Kai, Y., Matsumura, H., Inoue, T., Terada, K., Nagara, Y., Yoshinaga, T., Kihara, A., Tsumura, K., and Izui, K. (1999). Three-dimensional structure of phosphoenolpyruvate carboxylase: A proposed mechanism for allosteric inhibition. *Proceedings of the National Academy of Sciences* 96, 823–828.
- (80) Kalinowski, J. et al. (2003). The complete *Corynebacterium glutamicum* ATCC 13032 genome sequence and its impact on the production of L-aspartate-derived amino acids and vitamins. *Journal of Biotechnology* 104, 5–25.
- (81) Kallscheuer, N. and Marienhagen, J. (2018). *Corynebacterium glutamicum* as platform for the production of hydroxybenzoic acids. *Microbial Cell Factories* 17, 1–13.
- (82) Keilhauer, C, Eggeling, L, and Sahm, H (1993). Isoleucine synthesis in *Corynebacterium glutamicum*: Molecular analysis of the *ilvB-ilvN-ilvC* operon. *Journal of Bacteriology* 175, 5595–5603.
- (83) Kennedy, J. A. and Powell, J. K. J. (1985). Aluminium(III) and Iron(III) 1,2-Diphenolato Complexes: a Potentiometric Study. *Australian Journal of Chemistry* 38, 659–667.
- (84) Kinoshita, S., Udaka, S., and Shimono, M. (1957). Studies on the amino acid fermentation Part I. Production of L-glutamic acid by various microorganisms. *Journal of General and Applied Microbiology* 3, 193–205.
- (85) Kirchner, O. and Tauch, A. (2003). Tools for genetic engineering in the amino acid-producing bacterium *Corynebacterium glutamicum*. *Journal of Biotechnology* 104, 287–299.

-
- (86) Klaffl, S. and Eikmanns, B. J. (2010). Genetic and functional analysis of the soluble oxaloacetate decarboxylase from *Corynebacterium glutamicum*. *Journal of Bacteriology* 192, 2604–2612.
- (87) Knoll, A., Bartsch, S., Husemann, B., Engel, P., Schroer, K., Ribeiro, B., Stöckmann, C., Seletzky, J., and Büchs, J. (2007). High cell density cultivation of recombinant yeasts and bacteria under non-pressurized and pressurized conditions in stirred tank bioreactors. *Journal of Biotechnology* 132, 167–179.
- (88) Kracke, F., Vassilev, I., and Krömer, J. O. (2015). Microbial electron transport and energy conservation - The foundation for optimizing bioelectrochemical systems. *Frontiers in Microbiology* 6, 1–18.
- (89) Küberl, A., Fränzel, B., Eggeling, L., Polen, T., Wolters, D. A., and Bott, M. (2014). Pupylated proteins in *Corynebacterium glutamicum* revealed by MudPIT analysis. *Proteomics* 14, 1531–1542.
- (90) Küberl, A., Polen, T., and Bott, M. (2016). The pupylation machinery is involved in iron homeostasis by targeting the iron storage protein ferritin. *Proceedings of the National Academy of Sciences* 113, 4806–4811.
- (91) Kubota, T., Tanaka, Y., Takemoto, N., Watanabe, A., Hiraga, K., Inui, M., and Yukawa, H. (2014). Chorismate-dependent transcriptional regulation of quinate/shikimate utilization genes by LysR-type transcriptional regulator QsuR in *Corynebacterium glutamicum*: Carbon flow control at metabolic branch point. *Molecular Microbiology* 92, 356–368.
- (92) Lange, J., Müller, F., Takors, R., and Blombach, B. (2017). Harnessing novel chromosomal integration loci to utilize an organosolv-derived hemicellulose fraction for isobutanol production with engineered *Corynebacterium glutamicum*. *Microbial Biotechnology* 11, 257–263.
- (93) Lau, C. K. Y., Krewulak, K. D., and Vogel, H. J. (2015). Bacterial ferrous iron transport: the Feo system. *FEMS Microbiology Reviews* 40, 273–298.

- (94) Lee, S. J., Song, H., and Lee, S. Y. (2006). Genome-based metabolic engineering of *Mannheimia succiniciproducens* for succinic acid production. *Applied and environmental microbiology* 72, 1939–1948.
- (95) Lesuisse, E., Raguzzi, F., and Crichton, R. R. (1987). Iron uptake by the yeast *Saccharomyces cerevisiae*: involvement of a reduction step. *Journal of general microbiology* 133, 3229–3236.
- (96) Liebl, W. In *Handbook of Corynebacterium glutamicum*, Eggeling, L. and Bott, M., Eds.; CRC Press: 2005; Chapter 2, pp 7–34.
- (97) Liebl, W., Klamer, R., and Schleifer, K.-H. (1989). Requirement of chelating compounds for the growth of *Corynebacterium glutamicum* in synthetic media. *Applied Microbiology and Biotechnology* 32, 205–210.
- (98) Light, S. H., Su, L., Rivera-Lugo, R., Cornejo, J. A., Louie, A., Iavarone, A. T., Ajo-Franklin, C. M., and Portnoy, D. A. (2018). A flavin-based extracellular electron transfer mechanism in diverse Gram-positive bacteria. *Nature* 562, 140–157.
- (99) Lin, C. T., Wu, C. C., Chen, Y. S., Lai, Y. C., Chi, C., Lin, J. C., Chen, Y., and Peng, H. L. (2011). Fur regulation of the capsular polysaccharide biosynthesis and iron-acquisition systems in *Klebsiella pneumoniae* CG43. *Microbiology* 157, 419–429.
- (100) Lin, H., Fischbach, M. A., Liu, D. R., and Walsh, C. T. (2005). In Vitro Characterization of Salmochelin and Enterobactin Trilactone Hydrolases IroD, IroE, and Fes. *Journal of the American Chemical Society* 127, 11075–11084.
- (101) Litwin, C. M. and Calderwood, S. B. (1993). Role of iron in regulation of virulence genes. *Clinical Microbiology Reviews* 6, 137–149.
- (102) Lopes, M., Belo, I., and Mota, M. (2014). Over-pressurized bioreactors: Application to microbial cell cultures. *Biotechnology Progress* 30, 767–775.

-
- (103) Love, J. F., VanderSpek, J. C., Marin, V., Guerrero, L., Logan, T. M., and Murphy, J. R. (2004). Genetic and biophysical studies of diphtheria toxin repressor (DtxR) and the hyperactive mutant DtxR(E175K) support a multistep model of activation. *Proceedings of the National Academy of Sciences of the United States of America* 101, 2506–11.
- (104) Love, J. F., VanderSpek, J. C., and Murphy, J. R. (2003). The *src* homology 3-like domain of the diphtheria toxin repressor (DtxR) modulates repressor activation through interaction with the ancillary metal ion-binding site. *Journal of Bacteriology* 185, 2251–2258.
- (105) Lucena, J. J. (2000). Effects of bicarbonate, nitrate and other environmental factors on iron deficiency chlorosis. A review. *Journal of Plant Nutrition* 23, 1591–1606.
- (106) Martínez-Cuenca, M. R., Iglesias, D. J., Forner-Giner, M. A., Primo-Millo, E., and Legaz, F. (2013). The effect of sodium bicarbonate on plant performance and iron acquisition system of FA-5 (Forner-Alcaide 5) citrus seedlings. *Acta Physiologiae Plantarum* 35, 2833–2845.
- (107) Massé, E. and Gottesman, S. (2002). A small RNA regulates the expression of genes involved in iron metabolism in *Escherichia coli*. *Proceedings of the National Academy of Sciences* 99, 4620–4625.
- (108) Mekalanos, J. J. (1992). Environmental signals controlling expression of virulence determinants in bacteria. *Journal of Bacteriology* 174, 1–7.
- (109) Merkens, H., Beckers, G., Wirtz, A., and Burkovski, A. (2005). Vanillate Metabolism in *Corynebacterium glutamicum*. 51, 59–65.
- (110) Michel, A., Koch-Koerfges, A., Krumbach, K., Brocker, M., and Bott, M. (2015). Anaerobic Growth of *Corynebacterium glutamicum* via Mixed-Acid Fermentation. *Applied and Environmental Microbiology* 81, 7496–7508.

- (111) Milse, J., Petri, K., Rückert, C., and Kalinowski, J. (2014). Transcriptional response of *Corynebacterium glutamicum* ATCC 13032 to hydrogen peroxide stress and characterization of the OxyR regulon. *Journal of Biotechnology* 190, 40–54.
- (112) Morgan, L. R. (1962). Oxidation of Protocatechuic Acid with Peroxyacetic Acid. *Journal of Organic Chemistry* 27, 1208–1210.
- (113) Mori, M. and Shiio, I. (1985). Purification and some properties of phosphoenolpyruvate carboxylase from *Brevibacterium flavum* and its aspartate-overproducing mutant. *Journal of Biochemistry* 97, 1119–1128.
- (114) Mudasir, Arai, M., Yoshioka, N., and Inoue, H. (1998). Reversed-phase high-performance liquid chromatography of iron(II) and copper(II) chelates with 4,7-diphenyl-1,10-phenanthroline disulfonate. *Journal of Chromatography A* 799, 171–176.
- (115) Mullis, K. B. and Faloona, F. (1987). Specific synthesis of DNA in vitro via a polymerase catalyzed chain reaction. *Methods in Enzymology* 155, 335–350.
- (116) Müller, F., Rapp, J., Hacker, A.-L., Feith, A., Takors, R., and Blombach, B. (2020). CO₂/HCO₃⁻ accelerates iron reduction through phenolic compounds. *mBio [accepted]*, <https://doi.org/10.1128/mBio.00085-20>.
- (117) Nakayama, K., Sato, Z., and Kinoshita, S. (1964). Growth of a glutamic acid producing bacterium and related bacteria I. Effect of iron salts, ferrichrom, amino acids and some other compounds. *Journal of General and Applied Microbiology* 10, 143–155.
- (118) Nakayama, K., Sato, Z., Tanaka, H., and Kinoshita, S. (1964). Growth of a Glutamic Acid producing Bacterium and related Bacteria II. Effect of Chelating Agent and its Relation to Inorganic Salt. *Journal of General and Applied Microbiology* 10, 181–199.
- (119) Neilands, J. B. (1981). Iron absorption and transport in microorganisms. *Annual review of nutrition* 1, 27–46.

-
- (120) Niesen, F. H., Berglund, H., and Vedadi, M. (2007). The use of differential scanning fluorimetry to detect ligand interactions that promote protein stability. *Nature Protocols* 2, 2212–2221.
- (121) Nishimura, T., Vertes, A. a., Shinoda, Y., Inui, M., and Yukawa, H. (2007). Anaerobic growth of *Corynebacterium glutamicum* using nitrate as a terminal electron acceptor. *Applied Microbiology and Biotechnology* 75, 889–897.
- (122) Nyhus, K. J., Wilborn, A. T., and Jacobson, E. S. (1997). Ferric iron reduction by *Cryptococcus neoformans*. *Infection and immunity* 65, 434–8.
- (123) O’Brien, I. G., Cox, G. B., and Gibson, F. (1971). Enterochelin hydrolysis and iron metabolism in *Escherichia coli*. *Biochimica et Biophysica Acta* 237, 537–549.
- (124) Okino, S., Noburyu, R., Suda, M., Jojima, T., Inui, M., and Yukawa, H. (2008). An efficient succinic acid production process in a metabolically engineered *Corynebacterium glutamicum* strain. *Applied Microbiology and Biotechnology* 81, 459–464.
- (125) Pappenheimer, A. M. and Johnson, S. J. (1936). Studies in Diphtheria Toxin Production. I: The Effect of Iron and Copper . *The British Journal of Experimental Pathology* XVII, 335–341.
- (126) Perron, N. R. and Brumaghim, J. L. (2009). A review of the antioxidant mechanisms of polyphenol compounds related to iron binding. *Cell Biochemistry and Biophysics* 53, 75–100.
- (127) Peters, W. J. and Warren, R. A. (1968). Itoic acid synthesis in *Bacillus subtilis*. *Journal of Bacteriology* 95, 360–366.
- (128) Peters, W. J. and Warren, R. A. J. (1968). Phenolic acids and transport in *Bacillus subtilis*. *Biochimica et Biophysica Acta* 165, 225–232.
- (129) Peters-Wendisch, P. G., Schiel, B., Wendisch, V. F., Katsoulidis, E., Möckel, B., Sahm, H., and Eikmanns, B. J. (2001). Pyruvate Carboxylase is a Major Bot-

- tleneck for Glutamate and Lysine Production by *Corynebacterium glutamicum*. *Journal of Molecular Microbiology and Biotechnology* 3, 295–300.
- (130) Pfeifer-Sancar, K., Mentz, A., Rückert, C., and Kalinowski, J. (2013). Comprehensive analysis of the *Corynebacterium glutamicum* transcriptome using an improved RNAseq technique. *BMC Genomics* 14, 1–23.
- (131) Pohling, R. In *Chemische Reaktionen in der Wasseranalyse*, 2015, pp 119–125.
- (132) Posey, J. E., Hardham, J. M., Norris, S. J., and Gherardini, F. C. (1999). Characterization of a manganese-dependent regulatory protein, TroR, from *Treponema pallidum*. *Proceedings of the National Academy of Sciences of the United States of America* 96, 10887–10892.
- (133) Proulx-Curry, P. M. and Chasteen, N. D. (1995). Molecular aspects of iron uptake and storage in ferritin. *Coordination Chemistry Reviews* 144, 347–368.
- (134) Qiu, X., Pohl, E., Holmes, R. K., and Hol, W. G. J. (1996). High-resolution structure of the diphtheria toxin repressor complexed with cobalt and manganese reveals an SH3-like third domain and suggests a possible role of phosphate as co-repressor. *Biochemistry* 35, 12292–12302.
- (135) Qiu, X., Verlinde, C. L., Zhang, S., Schmitt, M. P., Holmes, R. K., and Hol, W. G. (1995). Three-dimensional structure of the diphtheria toxin repressor in complex with divalent cation co-repressors. *Structure* 3, 87–100.
- (136) Radoš, D., Turner, D. L., Fonseca, L. L., Carvalho, A. L., Blombach, B., Eikmanns, B. J., Neves, A. R., and Santos, H. (2014). Carbon flux analysis by ¹³C nuclear magnetic resonance to determine the effect of CO₂ on anaerobic succinate production by *Corynebacterium glutamicum*. *Applied and Environmental Microbiology* 80, 3015–3024.
- (137) Ratledge, C. and Chaudhry, M. A. (1971). Accumulation of Iron-binding Phenolic Acids by *Actinomycetales* and Other Organisms Related to the *Mycobacteria*. *Journal of General Microbiology* 66, 71–78.

-
- (138) Riemer, J., Hoepken, H. H., Czerwinska, H., Robinson, S. R., and Dringen, R. (2004). Colorimetric ferrozine-based assay for the quantitation of iron in cultured cells. *Analytical Biochemistry* 331, 370–375.
- (139) Saiki, R. K., Scharf, S., Faloona, F., Mullis, K. B., Horn, G. T., Erlich, H. A., and Arnheim, N. (1985). Enzymatic amplification of β -globin genomic sequences and restriction site analysis for diagnosis of sickle cell anemia. *Science* 230, 1350–1354.
- (140) Saiki, R. K., Gelfand, D. H., Stoffel, S., Scharf, S. J., Higuchi, R., Horn, G. T., Mullis, K. B., and Erlich, H. A. (1988). Primer-directed enzymatic amplification of DNA with a thermostable DNA polymerase. *Science* 239, 487–491.
- (141) Sambrook, J. and Russell, R. W., *Molecular Cloning: A Laboratory Manual*, 3rd; Spring Harbor Laboratory Press: Cold Spring Harbor N.Y., 2001.
- (142) Sandrini, S. M., Shergill, R., Woodward, J., Muralikuttan, R., Haigh, R. D., Lyte, M., and Freestone, P. P. (2010). Elucidation of the mechanism by which catecholamine stress hormones liberate iron from the innate immune defense proteins transferrin and lactoferrin. *Journal of Bacteriology* 192, 587–594.
- (143) Sasaki, T., Kurano, N., and Miyachi, S. (1998). Induction of Ferric Reductase Activity and of Iron Uptake Capacity in *Chlorococcum littorale* Cells under Extremely High-CO₂ and Iron-Deficient Conditions. *Plant and Cell Physiology* 39, 405–410.
- (144) Sauer, U. and Eikmanns, B. J. (2005). The PEP-pyruvate-oxaloacetate node as the switch point for carbon flux distribution in bacteria. *FEMS Microbiology Reviews* 29, 765–794.
- (145) Schäfer, A., Tauch, A., Jäger, W., Kalinowski, J., Thierbach, G., and Pühler, A. (1994). Small mobilizable multi-purpose cloning vectors derived from the *Escherichia coli* plasmids pK18 and pK19: selection of defined deletions in the chromosome of *Corynebacterium glutamicum*. *Gene* 145, 69–73.

- (146) Schaffer, S., Weil, B., Nguyen, V. D., Dongmann, G., Günther, K., Nickolaus, M., Hermann, T., and Bott, M. (2001). A high-resolution reference map for cytoplasmic and membrane-associated proteins of *Corynebacterium glutamicum*. *Electrophoresis* 22, 4404–4422.
- (147) Schiering, N, Tao, X, Zeng, H, Murphy, J. R., Petsko, G. a., and Ringe, D (1995). Structures of the apo- and the metal ion-activated forms of the diphtheria tox repressor from *Corynebacterium diphtheriae*. *Proceedings of the National Academy of Sciences of the United States of America* 92, 9843–9850.
- (148) Schluesener, D., Rögner, M., and Poetsch, A. (2007). Evaluation of two proteomics technologies used to screen the membrane proteomes of wild-type *Corynebacterium glutamicum* and an L-lysine-producing strain. *Analytical and Bioanalytical Chemistry* 389, 1055–1064.
- (149) Schluesener, D., Fischer, F., Kruij, J., Rögner, M., and Poetsch, A. (2005). Mapping the membrane proteome of *Corynebacterium glutamicum*. *Proteomics* 5, 1317–1330.
- (150) Schmitt, M. P., Predich, M., Doukhan, L., Smith, I., and Holmes, R. K. (1995). Characterization of an iron-dependent regulatory protein (IdeR) of *Mycobacterium tuberculosis* as a functional homolog of the diphtheria toxin repressor (DtxR) from *Corynebacterium diphtheriae*. *Infection and Immunity* 63, 4284–4289.
- (151) Schröder, I., Johnson, E., and De Vries, S. (2003). Microbial ferric iron reductases. *FEMS Microbiology Reviews* 27, 427–447.
- (152) Schweigert, N., Zehnder, A. J., and Eggen, R. I. (2001). Chemical properties of catechols and their molecular modes of toxic action in cells, from microorganisms to mammals. *Environmental Microbiology* 3, 81–91.
- (153) Schwentner, A., Feith, A., Münch, E., Stiefelmaier, J., Lauer, I., Favilli, L., Massner, C., Öhrlein, J., Grund, B., Hüser, A., Takors, R., and Blombach, B. (2019). Modular systems metabolic engineering enables balancing of relevant pathways

- for L-histidine production with *Corynebacterium glutamicum*. *Biotechnology for Biofuels* 12, 1–21.
- (154) Sengupta, A. K. and Nandi, A. K. (1974). Complex Carbonates of Iron (III). *Zeitschrift für anorganische und allgemeine Chemie* 403, 327–336.
- (155) Shen, X. H., Zhou, N. Y., and Liu, S. J. (2012). Degradation and assimilation of aromatic compounds by *Corynebacterium glutamicum*: Another potential for applications for this bacterium? *Applied Microbiology and Biotechnology* 95, 77–89.
- (156) Shen, X. and Liu, S. (2005). Key enzymes of the protocatechuate branch of the beta-ketoadipate pathway for aromatic degradation in *Corynebacterium glutamicum*. *Science in China. Series C, Life Sciences / Chinese Academy of Sciences* 48, 241–249.
- (157) Sirivech, S., Frieden, E., and Osaki, S. (1974). The release of iron from horse spleen ferritin by reduced flavins. *Biochemical Journal* 143, 311–315.
- (158) Smith, E (1968). *Escherichia coli* Phosphoenolpyruvate and Carboxylase: Characterization and Sedimentation Behavior. *Archives of Biochemistry and Biophysics* 128, 611–622.
- (159) Smith, G. F., McCurdy, W. H., and Diehl, H. (1952). The colorimetric determination of iron in raw and treated municipal water supplies by use of 4:7-diphenyl-1:10-phenanthroline. *The Analyst* 77, 418–422.
- (160) Smith, K. S. and Ferry, J. G. (2000). Prokaryotic carbonic anhydrases. *FEMS Microbiology Reviews* 24, 335–366.
- (161) Spiering, M. M., Ringe, D., Murphy, J. R., and Marletta, M. A. (2003). Metal stoichiometry and functional studies of the diphtheria toxin repressor. *Proceedings of the National Academy of Sciences of the United States of America* 100, 3808–3813.

- (162) Steere, A. N., Byrne, S. L., Chasteen, N. D., and Mason, A. B. (2013). Kinetics of iron release from transferrin bound to the transferrin receptor at endosomal pH. *Biochimica et Biophysica Acta* 1820, 326–333.
- (163) Sun, X., Baker, H. M., Ge, R., Sun, H., He, Q. Y., and Baker, E. N. (2009). Crystal structure and metal binding properties of the lipoprotein MtsA, responsible for iron transport in *Streptococcus pyogenes*. *Biochemistry* 48, 6184–6190.
- (164) Sun, X., Ge, R., Chiu, J. F., Sun, H., and He, Q. Y. (2008). Lipoprotein MtsA of MtsABC in *Streptococcus pyogenes* primarily binds ferrous ion with bicarbonate as a synergistic anion. *FEBS Letters* 582, 1351–1354.
- (165) Tait, G. H. (1975). The identification and biosynthesis of siderochromes formed by *Micrococcus denitrificans*. *The Biochemical journal* 146, 191–204.
- (166) Tao, X, Zeng, H. Y., and Murphy, J. R. (1995). Transition metal ion activation of DNA binding by the diphtheria tox repressor requires the formation of stable homodimers. *Proceedings of the National Academy of Sciences of the United States of America* 92, 6803–7.
- (167) Tao, X. and Murphy, J. R. (1993). Cysteine-102 is positioned in the metal binding activation site of the *Corynebacterium diphtheriae* regulatory element DtxR. *Proceedings of the National Academy of Sciences of the United States of America* 90, 8524–8528.
- (168) Tauch, A. In *Corynebacteria: Genomics and Molecular Biology*, Burkovski, A., Ed.; Horizon Scientific Press: Norwich, UK, 2008; Chapter 2, pp 9–10.
- (169) Teleki, A., Sánchez-Kopper, A., and Takors, R. (2015). Alkaline conditions in hydrophilic interaction liquid chromatography for intracellular metabolite quantification using tandem mass spectrometry. *Analytical Biochemistry* 475, 4–13.
- (170) Teramoto, H., Inui, M., and Yukawa, H. (2009). Regulation of expression of genes involved in quinate and shikimate utilization in *Corynebacterium glutamicum*. *Applied and Environmental Microbiology* 75, 3461–3468.

-
- (171) Thomson, J. J. and Withey, J. H. (2014). Bicarbonate increases binding affinity of *Vibrio cholerae* ToxT to virulence gene promoters. *Journal of Bacteriology* 196, 3872–3880.
- (172) Torres, V. J., Attia, A. S., Mason, W. J., Hood, M. I., Corbin, B. D., Beasley, F. C., Anderson, K. L., Stauff, D. L., McDonald, W. H., Zimmerman, L. J., Friedman, D. B., Heinrichs, D. E., Dunman, P. M., and Skaar, E. P. (2010). *Staphylococcus aureus* Fur regulates the expression of virulence factors that contribute to the pathogenesis of pneumonia. *Infection and Immunity* 78, 1618–1628.
- (173) Traxler, M. F., Seyedsayamdost, M. R., Clardy, J., and Kolter, R. (2012). Interspecies modulation of bacterial development through iron competition and siderophore piracy. *Molecular Microbiology* 86, 628–644.
- (174) Ueda, K., Tagami, Y., Kamihara, Y., Shiratori, H., Takano, H., and Beppu, T. (2008). Isolation of bacteria whose growth is dependent on high levels of CO₂ and implications of their potential diversity. *Applied and Environmental Microbiology* 74, 4535–4538.
- (175) Unthan, S., Grünberger, A., van Ooyen, J., Gätgens, J., Heinrich, J., Paczia, N., Wiechert, W., Kohlheyer, D., and Noack, S. (2014). Beyond growth rate 0.6: What drives *Corynebacterium glutamicum* to higher growth rates in defined medium. *Biotechnology and Bioengineering* 111, 359–371.
- (176) van der Rest, M. E., Lange, C., and Molenaar, D. (1999). A heat shock following electroporation induces highly efficient transformation of *Corynebacterium glutamicum* with xenogeneic plasmid DNA. *Applied Microbiology and Biotechnology* 52, 541–545.
- (177) Vassilev, I., Gießelmann, G., Schwechheimer, S. K., Wittmann, C., Viridis, B., and Krömer, J. O. (2018). Anodic electro-fermentation: Anaerobic production of L-Lysine by recombinant *Corynebacterium glutamicum*. *Biotechnology and Bioengineering* 115, 1499–1508.

- (178) Vivoli, M., Novak, H. R., Littlechild, J. A., and Harmer, N. J. (2014). Determination of protein-ligand interactions using differential scanning fluorimetry. *Journal of Visualized Experiments*, 51809.
- (179) von der Osten, C. H., Gioannetti, C., and Sinskey, A. J. (1989). Design of a defined Medium for Growth of *Corynebacterium glutamicum* in which Citrate facilitates Iron Uptake. *Biotechnology Letters* 11, 11–16.
- (180) Wendisch, V. F., de Graaf, A. A., Sahm, H., and Eikmanns, B. J. (2000). Quantitative determination of metabolic fluxes during cointilization of two carbon sources: comparative analyses with *Corynebacterium glutamicum* during growth on acetate and/or glucose. *Journal of Bacteriology* 182, 3088–96.
- (181) Wendisch, V. F. (2019). Metabolic engineering advances and prospects for amino acid production. *Metabolic Engineering*, 0–1.
- (182) Wennerhold, J. and Bott, M. (2006). The DtxR Regulon of *Corynebacterium glutamicum*. *Journal of Bacteriology* 188, 2907–2918.
- (183) Wennerhold, J., Krug, A., and Bott, M. (2005). The AraC-type regulator RipA represses aconitase and other iron proteins from *Corynebacterium* under iron limitation and is itself repressed by DtxR. *Journal of Biological Chemistry* 280, 40500–40508.
- (184) White, A, Ding, X, VanderSpek, J. C., Murphy, J. R., and Ringe, D (1998). Structure of the metal-ion-activated diphtheria toxin repressor/*tox* operator complex. *Nature* 394, 502–506.
- (185) Wilson, B. R., Bogdan, A. R., Miyazawa, M., Hashimoto, K., and Tsuji, Y. (2016). Siderophores in Iron Metabolism: From Mechanism to Therapy Potential. *Trends in Molecular Medicine* 22, 1077–1090.
- (186) Wisedchaisri, G., Chou, C. J., Wu, M., Roach, C., Rice, A. E., Holmes, R. K., Beeson, C., and Hol, W. G. J. (2007). Crystal structures, metal activation, and DNA-binding properties of two-domain IdeR from *Mycobacterium tuberculosis*. *Biochemistry* 46, 436–447.

-
- (187) Yang, J., Dogovski, C., Hocking, D., Tauschek, M., Perugini, M., and Robins-Browne, R. M. (2009). Bicarbonate-Mediated Stimulation of RegA, the Global Virulence Regulator from *Citrobacter rodentium*. *Journal of Molecular Biology* 394, 591–599.
- (188) Yang, J., Hart, E., Tauschek, M., Price, G. D., Hartland, E. L., Strugnell, R. A., and Robins-Browne, R. M. (2008). Bicarbonate-mediated transcriptional activation of divergent operons by the virulence regulatory protein, RegA, from *Citrobacter rodentium*. *Molecular Microbiology* 68, 314–327.
- (189) Yanisch-Perron, C, Vieira, J, and Messing, J (1985). Improved M13 phage cloning vectors and host strains: nucleotide sequences of the M13mp18 and pUC19 vectors. *Gene* 33, 103–119.
- (190) Yano, M., Terada, K., Umiji, K., and Izui, K. (1995). Catalytic role of an arginine residue in the highly conserved and unique sequence of phosphoenolpyruvate carboxylase. *Journal of Biochemistry* 117, 1196–1200.
- (191) Yu, T. and Chen, Y. (2019). Effects of elevated carbon dioxide on environmental microbes and its mechanisms: A review. *Science of the Total Environment* 655, 865–879.
- (192) Zondervan, N. A., Van Dam, J. C., Schaap, P. J., Dos Santos, V. A., and Suarez-Diez, M. (2018). Regulation of three virulence strategies of *Mycobacterium tuberculosis*: A success story. *International Journal of Molecular Sciences* 19, 9–12.

Appendix

Overview of aromatic compounds

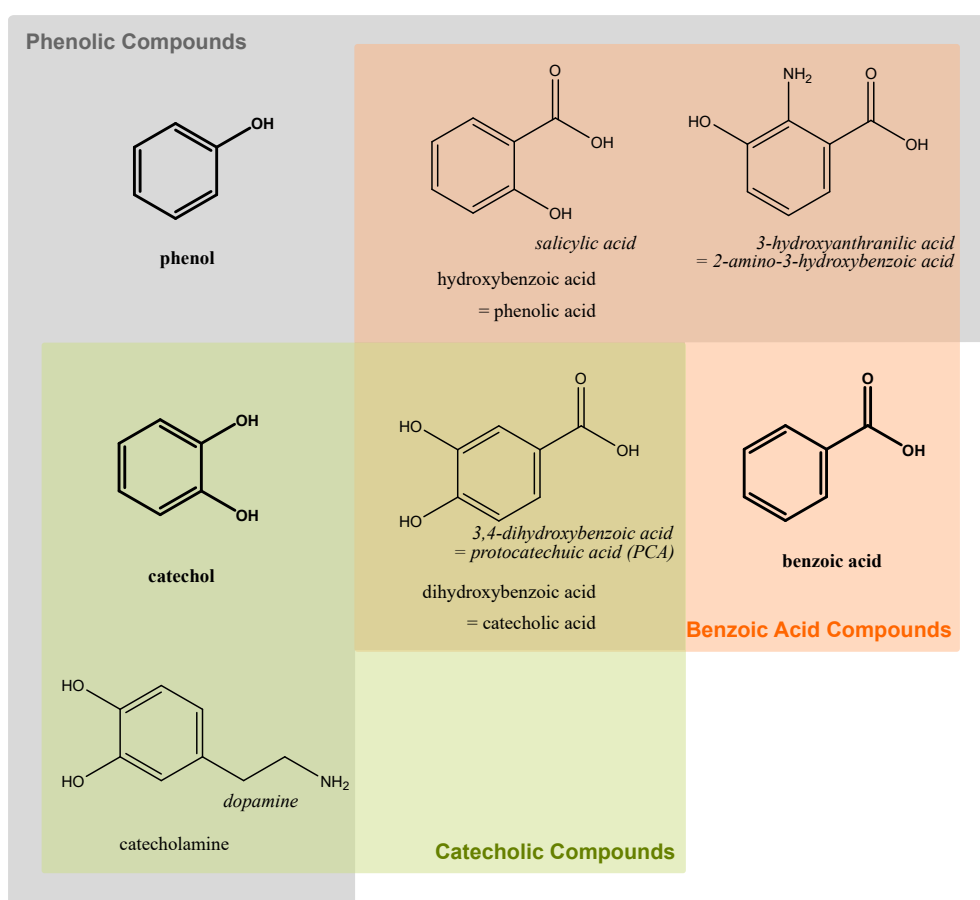


Figure S1: Overview of aromatic compounds and their (overlapping) classification into phenol, catechol or benzoic acid derivatives. The overview includes the compounds used or discussed in this study (or regioisomers). Specific and trivial names are *italicized*.

BioLector cultivation with 1 mM BPS

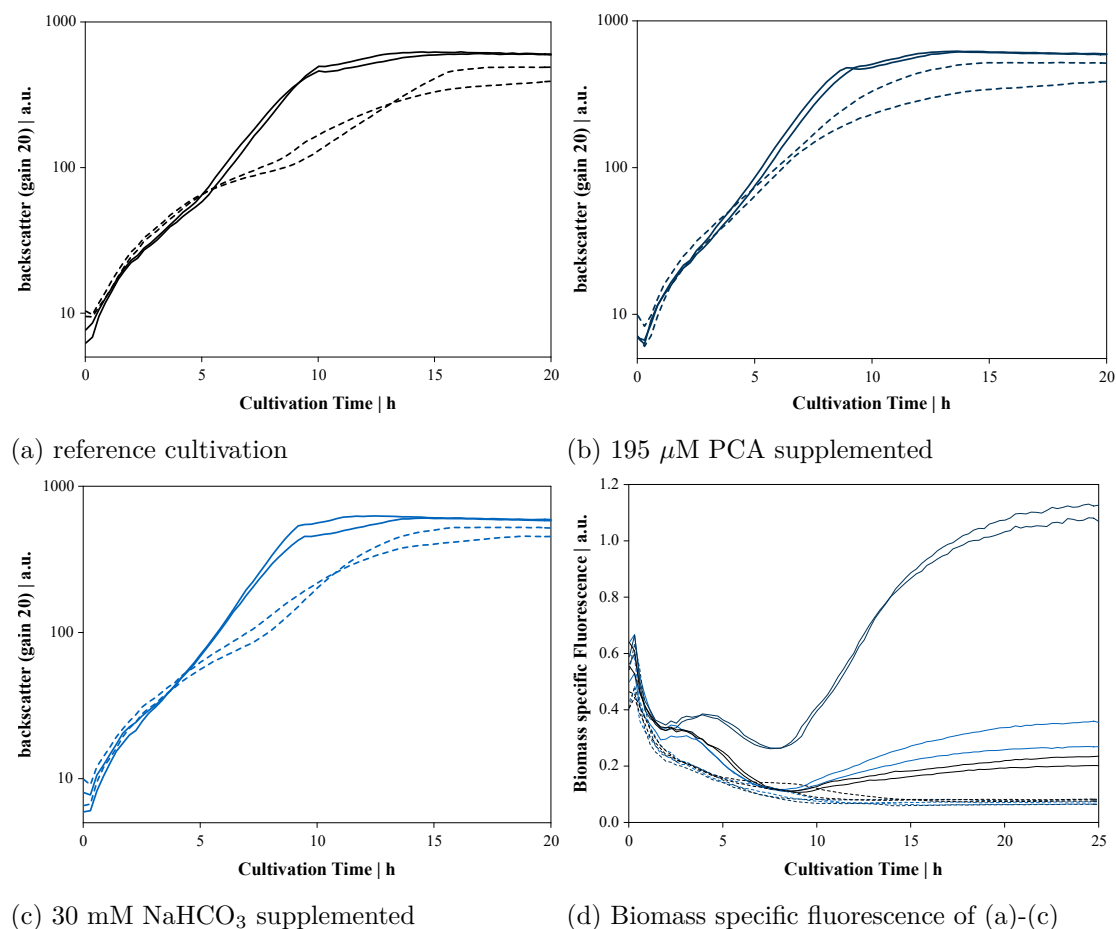


Figure S2: BioLector cultivation of *C. glutamicum* FEM3 in the absence (straight lines) and presence of 1 mM BPS (dashed lines). Subfigures show biomass generation under the individual cultivation conditions as indicated (a-c) or the biomass specific fluorescence (normalized to the backscatter value) under all cultivation conditions (d). Experiments were plotted individually.

Deletion mutants

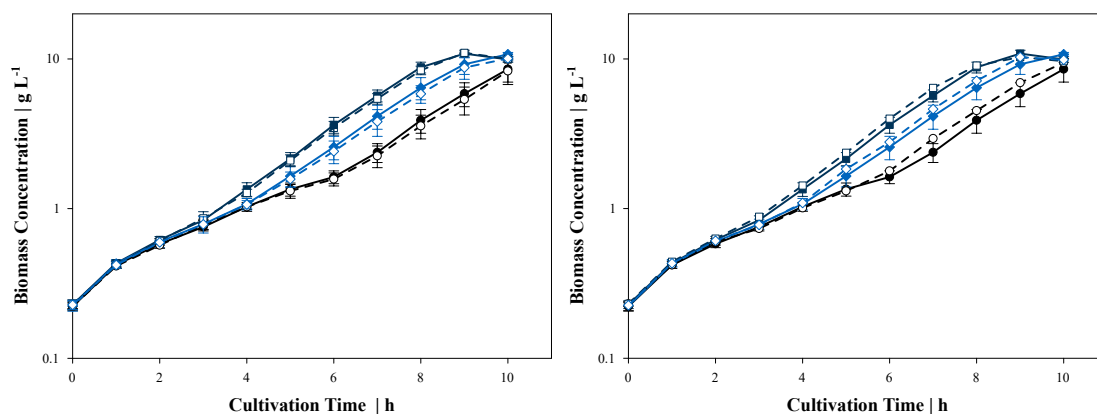
Corynebacterium glutamicum $\Delta cg2444$ & Δftn (a) *C. glutamicum* WT & $\Delta cg2444$ (b) *C. glutamicum* WT & Δftn

Figure S3: Biomass generation of *C. glutamicum* $\Delta cg2444$ (fig. a) and Δftn (fig. b) in parallel in shaking flask cultivations with *C. glutamicum* WT. In each figure, filled symbols indicate the WT cultivated in ●: standard conditions (no supplements), or medium with ■: 195 μ M protocatechuic acid (PCA) supplemented, ◆: 30 mM NaHCO_3 supplemented. Open symbols indicate the deletion strain cultivated in the same conditions ○: reference □: PCA, ◇: NaHCO_3 . Data points represent mean values and error bars indicate standard deviations of three independent experiments.

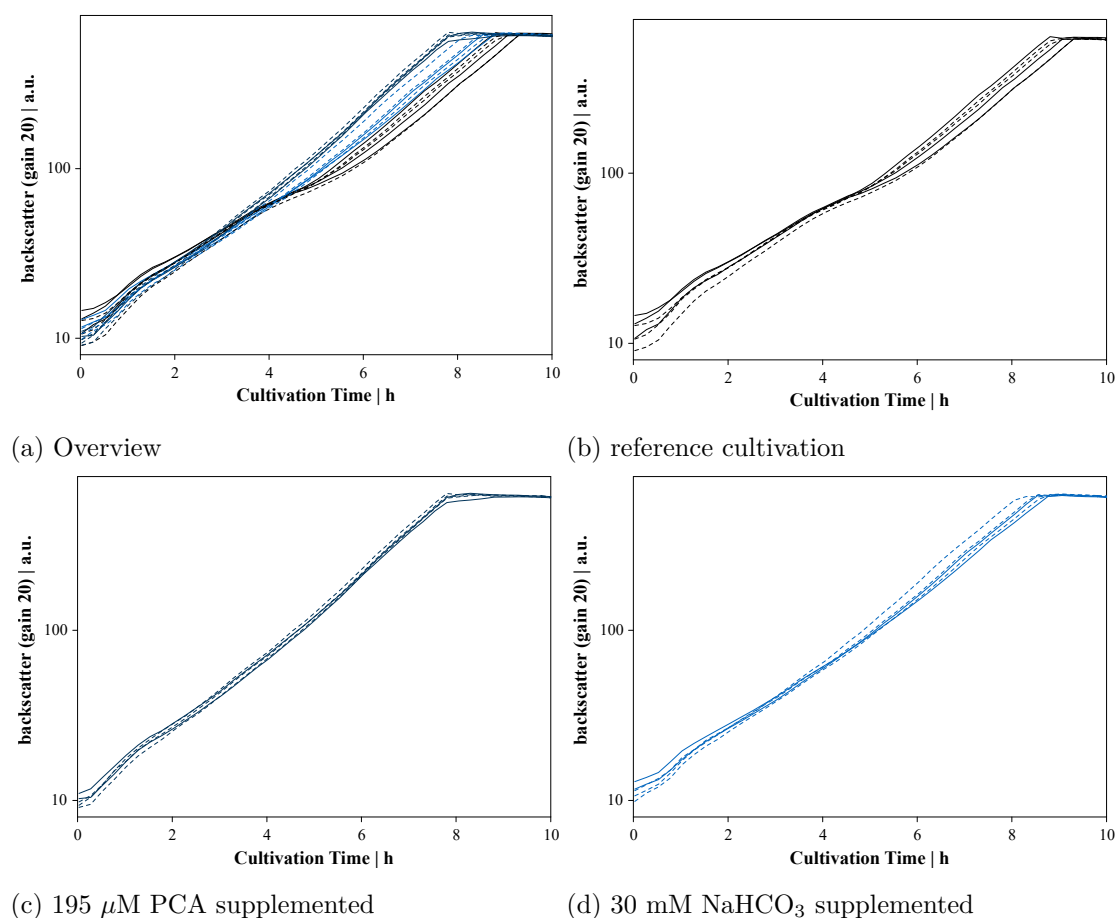
***Corynebacterium glutamicum* $\Delta cg0041-cg0042$** 

Figure S4: BioLector cultivation of *C. glutamicum* WT (straight lines) and *C. glutamicum* $\Delta(cg0041-cg0042)$ (dashed lines). Subfigures show an overview of all experiments (fig. a) as well as biomass generation under the individual cultivation conditions (fig. b- d). Experiments were plotted individually.

Chemicals

Table S1: List of chemicals

Substance	Company	Art.-No.
Acetic acid	Carl Roth	3738.2

Table S1: List of chemicals (continued)

Substance	Company	Art.-No.
Acetonitrile	VWR International	83639 320
40 % Acrylamide/Bis solution, 37.5:1	Bio-Rad Laboratories GmbH	1610148
Agarose	Sigma Aldrich	A5093
3-Amino-4-hydroxybenzoic acid	Sigma Aldrich	289647
3-Aminosalicylic acid	Sigma Aldrich	255300
4-Amino-3-hydroxybenzoic acid	Sigma Aldrich	339598
<i>para</i> -Aminosalicylic acid	Sigma Aldrich	A79604
Ammonia solution	Carl Roth	5460.4
Ammonium acetate	Sigma Aldrich	1011160500
Ammonium persulfate	Alfa Aesar	J61856.14
Ammonium sulphate	Carl Roth	9218.5
L-Ascorbic acid	Sigma Aldrich	795437
Ampicillin sodium salt	Carl Roth	K029.2
Bacto™ Brain Heart Infusion	BD Biosciences	237500
Bacto™ Tryptone	BD Biosciences	211699
Bathophenanthroline disulfonic acid	Sigma Aldrich	B1375
BBL™ Yeast Extract	BD Biosciences	211930
Biotin	Carl Roth	3822.1
2,2-Bipyridyl	Sigma Aldrich	D7505
Bromophenol blue	Sigma Aldrich	B8026
Calcium chloride	Merck Millipore	2389
Coomassie brilliant blue G250	Alfa Aesar	43318
Copper(II) sulfate pentahydrate	Sigma Aldrich	61240
Deoxynucleotide triphosphates (dNTPs)	Genaxxon Bioscience	M3015.4020

Table S1: List of chemicals (continued)

Substance	Company	Art.-No.
D-Desthiobiotin	Sigma Aldrich	D1411
Dimethyl sulfoxide (DMSO)	Thermo Fisher Scientific Inc.	F-515
Dithiothreitol (DTT)	Carl Roth	6908
di-Potassium hydrogen phosphate	Carl Roth	6875.3
Ethylenediamine tetraacetic acid (EDTA)	Carl Roth	X986.2
Ferritin	Sigma Aldrich	F4503
Ferrozin	Sigma Aldrich	82950
Formaldehyde (37 %)	Carl Roth	7398
α -D(+)-Glucose monohydrate	Carl Roth	6780.3
Glycerol	Carl Roth	3783.1
Glycine hydrochloride	Sigma Aldrich	G2879
4-(2-Hydroxyethyl)-1-piperazineethanesulfonic acid (HEPES)	Carl Roth	6763
Hydrochloric acid (32 %)	Carl Roth	P074.4
3-Hydroxyanthranilic acid	Sigma Aldrich	148776
2-(4-Hydroxyphenylazo)benzoic acid	Sigma Aldrich	H5126
Imidazole	Sigma Aldrich	56750
Iron(II) sulfate heptahydrate	Sigma Aldrich	31236
Iron(III) chloride hexahydrate	Alfa Aesar	11331839
Isopropyl- β -D-thiogalactoside (IPTG)	Sigma Aldrich	I5502
Kanamycin sulfate	Carl Roth	T832.3
Lysozyme from chicken egg white	Fluka BioChemika	62970
Magnesium chloride hexahydrate	VWR International	0288

Table S1: List of chemicals (continued)

Substance	Company	Art.-No.
Magnesium sulfate heptahydrate	Carl Roth	P027.3
Manganese(II) sulfate monohydrate	Sigma Aldrich	63555
Manganese(II) chloride monohydrate	Carl Roth	4320
Methanol	VWR International	20864 320
3-(<i>N</i> -morpholino)propanesulfonic acid (MOPS)	Carl Roth	6979.3
Neocuproin	Sigma Aldrich	N1501
Nickel chloride hexahydrate	Carl Roth	4489
Polyethyleneglycol 8000 (PEG8000)	VWR International	0159
Potassium chloride	VWR International	26760.295
Potassium dihydrogen phosphate	Carl Roth	P018.5
Potassium hydrogen carbonate	Carl Roth	X887
Potassium hydroxide	Carl Roth	6751.1
Protocatechuic acid	Carl Roth	8274.1
L(+)-Rhamnose monohydrate	Sigma Aldrich	R3875
Sodium carbonate	Carl Roth	A135.1
Sodium chloride	Merck Millipore	106404
Sodium dodecyl sulfate (SDS)	Carl Roth	0183
Sodium hydrogen carbonate	Sigma Aldrich	31437
Sodium hydroxide	Carl Roth	9356.2
Sodium dihydrogen phosphate monohydrate	Carl Roth	K300
Sorbitol	Carl Roth	6213.1
Struktol J 647	Schill + Seilacher	
D(+)-Sucrose	Fluka BioChemika	84105
SYPRO™ Orange	Sigma Aldrich	S5692

Table S1: List of chemicals (continued)

Substance	Company	Art.-No.
Tris base	Carl Roth	4855.2
TEMED	Carl Roth	2367.3
Urea	Fluka BioChemika	51460
Zinc sulfate heptahydrate	Sigma Aldrich	96501

Enzymes

Table S2: List of enzymes

Enzyme	Company	Specific Activity [U mL⁻¹]	Cat. No.	Buffer
<i>BamHI</i>	Thermo Fisher Scientific Inc.	10 000	ER0055	unique buffer (BamHI)
<i>HindIII</i>	Thermo Fisher Scientific Inc.	50 000	ER0503	Buffer R
<i>NdeI</i>	Thermo Fisher Scientific Inc.	10 000	ER0581	Buffer O
<i>NheI</i>	Thermo Fisher Scientific Inc.	10 000	ER0971	Tango Buffer
<i>NotI</i>	Thermo Fisher Scientific Inc.	10 000	ER0591	Buffer O
<i>PstI</i>	Thermo Fisher Scientific Inc.	10 000	ER0611	Buffer O
<i>XbaI</i>	Thermo Fisher Scientific Inc.	10 000	ER0681	Tango Buffer
FastAP	Thermo Fisher Scientific Inc.	1 000	EF0651	any
<i>Phusion</i> (HSII) polymerase	Thermo Fisher Scientific Inc.	2 000	F-549S	GC Buffer / HF Buffer

Table S2: List of enzymes (continued)

Enzyme	Company	Specific Activity [U mL⁻¹]	Cat. No.	Buffer
<i>Q5</i> polymerase	New England BioLabs	2 000	M0491	<i>Q5</i> reaction buffer
T4 DNA ligase	New England BioLabs	400 000	M0202	(Gibson ISO)
T5 exonuclease	New England BioLabs	10 000	M0363	(Gibson ISO)
<i>taq</i> polymerase	Genaxxon bioscience	5 000	M3001.0250	Buffer S

Kits

Table S3: List of kits

Kit	Company
DNeasy Blood & Tissue kit	Qiagen
E.Z.N.A. Plasmid DNA Mini Kit I	Omega bio-tek
Nucleo Spin Gel and PCR Clean	Macherey-Nagel
Pierce™ BCA Protein Assay kit	Thermo Fisher Scientific Inc.
QIAexpress Ni-NTA fast start kit	Qiagen

Laboratory equipment

Table S4: List of laboratory equipment

Equipment	Supplier	Art.-No.
96-well microplate	Greiner Bio-One	655101
Glass beads (0.1 mm)	Carl Roth	N029.1

Table S4: List of Laboratory Equipment (continued)

Equipment	Supplier	Art.-No.
Twin-tec [®] PCR plate 96	Eppendorf	951020401

Apparatus

Table S5: List of apparatus

Apparatus	Company
AM100	Mettler Toledo
Biofuge pico Microcentrifuge	Heraeus
Biometra Power Pack P25	Analytik Jena
Biometra T Advanced 96 G	Analytik Jena
Centrifuge 5417 R	Eppendorf
Centrifuge 5804 R	Eppendorf
Eporator	Eppendorf
LAS 3000 Imager	Fujifilm
M20 Water Bath Circulator	MGW Lauda
Mastercycler EP Gradient	Eppendorf
Mastercycler EP Realplex ² (epgradient S)	Eppendorf
Minispin	Eppendorf
Mini-Sub Cell System	BioRad
Nanodrop Spectrophotometer ND-1000	Thermo Fisher Scientific Inc.
PG4002-S Delta Range	Mettler Toledo
Precellys 24 homogenizer	Peqlab
S20 - Seven Easy pH Meter	Mettler Toledo
Synergy 2	BioTek Instruments
Techne Dri-Block DB 2A	Bibby Scientific

Table S5: List of apparatus (continued)

Apparatus	Company
Thermomixer 5436	Eppendorf
Vortex-Genie 2	Scientific Industries, Inc.
XP26 Delta Range	Mettler Toledo

Primer

Table S6: List of primers used in this study

Name	Sequence 5' → 3'	Purpose
amplification primer		
01fw_flank1 (cg3344)	CAGGTCGACTCTAGAGGATCCGTTCCGAAGA AGCCAAAG	forward primer 5'flank for integration between <i>cg3344</i> and <i>cg3345</i>
02rev_flank1 (cg3344)	CTTTGCGAGCAGGTCGCTGCGAAATGGAAAA CGCCCC	reverse primer 5'flank for integration between <i>cg3344</i> and <i>cg3345</i>
03fw_PripA	CCGGGGCGTTTTCCATTTTCGCAGCGACCTGC	forward primer P _{ripA} in pK19 <i>mobsacB</i> -P _{ripA} - <i>lacI</i>
04rev_PripA	ATCTCATCCTCACTACAAGC	reverse primer P _{ripA} in pK19 <i>mobsacB</i> -P _{ripA} - <i>lacI</i>
05fw_egfp	GCTTGTAGTGAGGATGAGATATGGTGAGCAAG GGCGAGGAG	forward primer for <i>egfp</i> cloning under control of P _{ripA}
06rev_TrrnB	CAGGAGAGCGTTCACC	reverse primer T _{rrnB} in pK19 <i>mobsacB</i> based integration plasmids
07fw_flank2 (cg3345)	GTCGGTGAACGCTCTCCTGACACATCTGTTTCG ACTCGC	forward primer 3'flank for integration between <i>cg3344</i> and <i>cg3345</i>
08rev_flank2 (cg3345)	GCGGCAGCGTGAAGCTAGCCGCGTGATTCCTG GAAAATTAG	reverse primer 3'flank for integration between <i>cg3344</i> and <i>cg3345</i>
09fw_lacI	GCTTGTAGTGAGGATGAGATATGGCGGAGCTG AATTAC	forward primer <i>lacI</i> in pK19 <i>mobsacB</i> -flank1(3' <i>cg3344</i>)- P _{ripA} - <i>lacI</i> -T _{rrnB} -flank2(5' <i>cg3345</i>)

Table S6: List of primers (continued)

Name	Sequence 5' → 3'	Purpose
10rev_lacI	CATCCGCCAAAACAGCCAAGCTCACTGCCCCGCTTTC	reverse primer <i>lacI</i> in pK19 <i>mobsacB</i> -flank1(3' <i>cg3344</i>)-P _{ripA} - <i>lacI</i> -T _{rrnB} -flank2(5' <i>cg3345</i>)
11fw_TrnB	GCTTGGCTGTTTTGGC	generic forward primer T _{rrnB}
15rev_Ptac	ATGGTATATCTCCTTCAATTCTG	generic reverse primer P _{tac}
16fw_egfp	GAATTGAAGGAGATATAACCATATGGTGAGCAA GGGCGAGGAG	forward primer <i>egfp</i> in pJC4-P _{tac} - <i>egfp</i>
19fw_Ptac	GCGACGCCGAGGGTCTAGACCCTGAATTGACTCTCTTCC	forward primer P _{tac} in pJC4-P _{tac} - <i>egfp</i>
20rev_TrnB	GATATCCATCACACTGGCGGCCCGCCAGGAGAG CGTTCACC	reverse primer T _{rrnB} in pJC4-P _{tac} - <i>egfp</i>
dtxR-1	GGGAATTCCATATGAAGGATCTGGTTCGATACC ACCG	forward primer for <i>dtxR</i> in pJOE6089- <i>dtxR</i>
dtxR-2	CGCGGATCCGCCCTCAACCTTTTCTACGCGG	reverse primer for <i>dtxR</i> in pJOE6089- <i>dtxR</i>
21fw_dtxR (NdeI)	CATATGAAGGATCTGGTTCGATAC	forward primer for <i>dtxR</i> (C102D) in pJOE6089- <i>dtxR</i> (C102D)
22rev_dtxR (BamHI)	GGATCCGCCCTCAACC	reverse primer for <i>dtxR</i> (C102D) in pJOE6089- <i>dtxR</i> (C102D)
23rev_dtxR (C102D)	CACGTGCTCCCAGCGGTCTGCTTCGTCGTGG	forward primer for <i>dtxR</i> (C102D) encoding point mutation in pJOE6089- <i>dtxR</i> (C102D)
24fw_dtxR (C102D)	CCACGACGAAGCAGACCGCTGGGAGCACGTG	reverse primer for <i>dtxR</i> (C102D) encoding point mutation in pJOE6089- <i>dtxR</i> (C102D)
56fw_dtxR (RBS)	GCCAAGCTTGCATGCCTGCAGGAGTTTGGAA AAACAAGGAAGGCAGCCTCCTATGAAG- GATC TGGTCGATAC	forward primer for <i>dtxR</i> in pVWEx1- <i>dtxR</i>
57rev_Strep (BamHI)	CGAGCTCGGTACCCGGGGATCCTTACTTTTCA AACTGCGG	reverse primer for <i>dtxR</i> in pVWEx1- <i>dtxR</i>
88fw_flank1 (cg2444)	AACAGCTATGACCATGATTACGCCAAGCTTAA ACACCACCTGGCGTGAC	forward primer 5'flank in pK19 <i>mobsacB</i> - Δ <i>cg2444</i>
89rev_flank1 (cg2444)	CCGACCGTAACCGGGTGAATTCCCTAACTTC CTGTC	reverse primer 5'flank in pK19 <i>mobsacB</i> - Δ <i>cg2444</i>
90fw_flank2 (cg2444)	TAGGAATTCCACCCGGTTACGGTCGGGTTTT AG	forward primer 3'flank in pK19 <i>mobsacB</i> - Δ <i>cg2444</i>
91rev_flank2 (cg2444)	AGTGAATTTCGAGCTCGGTACCCGGGGATCCG ATTTTCGCCGTCGCAAC	reverse primer 3'flank in pK19 <i>mobsacB</i> - Δ <i>cg2444</i>

Table S6: List of primers (continued)

Name	Sequence 5' → 3'	Purpose
100fw_flank1 (ftn)	AACAGCTATGACCATGATTACGCCAAGCTTAG CATCGTGAACACTGAG	forward primer 5'flank in pK19 <i>mobsacB-Δftn</i>
101rev_flank1 (ftn)	AACTGCGGGGAATGGCCCCAACGTACACAAC	reverse primer 5'flank in pK19 <i>mobsacB-Δftn</i>
102fw_flank2 (ftn)	TACGTTAGGGGCCATTCCCCGAGTTTTTAAT G	forward primer 3'flank in pK19 <i>mobsacB-Δftn</i>
103rev_flank2 (ftn)	AGTGAATTCGAGCTCGGTACCCGGGGATCCC AGCGAATGATGGACTTATC	reverse primer 3'flank in pK19 <i>mobsacB-Δftn</i>
110fw_flank1 (dps)	AACAGCTATGACCATGATTACGCCAAGCTTTG CGCTCTGCATCGGTGA	forward primer 5'flank in pK19 <i>mobsacB-Δdps</i>
111rev_flank1 (dps)	GCTTTTCGACGTTGACCCCTATTATAGCACTG CTTGATAAATTG	reverse primer 5'flank in pK19 <i>mobsacB-Δdps</i>
112fw_flank2 (dps)	TATAATAGGGGTCAACGTCGAAAAGCGTTAAG GCGC	forward primer 3'flank in pK19 <i>mobsacB-Δdps</i>
113rev_flank2 (dps)	AGTGAATTCGAGCTCGGTACCCGGGGATCCG GCAAGGCCCCAGGGAGG	reverse primer 3'flank in pK19 <i>mobsacB-Δdps</i>
116fw_flank1 (5'cg1438)	AACAGCTATGACCATGATTACGCCAAGCTTTC AGCAACATGAACTACTC	Forward primer 5'flank in pK19 <i>mobsacB-Δcg1438-cg1441</i>
117rev_flank1 (5'cg1438)	GGATGCTGCAATCTTTCTAACACGTCTTTTAA AGG	reverse primer 5'flank in pK19 <i>mobsacB-Δcg1438-cg1441</i>
118fw_flank2 (5'cg1441)	GTGTTAGAAAGATTGCAGCATCCTTAAATCAG	forward primer 3'flank in pK19 <i>mobsacB-Δcg1438-cg1441</i>
119rev_flank2 (5'cg1441)	AGTGAATTCGAGCTCGGTACCCGGGGATCCT CAAGGTCGATCTCACCAC	reverse primer 3'flank in pK19 <i>mobsacB-Δcg1438-cg1441</i>
130fw_flank1 (5'cg0041)	AACAGCTATGACCATGATTACGCCAAGCTTCG GTGGAGTAGGTGATGTC	forward primer 5'flank in pK19 <i>mobsacB-Δcg0041-cg0042</i>
131rev_flank1 (5'cg0041)	TCATTTTCAAACAGTCCTAAACAGTCTTAAAC AG	reverse primer 5'flank in pK19 <i>mobsacB-Δcg0041-cg0042</i>
132fw_flank2 (3'cg0042)	TTAGGACTGTTTGAAAATGATAACCGTTATCA TTAAGG	forward primer 3'flank in pK19 <i>mobsacB-Δcg0041-cg0042</i>
125rev_flank2 (3'cg0042)	AGTGAATTCGAGCTCGGTACCCGGGGATCCG AGGGTTTCGTGAGAAG	reverse primer 3'flank in pK19 <i>mobsacB-Δcg0041-cg0042</i>
sequencing primer		
25fw_pJoe6089 _seq	GCGATCACCACAATTCAG	generic forward primer for sequencing of pJOE6089 based plasmids

Table S6: List of primers (continued)

Name	Sequence 5' → 3'	Purpose
26rev_pJoe6089_seq	CCGCCAGGCAAATTTCTG	generic reverse primer for sequencing of pJOE6089 based plasmids
27fw_dtxR_seq	TCTGGTTCGATAACCACCG	forward sequencing primer binding inside <i>dtxR</i>
28rev_dtxR_seq	CCTCAACCTTTTCTACGC	reverse sequencing primer binding inside <i>dtxR</i>
43fw_pJC4_seq	CGATTGAAGACCGTCAAC	generic forward primer for sequencing of pJC4 based plasmids
44rev_pJC4_seq	GTCATCAGACCAAGGAG	generic reverse primer for sequencing of pJC4 based plasmids
45fw_pK19_seq	CAGGCTTTTACTTTTATGC	generic forward primer for sequencing of pK19 <i>mobsacB</i> based plasmids
46rev_pK19_seq	ACCTGCTTTTCTTTTGCG	generic reverse primer for sequencing of pK19 <i>mobsacB</i> based plasmids
47fw_Ptac_seq	AGCCATCGGAAGCTGTG	forward sequencing primer binding inside P _{tae}
48fw_PripA_seq	GAGATCCCAGAGGCATAG	forward sequencing primer binding inside P _{ripA}
49fw_egfp_seq	ACAACATCGAGGACGGC	forward sequencing primer binding inside <i>egfp</i>
50rev_egfp_seq	TCAGCTTGCCGTAGGTG	reverse sequencing primer binding inside <i>egfp</i>
51fw_lacI_seq	AGCAAATCGCGCTGTTAG	forward sequencing primer binding inside <i>lacI</i>
52rev_lacI_seq	GTTGAAAACCGGACATGG	reverse sequencing primer binding inside <i>lacI</i>
53rev_TrrnB_seq	TACGGCGTTTCACTTCTG	reverse sequencing primer binding inside T _{rrnB}
98fw_5'cg2444_seq	GCTTCTACTGCTTTGAAG	forward sequencing primer for <i>cg2444</i> deletion construct
99rev_3'cg2444_seq	CGATTTCCCTTTAGCTCCC	reverse sequencing primer for <i>cg2444</i> deletion construct
104fw_5'ftn_seq	TTAGACCTAGCTTTAGAGC	forward sequencing primer for <i>ftn</i> deletion construct

Table S6: List of primers (continued)

Name	Sequence 5' → 3'	Purpose
105rev_3'ftn_seq	TGTGGCAAAACAGTAATGC	reverse sequencing primer for <i>ftn</i> deletion construct
114fw_5'dps_seq	GTGACCGTTGATGATCGC	forward sequencing primer for <i>dps</i> deletion construct
115rev_3'dps_seq	CTTAGAGGCGATTCTAGG	reverse sequencing primer for <i>dps</i> deletion construct
120fw_5'cg1438_seq	CGCCGCATAGGAAATGC	forward sequencing primer for <i>cg1438-cg1441</i> deletion construct
121rev_3'cg1441_seq	GGCATCAAGTTCTGCTTTG	reverse sequencing primer for <i>cg1438-cg1441</i> deletion construct
136fw_5'cg0041_seq	CTCCTGCACTGTTGAGG	forward sequencing primer for <i>cg0041-cg0042</i> deletion construct
127rev_3'cg0042_seq	CAGTGAGTCGTTGCCAG	reverse sequencing primer for <i>cg0041-cg0042</i> deletion construct

GeneRuler™ 1 kb Plus DNA Ladder

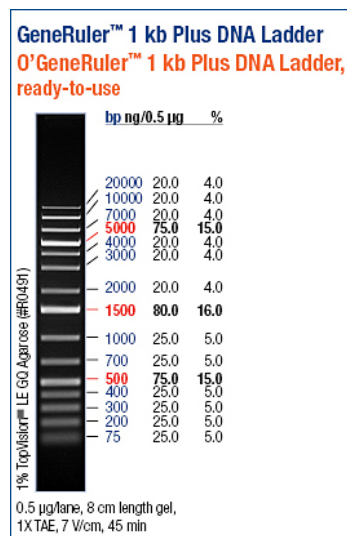
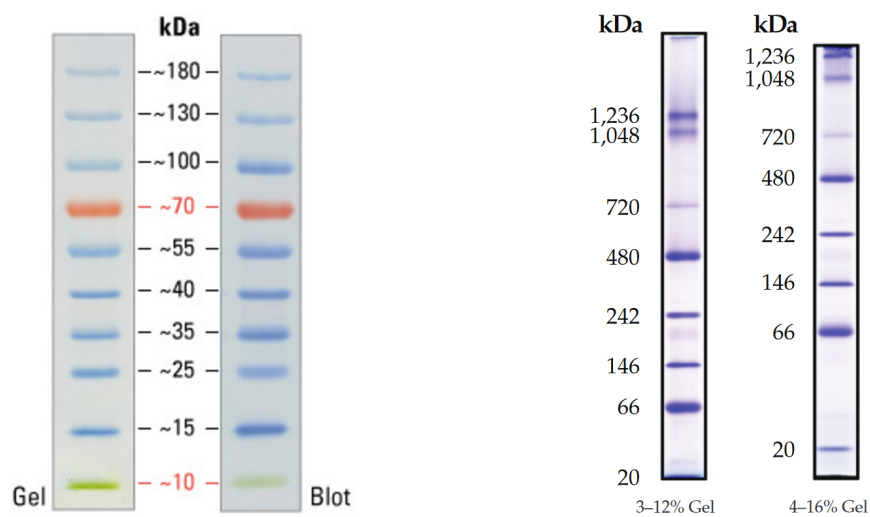


Figure S5: GeneRuler™ 1 kb Plus DNA Ladder, which was provided by Thermo Fisher Scientific Inc., Bremen, Germany

Protein ladders PageRuler™ and nativeMark™

(a) PageRuler™ Prestained Protein Ladder (b) nativeMark™ unstained protein standard

Figure S6: Protein ladders of known size for denatured (a) and native (b) acrylamide gels. Pictures provided by Thermo Fisher Scientific Inc., Bremen, Germany

mbo-mbio/mbo00120/mbo5125d20z | xppws | S=5 | 2/12/20 | 10:48 | ArtID: | DOI:10.1128/mBio.00085-20 | CE: CB

Editor: | Section: Research Article | Designation:

RESEARCH ARTICLE
Applied and Environmental Science

CO₂/HCO₃⁻ Accelerates Iron Reduction through Phenolic Compounds

AQ: au Felix Müller,^{a,b} Johanna Rapp,^a Anna-Lena Hacker,^a André Feith,^a Ralf Takors,^a Bastian Blombach^{a,b}^aInstitute of Biochemical Engineering, University of Stuttgart, Stuttgart, Germany^bMicrobial Biotechnology, Campus Straubing for Biotechnology and Sustainability, Technical University of Munich, Straubing, Germany

AQ: A

ABSTRACT Iron is a vital mineral for almost all living organisms and has a pivotal role in central metabolism. Despite its great abundance on earth, the accessibility for microorganisms is often limited, because poorly soluble ferric iron (Fe³⁺) is the predominant oxidation state in an aerobic environment. Hence, the reduction of Fe³⁺ is of essential importance to meet the cellular demand of ferrous iron (Fe²⁺) but might become detrimental as excessive amounts of intracellular Fe²⁺ tend to undergo the cytotoxic Fenton reaction in the presence of hydrogen peroxide. We demonstrate that the complex formation rate of Fe³⁺ and phenolic compounds like protocatechuic acid was increased by 46% in the presence of HCO₃⁻ and thus accelerated the subsequent redox reaction, yielding reduced Fe²⁺. Consequently, elevated CO₂/HCO₃⁻ levels increased the intracellular Fe²⁺ availability, which resulted in at least 50% higher biomass-specific fluorescence of a DtxR-based *Corynebacterium glutamicum* reporter strain, and stimulated growth. Since the increased Fe²⁺ availability was attributed to the interaction of HCO₃⁻ and chemical iron reduction, the abiotic effect postulated in this study is of general relevance in geochemical and biological environments.

IMPORTANCE In an oxygenic environment, poorly soluble Fe³⁺ must be reduced to meet the cellular Fe²⁺ demand. This study demonstrates that elevated CO₂/HCO₃⁻ levels accelerate chemical Fe³⁺ reduction through phenolic compounds, thus increasing intracellular Fe²⁺ availability. A number of biological environments are characterized by the presence of phenolic compounds and elevated HCO₃⁻ levels and include soil habitats and the human body. Fe²⁺ availability is of particular interest in the latter, as it controls the infectiousness of pathogens. Since the effect postulated here is abiotic, it generally affects the Fe²⁺ distribution in nature.

KEYWORDS iron homeostasis, iron reduction, carbon dioxide, bicarbonate, DtxR, pathogens, *Corynebacterium glutamicum*, iron homeostasis

Iron is a vital mineral for almost all living organisms and participates in inevitable electron transfer reactions since it serves a redox potential from -500 to +300 mV by switching between two oxidation states (Fe²⁺/Fe³⁺) (1). Despite its great abundance in the Earth's crust (representing the fourth most abundant element), its availability for organisms is limited, because it is mainly present as poorly soluble Fe³⁺ (10⁻¹⁸ M at pH 7.0) in an oxidative environment (2). Sophisticated strategies to increase its accessibility have evolved, including the secretion of siderophores and smaller iron chelators that enhance the solubility of Fe³⁺ (3). Iron complexes are then taken up via designated transport systems in an energy-dependent fashion (2). Since reduced Fe²⁺ is incorporated as a prosthetic group in a number of enzymes that belong to respiratory complexes or that participate in tricarboxylic acid (TCA) cycle reactions and stress response inside the cell, the reduction of Fe³⁺ is of central relevance. Several studies on the characterization of ferric reductase activity are reviewed by Schröder et al. (4). It

Citation Müller F, Rapp J, Hacker A-L, Feith A, Takors R, Blombach B. 2020. CO₂/HCO₃⁻ accelerates iron reduction through phenolic compounds. *mBio* 11:e00085-20. <https://doi.org/10.1128/mBio.00085-20>.

Editor Sang Yup Lee, Korea Advanced Institute of Science and Technology

Copyright © 2020 Müller et al. This is an open-access article distributed under the terms of the [Creative Commons Attribution 4.0 International license](https://creativecommons.org/licenses/by/4.0/).

Address correspondence to Bastian Blombach, bastian.blombach@tum.de.

Received 13 January 2020

Accepted 31 January 2020

Published

mbo-mbio/mbo00120/mbo5125d20z | xppws | S=5 | 2/12/20 | 10:48 | ArtID: | DOI:10.1128/mBio.00085-20 | CE: CB

Müller et al.



turned out that most designated ferric reductases are in fact flavin reductases that regenerate the substrate for chemical iron reduction. This is not limited to intracellular reactions, since it was shown recently that the human pathogen *Listeria monocytogenes* possesses an extracellular electron transfer apparatus, in which iron reduction is mediated by flavin (5).

In the Gram-positive soil bacterium *Corynebacterium glutamicum*, which is used in amino acid production on an industrial scale, little is known about iron uptake mechanisms because most annotated genes lack experimental validation (6, 7). During the development of a suitable minimal medium for *C. glutamicum*, the addition of citrate (8) or small amounts of the diphenolic compounds catechol or protocatechuic acid (PCA) (3,4-dihydroxybenzoic acid) revealed a growth-promoting effect, which was attributed to the improved iron uptake of Fe^{3+} chelates (9). To ensure sufficient initial iron uptake, PCA became a component of the widely used CgXII medium (10).

Excessive amounts of intracellular iron are deposited in specialized storage proteins (ferritin [Ftn] and Dps) and can be remobilized from there in times of iron starvation (2). A novel mode of iron remobilization was identified recently in *C. glutamicum*. Pupylation of a surface lysine residue of the Ftn and Dps proteins initiates the unfolding and subsequent Fe^{3+} release in the cytosol. However, the mechanism responsible for reduction of Fe^{3+} remains unclear (11).

Diphenolic substances (e.g., 2,3-dihydroxybenzoic acid [2,3-DHB] and derivatives) are secreted under iron-restricted growth conditions by a variety of organisms such as *Bacillus subtilis* and *Paracoccus (Micrococcus) denitrificans* (3, 12, 13). It was suggested that 2,3-DHB and derivatives are involved in iron uptake, as mutants deficient in the biosynthesis of 2,3-DHB and derivatives imported less iron, and adding these compounds enhanced iron transport (14). PCA is a structural relative of the common catecholate-type siderophore precursor 2,3-DHB and represents the basic compound of the rather unusual siderophore petrobactin (15). *Bacillus anthracis* and *Bacillus cereus* secrete great amounts of PCA in response to iron limitation (16–18). As a diphenolic Fe^{3+} chelator (19), it was expected to serve a function analogous to 2,3-DHB enhancing iron uptake, although evidence for this had not been provided (16).

Besides chelating iron, diphenols have the potential to reduce Fe^{3+} (20). The redox reaction in Fe^{3+} -PCA chelates (19, 21)—and generally speaking in Fe^{3+} -monocatecholate complexes—proceeds via the sequential oxidation of two adjacent hydroxyl groups to the respective semiquinone and quinone, providing two electrons per molecule for the reduction of Fe^{3+} (20). The reaction depends on an acidic pH, as iron and PCA bind in a 1:1 stoichiometry at a pH of <4.5 (19), and the redox reaction is inhibited by the presence of (at least) the biscatecholate complex (20, 21).

The phenotypical response of bacteria to different $\text{CO}_2/\text{HCO}_3^-$ levels has been extensively reviewed with a biotechnological, pathogenic, or environmental focus (22–25). On the one hand, the effect on cell viability might be detrimental, considering that CO_2 -based sterilization operating at high pressure is used in food processing. However, on the other hand, a class of bacteria called capnophiles demonstrates that HCO_3^- can be a vital substrate as they are unable to grow unless sufficiently high CO_2 levels are established (26). Carboxylation reactions might generally benefit from the increased availability of $\text{CO}_2/\text{HCO}_3^-$. *C. glutamicum* is especially well equipped with enzymes catalyzing these reactions, e.g., at the phosphoenolpyruvate (PEP)-pyruvate-oxaloacetate node (27). As a consequence, higher product (e.g., succinate) and biomass yields per substrate were reported in *C. glutamicum* at elevated CO_2 levels and could be attributed particularly to an increased flux via the anaplerotic reactions (28–30). Anaerobic growth on glucose and tryptone could be enhanced by increasing concentrations of CO_2 . The authors suggest that this might enhance acetyl coenzyme A (acetyl-CoA) carboxylation reactions, yielding greater levels of fatty and mycolic acids (31). Although the exponential growth rate of *C. glutamicum* could not be promoted under aerobic conditions, elevated CO_2 in the inlet air of a bioreactor cultivation provoked the transcriptional response of almost the entire DtxR regulon (30). The master regulator of iron homeostasis in *C. glutamicum* was originally named after its

mbo-mbio/mbo00120/mbo5125d20z xppws S=5 2/12/20 10:48 ArtID: DOI:10.1128/mBio.00085-20 CE: CB

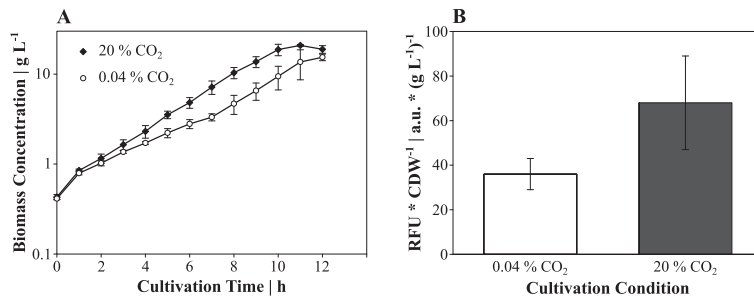
CO₂/HCO₃⁻ Accelerates Chemical Iron Reduction

FIG 1 Biomass formation of *C. glutamicum* FEM3 (A) and biomass-specific fluorescence after 24-h cultivation in a parallel bioreactor setup (B). *C. glutamicum* FEM3 was cultivated aerobically in minimal medium with 20 g glucose liter⁻¹ with synthetic air containing 20% CO₂ (21% O₂, 59% N₂) or ambient air (0.04% CO₂). Data points (A) and bars (B) represent mean values, and error bars indicate standard deviations for three biological independent replicates.

functional homologue in the pathogenic *C. diphtheriae*, where it controls the toxin production in response to the iron availability (32). In fact, to date, many pathogens that induce the expression of toxin genes under iron starvation conditions and typically integrate this signal via the transcriptional regulators Fur, DtxR and homologues thereof are known (33–35). In analogy with the iron limitation, elevated CO₂/HCO₃⁻ levels represent another suitable indicator for the host environment (2). The expression of toxin-encoding genes in *Vibrio cholerae* or *Pseudomonas aeruginosa* is mediated by the transcriptional regulators ToxT and RegA in response to elevated HCO₃⁻ concentrations (23). Interestingly, *regA* expression in *P. aeruginosa* is in turn repressed in an iron-dependent manner by a Fur homologue (33). Hence, understanding the interaction between CO₂/HCO₃⁻ and iron availability is particularly interesting with regard to toxin production by pathogenic bacteria (23).

RESULTS

Elevated levels of CO₂/HCO₃⁻ increase intracellular Fe²⁺ availability. To monitor intracellular Fe²⁺ availability, we constructed the fluorescence-based reporter strain *C. glutamicum* FEM3 which responds to the activation state of DtxR (see Fig. S1 in the supplemental material). Therefore, we chromosomally integrated the *lacI* gene under the control of the *ripA* promoter (*P_{ripA}*), which is controlled by DtxR. High Fe²⁺ concentrations induce DtxR binding to *P_{ripA}*, thus provoking repression of *lacI* and ultimately resulting in *egfp* expression under the control of the strong *tac* promoter (*P_{tac}*). Thus, the genetic circuit of *C. glutamicum* FEM3 constitutes a signal amplifier and a converter of the native repression mechanism.

Under all conditions tested, *C. glutamicum* FEM3 and the wild type (WT) showed identical growth. Cultivating *C. glutamicum* FEM3 under iron starvation (1 μM) resulted in a marginal increase of the fluorescence per biomass [78 ± 4 arbitrary units (a.u.) · (g_{CDW} liter⁻¹)⁻¹ where g_{CDW} is the cell weight (dry weight) in grams] over the autofluorescence of the WT [64 ± 3 a.u. · (g_{CDW} liter⁻¹)⁻¹] after 24 h. At iron excess (100 μM), *C. glutamicum* FEM3 yielded a fluorescence per biomass which was about fourfold higher [313 ± 20 a.u. · (g_{CDW} liter⁻¹)⁻¹] at the end of the cultivation compared to conditions under iron starvation (Fig. S2).

Having proven the functionality at different iron concentrations, we cultivated *C. glutamicum* FEM3 aerobically in a parallel bioreactor system to evaluate the intracellular Fe²⁺ availability in response to altering CO₂/HCO₃⁻ levels. With 20% CO₂ in the inlet air, *C. glutamicum* FEM3 grew exponentially (growth rate [μ] = 0.36 ± 0.02 h⁻¹) until the carbon source glucose was exhausted (Fig. 1A). In contrast, aeration with an ambient CO₂ concentration (0.04%) provoked biphasic growth of *C. glutamicum* FEM3 with a growth rate of 0.26 ± 0.05 h⁻¹ and 0.32 ± 0.02 h⁻¹ in growth phase one and two, respectively (Fig. 1A). Biomass-specific fluorescence started at similar levels in both

FI

mbo-mbio/mbo00120/mbo5125d20z xppws S=5 2/12/20 10:48 ArtID: DOI:10.1128/mBio.00085-20 CE: CB

Müller et al.

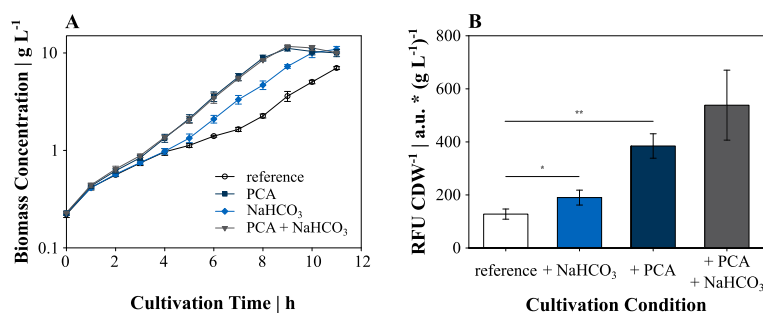


FIG 2 (A) Shaking flask cultivations of wild-type (WT) *C. glutamicum* in minimal medium with 20 g glucose liter⁻¹ without supplement (reference), with 195 μ M PCA, 50 mM NaHCO₃ or a combination of both supplements. (B) Biomass-specific fluorescence of *C. glutamicum* FEM3 after 24 h of cultivation with the indicated supplements. Data points and bars represent mean values with error bars indicating standard deviations for 3 to 10 independent biological replicates. Values that are significantly different by a two-sample t test are indicated by bars and asterisks as follows: *, $P < 0.05$; **, $P < 0.01$.

F2

conditions but after 24 h on average reached almost twofold-higher values at 20% CO₂ content, whereas it remained at a low level at the ambient CO₂ concentration (Fig. 1B). Biphasic growth of *C. glutamicum* FEM3 and the WT was also observed on minimal medium containing glucose in shaking flasks at an ambient CO₂ concentration (Fig. 2A). In accordance with the bioreactor cultivations, growth was stimulated by adding 30 mM NaHCO₃, which shortened the initial (nonexponential) growth phase from about 7 h under reference conditions to 4 h and led to a growth rate of 0.40 ± 0.03 h⁻¹ during the second growth phase. The addition of 195 μ M of the iron chelator PCA restored exponential growth throughout the cultivation (Fig. 2A) and resulted in a slightly higher growth rate compared to the rate for the second growth phase of the reference condition (reference, $\mu = 0.37 \pm 0.01$ h⁻¹; PCA, $\mu = 0.43 \pm 0.01$ h⁻¹).

The biomass-specific fluorescence of the shaking flask approach showed a 0.5- and 3.0-fold increase in response to supplementing with NaHCO₃ or PCA compared to the reference cultivation after 24 h, respectively (Fig. 2B). Although growth of *C. glutamicum* FEM3 was not further improved by the combined addition of NaHCO₃ and PCA (Fig. 2A), there might be a synergistic effect on fluorescence level (4.2-fold compared to the reference; Fig. 2B), which was, however, not significantly higher than in the PCA-supplemented condition (by Student's *t* test). Supplementing with PCA or NaHCO₃ did not show a growth-stimulating effect in iron-depleted medium (Fig. S3), where biomass stagnated at a final 0.9 to 1.1 g liter⁻¹ regardless of supplementation. In summary, these results demonstrate that in the presence of the extracellular iron source (FeSO₄), elevated levels of CO₂/HCO₃⁻ and/or the addition of PCA to the minimal medium results in an increased intracellular Fe²⁺ availability in *C. glutamicum*.

CO₂/HCO₃⁻ does not increase thermal stability of the DtxR protein or interact with iron storage and mobilization. The DtxR protein of *C. glutamicum* shares 72% sequence identity with its extensively characterized homologue from *Corynebacterium diphtheriae*, including conserved ligand binding sites. Dimerization of the latter and subsequent DNA recognition are induced by sequential binding of two divalent metal ions per monomer. Besides the physiological effector of DtxR, Fe²⁺, *in vitro* activation was demonstrated with Ni²⁺, Mn²⁺, and Co²⁺ at various affinities (36). As they are stable in an oxidative environment, they are commonly found in crystallographic structures of DtxR. An anion binding site is located in close proximity to the low-affinity binding site and essential for coordination of the metal ion (37–39). To address the question whether binding of HCO₃⁻ to the anion binding site of DtxR could cause the higher activation, we performed differential scanning fluorimetry. The thermal stability of purified DtxR protein was enhanced by increasing concentrations of divalent metal ions (Ni²⁺ and Mn²⁺) and dissociation constants (K_D) were calculated to 5.3 ± 1.1 μ M

mbo-mbio/mbo00120/mbo5125d20z xppws S=5 2/12/20 10:48 ArtID: DOI:10.1128/mBio.00085-20 CE: CB

CO₂/HCO₃⁻ Accelerates Chemical Iron Reduction

mBio

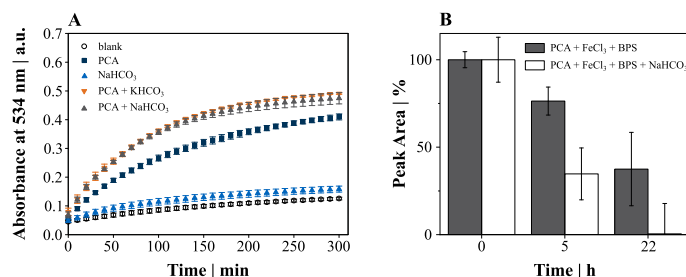


FIG 3 (A) Kinetic analysis of the Fe²⁺-BPS complex formation at 534 nm with 19.5 μM PCA and/or 50 mM HCO₃⁻. (B) Relative PCA degradation over time in the presence and absence of 50 mM NaHCO₃. Data points and bars represent mean values with error bars indicating standard deviations for three to six independent replicates.

and 21.8 ± 3.6 μM, respectively. However, addition of up to 100 mM NaHCO₃ did not stabilize DtxR further at any concentration of metal ions (data not shown).

To investigate whether elevated CO₂/HCO₃⁻ levels have an impact on iron storage or mobilization, we created deletion mutations (Δ *ftn*, Δ *dps*, Δ *ftn* Δ *dps*, and Δ *pup*) in *C. glutamicum* FEM3 and the WT. The deletion mutants lack either one (Δ *ftn*, Δ *dps*) or both iron storage proteins (Δ *ftn* Δ *dps*) or are unable to initiate remobilization of the stored iron by pupylation (Δ *pup*). With the exception of *C. glutamicum* Δ *pup*, none of the deletion mutants showed a difference regarding growth and fluorescence in any of the conditions tested (data not shown). *C. glutamicum* Δ *pup* revealed an even stronger growth defect than the WT under reference conditions. However, supplementation of PCA or NaHCO₃ restored the respective growth phenotype with the result that *C. glutamicum* Δ *pup* and the WT grew identically again (Fig. S4).

CO₂/HCO₃⁻ accelerates Fe³⁺ reduction through phenolic compounds. Since we could not attribute the improved Fe³⁺ reduction capacity in the presence of elevated CO₂/HCO₃⁻ levels to an interaction with stored intracellular iron, we focused on the chemical reduction by PCA and HCO₃⁻ using the Fe²⁺-specific iron chelator bathophenanthroline disulfonic acid (BPS) for detection. After 5 h of incubation, the amount of Fe²⁺-BPS complexes was about sevenfold higher in the presence of 19.5 μM PCA compared to a sample without additives (blank control; Fig. 3A). Although the addition of 50 mM NaHCO₃ alone increased the final absorbance only marginally, it promoted the iron reduction in the presence of PCA significantly. Differences caused by the presence of NaHCO₃ were most remarkable during the initial reduction phase with a >50% greater amount of Fe²⁺-BPS complexes up to 100 min after the start of the assay (Fig. 3A). The sample pH was maintained at 7.4 throughout the incubation in 200 mM 3-(*N*-morpholino)propanesulfonic acid (MOPS) buffer, thus proving that a shift in pH was not causing the increase in absorbance. We also replaced NaHCO₃ with KHCO₃, which led to the identical improvement in iron reduction (Fig. 3A). An equimolar NaCl concentration did not trigger iron reduction (data not shown).

We monitored the degradation of PCA by liquid chromatography-quadrupole time of flight mass spectrometry (LC-MS-QTOF) analysis and found only about half of the residual amount of PCA when samples were incubated for 5 h in the presence of HCO₃⁻ compared to samples incubated without HCO₃⁻ (Fig. 3B). Furthermore, we identified oxidation products with the chemical formula C₇H₆O₆ and C₇H₅O₆.

Concluding that PCA serves as electron donor in the reduction of Fe³⁺, we tested other aromatic compounds at identical concentrations that could be associated with iron reduction.

Catechol and 2-amino-3-hydroxybenzoic acid (3-hydroxyanthranilic acid [3-HAA]) carrying two adjacent hydroxyl groups or a mix of amino and hydroxyl groups, respectively, exhibited reduction capacities that were at least as high as PCA. Iron

mbo-mbio/mbo00120/mbo5125d20z xppws S=5 2/12/20 10:48 ArtID: DOI:10.1128/mBio.00085-20 CE: CB

Müller et al.

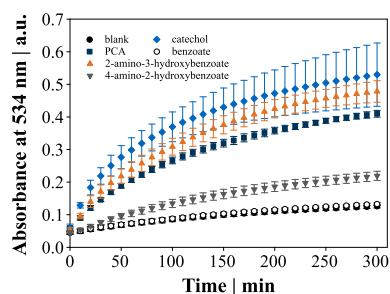


FIG 4 Kinetic analysis of the Fe^{2+} -BPS complex formation at 534 nm with different functionalized aromatic compounds. Data points represent mean values with error bars indicating standard deviations of three to six independent replicates.

reduction by 4-amino-2-hydroxybenzoic acid (*para*-aminosalicylic acid), where the amino and hydroxyl groups are not positioned adjacent to each other, was only intermediate, whereas benzoic acid lacking hydroxyl and amino groups did not reduce iron at all (Fig. 4). The addition of 50 mM NaHCO_3 alongside with either of the above compounds (except for benzoic acid) accelerated the iron reduction in the same way as observed with PCA.

To further elucidate the role of HCO_3^- in the reduction of iron, we analyzed the complex formation between Fe^{3+} and the iron chelator PCA that is required prior to reduction. In accordance with iron reduction, the initial rate of Fe^{3+} -PCA complex formation (0 to 35 min) was increased by 46% through the addition of 50 mM NaHCO_3 ($5.2 \pm 1.0 \Delta\text{mA}_{560} \text{ min}^{-1}$ [change in milli absorbance units at 560 nm per minute] versus $7.6 \pm 1.3 \Delta\text{mA}_{560} \text{ min}^{-1}$; Fig. 5A). In addition to the altered kinetics, the maximum absorbance of those complexes shifted to a shorter wavelength (λ_{max}). The assay pH was again not affected by the addition of NaHCO_3 , and intentional pH perturbation with 50 mM KOH or HCl failed to reproduce the λ_{max} shift (Fig. 5B).

DISCUSSION

Recently, Blombach et al. (30) initially disclosed a link between a high CO_2 proportion in the inlet air and a transcriptional response of almost the complete DtxR regulon in *C. glutamicum*. In this study, we demonstrate that elevated $\text{CO}_2/\text{HCO}_3^-$ levels increased the intracellular Fe^{2+} availability and thus stimulated growth of *C. glutamicum*. The higher Fe^{2+} concentration was not coupled to biological activity. Instead, we

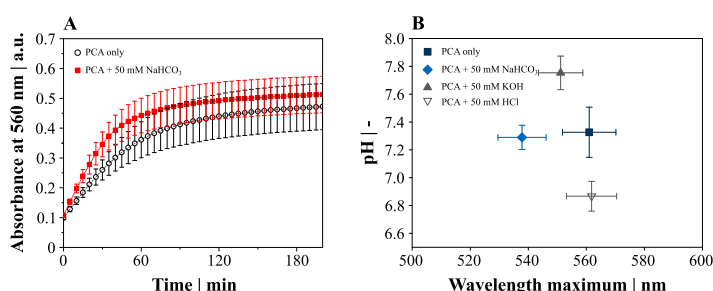


FIG 5 Complex formation between Fe^{3+} and PCA in the presence and absence of 50 mM NaHCO_3 . (A) The kinetics of complex formation was monitored by an increase of the absorbance at 560 nm. (B) Wavelength of the maximum absorbance (λ_{max}) of the Fe^{3+} -PCA complexes formed in the presence and absence of NaHCO_3 correlated with pH. Data points represent mean values, and error bars indicate standard deviations for three to five independent replicates.

January/February 2020 Volume 11 Issue 1 e00085-20

mbio.asm.org 6

mbo-mbio/mbo00120/mbo5125d20z | xppws | S=5 | 2/12/20 | 10:48 | ArtID: | DOI:10.1128/mBio.00085-20 | CE: CB

CO₂/HCO₃⁻ Accelerates Chemical Iron Reduction

identified an abiotic interaction of CO₂/HCO₃⁻ with chemical iron reduction through phenolic compounds.

Growth retardation had not been reported previously, when *C. glutamicum* cultures were aerated with pressurized air and has been introduced in this study presumably by the insertion of an additional minimal medium preculture, since all other process parameters were kept the same (30). The growth defect could be transferred to a shaking flask approach and was apparently caused by a limitation of intracellular iron availability, as suggested (i) by the lower fluorescence of FEM3, (ii) by the stronger growth retardation of *C. glutamicum* Δ pup in the reference culture, which was found to exhibit a growth retardation only in iron starvation (11) and (iii) by the fact that PCA supplementation restored exponential growth (9). Analogously, an extended lag phase of *C. glutamicum* in minimal medium had been observed when the main culture was inoculated from a preculture in minimal medium or when the inoculum was washed excessively and, consequently, the addition of iron chelators like catechol, PCA, or citrate to minimal medium was suggested (8, 9). Interestingly, this requirement for iron chelators became apparent only when carbonate was omitted from the medium (8, 9, 40). However, the role of CO₂ with regard to the iron availability was not addressed further until noting a transcriptional response of the DtxR regulon (30).

The cometabolization of glucose and PCA can improve the growth rate of *C. glutamicum* to about 0.61 h⁻¹. However, this requires essentially higher PCA concentrations and lower cell densities (40). At standard PCA concentrations (as applied in this study), growth was not found to be increased over the maximum of $\mu = 0.42$ h⁻¹ when glucose was utilized as the sole carbon and energy source (41). Thus, growth of PCA-supplemented and nonsupplemented shaking flask cultures recorded herein was in qualitative and quantitative accordance with the literature (40, 41).

If NaHCO₃ supplementation were required for an increased flux via the anaplerotic reactions, and thus explaining the growth stimulation over a reference cultivation, the effect should persist in the simultaneous addition of PCA and NaHCO₃, because the small amount of PCA is readily consumed and cannot provide a long-lasting surplus of necessary precursors. However, supplementing with both PCA and NaHCO₃ did not result in a further growth improvement, and we found instead that the growth-stimulating effect of PCA and NaHCO₃ was related to the presence of the extracellular iron source. In iron-depleted medium, growth ceased after two to three cell divisions as reported previously (42).

Upon dissolution of the iron source FeSO₄ in CgXII medium, iron is present as reduced Fe²⁺. However, it will be quickly oxidized under aerobic conditions, yielding 99% of the initial iron concentration as Fe³⁺ after 15 min (43). Considering the standard preparation times of a shaking flask experiment and estimating the initially dissolved oxygen concentration at 7.5 to 8 mg liter⁻¹ (22), the entire amount of iron provided in the medium will be oxidized before inoculation. This highlights the need of enhanced iron reduction mechanisms to obtain increased intracellular Fe²⁺ levels. Since the increased Fe²⁺ availability in the presence of elevated CO₂/HCO₃⁻ levels could not be attributed to a biological function, we analyzed the chemical reduction capacity of PCA and HCO₃⁻. Results of iron reduction assays and the LC-MS-QTOF approach show that PCA served as an electron donor for the redox reaction. Having performed the experiments at physiological pH (7.4), our results are in contrast with the common understanding that these redox reactions are restricted to acidic pH values (19–21). At pH 7.4, PCA coordination with Fe³⁺ represents a mix of 2:1 and 3:1 stoichiometry (20) and was expected to inhibit redox reactions of the iron monocatecholate complexes, which are favored at pH < 4.5 (21). Furthermore, our results indicate that the primary oxidation products of PCA (quinone and semiquinone) are further degraded. The chemical formula C₇H₆O₆ and C₇H₈O₆ obtained by the LC-MS-QTOF approach might represent β -carboxy-(*cis-cis*)-muconic acid or β -carboxy- γ -carboxymethyl- $\Delta^{\alpha,\beta}$ -butenolide and butene-1,2,3-tricarboxy acid that were postulated to be degradation products, when PCA was oxidized with peroxyacetic acid (44). Interestingly, these

January/February 2020 Volume 11 Issue 1 e00085-20

mbio.asm.org 7

mbo-mbio/mbo00120/mbo5125d20z xppws S=5 2/12/20 10:48 ArtID: DOI:10.1128/mBio.00085-20 CE: CB

Müller et al.



products also form part of the enzymatic degradation of PCA via the β -ketoacid pathway (45).

Beyond PCA, other phenolic compounds can promote bacterial growth and have been associated with iron reduction and transport in the past. Examples are the reductive mobilization of ferritin iron through PCA and derivatives (46) as well as 2-amino-3-hydroxybenzoic acid secretion by *Cryptococcus neoformans* which mediated the iron reduction required for Fe^{2+} uptake (47). Supplementing with catechol stimulated growth of *C. glutamicum* comparably to PCA (9), and the chemical reduction of Fe^{3+} through catechol oxidation is well-known and has been reviewed (20). Our results provide evidence that the postulated iron reduction is not unique to PCA but characteristic of other functionalized phenolic compounds. Reduction assays with benzoic acid and 4-amino-2-hydroxybenzoic acid suggest that the carboxyl group was not required for iron reduction and that the stabilization of the semiquinone in adjacent hydroxyl (or mixed functional) groups was advantageous for the reduction of iron (drastically reduced in 4-amino-2-hydroxybenzoic acid).

The beneficial effect of HCO_3^- on the reduction of iron has not been postulated before. Remarkably, the iron reduction capacity of all aromatic compounds was enhanced in the presence of HCO_3^- , although iron reduction in the presence of HCO_3^- alone was negligible. The promoting effect of HCO_3^- on iron reduction was apparently related to the complex formation between Fe^{3+} and chelates, as exemplarily shown for PCA. Since we could not clarify the precise mechanism of interaction, one could assume that H^+ and OH^- concentrations were the reason for the λ_{max} shift in analogy with an overall alteration of the absorbance due to the formation of $\text{Fe}(\text{OH})$ -PCA complexes (19). However, we carefully performed pH buffering and control experiments in order to rule out this possibility. The sample pH was not varied in our experiments by the addition of NaHCO_3 , and intentionally changing the pH failed to reproduce a comparable λ_{max} shift. It might be further speculated that HCO_3^- enhances the iron accessibility to PCA in the form of ferric bicarbonate, since the initial complex formation rate was accelerated by 46%.

Although the presence of HCO_3^- alone had no effect on the reduction of iron *in vitro*, the growth-promoting effect of $\text{CO}_2/\text{HCO}_3^-$ correlated with increased intracellular Fe^{2+} levels reported *in vivo*. We conclude that the growth-promoting effect of $\text{CO}_2/\text{HCO}_3^-$ requires the natural production of suitable reductants by *C. glutamicum*. Surprisingly, PCA production in *C. glutamicum* does not appear to be regulated in response to iron availability, unlike other organisms (16). The expression of *qsuB* encoding the dehydroshikimate dehydratase that catalyzes the conversion of 3-dehydroshikimate to PCA is controlled by QsuR in *C. glutamicum* and provides a shunt when chorismate accumulates (48, 49). The question of major iron reductants produced by *C. glutamicum* must be addressed in future research.

There is continuous debate about the redox reaction in Fe^{3+} -catecholate complexes and its interpretation as antioxidant or prooxidant, since contradictory observations have been published (20, 50). It must be noted that the experimental setup is essentially decisive for the outcome. Many studies emphasized the antioxidant effect of PCA and other catecholates in the past (20). Fe^{2+} generation was monitored, e.g., by lipid oxidation experiments, which in contrast to BPS detection, do not exhibit high affinity for Fe^{2+} . As a consequence, observations might differ from ours. The detection of Fe^{2+} with BPS in this study might have been beneficial for two reasons. (i) Fe^{2+} and BPS form a stable complex, thus preventing Fe^{2+} from reoxidation. (ii) Capturing Fe^{2+} in the complex constantly shifts the chemical equilibrium in favor of reduction. Thus, our *in vitro* screening system might be well suited for representing a biological context, considering the high Fe^{2+} affinity of iron processing enzymes, e.g., *Escherichia coli* IscA (the first enzyme of the iron sulfur cluster assembly machinery, $K_D = 3.3 \times 10^{-20}$ to 5×10^{-20} M) (51, 52). Dissociation constants between iron and human transferrin (53) have been determined in a very similar range (2.1×10^{-21} and 4.2×10^{-20} M). However, the most obvious support of these hypothetical considerations is provided by the consistency of the results of *in vitro* and *in vivo* experiments in this study.

mbo-mbio/mbo00120/mbo5125d20z xppws S=5 2/12/20 10:48 ArtID: DOI:10.1128/mBio.00085-20 CE: CB

CO₂/HCO₃⁻ Accelerates Chemical Iron Reduction

Given the predominance of Fe³⁺ in an oxygenic environment, the abiotic acceleration of iron reduction through HCO₃⁻ is of global importance. The two prerequisites—the presence of functional aromatic compounds on one hand and high HCO₃⁻ concentrations on the other hand—combine in a number of habitats. Aromatic compounds are ubiquitous in cellular metabolism, and plant-derived catecholic compounds can be released, e.g., in soils during biomass degradation or reach high concentrations in human plasma shortly after ingestion (20). A number of stress hormones and neurotransmitters, including dopamine, adrenaline, and norepinephrine, contain a functional catechol group and exhibit interesting features with regard to the iron homeostasis. The stimulating role of catecholamine on growth of a number of pathogenic bacteria in iron-restricted growth media containing serum, transferrin, or lactoferrin has been reported (54–58). Pathogens possess an outstanding role within the inhabitants of the human body as they encounter a constant battle for iron, the majority of which is sequestered in host transferrin and lactoferrin (35). Several studies demonstrated that catecholamines or dietary catechols can liberate iron from transferrin and lactoferrin (55, 59, 60) and might even reduce Fe³⁺ by promoting bacterial growth (61). The greater availability of liberated Fe³⁺ and Fe²⁺ resulting from this mechanism might be further increased at the high concentrations of CO₂ species typically found in calcareous soils, but also in the human body, where HCO₃⁻ concentrations can reach up to 140 mM (22). Considering the HCO₃⁻ interaction with iron reduction demonstrated in this study thus might be of particular interest in understanding pathogenicity. Of the currently most threatening human pathogens, *Pseudomonas aeruginosa*, *Staphylococcus aureus*, *Klebsiella pneumoniae*, *Mycobacterium tuberculosis*, and pathogenic *Escherichia coli* strains as well as several other pathogenic bacteria regulate toxin expression on the transcriptional level in response to iron availability (33, 62–64).

In summary, we show that high CO₂/HCO₃⁻ concentrations accelerate the chemical reduction of Fe³⁺ through various phenolic compounds. This increases the intracellular Fe²⁺ availability and stimulates growth of *C. glutamicum*.

MATERIALS AND METHODS

Genetic manipulation, cloning, and strain construction. Standard techniques of molecular biology were applied in accordance with the literature (65). Kits for purification of plasmids and PCR products and for isolation of genomic DNA were used according to Lange et al. (66). Cloning of plasmids and construction of *C. glutamicum* integration and deletion mutants have been performed as described in detail previously (66). All cloned fragments were verified by Sanger sequencing (GATC, Constance, Germany).

C. glutamicum FEM3 was composed of the chromosomally integrated sensor part and a replicative plasmid carrying the reporter gene. Expression of *lacI* was placed under the control of the DtxR-regulated promoter of the *ripA* gene (*P_{ripA}*), followed by the strong *rrnB* terminator (*T_{rrnB}*). Chromosomal integration of the cassette in *C. glutamicum* was targeted to CgLP13 (between *cg3344* and *cg3345*) by two 500-bp homologous sequences (66). *C. glutamicum* endogenous elements (500-bp flanks, *P_{ripA}*) were amplified from genomic DNA using the primer pairs 5' (cg3344)-1 plus 5' (cg3344)-2, 3' (cg3344)-1 plus 3' (cg3344)-2, and PripA-1 plus PripA-2, respectively, and exogenous elements (*lacI*, *T_{rrnB}*) were amplified from plasmid pJOE7706.1 (67) with *lacI*-1 plus *lacI*-2 and *TrrnB*-1 plus *TrrnB*-2, respectively. All PCR amplification products were simultaneously inserted into BamHI- and NheI-linearized pK19*mobsacB* (68) by isothermal assembling (69). The *egfp* gene under the control of the strong hybrid promoter *P_{tac}* and *T_{rrnB}* was amplified from pJOE7706.1 with primer pairs *P_{tac}*-1 plus *P_{tac}*-2 and *egfp*-1 plus *egfp*-2, respectively, and inserted into XbaI- and NotI-linearized pJC4 plasmid (70) in the same way.

For markerless deletions of the genes *pup* (*cg1689*), *ftn* (*cg2782*), and *dps* (*cg3327*) in *C. glutamicum*, 500-bp homologous sequences flanking the target gene were amplified with the respective primer pair (see Table S1 in the supplemental material) and simultaneously inserted in BamHI- and HindIII-linearized pK19*mobsacB* as described before.

For purification of the DtxR regulator protein, the *dtxR* gene was amplified from the *C. glutamicum* chromosomal DNA via PCR using the primer pair *dtxR*-1 and *dtxR*-2 and cloned into pJOE6089.4 by restriction and ligation using the NdeI and BamHI restriction sites. Competent *E. coli* DH5α was transformed with the resulting plasmid pJOE6089-*dtxR* carrying a C-terminal *Strep*-tag II fused to the *dtxR* gene by electroporation (66).

Bacterial strains and cultivation conditions. An overview of all bacterial strains and plasmids used in this work is given in Table S2. Permanent cultures were maintained at -70°C in 30% (vol/vol) glycerol. *C. glutamicum* strains were cultivated at 30°C on a rotary shaker in baffled shaking flasks (500 ml filled with 50 ml medium, 120 rpm). Kanamycin was added at a working concentration of 50 μg ml⁻¹ when appropriate.

January/February 2020 Volume 11 Issue 1 e00085-20

mbio.asm.org 9

mbo-mbio/mbo00120/mbo5125d20z xppws S=5 2/12/20 10:48 ArtID: DOI:10.1128/mBio.00085-20 CE: CB

Müller et al.



Permanent cultures were streaked on 2× yeast tryptone (2× YT) (65) agar (18 g liter⁻¹) plates and grown for 2 days. Liquid cultures (5 ml of 2× YT) were inoculated from the plate, grown overnight (O/N), and used to inoculate a 50-ml 2× YT culture, which was incubated for another 6 to 8 h. An appropriate volume of the complex preculture was harvested and resuspended in 2 ml of 0.9% (wt/vol) NaCl to inoculate a CgXII preculture to a starting optical density at 600 nm (OD₆₀₀) of 1. The main cultures were inoculated in the same way from the CgXII O/N culture and incubated for at least 25 h.

Shaking flask cultivation. *C. glutamicum* cultivations were performed in CgXII medium (pH 7.4) containing 20 g glucose liter⁻¹ supplemented with protocatechuic acid (PCA) to a final concentration of 195 μM (10) or with 30 mM NaHCO₃ or not supplemented (71) as indicated. Since slight variations occurred in the past, the exact composition of the CgXII medium used in this study is outlined in Lange et al. (66). The functionality of the reporter strain *C. glutamicum* FEM3 was validated under iron starvation (1 μM FeSO₄) and iron excess (100 μM FeSO₄) conditions in the presence of 195 μM PCA and starting from identical precultures as described before (32). Iron-depleted growth medium was prepared with a trace element solution lacking the iron source (FeSO₄), and the ferrous iron chelator 2,2-dipyridyl was added at a final concentration of 250 μM immediately before inoculation to remove any residual iron from the medium (42). Precultures were performed in iron excess conditions (100 μM FeSO₄, instead of the usual 59 μM FeSO₄).

Bioreactor cultivation. Bioreactor cultivations were performed in batch mode in 1.5-liter stainless steel bioreactors (30) with a starting volume of 800 ml CgXII medium containing 40 g glucose liter⁻¹ as the sole carbon and energy source but lacking 3-(*N*-morpholino)propanesulfonic acid (MOPS) buffer and urea. The cultivation pH was maintained at pH 7.4 by the addition of 25% ammonium hydroxide. Two parallel fermentations were always inoculated from identical precultures to a starting OD₆₀₀ of 2. Both reactors were operated at a total pressure of 1.5 bar and contained two six-blade Rushton-type impellers. The stirrer speed started at 300 rpm and was gradually increased to maintain the dissolved oxygen concentration above 35%. Reactor 1 was aerated with 0.5 vvm (volume of gas per volume of liquid per minute) pressurized air (0.04% CO₂), and reactor 2 was aerated with synthetically mixed gas containing 20% CO₂, 21% O₂, and 59% N₂ (20% CO₂).

Biomass formation. Cell density was determined by measuring the optical density of a culture at 600 nm (OD₆₀₀). Biomass concentration (cell weight [dry weight] [CDW] in grams liter⁻¹) was calculated from it using the correlation coefficient CDW = 0.21 × OD₆₀₀ (72) specific for the spectrophotometer (Ultrospec 10 cell density meter; GE Healthcare, Little Chalfont, UK).

Fluorescence readings. Fluorescence (relative fluorescence units [RFU]) was detected in 100-μl samples of the pure culture using 96-well microtiter plates in the Synergy 2 device (BioTek Instruments, Bad Friedrichshall, Germany) at 37°C (excitation wavelength/bandwidth, 485/20 nm; emission wavelength/bandwidth 528/20 nm) as described before (73). The culture background (after removing cells by centrifugation, 13,300 rpm, 1 min) was subtracted from the sample value and normalized with respect to the biomass concentration (RFU CDW⁻¹).

LC-MS-QTOF. PCA degradation was detected by a relative decrease of the respective peak area via liquid chromatography-quadrupole time of flight mass spectrometry (LC-MS-QTOF). Samples (1-ml samples) containing 0.5 mM FeCl₃ (from a stock in 10 mM HCl) were prepared in 1.5-ml Eppendorf cups. Samples were neutralized with 50 mM NaOH and 19.5 μM PCA, and 6.5 mM BPS and 50 mM NaHCO₃ were added when appropriate. At the indicated time points, 200-μl samples were transferred to fresh 1.5-ml Eppendorf cups and stored frozen at -20°C until further processing. After thawing, samples or respective standards were prepared in 60% (vol/vol) acetonitrile, 0.75 mM EDTA, and 10 mM ammonium acetate buffer (adjusted to pH 9.2) and analyzed by an Agilent 1260 bio-inert high high-performance liquid chromatography (HPLC) system (Agilent Technologies, Waldbronn, Germany) coupled to an Agilent 6540 accurate-mass QTOF (Agilent Technologies, Santa Clara, CA, USA). Alkaline hydrophilic interaction liquid chromatography (HILIC) (74) and QTOF-MS (75) parameters were set as previously described, and analysis was conducted in the negative mode with a fragmentor voltage of 100 V in the MS mode. The extraction of chromatograms and integration were done in MassHunter Qualitative Analysis with the "Find by Formula" algorithm. Potential oxidation products were identified via the molecular formula calculator feature based on the accurate mass, isotope abundances, and isotope spacing (B.07.00, Agilent Technologies, Santa Clara, CA, USA).

Iron reduction assays. The kinetics of Fe³⁺ reduction was monitored by an increase of the absorbance at 534 nm due to complex formation with the Fe²⁺-specific chelator bathophenanthroline disulfonic acid (BPS) (76, 77) in 96-well microtiter plates containing 100 μl of sample. The iron reduction assay was performed in 200 mM MOPS buffer (pH 7.4). 0.5 mM FeCl₃ was added from a stock in 10 mM HCl neutralized with 50 mM NaOH immediately before use. 19.5 μM PCA, other benzoic acid derivatives, or 50 mM NaHCO₃ was applied as indicated. The reaction was started by the addition of 6.5 mM BPS and measured every 10 min.

Fe³⁺-PCA complex formation. Complex formation between Fe³⁺ and PCA was monitored in a setup identical to the setup used in the iron reduction assay but in the absence of Fe²⁺-specific BPS. The Fe³⁺-PCA complex formation assay was started by the addition of 1.5 mM PCA to provide it in a 3:1 stoichiometry with iron. Fe³⁺-catecholate complexes show characteristic λ_{max} values between 561 and 586 nm (20), and for Fe³⁺-PCA, 575 nm was reported as λ_{max} (19). Wavelength scans of the complexes were performed with 100-μl samples in 96-well plates (1-nm step size) after 5 h of incubation. Since the absorbance peaked around 560 nm in the standard setup (see Fig. S5 in the supplemental material), kinetic measurements of complex formation was performed in the following every 5 min at 560 nm in the same setup.

AQ: B

mbo-mbio/mbo00120/mbo5125d20z xppws S=5 2/12/20 10:48 ArtID: DOI:10.1128/mBio.00085-20 CE: CB

CO₂/HCO₃⁻ Accelerates Chemical Iron Reduction

Purification of DtxR. For the production of DtxR protein, a cryogenic culture of *E. coli* DH5 α (pJ0E6089-*dtxR*) was streaked on a 2 \times YT agar plate containing 100 μ g ampicillin (Amp¹⁰⁰) ml⁻¹ and incubated for 24 h at 37°C. A single cell was used to inoculate 5 ml of 2 \times YT (Amp¹⁰⁰) which was incubated overnight (O/N) at 37°C on a rotary shaker at 120 rpm before 1.5 ml of this culture was transferred to fresh 150 ml of 2 \times YT (Amp¹⁰⁰) medium in a 1-liter baffled shaking flask. This culture was incubated at 37°C on a rotary shaker at 120 rpm until an OD₆₀₀ of 0.84 was reached. The expression of *dtxR* was induced by the addition of L-rhamnose to a final concentration of 2 g liter⁻¹, and incubation continued for 6 h at 30°C before the cells were harvested by centrifugation (10 min, 5,000 rpm at 4°C in an Eppendorf centrifuge 5804 R). The cell pellets were stored frozen at -20°C until further processing.

Strep-tagged protein was purified with the Strep-tagged protein purification kit (Qiagen, Hilden, Germany) after lysing cells by sonication (five cycles, Sonopuls HD2200, Bandelin, Berlin, Germany; tip type MS73, 30 s, power 40%).

Thermal shift assay. Differential scanning fluorimetry experiments were performed in a final sample volume of 50 μ l in 96-well plates using the Mastercycler EP Realplex² (epgradient S; Eppendorf, Hamburg, Germany). Briefly, at a gradually increasing temperature, protein denaturation is monitored by an increase of the fluorescence which is caused by the binding of a dye that successively presents hydrophobic areas of the protein (78). Ligand binding might increase the protein stability. Thermal protein denaturation was monitored by an increase of the absorbance at 550 nm due to binding of SYPRO Orange (Thermo Fisher Scientific Inc., Bremen, Germany).

Protein samples (50 μ g ml⁻¹) were prepared in 100 mM potassium phosphate buffer (pH 7.4) containing 600 mM NaCl and 5 mM dithiothreitol (DTT). Divalent metal ions were applied at various concentrations (0.1 μ M to 1 mM NiCl₂ or 0.1 μ M to 5 mM MnCl₂). When 10 to 200 mM NaHCO₃ was added to the sample, osmolarity was maintained at an identical level by adjusting the NaCl concentration. One microliter of SYPRO Orange was added to each sample immediately before starting the assay. Then, the 96-well microtiter plate was sealed with adhesive foil and incubated in the mastercycler (20°C for 15 s, 20°C to 90°C in 30 min, 90°C for 15 s). The range of the greatest absorbance increase over temperature was fitted by a fourth order polynomial (best fit), and the melting temperature (T_m) was determined at the inflection point. The T_m at a given ligand concentration eventually represents the mean value \pm standard deviation for at least four replicates. Dissociation constants (K_D) were calculated for the inflection point of the T_m on the ligand concentration curve (79).

Statistical analysis. All growth experiments were performed as independent biological triplicates on different days. (Bio)chemical assays were replicated 4 to 6 times, and LC-MS-QTOF analysis was performed on the three biological replicate samples. All values represent mean values with error bars indicating standard deviations. When appropriate, statistically significant differences of sample means were tested with a two-sample t test.

SUPPLEMENTAL MATERIAL

Supplemental material is available online only.

FIG S1, EPS file, 0.2 MB.

FIG S2, EPS file, 0.2 MB.

FIG S3, EPS file, 0.2 MB.

FIG S4, EPS file, 0.2 MB.

FIG S5, EPS file, 0.2 MB.

TABLE S1, DOCX file, 0.01 MB.

TABLE S2, DOCX file, 0.02 MB.

ACKNOWLEDGMENTS

This work was funded by the Deutsche Forschungsgemeinschaft (grant TA241/5-2).

We thank Michael Bott for kindly providing the deletion plasmid pK19*mobsacB-Δpup*. We thank Herbert Riepl (Organic-Analytical Chemistry, Weihenstephan-Triesdorf University of Applied Sciences, Technical University of Munich, Campus Straubing), Stephan Hammer, Bettina Nestl, and Bernd Nebel (Department of Technical Biochemistry, University of Stuttgart) for discussions of chemical aspects of this work.

F.M., R.T., and B.B. conceived and designed the experiments. F.M., J.R., A.-L.H., and A.F. performed the experiments. F.M., J.R., A.-L.H., A.F., and B.B. analyzed the data. F.M. and B.B. wrote the manuscript.

REFERENCES

1. Proulx-Curry PM, Chasteen ND. 1995. Molecular aspects of iron uptake and storage in ferritin. *Coord Chem Rev* 144:347–368. [https://doi.org/10.1016/0010-8545\(95\)01148-1](https://doi.org/10.1016/0010-8545(95)01148-1).
2. Andrews SC, Robinson AK, Rodriguez-Quinones F. 2003. Bacterial iron homeostasis. *FEMS Microbiol Rev* 27:215–237. [https://doi.org/10.1016/S0168-6445\(03\)00055-X](https://doi.org/10.1016/S0168-6445(03)00055-X).
3. Neilands JB. 1981. Microbial iron compounds. *Annu Rev Biochem* 50: 715–731. <https://doi.org/10.1146/annurev.bi.50.070181.003435>.
4. Schröder I, Johnson E, De Vries S. 2003. Microbial ferric iron reductases. *FEMS Microbiol Rev* 27:427–447. [https://doi.org/10.1016/S0168-6445\(03\)00043-3](https://doi.org/10.1016/S0168-6445(03)00043-3).
5. Light SH, Su L, Rivera-Lugo R, Cornejo JA, Louie A, Iavarone AT, Ajo-

mbo-mbio/mbo00120/mbo5125d20z xppws S=5 2/12/20 10:48 ArtID: DOI:10.1128/mBio.00085-20 CE: CB

Müller et al.



- Franklin CM, Portnoy DA. 2018. A flavin-based extracellular electron transfer mechanism in diverse Gram-positive bacteria. *Nature* 562: 140–157. <https://doi.org/10.1038/s41586-018-0498-z>.
6. Kalinowski J, Bathe B, Bartels D, Bischoff N, Bott M, Burkovski A, Dusch N, Eggeling L, Eikmanns BJ, Gaigalat L, Goesmann A, Hartmann M, Huthmacher K, Krämer R, Linke B, McHardy AC, Meyer F, Möckel B, Pfeufferle W, Pühler A, Rey DA, Rückert C, Rupp O, Sahn H, Wendisch VF, Wiegräbe I, Tauch A. 2003. The complete *Corynebacterium glutamicum* ATCC 13032 genome sequence and its impact on the production of L-aspartate-derived amino acids and vitamins. *J Biotechnol* 104:5–25. [https://doi.org/10.1016/s0168-1656\(03\)00154-8](https://doi.org/10.1016/s0168-1656(03)00154-8).
 7. Frunzke J, Bott M. 2008. Regulation of iron homeostasis in *Corynebacterium glutamicum*, p 241–266. In Burkovski A (ed), *Corynebacteria: genomics and molecular biology*. Horizon Scientific Press, Norwich, United Kingdom.
 8. von der Osten CH, Giannetti C, Sinskey AJ. 1989. Design of a defined medium for growth of *Corynebacterium glutamicum* in which citrate facilitates iron uptake. *Biotechnol Lett* 11:11–16. <https://doi.org/10.1007/BF01026778>.
 9. Liebl W, Klamer R, Schleifer K-H. 1989. Requirement of chelating compounds for the growth of *Corynebacterium glutamicum* in synthetic media. *Appl Microbiol Biotechnol* 32:205–210. <https://doi.org/10.1007/BF00165889>.
 10. Keilhauer C, Eggeling L, Sahn H. 1993. Isoleucine synthesis in *Corynebacterium glutamicum*: molecular analysis of the *ilvB-ilvN-ilvC* operon. *J Bacteriol* 175:5595–5603. <https://doi.org/10.1128/jb.175.17.5595-5603.1993>.
 11. Kübel A, Polen T, Bott M. 2016. The pupylation machinery is involved in iron homeostasis by targeting the iron storage protein ferritin. *Proc Natl Acad Sci U S A* 113:4806–4811. <https://doi.org/10.1073/pnas.1514529113>.
 12. Peters WJ, Warren RA. 1968. Itoic acid synthesis in *Bacillus subtilis*. *J Bacteriol* 95:360–366. <https://doi.org/10.1128/JB.95.2.360-366.1968>.
 13. Tait GH. 1975. The identification and biosynthesis of siderochromes formed by *Micrococcus denitrificans*. *Biochem J* 146:191–204. <https://doi.org/10.1042/bj1460191>.
 14. Peters WJ, Warren R. 1968. Phenolic acids and iron transport in *Bacillus subtilis*. *Biochim Biophys Acta* 165:225–232. [https://doi.org/10.1016/0304-4165\(68\)90050-0](https://doi.org/10.1016/0304-4165(68)90050-0).
 15. Barbeau K, Zhang G, Live DH, Butler A. 2002. Petrobactin, a photoreactive siderophore produced by the oil-degrading marine bacterium *Marinobacter hydrocarbonoclasticus*. *J Am Chem Soc* 124:378–379. <https://doi.org/10.1021/ja0119088>.
 16. Garner BL, Arceneaux JEL, Byers BR. 2004. Temperature control of a 3,4-dihydroxybenzoate (protocatechuate)-based siderophore in *Bacillus anthracis*. *Curr Microbiol* 49:89–94. <https://doi.org/10.1007/s00284-004-4286-7>.
 17. Ratledge C, Chaudhry MA. 1971. Accumulation of iron-binding phenolic acids by Actinomycetales and other organisms related to the Mycobacteria. *J Gen Microbiol* 66:71–78. <https://doi.org/10.1099/00221287-66-1-71>.
 18. Zawadzka AM, Abergel RJ, Nichiporuk R, Andersen UN, Raymond KN. 2009. Siderophore-mediated iron acquisition systems in *Bacillus cereus*: identification of receptors for anthrax virulence-associated petrobactin. *Biochemistry* 48:3645–3657. <https://doi.org/10.1021/bi8018674>.
 19. Kennedy JA, Powell J. 1985. Aluminium(III) and iron(III) 1,2-diphenolato complexes: a potentiometric study. *Aust J Chem* 38:659–667. <https://doi.org/10.1071/CH9850659>.
 20. Perron NR, Brumaghim JL. 2009. A review of the antioxidant mechanisms of polyphenol compounds related to iron binding. *Cell Biochem Biophys* 53:75–100. <https://doi.org/10.1007/s12013-009-9043-x>.
 21. Avdeef A, Sofen SR, Bregante TL, Raymond KN. 1978. Coordination chemistry of microbial iron transport compounds. 9. Stability constants for catechol models of enterobactin. *J Am Chem Soc* 100:5362–5370. <https://doi.org/10.1021/ja00485a018>.
 22. Blombach B, Takors R. 2015. CO₂ – intrinsic product, essential substrate, and regulatory trigger of microbial and mammalian production processes. *Front Bioeng Biotechnol* 3:108. <https://doi.org/10.3389/fbioe.2015.00108>.
 23. Cummins EP, Selfridge AC, Sporn PH, Sznajder J, Taylor CT. 2014. Carbon dioxide-sensing in natural systems and its implications for human disease. *Cell Mol Life Sci* 71:831–845. <https://doi.org/10.1007/s00018-013-1470-6>.
 24. Lopes M, Belo I, Mota M. 2014. Over-pressurized bioreactors: application to microbial cell cultures. *Biotechnol Prog* 30:767–775. <https://doi.org/10.1002/btpr.1917>.
 25. Yu T, Chen Y. 2019. Effects of elevated carbon dioxide on environmental microbes and its mechanisms: a review. *Sci Total Environ* 655:865–879. <https://doi.org/10.1016/j.scitotenv.2018.11.301>.
 26. Ueda K, Tagami Y, Kamihara Y, Shiratori H, Takano H, Beppu T. 2008. Isolation of bacteria whose growth is dependent on high levels of CO₂ and implications of their potential diversity. *Appl Environ Microbiol* 74:4535–4538. <https://doi.org/10.1128/AEM.00491-08>.
 27. Sauer U, Eikmanns BJ. 2005. The PEP-pyruvate-oxaloacetate node as the switch point for carbon flux distribution in bacteria. *FEMS Microbiol Rev* 29:765–794. <https://doi.org/10.1016/j.femsre.2004.11.002>.
 28. Inui M, Murakami S, Okino S, Kawaguchi H, Vertés AA, Yukawa H. 2004. Metabolic analysis of *Corynebacterium glutamicum* during lactate and succinate productions under oxygen deprivation conditions. *J Mol Microbiol Biotechnol* 7:182–196. <https://doi.org/10.1159/000079827>.
 29. Okino S, Noburyu R, Suda M, Jojima T, Inui M, Yukawa H. 2008. An efficient succinic acid production process in a metabolically engineered *Corynebacterium glutamicum* strain. *Appl Microbiol Biotechnol* 81: 459–464. <https://doi.org/10.1007/s00253-008-1668-y>.
 30. Blombach B, Buchholz J, Busche T, Kalinowski J, Takors R. 2013. Impact of different CO₂/HCO₃⁻ levels on metabolism and regulation in *Corynebacterium glutamicum*. *J Biotechnol* 168:331–340. <https://doi.org/10.1016/j.jbiotec.2013.10.005>.
 31. Michel A, Koch-Koerfges A, Krumbach K, Brocker M, Bott M. 2015. Anaerobic growth of *Corynebacterium glutamicum* via mixed-acid fermentation. *Appl Environ Microbiol* 81:7496–7508. <https://doi.org/10.1128/AEM.02413-15>.
 32. Wennerhold J, Bott M. 2006. The DtxR regulon of *Corynebacterium glutamicum*. *J Bacteriol* 188:2907–2918. <https://doi.org/10.1128/JB.188.8.2907-2918.2006>.
 33. Litwin CM, Calderwood SB. 1993. Role of iron in regulation of virulence genes. *Clin Microbiol Rev* 6:137–149. <https://doi.org/10.1128/cmr.6.2.137>.
 34. Mekalanos JJ. 1992. Environmental signals controlling expression of virulence determinants in bacteria. *J Bacteriol* 174:1–7. <https://doi.org/10.1128/jb.174.1.1-7.1992>.
 35. Wilson BR, Bogdan AR, Miyazawa M, Hashimoto K, Tsuji Y. 2016. Siderophores in iron metabolism: from mechanism to therapy potential. *Trends Mol Med* 22:1077–1090. <https://doi.org/10.1016/j.molmed.2016.10.005>.
 36. D'Aquino JA, Denninger AR, Moulin AG, D'Aquino KE, Ringe D. 2009. Decreased sensitivity to changes in the concentration of metal ions as the basis for the hyperactivity of DtxR(E175K). *J Mol Biol* 390:112–123. <https://doi.org/10.1016/j.jmb.2009.05.003>.
 37. Qiu X, Verlinde CL, Zhang S, Schmitt MP, Holmes RK, Hol WG. 1995. Three-dimensional structure of the diphtheria toxin repressor in complex with divalent cation co-repressors. *Structure* 3:87–100. [https://doi.org/10.1016/s0969-2126\(01\)00137-x](https://doi.org/10.1016/s0969-2126(01)00137-x).
 38. Qiu X, Pohl E, Holmes RK, Hol W. 1996. High-resolution structure of the diphtheria toxin repressor complexed with cobalt and manganese reveals an SH3-like third domain and suggests a possible role of phosphate as co-repressor. *Biochemistry* 35:12292–12302. <https://doi.org/10.1021/bi960861d>.
 39. Goranson-Siekierke J, Pohl E, Hol WGJ, Holmes RK. 1999. Anion-coordinating residues at binding site 1 are essential for the biological activity of the diphtheria toxin repressor. *Infect Immun* 67:1806–1811.
 40. Unthan S, Grünberger A, van Ooyen J, Gätgens J, Heinrich J, Paczia N, Wiechert W, Kohlheyer D, Noack S. 2014. Beyond growth rate 0.6: what drives *Corynebacterium glutamicum* to higher growth rates in defined medium. *Biotechnol Bioeng* 111:359–371. <https://doi.org/10.1002/bit.25103>.
 41. Grünberger A, van Ooyen J, Paczia N, Rohe P, Schiendzielorz G, Eggeling L, Wiechert W, Kohlheyer D, Noack S. 2013. Beyond growth rate 0.6: *Corynebacterium glutamicum* cultivated in highly diluted environments. *Biotechnol Bioeng* 110:220–228. <https://doi.org/10.1002/bit.24616>.
 42. Frunzke J, Gätgens C, Brocker M, Bott M. 2011. Control of heme homeostasis in *Corynebacterium glutamicum* by the two-component system HrrSA. *J Bacteriol* 193:1212–1221. <https://doi.org/10.1128/JB.01130-10>.
 43. Davison W, Seed G. 1983. The kinetics of the oxidation of ferrous iron in synthetic and natural waters. *Geochim Cosmochim Acta* 47:67–79. [https://doi.org/10.1016/0016-7037\(83\)90091-1](https://doi.org/10.1016/0016-7037(83)90091-1).
 44. Morgan LR. 1962. Oxidation of protocatechuic acid with peroxyacetic acid. *J Org Chem* 27:1208–1210. <https://doi.org/10.1021/jo10151a020>.

January/February 2020 Volume 11 Issue 1 e00085-20

mbio.asm.org 12

mbo-mbio/mbo00120/mbo5125d20z xppws S=5 2/12/20 10:48 ArtID: DOI:10.1128/mBio.00085-20 CE: CB

CO₂/HCO₃⁻ Accelerates Chemical Iron Reduction

45. Shen XH, Zhou NY, Liu SJ. 2012. Degradation and assimilation of aromatic compounds by *Corynebacterium glutamicum*: another potential for applications for this bacterium? *Appl Microbiol Biotechnol* 95:77–89. <https://doi.org/10.1007/s00253-012-4139-4>.
46. Boyer RF, Clark HM, LaRoche AP. 1988. Reduction and release of ferritin iron by plant phenolics. *J Inorg Biochem* 32:171–181. [https://doi.org/10.1016/0162-0134\(88\)80025-4](https://doi.org/10.1016/0162-0134(88)80025-4).
47. Nyhus KJ, Wilborn AT, Jacobson ES. 1997. Ferric iron reduction by *Cryptococcus neoformans*. *Infect Immun* 65:434–438. <https://doi.org/10.1128/IAI.65.2.434-438.1997>.
48. Teramoto H, Inui M, Yukawa H. 2009. Regulation of expression of genes involved in quinate and shikimate utilization in *Corynebacterium glutamicum*. *Appl Environ Microbiol* 75:3461–3468. <https://doi.org/10.1128/AEM.00163-09>.
49. Kubota T, Tanaka Y, Takemoto N, Watanabe A, Hiraga K, Inui M, Yukawa H. 2014. Chorismate-dependent transcriptional regulation of quinate/shikimate utilization genes by LysR-type transcriptional regulator QsuR in *Corynebacterium glutamicum*: carbon flow control at metabolic branch point. *Mol Microbiol* 92:356–368. <https://doi.org/10.1111/mmi.12560>.
50. Schweigert N, Zehnder AJB, Eggen R. 2001. Chemical properties of catechols and their molecular modes of toxic action in cells, from microorganisms to mammals. *Environ Microbiol* 3:81–91. <https://doi.org/10.1046/j.1462-2920.2001.00176.x>.
51. Ding H, Clark RJ. 2004. Characterization of iron binding in IscA, an ancient iron-sulphur cluster assembly protein. *Biochem J* 379:433–440. <https://doi.org/10.1042/BJ20031702>.
52. Ding H, Harrison K, Lu J. 2005. Thioredoxin reductase system mediates iron binding in IscA and iron delivery for the iron-sulfur cluster assembly in IscU. *J Biol Chem* 280:30432–30437. <https://doi.org/10.1074/jbc.M504638200>.
53. Aisen P, Leibman A, Zweier J. 1978. Stoichiometric and site characteristics of the binding of iron to human transferrin. *J Biol Chem* 253:1930–1937.
54. Burton CL, Chhabra SR, Swift S, Baldwin TJ, Withers H, Hill SJ, Williams P. 2002. The growth response of *Escherichia coli* to neurotransmitters and related catecholamine drugs requires a functional enterobactin biosynthesis and uptake system. *Infect Immun* 70:5913–5923. <https://doi.org/10.1128/iai.70.11.5913-5923.2002>.
55. Freestone PPE, Haigh RD, Williams PH, Lyte M. 2003. Involvement of enterobactin in norepinephrine-mediated iron supply from transferrin to enterohaemorrhagic *Escherichia coli*. *FEMS Microbiol Lett* 222:39–43. [https://doi.org/10.1016/S0378-1097\(03\)00243-X](https://doi.org/10.1016/S0378-1097(03)00243-X).
56. Anderson MT, Armstrong SK. 2008. Norepinephrine mediates acquisition of transferrin-iron in *Bordetella bronchiseptica*. *J Bacteriol* 190:3940–3947. <https://doi.org/10.1128/JB.00086-08>.
57. Coulanges V, Andre P, Vidon D. 1998. Effect of siderophores, catecholamines, and catechol compounds on *Listeria* spp. growth in iron-complexed medium. *Biochem Biophys Res Commun* 249:526–530. <https://doi.org/10.1006/bbrc.1998.9184>.
58. Lyte M, Ernst S. 1992. Catecholamine induced growth of Gram negative bacteria. *Life Sci* 50:203–212. [https://doi.org/10.1016/0024-3205\(92\)90273-r](https://doi.org/10.1016/0024-3205(92)90273-r).
59. Freestone PPE, Lyte M, Neal CP, Maggs AF, Haigh RD, Williams PH. 2000. The mammalian neuroendocrine hormone norepinephrine supplies iron for bacterial growth in the presence of transferrin or lactoferrin. *J Bacteriol* 182:6091–6098. <https://doi.org/10.1128/jb.182.21.6091-6098.2000>.
60. Freestone PPE, Walton NJ, Haigh RD, Lyte M. 2007. Influence of dietary catechols on the growth of enteropathogenic bacteria. *Int J Food Microbiol* 119:159–169. <https://doi.org/10.1016/j.jifoodmicro.2007.07.039>.
61. Sandrini SM, Shergill R, Woodward J, Muralikuttan R, Haigh RD, Lyte M, Freestone PP. 2010. Elucidation of the mechanism by which catecholamine stress hormones liberate iron from the innate immune defense proteins transferrin and lactoferrin. *J Bacteriol* 192:587–594. <https://doi.org/10.1128/JB.01028-09>.
62. Torres VJ, Attia AS, Mason WJ, Hood MI, Corbin BD, Beasley FC, Anderson KL, Stauff DL, McDonald WH, Zimmerman LJ, Friedman DB, Heinrichs DE, Dunman PM, Skaar EP. 2010. *Staphylococcus aureus* Fur regulates the expression of virulence factors that contribute to the pathogenesis of pneumonia. *Infect Immun* 78:1618–1628. <https://doi.org/10.1128/IAI.01423-09>.
63. Lin CT, Wu CC, Chen YS, Lai YC, Chi C, Lin JC, Chen Y, Peng HL. 2011. Fur regulation of the capsular polysaccharide biosynthesis and iron-acquisition systems in *Klebsiella pneumoniae* CG43. *Microbiology* 157:419–429. <https://doi.org/10.1099/mic.0.044065-0>.
64. Zondervan NA, Van Dam JCJ, Schaap PJ, Martins Dos Santos VAP, Suarez-Diez M. 2018. Regulation of three virulence strategies of *Mycobacterium tuberculosis*: a success story. *Int J Mol Sci* 19:E347. <https://doi.org/10.3390/ijms19020347>.
65. Sambrook J, Russell RW. 2001. *Molecular cloning: a laboratory manual*, 3rd ed. Cold Spring Harbor Laboratory Press, Cold Spring Harbor, NY.
66. Lange J, Müller F, Takors R, Blombach B. 2018. Harnessing novel chromosomal integration loci to utilize an organosolv-derived hemicellulose fraction for isobutanol production with engineered *Corynebacterium glutamicum*. *Microb Biotechnol* 11:257–263. <https://doi.org/10.1111/1751-7915.12879>.
67. Hoffmann J, Altenbuchner J. 2014. Hyaluronic acid production with *Corynebacterium glutamicum*: effect of media composition on yield and molecular weight. *J Appl Microbiol* 117:663–678. <https://doi.org/10.1111/jam.12553>.
68. Schäfer A, Tauch A, Jäger W, Kalinowski J, Thierbach G, Pühler A. 1994. Small mobilizable multi-purpose cloning vectors derived from the *Escherichia coli* plasmids pK18 and pK19: selection of defined deletions in the chromosome of *Corynebacterium glutamicum*. *Gene* 145:69–73. [https://doi.org/10.1016/0378-1119\(94\)90324-7](https://doi.org/10.1016/0378-1119(94)90324-7).
69. Gibson DG. 2011. Enzymatic assembly of overlapping DNA fragments. *Methods Enzymol* 498:349–361. <https://doi.org/10.1016/B978-0-12-385120-8.00015-2>.
70. Cordes C, Möckel B, Eggeling L, Sahn H. 1992. Cloning, organization and functional analysis of *ilvA*, *ilvB* and *ilvC* genes from *Corynebacterium glutamicum*. *Gene* 112:113–116. [https://doi.org/10.1016/0378-1119\(92\)90311-c](https://doi.org/10.1016/0378-1119(92)90311-c).
71. Eikmanns BJ, Metzger M, Reinscheid D, Kircher M, Sahn H. 1991. Amplification of three threonine biosynthesis genes in *Corynebacterium glutamicum* and its influence on carbon flux in different strains. *Appl Microbiol Biotechnol* 34:617–622. <https://doi.org/10.1007/bf00167910>.
72. Schwentner A, Feith A, Münch E, Stiefelmaier J, Lauer J, Favilli L, Massner C, Öhrlein J, Grund B, Hüser A, Takors R, Blombach B. 2019. Modular systems metabolic engineering enables balancing of relevant pathways for L-histidine production with *Corynebacterium glutamicum*. *Biotechnol Biofuels* 12:1–21. <https://doi.org/10.1186/s13068-019-1410-2>.
73. Fällmeizger J, Nitschel R, Sánchez-Kopper A, Kraml M, Siemann-Herzberg M. 2016. Site-specific cleavage of ribosomal RNA in *Escherichia coli*-based cell-free protein synthesis systems. *PLoS One* 11:e0168764. <https://doi.org/10.1371/journal.pone.0168764>.
74. Teleki A, Sánchez-Kopper A, Takors R. 2015. Alkaline conditions in hydrophilic interaction liquid chromatography for intracellular metabolite quantification using tandem mass spectrometry. *Anal Biochem* 475:4–13. <https://doi.org/10.1016/j.ab.2015.01.002>.
75. Feith A, Teleki A, Graf M, Favilli L, Takors R. 2019. HILIC-enabled ¹³C metabolomics strategies: comparing quantitative precision and spectral accuracy of QTOF high- and QQQ low-resolution mass spectrometry. *Metabolites* 9:E63. <https://doi.org/10.3390/metabo904063>.
76. Cowart RE, Singleton FL, Hind JS. 1993. A comparison of bathophenanthrolinedisulfonic acid and ferrozine as chelators of iron(II) in reduction reactions. *Anal Biochem* 211:151–155. <https://doi.org/10.1006/abio.1993.1246>.
77. Blair D, Diehl H. 1961. Bathophenanthrolinedisulphonic acid and bathocuproinedisulphonic acid, water soluble reagents for iron and copper. *Talanta* 7:163–174. [https://doi.org/10.1016/0039-9140\(61\)80006-4](https://doi.org/10.1016/0039-9140(61)80006-4).
78. Niesen FH, Berglund H, Vedadi M. 2007. The use of differential scanning fluorimetry to detect ligand interactions that promote protein stability. *Nat Protoc* 2:2212–2221. <https://doi.org/10.1038/nprot.2007.321>.
79. Vivoli M, Novak HR, Littlechild JA, Harmer NJ. 2014. Determination of protein-ligand interactions using differential scanning fluorimetry. *J Vis Exp* 2014:51809. <https://doi.org/10.3791/51809>.

Clarification on the work contributions

The greatest part of the work presented here was designed, performed and analysed by myself and experimentally assisted by my master student Johanna Rapp and my bachelor student Anna-Lena Hacker. Exceptions from this are outlined here for the clarification of further contributions:

André Feith performed the LC-MS-QTOF analysis of culture supernatants (outlined in 4.3) as well as samples that derived from iron reduction assays with PCA (as part of 4.8.1). This included sample preparation, measurements and interpretation of the data.

PCR amplified DNA fragments were always verified by sequencing to be free of undesired mutations. Premixed samples for this were sent to GATC Biotech AG (Constance, Germany) and analysed by the commercial *GATC LIGHTrun* service. GATC Biotech AG provided the sequencing results online, that were further processed as outlined in the Materials & Methods section (3.4.11).

The sequence of unknown peptides was analysed by the commercial service offered by Proteome Factory AG (Berlin, Germany). The initial sample preparation in our laboratory is described in 3.7.3. Proteome Factory AG processed the samples further, identified the amino acid sequence of unknown peptides and delivered a preliminary interpretation of the results (as outlined in 3.7.4).

DNA oligonucleotides for PCR amplification and sequencing (tab. S6) were ordered from Biomers.net GmbH (Ulm, Germany).